

NASA Contractor Report 185175
Aerojet 2459-54-2

AD-A234 629

Orbital Transfer Vehicle Oxygen Turbopump Technology

Final Report, Volume I—Design, Fabrication,
and Hydrostatic Bearing Testing

P.S. Buckmann, W.R. Hayden, S.A. Lorenc,
R.L. Sabiers, and N.R. Shimp

*GENCORP Aerojet TechSystems
Sacramento, California*

DTIC
ELECTE
APR 15 1991

C

D

December 1990

Prepared for
Lewis Research Center
Under Contract NAS3-23772

DTIC FILE COPY

Best Available Copy

NASA

National Aeronautics and
Space Administration

91 4 12 035

FOREWORD

This document is the first volume of the final report to the National Aeronautics and Space Administration for that portion of the oxygen turbopump technology work done under Task Orders B.2, B.3, and B.4. Volume II covers the work done under Task Orders B.6 and B.7. All work in this volume was presented to NASA LeRC during program reviews, in the monthly technical reports, or in ATC Report 2459-54-1, April 1988, which documented the hydrostatic bearing (Series A and B) testing.

The time span of the activities covered in this report is from July 1983 to 31 March 1987. Task B.2, Preliminary Design, extended from July 1983 to April 1984; Task B.3, Detail Design, from July 1984 to April 1986; and Task B.4, OX TPA Bearing test, from September 1985 to 31 March 1987. Following the Task B.4 testing, the test article required completion of machining and pump housing surface plating to convert it from a bearing test unit to a functioning turbopump. Task Order B.6 covered the machining and preparations for testing. Actual testing was done under Task Order B.7 where successful operation with gaseous oxygen turbine drive was demonstrated. Task Order B.8 extends the testing from July 1989 to the completion of hot gaseous oxygen turbine drive testing (Series F) in late 1990.

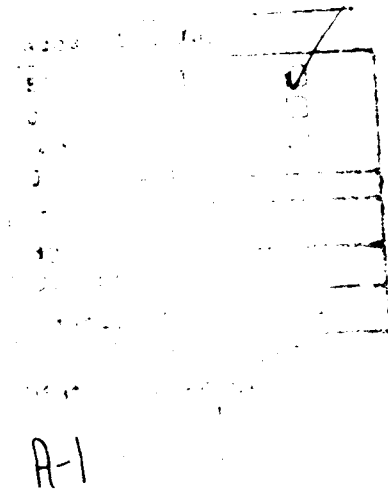


TABLE OF CONTENTS

	<u>Page</u>
List of Tables.....	iv
List of Figures	v
Summary.....	1
1.0 Introduction.....	3
1.1 Background	3
1.1.1 Orbital Transfer Vehicle.....	3
1.1.2 Aerojet Dual Propellant Expander Cycle Engine	5
1.1.3 Oxygen Turbopump	7
1.2 Scope.....	9
1.2.1 Task Order B.2 - TPA/Bearing Tester Preliminary Design	9
1.2.2 Task Order B.3 - Detail Design and Fabrication.....	9
1.2.3 Task Order B.4 - TPA Bearing Test, Series A and B.....	9
1.3 Relevance to Current Rocket Engine Turbopump Design.....	13
1.4 Significance of the Program.....	13
2.0 Design	15
2.1 Design Requirements.....	15
2.2 Selected Approach	18
2.3 Materials Selection	25
2.3.1 Material Ignition in Oxygen	25
2.3.2 Particle Impact Ignition and Design Strategy.....	28
2.3.3 Rubbing Contact Induced Ignition.....	32
2.3.4 Burn Factor and Materials Selection Matrix.....	34
2.3.5 Final Materials Selection.....	39
2.4 Design Baseline	39
2.4.1 Power Balance Results.....	39
2.4.2 Design Point and Predicted Performance	43
2.5 Detailed Design.....	51
2.5.1 Bearing and Seal Design.....	51
2.5.2 Pump Section and Crossovers	75
2.5.3 Turbine Section Design.....	93
2.5.4 Housing Design.....	125
2.5.5 Tester Drive Unit Design	131
2.5.6 Thermal and Stress Analyses.....	131

TABLE OF CONTENTS (cont.)

	<u>Page</u>
3.0 Fabrication.....	149
3.1 Vendor Survey and Selection.....	149
3.2 Vendor Capability/Productibility	149
3.3 Fabricated Items.....	153
4.0 Oxygen Turbopump Testing.....	159
4.1 Facility and Hardware Description.....	159
4.2 Test Approach and Rationale.....	162
4.3 Facility Buildup.....	166
4.3.1 Facility Schematic and Flow Loop Description	166
4.3.2 Facility Instrumentation	166
4.4 Test Procedures.....	170
4.4.1 Test Plan Requirements	170
4.4.2 Test Conduct	170
4.5 Testing.....	175
4.5.1 Facility Checkout and Tester Chilldown	175
4.5.2 Series A Testing.....	182
4.5.3 Series B Testing.....	184
4.5.4 Teardown Inspection	191
5.0 Discussion of Results and Conclusions	201
5.1 Discussion.....	201
5.2 Conclusions.....	212
6.0 References.....	215
7.0 Symbols and Units.....	217
Appendices	
A. Port Instrument Location/Identification Scheme.....	A-1
B. Instrumentation List.....	B-1

LIST OF TABLES

<u>Table No.</u>		<u>Page</u>
1.1-1	Goals for the New OTV Engine.....	4
2.1-1	Dual Expander Engine Features.....	16
2.1-2	LOX Turbopump Design Point	17
2.2-1	Bearing Life Requirement.....	20
2.2-2	Bearing Selection/Rationale	21
2.2-3	TPA Design Conditions.....	22
2.2-4	Design Basis and Reference	23
2.3-1	Materials Selection Matrix.....	29
2.4-1	LOX Pump Design Point.....	45
2.4-2	Inducer Design Point.....	46
2.4-3	OTV 1st Stage Pump.....	47
2.4-4	OTV 2nd Stage Pump.....	47
2.5-1	Inducer Design Parameters.....	82
2.5-2	Impeller Design Parameters	84
2.5-3	Second Stage Inlet Guide Vanes.....	90
2.5-4	Turbine Section Design Point	95
2.5-5	LOX Turbopump Speed Selection.....	100
2.5-6	Turbine Design Values.....	106
2.5-7	Nozzle and Rotor Blade Loss Analysis	109
2.5-8	Design Point Performance Prediction	110
2.5-9	Effect of Rotor Tip Clearance on Efficiency	110
2.5-10	Nozzle Vane Profile Parameters	114
2.5-11	Rotor Blade Profile Parameters.....	114
2.5-12	Turbine Power Balance at Minimum Thrust Point.....	120
2.5-13	Important Properties of Candidate Materials	127
2.5-14	OTV TPA Stress Summary.....	148
3.3-1	OTV Oxygen TPA Fabricated Parts List	155
4.4-1	Oxygen Turbopump Test Plan Highlights.....	173
4.5-1	Test Series "B" Summary.....	194

LIST OF FIGURES

<u>Figure No.</u>		<u>Page</u>
1.1-1	Dual Expander Cycle Engine Original Concept.....	6
1.1-2	Engine Control Schematic.....	8
1.1-3	Bearing Tester.....	10
1.1-4	Disassembled Housings With Pump and Quill Shaft.....	11
1.1-5	Disassembled Turbine and Pump Bearings.....	12
2.2-1	Disassembled Rotating Assembly Showing Impeller and Turbine Discs Prior to Finish Machining.....	19
2.2-2	Critical Speed Operating Zones.....	24
2.3-1	Bearing Tester Nitrogen Service.....	26
2.3-2	Oxygen Compatible Materials for OTV Engine Turbopump.....	27
2.3-3	Effect of O ₂ Pressure on Ignition Temperature.....	30
2.3-4	Results of Particle Impact Tests on Impact Plates.....	31
2.3-5	Effect of O ₂ Pressure on Heating Rates of Monel 400.....	33
2.3-6	Time to Ignition vs Oxygen Pressure.....	33
2.3-7	Load at Ignition vs Oxygen Pressure.....	35
2.3-8	Heat Rate per Unit Area Required for Ignition vs O ₂ Pressure..... (From Benz & Stoltzfus)	35
2.3-9	Correlation of Heat of Combustion With PV Product for..... Metal Ignition	36
2.3-10	Burn Factor vs Ignition Temperature in 6.9 MPa (1000 psi) O ₂	37
2.3-11	Structural and Thermal Properties of Materials for Use..... in Oxygen	38
2.4-1	O ₂ Turbopump Power Balance at Minimum Thrust.....	40
2.4-2	Power Balance at Maximum Thrust.....	44
2.4-3	Predicted OTV Stage Performance.....	48
2.4-4	Predicted OTV Combined Stage Performance.....	49
2.5-1	Two Piece Shaft, Self-Aligning Pump Bearing.....	52
2.5-2	Rotating Assembly Mass-Elastic System and Mode Shapes.....	53
2.5-3	Critical Speed as a Function of Bearing Stiffness.....	54
2.5-4	Rotor Maximum Misalignment.....	55
2.5-5	Rotor Axial Thrust.....	57
2.5-6	Summary of Rotor Loads.....	58
2.5-7	Pump End Hydrostatic Thrust and Journal Bearing.....	59
2.5-8	Bearing Surface Velocity as a Function of Shaft Speed.....	62

LIST OF FIGURES (cont.)

<u>Figure No.</u>		<u>Page</u>
2.5-9	Fluid Film Reynolds Number Due to Shaft Rotation.....	63
2.5-10	Reynolds Number Due to Pressure Induced Velocity.....	64
2.5-11	Pump End Journal Bearing Performance Prediction.....	65
2.5-12	First Stage Thrust Bearing Performance Prediction.....	66
2.5-13	First Stage Thrust Bearing.....	67
2.5-14	LO ₂ TPA Axial Load Capacity vs Axial Clearance.....	68
2.5-15	Second Stage Thrust Bearing.....	69
2.5-16	Second Stage Thrust Bearing.....	70
2.5-17	Spherical Socket Performance.....	71
2.5-18	Turbine End Journal Bearing.....	73
2.5-19	OTV LO ₂ TPA - Turbine End Journal.....	74
2.5-20	Turbine End Journal Bearing.....	76
2.5-21	Turbine End Journal Bearing.....	77
2.5-22	Turbine End Journal Bearing.....	78
2.5-23	Turbine End Journal Bearing.....	79
2.5-24	Volute Configuration Based on Constant Velocity Concept.....	86
2.5-25	Second Stage Inlet for External Interstage Passages.....	87
2.5-26	OTV LOX Turbopump Flight Configuration.....	89
2.5-27	Second Stage Inlet Guide Vane.....	91
2.5-28	Second Stage Inlet Guide Vanes Mean Streamline Unwrapped..... View	92
2.5-29	Predicted OTV Performance Overall Performance	94
2.5-30	OTV LOX Turbopump.....	97
2.5-31	OTV LOX Turbine Maximum Thrust Point Turbine..... Mach Numbers	98
2.5-32	Relation Between F and E.....	104
2.5-33	OTV LOX Turbine Velocity Diagram.....	108
2.5-34	Turbine Performance Characteristics	111
2.5-35	Turbine Performance Characteristics	112
2.5-36	OTV LOX Turbine Nozzle Contour.....	113
2.5-37	Preliminary Sketch of Rotor Blade Contour.....	116
2.5-38	OTV LOX Turbine Flow Passage.....	117
2.5-39	OTV LOX Turbopump.....	118

LIST OF FIGURES (cont.)

<u>Figure No.</u>		<u>Page</u>
2.5-40	O ₂ Turbopump Power Balance at Minimum Thrust	121
2.5-41	Bearing Tester Initial Installation	126
2.5-42	OTV Oxidizer Turbopump Assembly Bearing Tester..... Configuration	128
2.5-43	Housing, Turbopump	129
2.5-44	Housing, Turbopump	130
2.5-45	Housing, Turbopump	132
2.5-46	IR&D Turbine Drive Assembly	133
2.5-47	Drive Turbine And Torquemeter Assembly	134
2.5-48	Bearing Tester Shaft With Bearings and Quill Drive Shaft	135
	With Floating Ring Seal, Post Test 2459-120-A7-32	
2.5-49	Post Test View of Test Setup Looking Obliquely at the Bearing.....	136
	Tester End	
2.5-50	Post Test View of Test Setup Looking at the Test Drive Turbine	138
	Exhaust End	
2.5-51	Turbine Blade In-Plane Bending Stress	139
2.5-52	OTV TPA Shaft and Impellers - Deformed Shape.....	140
2.5-53	OTV Rotor with Bolt, Deformed Shape, Steady State-Full Thrust.....	141
	Thermal Pressure and Speed Effects (75,000 rpm)	
2.5-54	Turbine Disk Effective Stress Due to Clamping and Rotating Loads ...	142
2.5-55	First Stage Housing Deformed Shape.....	144
2.5-56	Pump Housings - Deformed Shape Summary.....	145
2.5-57	Turbine Housing Effective Stress	146
2.5-58	Turbine Shaft Coolant Path.....	147
2.5-59	Steady State Temperature Map at Turbine End and Adjacent Parts.....	148
3.1-1	Pump Bearing, Sheet 1	150
3.1-2	Pump Bearing, Sheet 2	151
3.1-3	Turbine Bearing, Sheet 3	152
4.1-1	Bearing Tester and Test Drive Turbine Assemblies at Mockup.....	160
	Installation in Test Bay A7	
4.1-2	LOX Bearing Tester - OTV Turbopump.....	161
4.1-3	Floating Shaft Seal and Quill Shaft With Seal Housing.....	163
4.1-4	Assembled Turbine and Pump Bearings.....	164
4.1-5	Turbopump Housing Seal Split Rings.....	165

LIST OF FIGURES (cont.)

<u>Figure No.</u>	<u>Page</u>
4.3-1	OTV Test Series "A" and "B" LN2 Bearing Tester Flow Diagram..... 167
4.3-2	OTV Bearing Tester NETSIM Nodes and Branches..... 168
4.3-3	Inductance Distance Probe With Signal Conditioning Box..... 169
4.3-4	Inlet Housing Distance Probe Port P/N 1197575 171
4.3-5	Inlet Housing-Distance Probe Tip End P/N 119755..... 172
4.5-1	Temperature as a Function of Time..... 176
4.5-2	Fluid and Housing Exterior-Temperature vs Time Test..... 178 No. 2459-120-A7-042 Plot No. 1 Test Stand A287 Test Date 06-03-89
4.5-3	Drive Turbine Bearing Temperature vs Time Test No..... 179 2459-120-A7-042 Plot No. 2 Test Stand A287 Test Date 06-03-87
4.5-4	Test No. 2459-120-A7-32 OTV Bearing Tester Digitalized Data..... 185
4.5-5	Quill Shaft..... 186
4.5-6	Cryogenic and Ambient Temperature Distance Sensors-..... 188 Start Transient
4.5-7	Distance Sensor Signal as a Function of Speed 189
4.5-8	Distance Sensor Signal as a Function of Speed 190
4.5-9	Cryogenic Operation of Distance Sensors at 72,000 RPM 192 Steady State
4.5-10	Cryogenic Operation of Distance Sensor Through Start..... 193 Transient Speed and Flow Meters
4.5-11	Pressure/Flow/Speed/Temperature vs Time Test No..... 195 2459-120-A7-A042 Plot No. 3
4.5-12	Pressure vs Time-Test No. 2459-120-A7-042 Plot No. 4..... 196
4.5-13	Pressure/Temperature/Speed/Torque vs Time..... 197 Test No. 2459-120-A7-042 Plot No. 5
4.5-14	Voltage/Speed vs Time Test No. 2459-120-A7-042 Plot No. 6..... 198 Test Stand A287 Test Date 06-03-87
4.5-15	Bearing Tester Shaft With Bearings and Quill Drive Shaft..... 199 With Floating Ring Seal, Post Test 2459-120-A7-32
5.1-1	First Stage Impeller Disk Pressure..... 204
5.1-2	Axial Loads at Each Impeller and Turbine..... 205
5.1-3	Net Load on Pump Hydrostatic Bearing..... 207
5.1-4	Net Load on Spherical Socket 208
5.1-5	OTV LOX Pump End Self-Aligning Hydrostatic Bearing Flow Rate... 210

LIST OF FIGURES (cont.)

<u>Figure No.</u>		<u>Page</u>
5.1-6	OTV LOX Turbine End Self-Aligning Hydrostatic Bearing Flow Rate	211
5.1-7	"X" vs "Y" Orbits at 72,000.....	213

SUMMARY

This report covers the design, fabrication, and initial testing of a rocket engine turbopump (TPA) for the delivery of high pressure liquid oxygen using hot oxygen for the turbine drive fluid. This TPA is basic to the dual expander engine which uses both oxygen and hydrogen as working fluids. Separate tasks addressed the key issue of materials for this TPA. All material selections emphasized compatibility with hot oxygen. Monel K-500 or 400 are used where high strength is required while Nickel 200 is used in lower stress areas. Bearing areas are silver plated for low rubbing friction contact with hard chrome plated rotating element surfaces.

The OX TPA design uses a two-stage centrifugal pump driven by a single-stage axial turbine on a common shaft. The first pump stage incorporates an inducer section for improved suction performance. Inter-stage pump flow is routed external to the main housing through two ducts connecting first-stage discharge to second stage entry. The shaft is supported by two journal type hydrostatic bearings supplied with high pressure LOX from the second-stage pump discharge. Both bearings articulate on spherical seats giving some capability to correct for initial misalignment and/or transient thermal distortion. Design speed is 75,000 rpm at a flowrate of 5.5 lbm/sec. The very stiff support provided by the hydrostatic bearing system to the rotor facilitates a sub-critical speed design over a speed range comparable to 20:1 throttling of the engine. The very small shaft displacements and low vibration associated with subcritical operation allow the tight running clearances needed for high efficiency open impellers without contact.

The design includes provision for future addition of a low speed boost pump to the engine for operation with the low pump suction pressure of flight tankage. A portion of the inducer discharge is tapped off to drive the boost pump. The design also includes ports for three shaft displacement/speed sensors, various temperature measurements, and accelerometers. Flow measurements are made on streams to and from the TPA.

The unique spherical hydrostatic bearing design was considered a radical enough departure from current design to warrant a bearing test program. The bearing tester used the semi-finished TPA housing, the rotating assembly prior to finish

Summary (cont.)

machining of impellers and turbine blades, and provision for a quill shaft connection to the drive unit. The drive unit was a workhorse gaseous nitrogen driven turbine capable of 75,000 rpm. The unit proved difficult to setup and checkout. Trying to simulate a turbopump pressure environment proved very time consuming. Testing proceeded with great care as nearly all the hardware was unique, required considerable fabrication time, and there were no spares.

The Series A testing demonstrated bearing chilldown and integrity at low speed operation. An incompletely resolved problem was the rotor binding caused by pressure changes as the tester was chilled to liquid nitrogen temperatures. Series B testing demonstrated the bearing operation at high speed. The maximum speed attained was 72,000 rpm. The bearing operated satisfactorily with no load or stability problems. Post test examination of the journal and thrust bearing surfaces showed no evidence of operating wear.

The successful completion of the Series B testing led to a lengthy hiatus in the program while the TPA housing and rotating assembly were finish machined and selectively silver plated to form the operational turbopump assembly. Additional testing which used ambient oxygen as the turbine drive gas and liquid oxygen in the pump is discussed in Volume II of this report.

1.0 INTRODUCTION

1.1 BACKGROUND

1.1.1 Orbit Transfer Vehicle

The orbit or orbital transfer vehicle (OTV) is one in a series of vehicle concepts for the transfer of payloads from low earth orbit (LEO) to geostationary orbit (GEO) or other inner solar system missions. Various NASA organizations have funded study and hardware programs for developing the technology for these vehicles and their propulsion systems since the completion of the Apollo program. NASA Lewis Research Center has had responsibility for the engine technology while NASA Marshall has supervised vehicle study contracts and developed the mission model. Aerojet has done active contract work on various engine concepts directly applicable to the current work since 1978.

This turbopump technology program is a part of a task order contract initiated in April 1983. The turbopump tasks began in July 1983 and will conclude in late 1990. The OTV technology contract will be continued under the Chemical Transfer Propulsion program under Project Pathfinder. The rocket engine technology developed under this program will support such missions as a return to the moon and piloted missions to Mars and its moons. In keeping with the Pathfinder (and OTV) program goals of developing emerging, innovative technologies, and rocket engines with capabilities superior to available engines, NASA LeRC has encouraged Aerojet and other companies in the industry to work to requirements representing a significant advance in the state-of-the-art. The technology goals for the OTV engine are presented in Table 1.1-1. The three columns in the table show the evolution of both the state-of-the-art and the requirements developed by the Prime contractors doing the Phase A vehicle studies for NASA-MSFC. The requirements in 1984 and those listed in the center column for 1986 were similar.

The turbopump design reported herein was prepared to meet requirements as they were in 1984. Since that time both the NASA requirements and the Aerojet design have evolved. In 1984, Aerojet proposed a set of four 3000 lbf thrust engines per vehicle to meet LEO-to-GEO mission requirements. The engine was a radical departure from then available LOX/LH₂ engines. It featured a hot oxy-

TABLE 1.1-1

TECHNOLOGY GOALS FOR THE NEW OTV ENGINE

Parameters	Reference		Updated	
	Engine System	October 1986	1988	Goals or Requirements
	Characteristics	Goals and/or Requirements	Requirements	
basin	Earth	Not Specified	Space	
Human-rating	No	Not Specified	Yes	
Safety Criteria	Not Specified	Not Specified	Fail Operational, Fail Safe	
Propellants - Fuel	Hydrogen	Hydrogen	Hydrogen	
- Oxidizer	Oxygen	Oxygen	Oxygen	
Vacuum Thrust (Design Point)	15,000 lbf	10,000 - 25,000 lbf*	7500 lbf (per engine)	
Number of Engines per Vehicle		Not Specified	2 Minimum	
Engine Mixture Ratio, O/F	5.0	6.0	6.0	
(Design Point)				
Engine Mixture Ratio Range, O/F	4.4 to 5.6	5 - 7	5 - 7	
Propellant Inlet Temperature - Hydrogen	38.3°R	37.8°R	37.8°	
Oxygen	175.3°R	162.7°R	162.7°R	
Gimbal	±4.0 Degrees	±6.0 Degrees (Sq. Pattern)	±20 degrees Pitch & Yaw	
Aerobraking Design Criteria	The engine must be compatible with aeroassist return of the vehicle to low-earth orbit.			
Vacuum Specific Impulse	444 lbf-sec/lbm	520 lbf-sec/lbm	490 lbf-sec/lbm	
Vacuum Thrust Throttling Ratio	No Throttling	30:1	10:1	
Net Positive Suction Head (NPSH) - Hydrogen	133.0 ft-lbf/lbm	0	15 ft-lbf/lbm	
Oxygen	16.7 ft-lbf/lbm	0	2 ft-lbf/lbm	
Weight	290 lbm	360 lbm	360 lbm (2 engines)	
Length	70.1 in.	40	TBD (Assume 60", Stowed)	
Reliability (90% Confidence Level)	0.9982	1.0	.9975 Single engine, .99958 Dual engine**	
Operational Life	3 Starts, 4000 sec	500 Starts, 20 Hours	500 Starts, 20 Hours	
Service Free-Life		100 Starts, 4 Hours	100 Starts, 4 Hours	
Start Cycle		Chilldown with propulsive dumping of propellants, tankhead start, pumped idle operation, autogenous tank pressurization required		

Updated March 1990

*Vehicle engine set total thrust must be in this range

**MSFC/Boeing Vehicle Studies

1.1, Background, cont.

gen driven oxygen TPA located in the center of the engine chamber. The oxygen was to be heated by the combustion gas in the chamber and fed directly to the turbine. The engine injector had two annular rows of elements. The basic engine configuration is shown in Figure 1.1-1. This radical concept posed numerous challenges to the TPA design team. The chamber mounting made the design task more manhour intensive than for a conventional TPA mounted external to the combustor. The actual test article compromised the flight type design by using external interstage crossovers and a conventional machined case. By the time the TPA was in test the engine concept had changed to use an externally mounted TPA and the test article was actually much more representative of the proposed flight unit. The Aerojet engine concept, however, continues to use the dual expander cycle with an all oxygen TPA. The most critical technology needed to validate the cycle is this turbopump.

1.1.2 Aerojet Dual Propellant Expander Cycle Engine

In a conventional expander cycle engine, hydrogen is routed through passages in the combustion chamber wall where it both cools the wall and acquires sufficient thermal energy to power the turbine drives of pumps for both the hydrogen and oxygen flow circuits. It is then routed to the injector for combustion. This cycle is fairly simple, plumbing is straight forward, it offers good performance potential, and, as all propellant is burned in the combustion chamber, it does not have the losses associated with open cycles. Its limitations are related to dependence on only one propellant as a turbine drive fluid which, in turn, requires interpropellant seals and a purge gas in the oxygen turbopump. To obtain the needed power the hydrogen must be heated to a temperature very near to the design limit for the copper based alloys employed for the chamber liner. With the added limits imposed by high cycle life, long operating times without maintenance, and a 10:1 or greater throttling requirement, the hydrogen expander cycle is capable of only a modest improvement over the current production expander cycle engine, the RL-10.

The Aerojet dual expander cycle alleviates these limitations by using oxygen as a working fluid as well as hydrogen. This reduces the demands on the hydrogen circuit as the oxygen turbopump is driven by heated oxygen. It also eliminates the need for an interpropellant seal and the associated helium purge

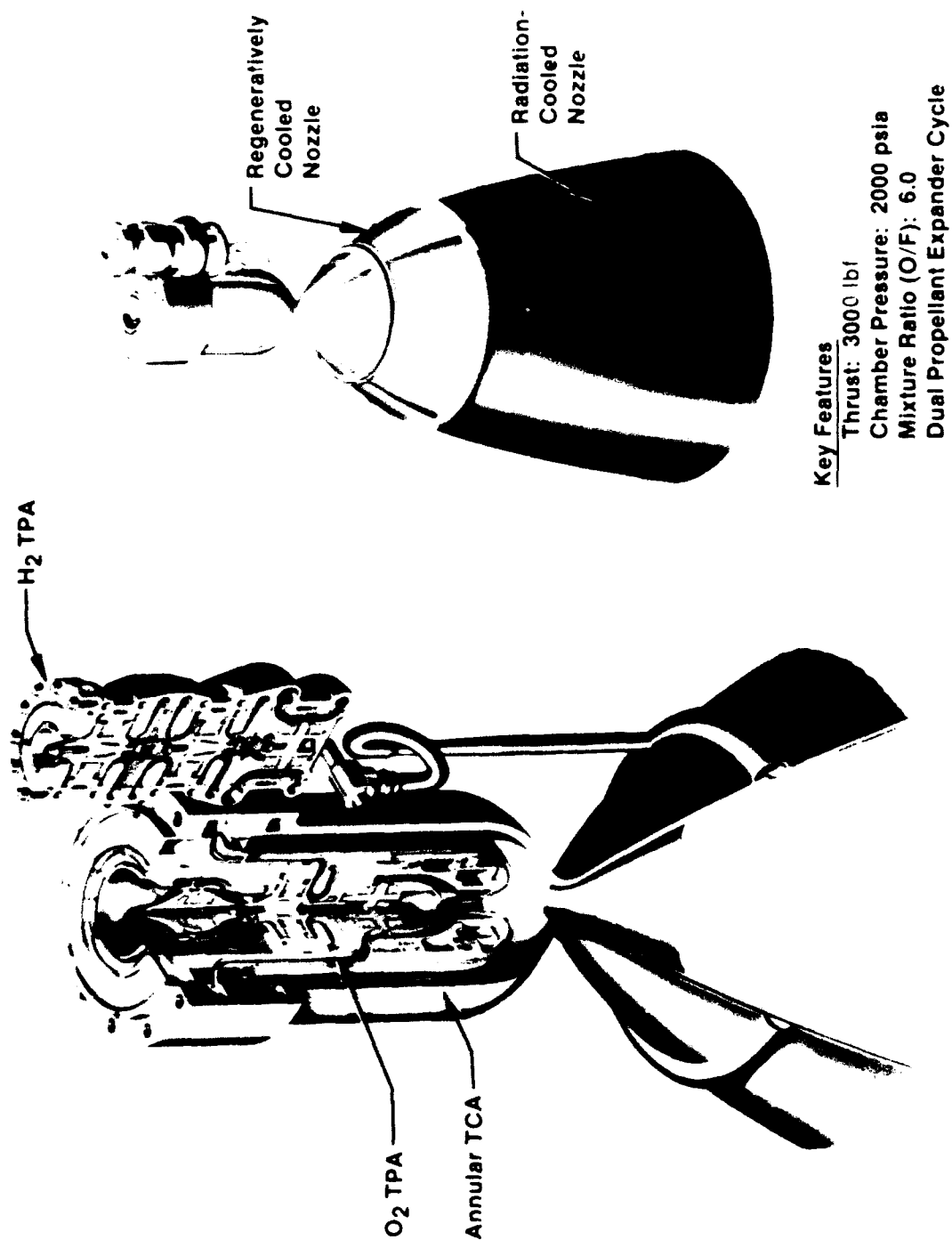


Figure 1.1-1. Dual Expander Cycle Engine Original Concept

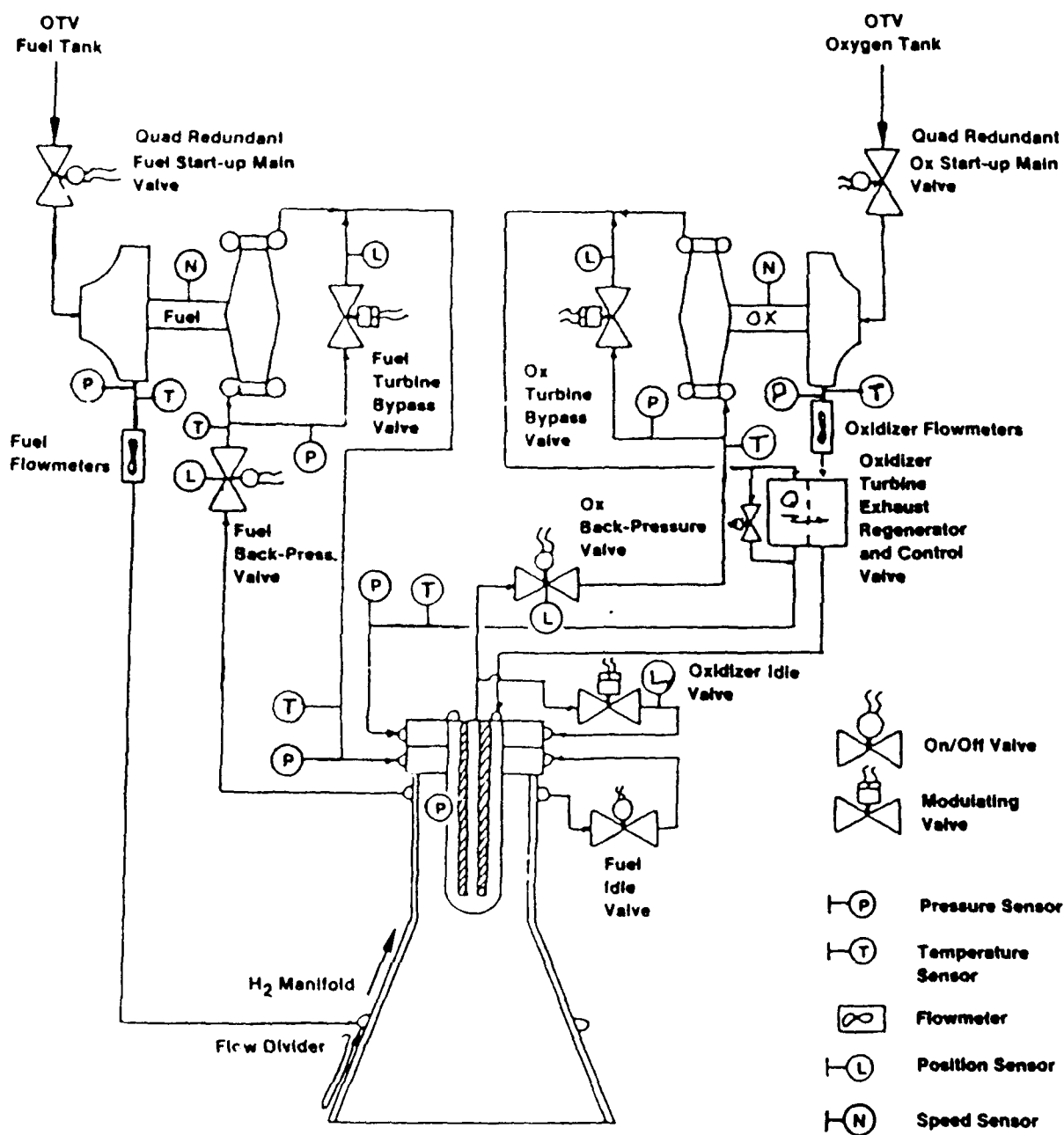
1.1, Background, cont.

requirement. The gasified oxygen is also needed for the I-triplet gas-gas injector element which provides high (100%) energy release efficiency and excellent combustion stability over a wide throttling range. The oxygen is heated to approximately 400°F by flowing through a LOX/GH₂ heat exchanger and then through the regeneratively cooled nozzle extension. The flow schematic is shown in Figure 1.1-2. This is the schematic used during the TPA design. It has evolved considerably since that time. The hydrogen used to heat the cold oxygen in the heat exchanger is the exhaust from the hydrogen TPA turbine and provides the thermal energy to the oxygen at a cost of some pressure drop across the heat exchanger.

1.1.3 Oxygen Turbopump

Key to this design is the use of an oxygen turbopump driven by 400°F (maximum) oxygen. Many turbopumps have been successfully used to pump liquid oxygen, but hot oxygen has been considered too reactive to use as a turbine drive fluid. The NASA LeRC has sponsored an extensive program of oxygen compatibility experiments with various materials under a variety of conditions of pressure, temperature, and mechanical stress. The pertinent papers are given in the list of References 1-6 at the end of this report. A number of materials have been identified that can be used in an oxygen turbopump with good confidence that the materials will not ignite under either particle impact or minor rubbing. Despite the experimental data, verification of an oxygen turbopump requires successful completion of an extensive test program with a TPA in oxygen service. This volume of the report covers the first two series of tests in a complete oxygen TPA verification program. At the completion of the program the TPA will have demonstrated compatibility of the selected materials with cryogenic oxygen, ambient oxygen, and 400°F oxygen in conditions approximating that of actual service.

The oxygen TPA also uses a number of design innovations other than materials selection. The most critical is the self aligning hydrostatic bearing system. The long life requirements of the OTV engine are incompatible with conventional ball bearing systems that require rolling and sliding contact in liquid oxygen at high speeds. A hydrostatic bearing was chosen for this TPA as it had potential for very long service life free of wear or fatigue life limits. The Series "A" and "B" tests were planned to verify the bearing design prior to actual testing with oxygen.



As of 1 June 87

Figure 1.1-2. OTV Engine Control Schematic

1.1, Background, cont.

This required use of a special bearing test assembly as shown in longitudinal sectional view in Figure 1.1-3. The housing was designed for later modification into an actual turbopump housing after completion of Series "A" and "B" testing. Actual photographs of the TPA in bearing tester configuration and the hydrostatic bearing parts are shown in Figure 1.1-4 and 1.1-5, respectively.

1.2 SCOPE

The scope for each subtask is summarized below based on the task order requirements.

1.2.1 Task Order B.2 - TPA/Bearing Tester Preliminary Design

Conduct a design and analysis program for the preliminary design of the oxygen turbopumps and the preliminary and detail design of hydrostatic bearing tester assemblies. Test plans for subcomponent and TPA testing were written under this task order.

1.2.2 Task Order B.3 - Detail Design and Fabrication

Conduct a detail design program and complete the design of the oxygen TPA and bearing tester with detail drawings ready for fabrication. Fabricate and/or procure one set plus critical spares of TPA components and bearing tester components using the drawings from the detail design. Initial test site preparation and completion of a detailed test plan were included in the scope.

1.2.3 Task Order B.4 - TPA Bearing Test, Series A and B

Conduct a test program to determine the performance and operating characteristics of the oxygen TPA bearing. Two series of tests, Series A and B, were to operate the bearing at low speed and at high speed in liquid nitrogen. An interim report was prepared and distributed at the completion of the task.

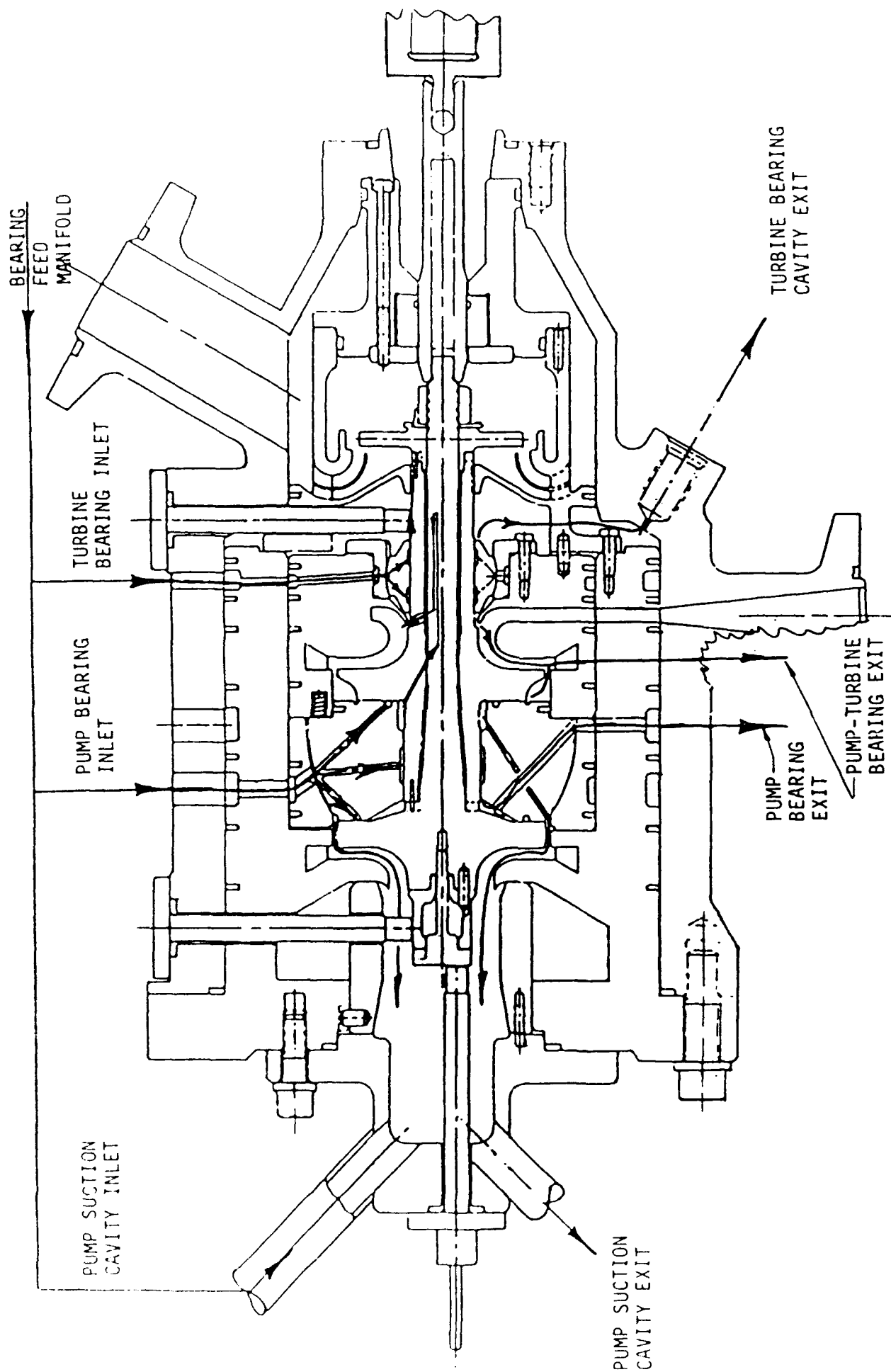


Figure 1.1-3. OTV Bearing Tester

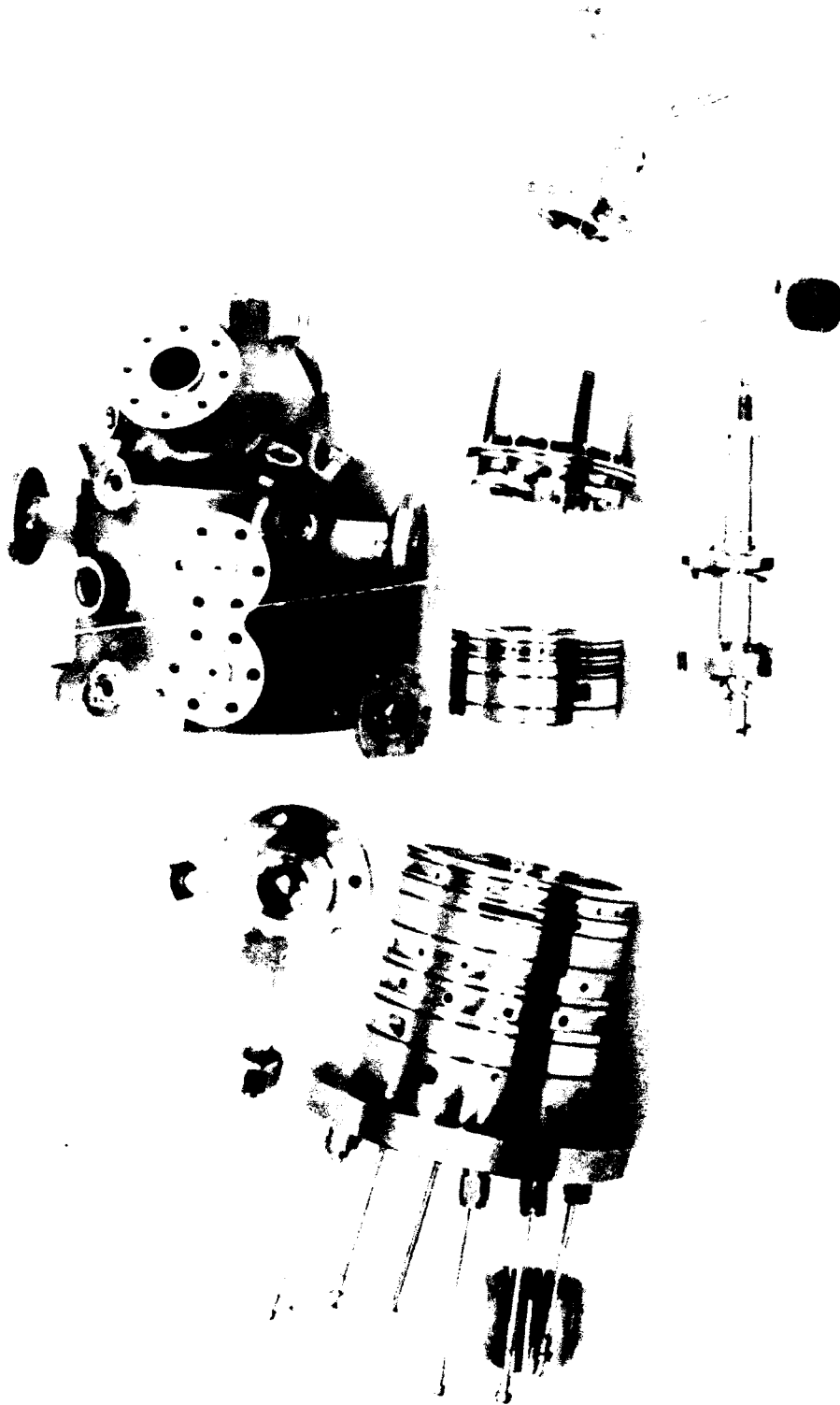


Figure 1.1-4. Disassembled Housings With Pump and Quill Shaft

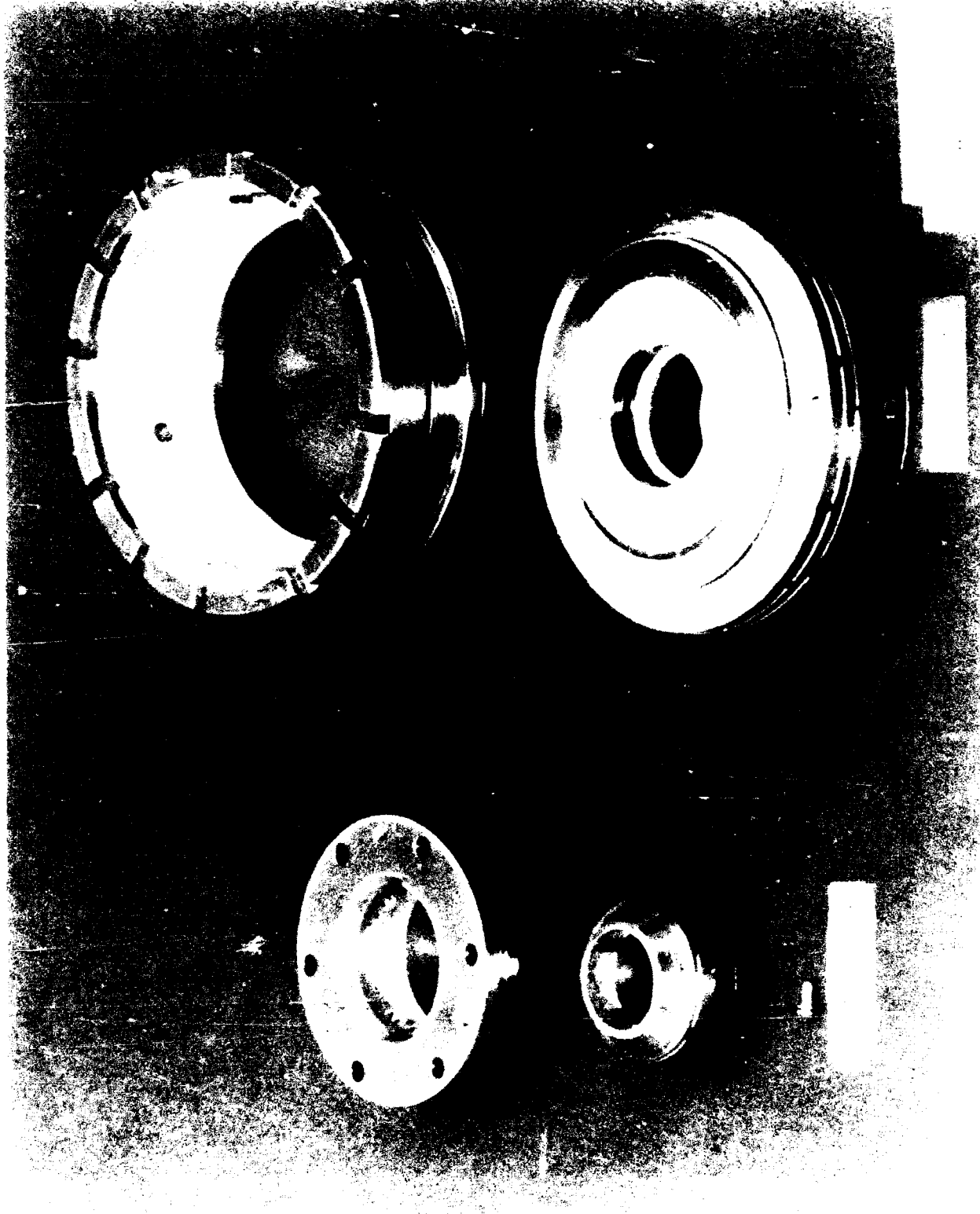


Figure 1.1-5. Disassembled Turbine and Pump Bearings

1.0, Introduction, cont.

1.3 RELEVANCE TO CURRENT ROCKET ENGINE TURBOPUMP DESIGN

The intent of this technology program is to demonstrate and reduce to practice several key design innovations that, taken together, significantly advance the design base for rocket engine turbopumps. These design innovations are:

- 1) Use of hot (400°F) oxygen as a turbine drive fluid.
- 2) Use of the monel family of alloys along with various platings for materials compatible with hot oxygen.
- 3) Use of a hydrostatic bearing system for non-contact operation without the fatigue life limits of rolling contact bearings to meet operating life goals well beyond current rocket engine requirements.
- 4) Use of an articulating, self adjusting spherical bearing system to accommodate minor motion and misalignment for the very close clearances required in a hydrostatic bearing system.
- 5) Demonstration of a rotating assembly design that will operate in a subcritical mode over the full range of turbopump speeds for a throttling engine.
- 6) Incorporation of several design features for smooth, predictable operation over a 20:1 throttling range.
- 7) Elimination of an interpropellant seal and a purge gas by having an oxygen drive with an oxygen pump.

1.4 SIGNIFICANCE OF THE PROGRAM

This turbopump not only made use of the design innovations listed above, but proved in testing that they form a workable design. At the time of this writing the TPA has been tested up through the series with ambient temperature oxygen drive while pumping liquid oxygen. As with any first article test unit there are details that would benefit from a redesign, but the unit actually operates quite

1.4, Significance of the Program, cont.

well as is. This is a very respectable technical achievement which should be of use in future turbopump designs.

Final verification of the TPA design approach will come from the hot oxygen test series. When the TPA has operated successfully with 400°F oxygen drive it is suitable for use in a dual expander cycle engine. This is the most critical technology demonstration needed to validate that engine cycle. The dual expander cycle has, in concept, the highest chamber pressure capability of any expander cycle engine. This is the key to wide throttling range, high delivered specific impulse, and the smallest engine size for a given thrust. Without the oxygen turbopump, it is of theoretical interest; with an operating oxygen turbopump an engine using the cycle can be built.

2.0 DESIGN

The following design discussion benefits from the hindsight afforded by report preparation 6 1/2 years after the oxygen TPA design was first considered. No discussion of design detours and blind alleys is included. The intent is to focus on the fruitful approaches and pertinent analysis that culminated in a testable TPA. There is some comment on the changes in mission requirements that impacted the design.

2.1 DESIGN REQUIREMENTS

The overall engine design requirements are presented in Table 1.1-1. Deriving TPA requirements from this list required an engine concept definition be prepared first. The basic mechanical layout of the proposed engine is shown in Figure 1.1-1. Table 2.1-1 summarizes the features that make up this concept. It is fairly radical in appearance and required two critical technologies to be practical: 1) the oxygen driven LOX TPA, and 2) a centerbody cooled by the liquid oxygen from the turbopump. A rigorous thermal design analysis completed during the 7.5K Thrust Chamber Assembly (TCA) design (Task C.3) showed oxygen cooling impractical for the heat transfer rates and gas side wall temperatures predicted with the I-triplet injector element at 2000 psia chamber pressure. This forced the removal of the OX TPA from the centerbody and the use of a GH₂/LOX heat exchanger (HEX) to heat the oxygen for the TPA turbine drive. The oxygen driven TPA remained as a critical technology for the cycle.

The TPA design point is given in Table 2.1-2. Pressures and temperatures were determined from power balances run with the original engine schematic. Simplifying assumptions were made for component pressure drops where no designs had actually been completed. Reworking the power balance for the 7.5K lbf thrust engine design (Task D.5) in 1987-88 showed that the selected design point was well chosen. The flow rate corresponds to operation at an oxidizer to fuel mixture ratio of $MR = 7$. The original Aerojet concept of four engines on each vehicle would meet a total 15,000 lbf thrust, if each engine produced 3750 lbf at $MR = 6$. The 7.5K lbf thrust engine would meet the same total thrust with just two engines.

A critical requirement for a hot oxygen driven TPA is the selection of materials that will not burn in the hot oxygen or be ignited by a high speed particle impact.

TABLE 2.1-1

DUAL EXPANDER ENGINE FEATURES
3000 LBF THRUST VERSION

<u>Parameter/Feature</u>	<u>Design Point</u>
Propellants	LOX/LH2
Engine Cycle	Dual Expander
Thrust	3000 lbf
Chamber Pressure	2000 psia
Mixture Ratio	6 ± 1
Injector Type	2 Row, Annular
Injector Element	I-Triplet (Gas-Gas)
Chamber Regen Coolant	85% of Hydrogen Flow
Cooled Nozzle Coolant	15% of Hydrogen Flow
Oxygen Heating	Oxygen Cooled Centerbody
Oxygen Turbopump Location	Inside the Centerbody
Hydrogen Turbopump Location	Conventional External Mounting
Extendible/Retractable Nozzle	Packages for 40 inch Envelope when Stowed

Table 2.1-2.
LOX Turbopump Design Point

Pump

Flow Rate,	$\dot{W}_p = 5.5 \text{ lb/sec}$
Pressure Rise,	$\Delta P_p = 4600 \text{ psi}$
Efficiency,	$\eta_p \eta_m = 0.585$
Horsepower,	$HP = 156.4$

Turbine

Inlet Total Pressure,	$P_o = 4315 \text{ psia}$
Inlet Total Temperature,	$T_o = 860^\circ R$
Exit Total Pressure,	$P_{o_2} = 2300 \text{ psia}$
Specific Heat at Constant Pressure,	$C_p = 0.22 \text{ BTU/lb.}^\circ R$
Specific Heat Ratio,	$\gamma = 1.4$
Gas Constant,	$R = 48.29 \text{ FT.LB/LB.}^\circ R$

2.1, Design Requirements, cont

There was enough concern regarding the current knowledge of materials/oxygen compatibility that NASA LeRC funded two separate tasks to evaluate various materials under the expected operating conditions (Tasks B.1 and B.5). The results of this and related research are given in the References 1-5 cited at the end of this report, and are summarized in Section 2.3 below.

2.2 SELECTED APPROACH

The limited experience with hydrostatic bearing systems and the unique spherical bearing configuration were considered of sufficient technical risk that a bearing test was needed. This could be done with a specially designed test article or it could be done with the actual TPA bearing system using an external drive unit. Program economics dictated the use of actual TPA hardware adapted for use with an external drive unit. The rotating assembly was used without the final machining of impellers and turbine blades (see Figure 2.2-1), and the TPA housing ports were pilot drilled with finish machining to come after the bearing test (see Figure 1.3-2). This approach to verification of the bearing design and operation placed some limits on the mechanical design of the TPA and consumed nearly two years of program time and TPA task resources.

The hydrostatic bearing selection was based on mission requirements as they applied to the turbopump. The goal of a four hour service life multiplied by the 5X service factor yields a 20 hour design life for turbopump components. The assumption of bearing reliability to be 10X the 0.9997 engine reliability results in a 12,500 hour bearing design life. This is incompatible with any known rolling element design. Ball loads due to centrifugal force alone can be 15 times the allowable fatigue life load limit for a 12,500 hour life. The hydrostatic bearing was the only reasonable selection. The hydrostatic bearing is more sensitive to wear from rubbing during the start and shutdown transients. In operation, there is a high pressure fluid film separating the rotating assembly from the bearing surface. Only particulate contaminants or asymmetrical shaft motion could cause contact type wear. Filters and a

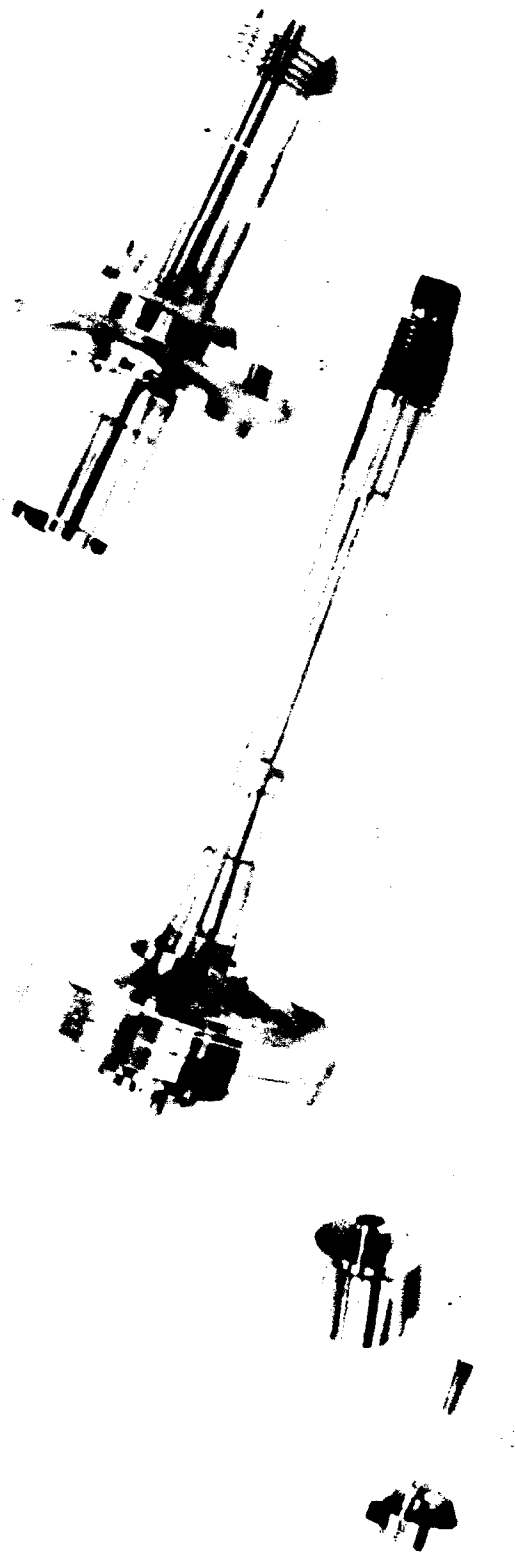


Figure 2.2-1. Disassembled Rotating Assembly Showing Impeller and Turbine Discs Prior to Finish Machining

2.2, Selected Approach, cont.

stable dynamic design eliminate these factors from serious concern. The bearing life requirement is summarized in Table 2.2-1. The selection rationale is given in Table 2.2-2.

TABLE 2.2-1

OTV BEARING LIFE REQUIREMENT

Engine Reliability	= 0.997
Engine Service Life	= 4 hours
Assume Bearing Reliability	= 100 x Engine Reliability
Bearing Reliability	= 0.99999
Bearing Design Life	= 5 x Service Life
∴ Bearing B ₁₀ Life ≈ 5 x 4 x 5 ⁴	= 12,500 hours
Since B _n ~ 5 x B _n /10	

The baseline design selection is summarized in Table 2.2-3. The background for the design selection includes a number of past and recent TPA programs conducted at Aerojet. Some of the more important sources are listed in Table 2.2-4. The design is very much a product of the Aerojet Rotating Machinery Group with a clearly evident design history. One of the Aerojet criteria employed whenever the physical size of the turbopump will allow is the use of a subcritical rotating assembly and bearing design. Figure 2.2-2 is a representation of the TPA critical speed as plotted against a bearing stiffness factor. The curves for the first four critical speeds are shown along with three zones commonly used by TPA designers. Zone 1 is the subcritical zone characterized by a rigid rotor and a stiff bearing system. The advantage of subcritical design is that a throttling engine can operate over its entire thrust range without encountering any forbidden speeds or speed ranges where vibration levels are at high levels. Successful designs are possible in all three zones indicated, but the OTV OX TPA is particularly suitable for subcritical design due to the small size (rotor weight of about 9 ounces), reasonable speed range, and use of a hydrostatic bearing.

TABLE 2.2-2

BEARING SELECTION/RATIONALE

• Life Requirements Can Only Be Met By a Hydrostatic Bearing Design
• At Least Two Bearing Geometries Will Meet the Requirements
• Selected a self aligning hydrostatic bearing for baseline <ul style="list-style-type: none">• Permits high speed operation• Provides high support stiffness for subcritical operation• Has self-alignment capability• Allows close running clearance - high efficiencies
• Design Fixed Hydrostatic Bearing for Backup <ul style="list-style-type: none">• Development risk is similar to the baseline• Fabrication is somewhat simpler (non-spherical surfaces)• Easy substitution for baseline during development
• Develop Self Aligning Hydrostatic Bearing for Test Unit. Alternate Design to Be Completed as Program Resources Permit.

TABLE 2.2-3

TPA DESIGN CONDITIONS

1. <u>The Baseline Turbine will be a Single Stage Design</u> However, a 2-stage design was carried through the concept phase so that a conversion could be made at some later date in the event that WSTF or other data indicated a high ignition potential due to the higher gas velocities experienced with the single stage. The conversion to a 2-stage design, would not be allowed to compromise the mechanical design.
2. <u>The TPA Design Point will be at 100% Thrust</u> (3000 lbf)
3. <u>LOX Pump Design Point Flowrate is 5.5 lbm/sec.</u> This is coincident with a mixture ratio of 7 at 3000 lbf thrust or a mixture ratio of 6 at 3750 lbf thrust.
4. <u>LOX Pump Design Point Discharge Pressure Will Be 4600 Psi</u> The pump impellers, however, will be sized for 4800 psi for design margin and trimming as necessary.
5. <u>Turbine Design Point Conditions</u> <ul style="list-style-type: none">• Turbine inlet pressure 4300 psi• Turbine inlet temperature, 860°R (400°F)• A turbine by-pass minimum of 10% at design point (100% thrust) is achievable providing that the estimated efficiencies of 72.3% turbine, 65% pumps, 90% mechanical are met.
6. <u>Machine Design Safety Margins, Life Goals, Etc.</u> As defined in the OTV program review dated 15, 16 November 1982, the ALRC Development Spec. #40440, and as evolved during the design process.
7. <u>TPA Throttling Performance, Operation and Start-Up</u> Dependent on an engine controls study. See NASA CR 182122 (full citation in Reference 7). TPA design shall be capable of 10:1 throttling with 20:1 desired.

TABLE 2.2-4
DESIGN BASIS AND REFERENCES

- Design Guide for High Pressure Oxygen Systems - NASA 1113.
- WSTF Materials Rubbing and Particle Impact Testing. (See References 1-5)
- OTV Technology Program Work Plan - NAS3-23772
- OTV Transfer Rocket Engine Technology Program Review
15/16 November 1982- NAS3-23170
- OTV Advanced Expander Cycle Engine Design Point Study
NAS 8-33574 June 1980
- High Speed Turbine Shaft Dynamics, Bearings and Seals for Rankine Cycle
Aerojet IR&D 8724
- Hydrostatic Bearing Program (ARES) - 7439-Q-1
- Steady State Performance Prediction Methods for Self-compensating Thrust
Balance - NASA CR72430
- 8 stage Overhung, 60,000 RPM Steam Turbine for EPA -
Contract 68-04-0005
- NERVA Turbo Pump Design Report - N-8300R:71-076

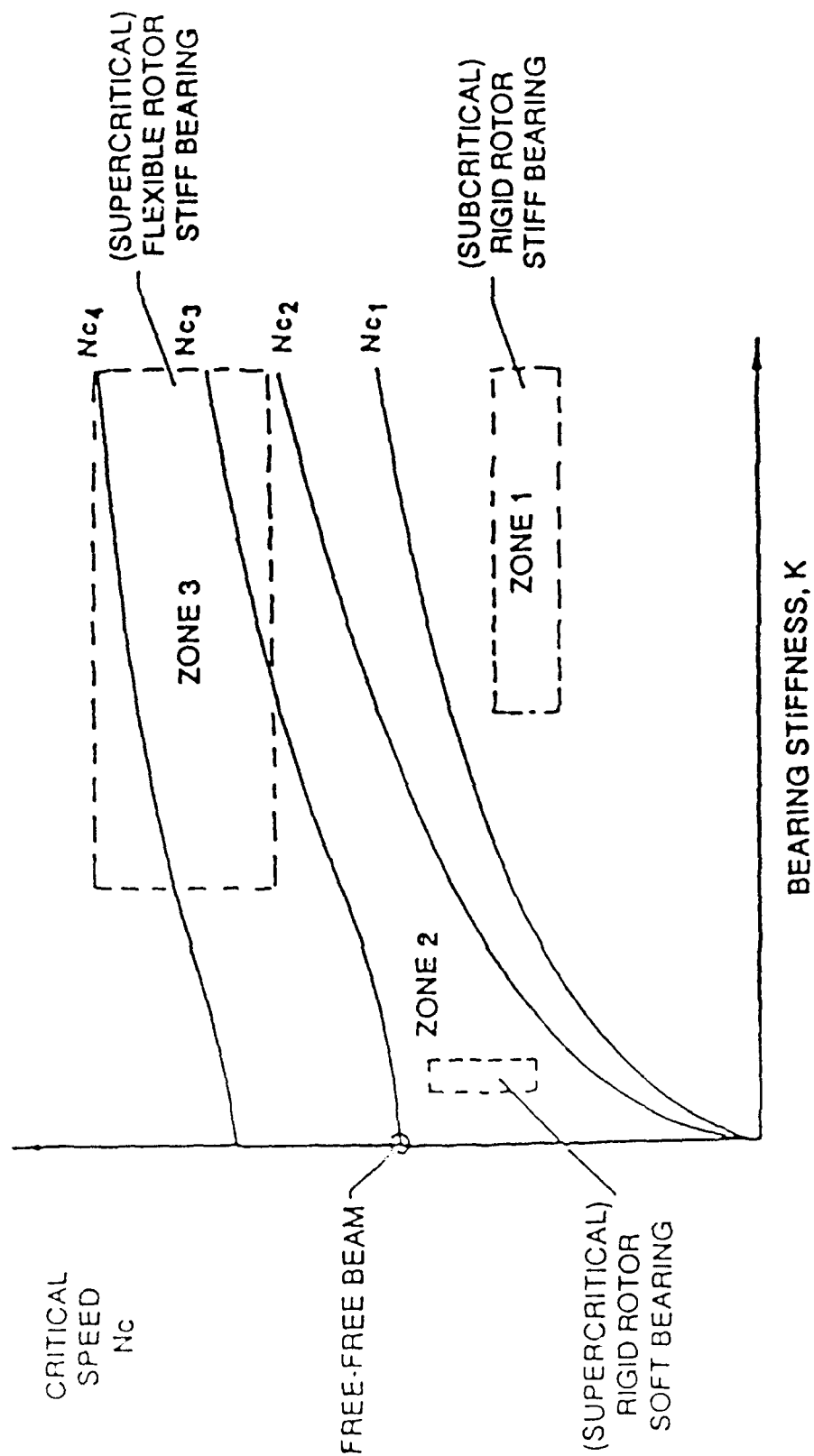


Figure 2.2-2. Critical Speed Operating Zones

2.0, Design, cont.

2.3 MATERIALS SELECTION

The success of the oxygen TPA design is directly dependent on the selection of materials that can be exposed to high pressure and, in the turbine section, high temperature oxygen over many hours of high speed operation without ignition or mechanical degradation due to oxide formation. This is a significant design challenge. Oxygen is a common material; so much a part of life that its reactivity in high concentrations and at high temperatures nearly always surprises people without a scientific background. The success of the propulsion industry in handling large quantities of liquid oxygen with few problems is a reflection of the great investment of engineering time and design experience, and should not be taken to mean that working with pure oxygen is a simple task. There are hardly any processes or established operations that use hot oxygen due to its well-proven hazards. The Aerojet and the NASA LeRC engineering staffs were well aware of this and also recognized that the compatibility of various structural materials with pure oxygen was not well established. Tasks B.1 and B.5 of contract NAS 3-23772 were funded by NASA LeRC to investigate both theoretical aspects of materials reaction with oxygen and the kind of sample testing that could characterize reaction under particle impact and material rubbing in oxygen. The reports on these tasks are given in the References 1-5. The discussion that follows makes use of the information developed in Tasks B.1 and B.5 and related work at the White Sands Test Facility (WSTF). The results of the materials selection are shown in Figures 2.3-1 and 2.3-2. Figure 2.3-1 shows the TPA in its configuration for the bearing tests reported in this volume. Figure 2.3-2 shows the TPA in the completed configuration for full function and testing as a turbopump.

2.3.1 Materials Ignition in Oxygen

In order for ignition to occur three things are required; a fuel, an oxidizer and an ignition source. The turbopump material or other particles that enter the system are the fuel and the ignition source is the energy contained in the high speed rotational parts and in the high velocity, high pressure oxygen. The present approach to the design/material selection is to remove as much of the energy contained in the fuel as possible and to preclude the conversion of kinetic and



2.3, Materials Selection, cont.

potential energy to concentrated thermal energy at local spots subject to rubbing or impact. The material physical properties of interest in oxygen applications are, therefore: heat of combustion, thermal conductivity or diffusivity, melting point, ignition temperatures, and plastic deformation under load at elevated temperatures. Information on some of these properties is given in Table 2.3-1 for various materials considered.

Materials that appear unreactive with oxygen at conditions of low temperature or low velocity contact can spontaneously ignite if a protective oxide layer is removed, if a high speed, high energy particle impacts the material, or if the material is rubbed against another material to generate frictional heating. Other factors of importance are the oxygen temperature and pressure. Of these, temperature is the most important as reaction rates essentially increase exponentially with increasing temperature. Contrary to expectations at the start of the oxygen/materials test program, the reactivity for some metals actually declines at very high pressures. This is shown graphically in Figure 2.3-3. The implication is that pump section operations at high oxygen pressure is no more hazardous than, say, a low pressure operation, especially if there is any cavitation. The significant environmental factors, then, are particle impact, materials rubbing, and temperature.

2.3.2 Particle Impact Ignition and Design Strategy

A hard, high speed particle impacting on a metal surface in pure oxygen has sufficient energy to start a local ignition. At that time the fire can be self-propagating or self-quenching, depending on impact energy, internal conditions, and, in particular, the material's thermal conductivity and resistance to oxidation. Figure 2.3-4 shows the effect of a calibrated particle impact on various structural materials with oxygen temperature as the variable. Note that zirconium copper, Nickel 200, Monel 400, and , Monel K-500 either did not ignite at all or were self-quenching. In contrast, the 316 stainless steel alloy ignites over a wide range of temperatures. This kind of test data was used in the oxygen TPA material selection, but another design strategy was to reduce stream velocities as low as practical and to make all flow passage directional changes gradual so that any particles entrained in the flowing oxygen would have lower impact energies. This strategy could not be

Table 2.3-1.
Materials Selection Matrix

Alloy	Composition	Burn Factor	Strength, ksi 800°R	Ductile/Brittle Transition Temperature	Oxidation** Resistance	Coefficient Expansion*	Typical Use and Reason
Silver	99 Ag	2	8	None	Fair	10.9	Bearings low friction
Nickel 201	99 Ni	550	11A	None	Good	8.5	Not in common use low strength
Zr-Cu	99.8 Cu .2 Zr	35	45	None	Poor	18.4 (1200°R), TBD (140°R)	Not in common use
Monel 400	BAL Ni 31.5 Cu Mn 2	1390	40 to 100	None	Good	8.9 (1200°R), 6.1 (140°R)	Fire brakes not in common use
Monel K-500	BAL Ni 29.5 Cu 2.7 Al .6 Ti	2090	105	None	Good	8.5 (1200°R), 6.2 (140°R)	Fire brakes when higher strength is required
Duranickel 301	95 Ni 4.4 Al .6 Ti	2900	120	None	Good	N/A	Not in common use
CRES 316	BAL Fe 17 Cr 12 Ni 3 Mo	4515	33	None	Good	9.3 (1200°R), 7.2 (140°R)	Low cost structural material
Invar	64 Fe 36 Ni	5444	N/A	None	Poor	3.5 (1200°R), .9 (140°R)	Low expander coefficient
Hastalloy X	BAL Ni 22 Cr 18 Fe 9 Mo	7160	50	None	Excellent	8.3 (1200°R)	Oxidation resistant
CRES 440	BAL Fe 17 Cr 2 Mn/Si	2783	55	0°F	Good	11 (1200°R)	Bearings, wear resistance
Graphite	Carbon	5156	-	None	Poor	.2 (800°F), .1 (-320°F)	
SiC	-	1145	-	None	Good	.6 (800°F), .5 (-320°F)	Bearings low friction
Inc 600	76 Ni 8 Fe 15 Cr	3226	80	None	Good	8.5	
Inc 718	52 Ni 18 Fe 19 Cr 8 TA MoCb	4600	147	None	Good	7.8	Structural housing high strength

As determined by Gluzek, et al B.F. = $\frac{\Delta H_f}{\text{Therm Diff.}}$ for 100g samples
Typical Fty (ksi)

*10⁻⁶ in./in./°F
**Est. for 4000 psi oxygen at 1200°R
N/A - Not Available

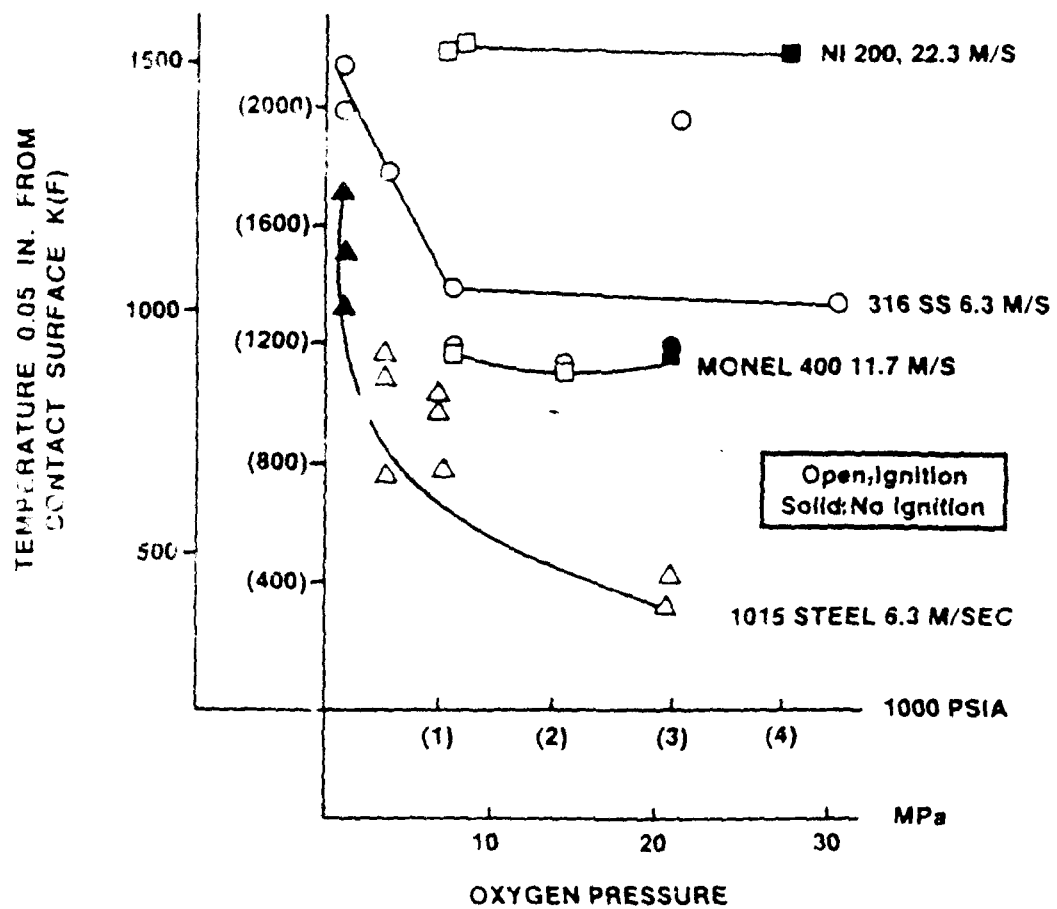


Figure 2.3-3. Effect of O₂ Pressure on Ignition Temperature

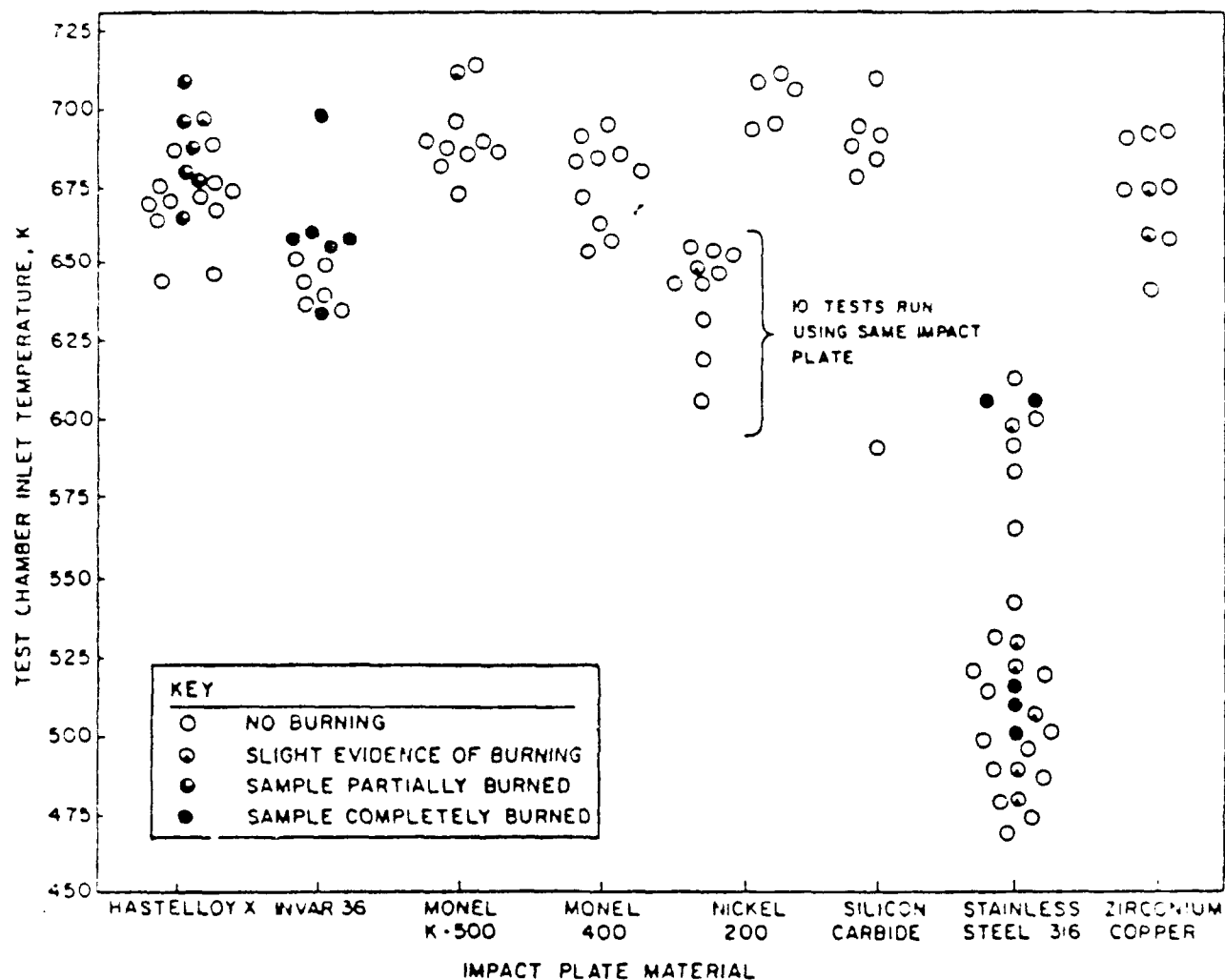


Figure 2.3-4. Results of Particle Impact Tests on Impact Plates

2.3, Materials Selection, cont.

used in the design of the turbine inlet without seriously reducing the efficiency. A two-stage turbine was considered to improve efficiency with lower turbine inlet velocity, but the final design stayed with a high velocity single turbine stage. The turbine section is highly dependent on materials selection for safe operation with some particle impingement. This is of reduced concern if the TPA inlet oxygen is filtered to remove most particulates. The regeneratively cooled nozzle design baseline includes a filter in the inlet manifold to prevent particles from clogging the nozzle coolant channels. Each valve will also have an inlet filter so that the turbine drive oxygen will have been filtered two or three times prior to entering the TPA.

2.3.3 Rubbing Contact Induced Ignition

The rotating elements of a turbopump will always have some point in the operating cycle where there is contact with a bearing surface despite the use of a "non-contact" hydrostatic bearing. For the Aerojet oxygen TPA this is during startup and shutdown. A rubbing start is expected and materials were selected to accommodate it. Tests in Series D and E demonstrated rubbing starts without ignition. Testing under the materials/oxygen compatibility tests actually forced a rotating material in contact with a fixed material at various rotation speeds and contact forces and at various oxygen pressures. Figure 2.3-5 plots the effect of oxygen pressure on the heating rate of Monel 400. Note that at lower pressures the monel will ignite after a fairly lengthy rubbing time as the surface temperature exceeds 1000°F. At 3000 psia the monel did not ignite. An appropriate design strategy to make use of this data would be to geometrically fix the first possible rubbing surface within the high pressure pump section so that initial contact would be with a non-ignitable material. Silver plate is used in the LOX TPA for all initial bearing contact surfaces. Gold is used for the turbine shroud ring. Figure 2.3-6 is a similar plot but includes other materials. Note that the threshold for ignition of carbon steel and 316 stainless is appreciably lower than for Monel 400.

The effect of varying the loading force at various oxygen pressures is shown in Figure 2.3-7. Despite high loading forces the Monel 400 was very resistant to ignition, and at 3000 psia did not ignite at the maximum load in the tester. The

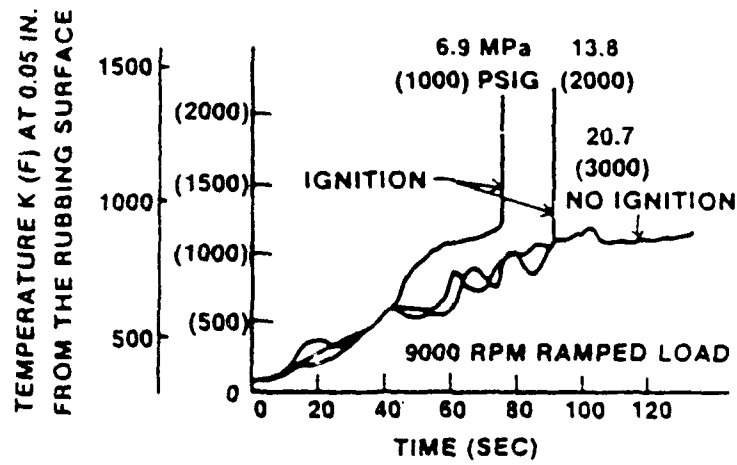


Figure 2.3-5. Effect of O₂ Pressure on Heating rates of Monel 400

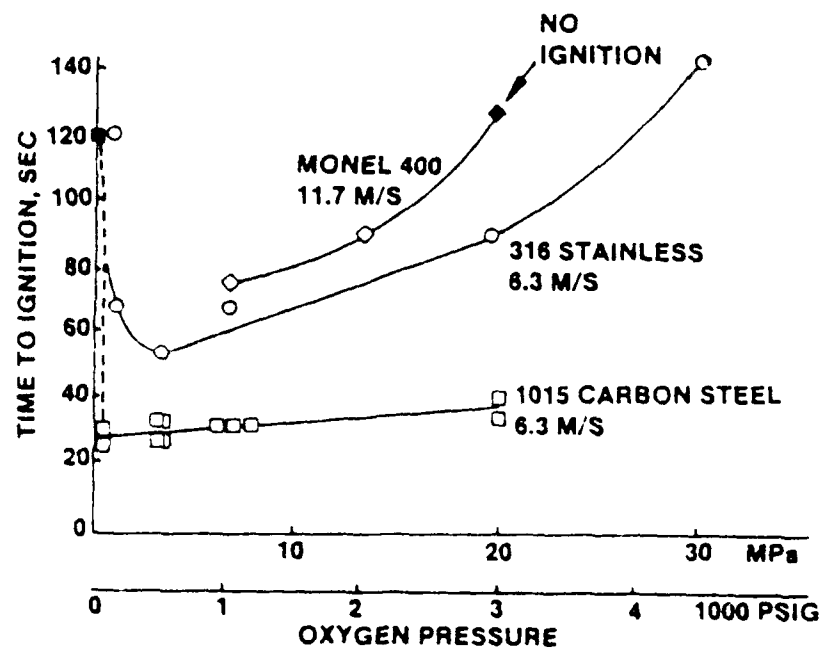


Figure 2.3-6. Time to Ignition vs. Oxygen Pressure

2.3, Materials Selection, cont.

good performance of the 316 stainless steel is attributed to the high chrome content and a smooth, galling resistant surface. These favorable properties of chromium were exploited by using a polished electroless chrome surface on the rotating assembly which would contact a yielding silver surface on rubbing.

Rubbing contact generates heat in a limited area. If not rapidly conducted away the material will either yield or ignite. The factor of heat generation per unit area was assessed for six materials under constant contact forces but with varying oxygen pressures. The results are given Figure 2.3-8 Reference 5.

A significant variable in assessing the hazards of rubbing friction is the force that pushes the materials together. A second important variable is the velocity of the rotating element. The compatibility work found a means of combining these two variables in a pressure-velocity product that was correlated with the metal heat of combustion. The results of this work are given in Figure 2.3-9. An important result of this correlation is the identification of several materials as more resistive to ignition than the heat of combustion would imply if taken alone. In particular the alloy Inconel 600 is identified as a likely high strength candidate for this application. The monels were good but not outstanding according to this correlation.

2.3.4 Burn Factor and Materials Selection Matrix

The oxygen/materials compatibility work attempted to develop a screening method that would identify the best materials for oxygen service. The factors used were thermal diffusivity and heat of combustion. The result is a "burn factor" that can be calculated for nearly any material. The results of this approach are presented in Figure 2.3-10. It is of some use as a screening aid, but the correlation does not appear to be so strong that a material can be used without further testing. Of more help are plots relating structural strength to temperature for alloys already deemed suitable for oxygen service (See Figure 2.3-11). A materials selection matrix can then be developed using these screening aids.

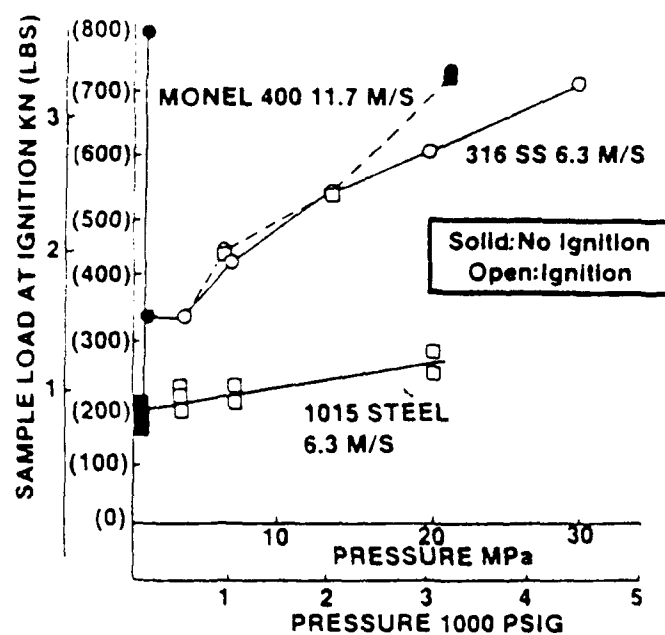


Figure 2.3-7. Load at Ignition vs Oxygen Pressure

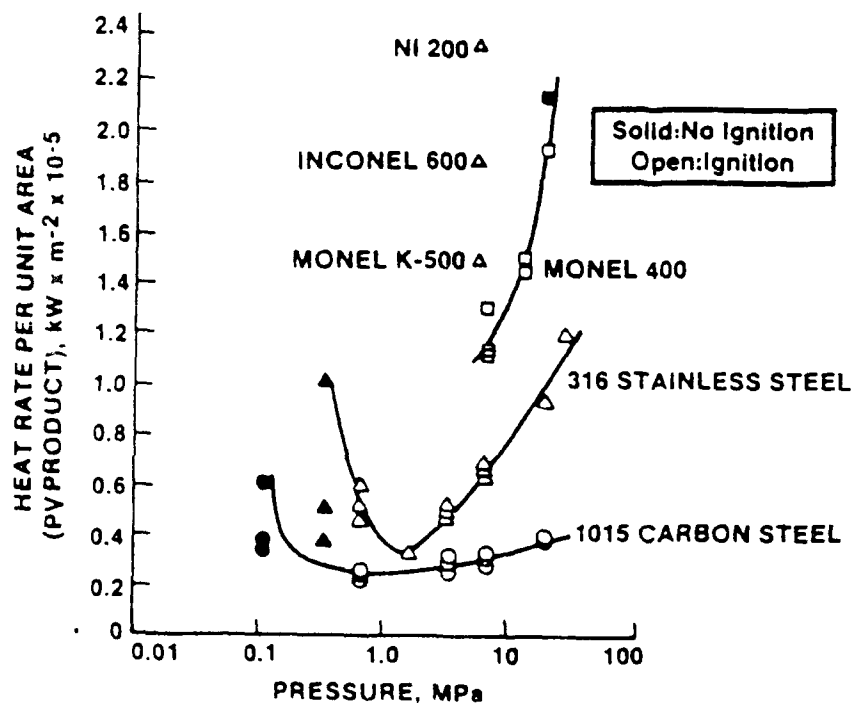


Figure 2.3-8. Heat Rate per Unit Area Required for Ignition vs. O₂ Pressure

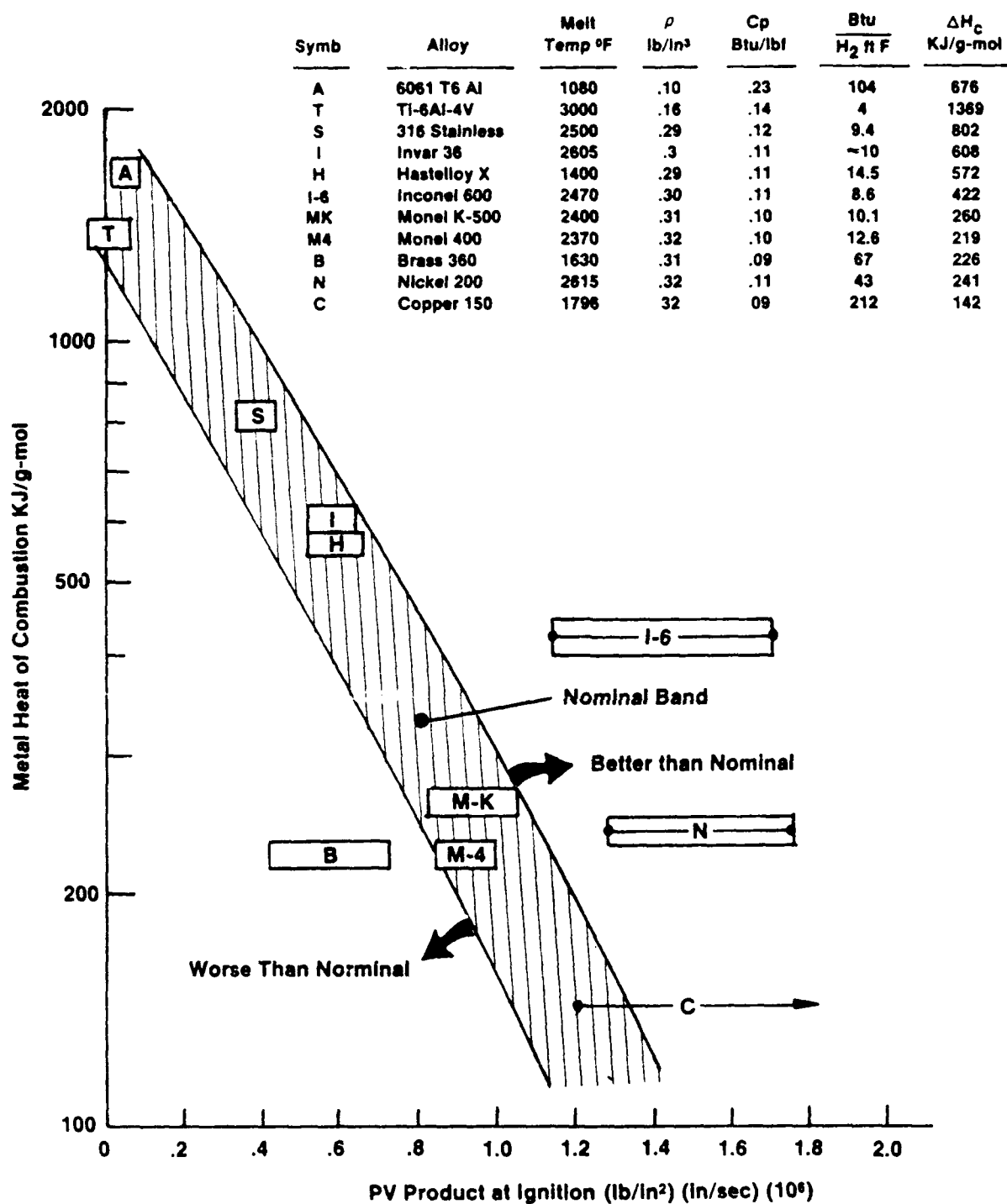


Figure 2.3-9. Correlation of Heat of Combustion with PV Product for Metal Ignition

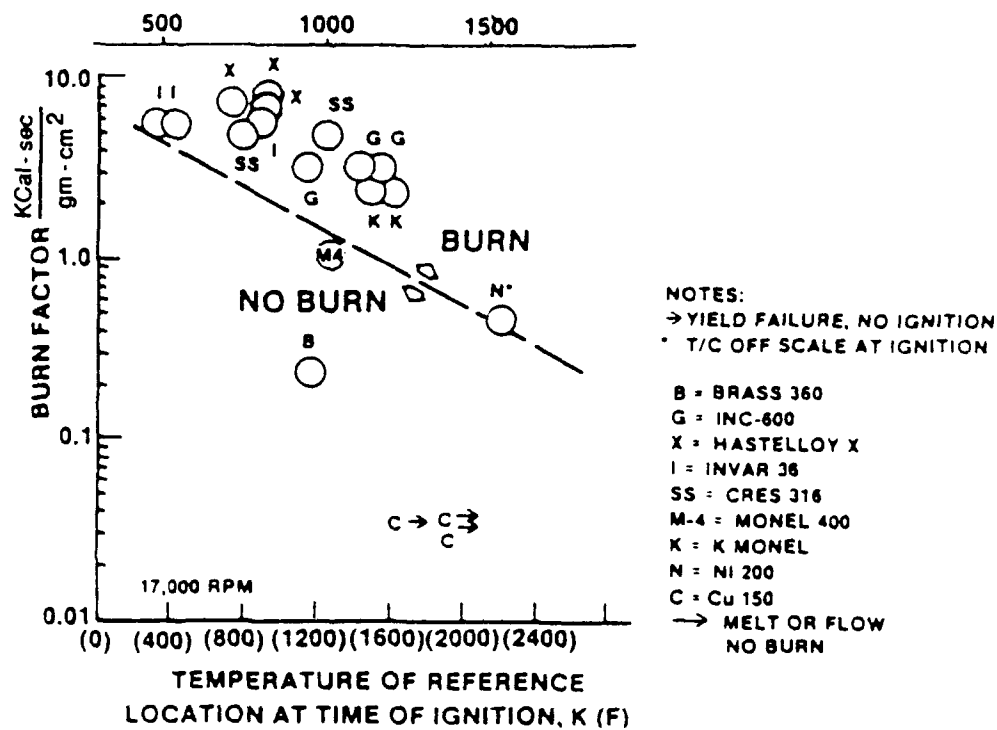


Figure 2.3-10. Burn Factor vs. Ignition Temperature in 6.9 MPa (1000 psi) O₂

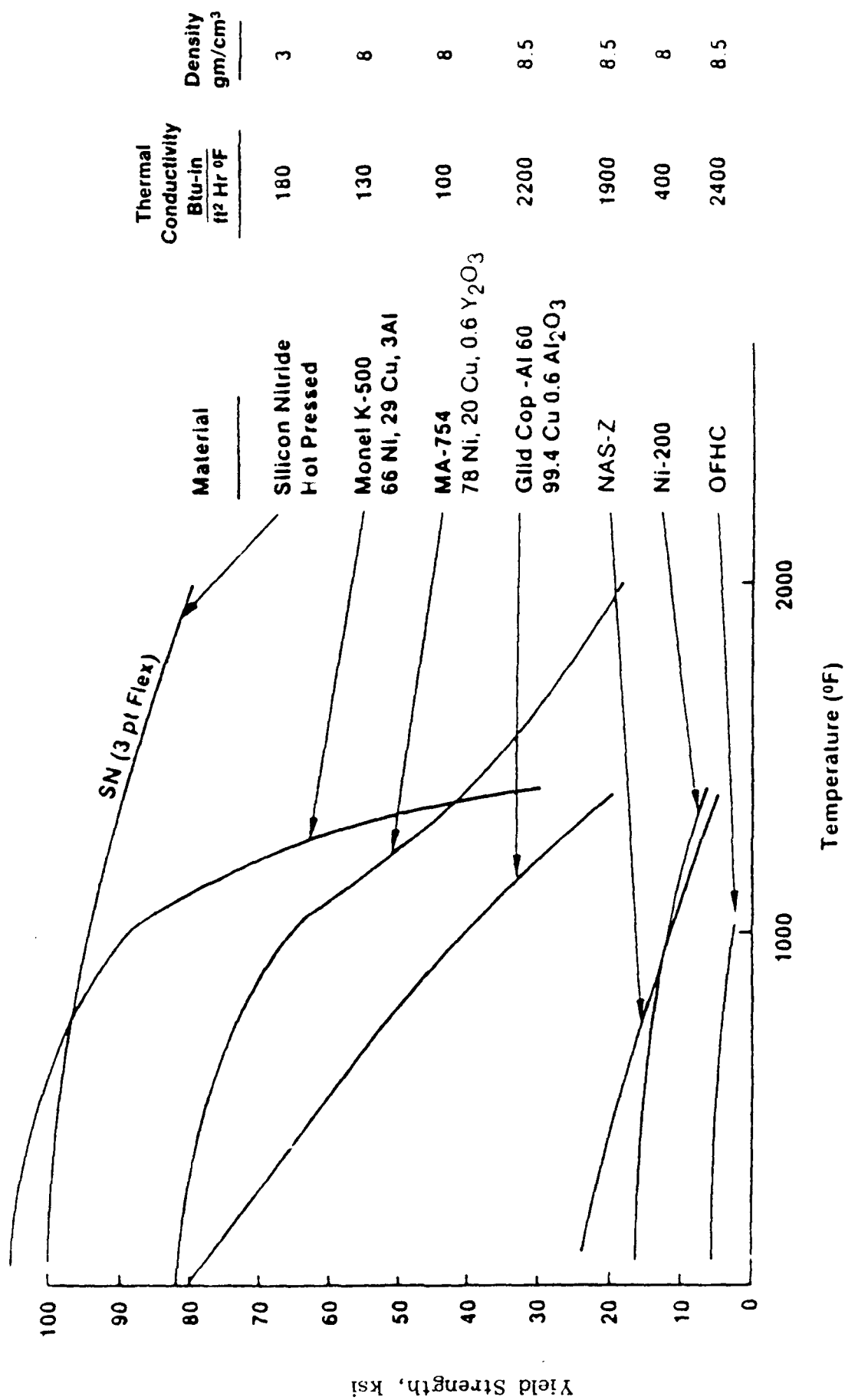


Figure 2.3-11. Structural and Thermal Properties of Materials for Use in Oxygen

2.3, Materials Selection, cont.

2.3.5 Final Materials Selection

Materials such as Inconel 600 were considered excellent candidates for structural materials, but final selection was of materials available within program schedule and budget. The result was a TPA using Monel 400 and Monel K-500 as the principal structural materials. Rotating assembly bearing surfaces were coated with electroless chrome. Stationary bearing surfaces were silver plated. Other materials selections are as indicated in Figure 2.3-1 and 2.3-2.

2.4 DESIGN BASELINE

2.4.1 Power Balance Results

An expander cycle requires a careful balancing of component pressures, temperatures, and power requirements for successful operation. In contrast, a gas generator cycle can compensate for a variety of component performance shortcomings by simply increasing the gas generator output. A new expander cycle design starts with such engine requirements as thrust, mixture ratio, and specific impulse. An engine cycle schematic is developed and preliminary component pressure drops, operating temperatures, and efficiencies are calculated. These preliminary values are then used for an overall engine energy balance. This is commonly called a power balance as the most critical variable over the engine operating range is the turbopump power requirement. For a dual expander engine cycle the balance has some additional complexity as the hydrogen and oxygen circuits are separate and both must balance over the entire range. An input parameter in a computerized power balance is the engine chamber pressure at rated thrust. For the OTV engine this was chosen as 2000 psia. A 20:1 throttling range would then yield a low thrust chamber pressure of 100 psia. This was considered a practical minimum for the chamber thermal design as well as for turbopump operation. A balance was attained at 2000 psia but the engine also had to balance at low pressure with the same components. A graphical representation of the low pressure power balance is given in Figure 2.4-1 for a 150 psia chamber pressure at a 13:1 throttling range. The intent is to show the interaction of various component performance curves and engine control effectiveness. Note that at very low thrust the baseline turbine bypass

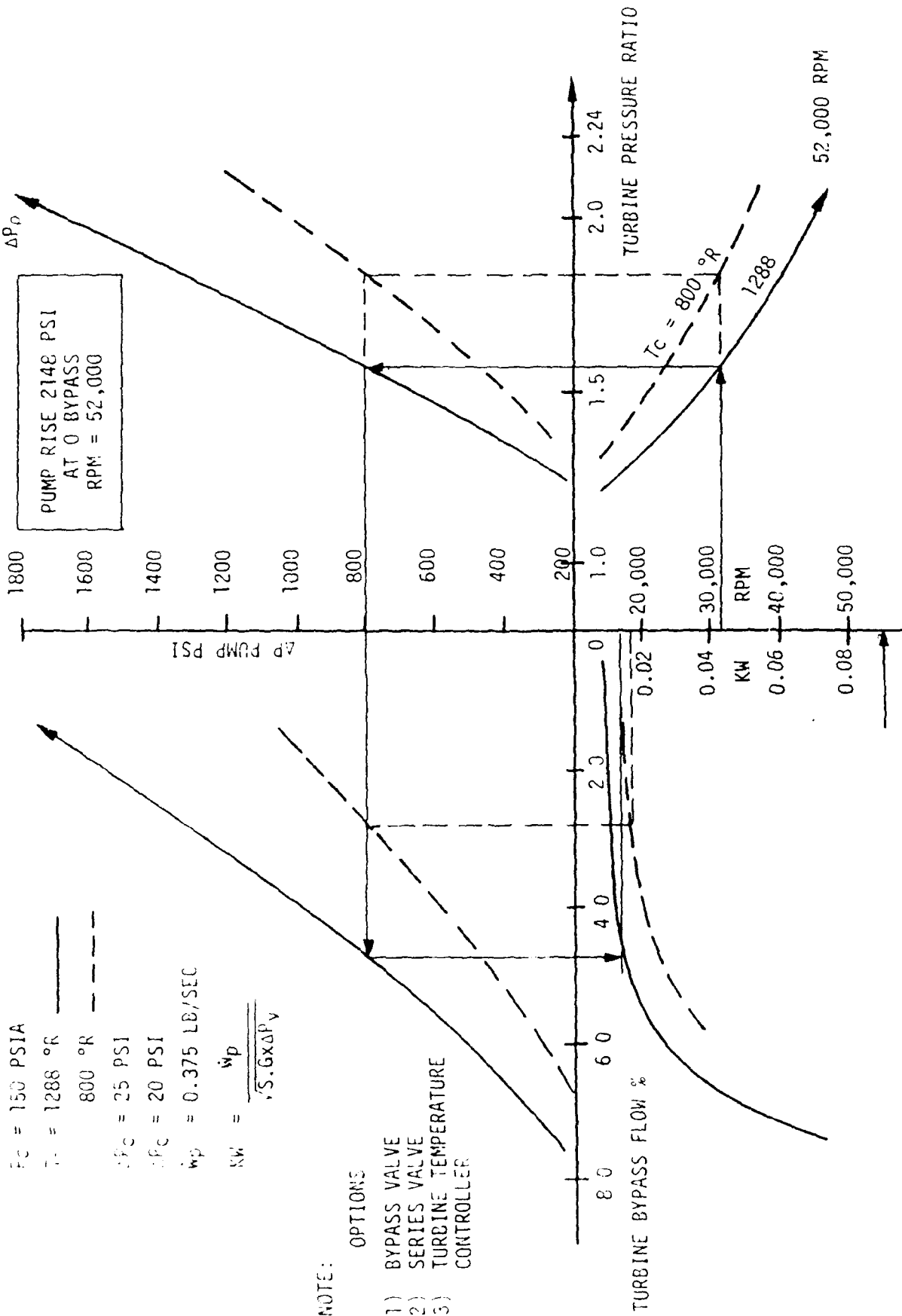


Figure 2.4-1. O₂ Turbopump Power Balance Options at Minimum Thrust

2.4, Design Baseline, cont.

control curve flattens to the point that bypass control is ineffective. At the same conditions the TPA speed has dropped below 10,000 rpm. A 10:1 throttling range is practical. A 20:1 range may be impossible using the selected component design point in this example. Trade studies were done for several TPA configurations until power balance results indicated that a near optimum design point had been selected.

The engine power balance at the maximum thrust point of 3000 lbf was performed assuming the following:

$$\Delta P_c = 300 \text{ psi}$$

$$\Delta P_i = 300 \text{ psi}$$

$$T_o = 800, 850, 900^\circ\text{R}$$

$$\dot{W}_p / \dot{W}_T = 1.1$$

These assumed values were used in the equation:

$$P_c = \left\langle \frac{\Delta P_p - \Delta P_c}{PR_T} \right\rangle - \Delta P_i \quad (1)$$

where P_c = Chamber pressure, psia

$$\Delta P_p = \text{Pump Pressure Rise, psid}$$

$$\Delta P_c = \text{Cooling System Pressure Drop, psid}$$

$$\Delta P_i = \text{Injector Pressure Drop, psid}$$

$$PR_T = \text{Turbine Total Pressure Ratio}$$

2.4, Design Baseline, cont.

The turbopump power balance is:

$$PR_T = \left[1 - \frac{\Delta P_P \frac{\dot{W}_P}{\dot{W}_T}}{J P_P C_p T_0 \eta_T \eta_P \eta_m} \right]^{\frac{\gamma-1}{\gamma}} \quad (2)$$

where \dot{W}_P = Pump flow Rate, lb/sec

\dot{W}_T = Turbine Flow Rate, lb/sec

P_P = Propellant Density = 72.4 lb/ft³

C_p = Gas Specific Heat = 0.22 Btu/lb °R

γ = Ratio of Specific Heats = 1.4

T_0 = Turbine Inlet Total Temperature, °R

η_T = Turbine Efficiency

η_P = Pump Efficiency

η_m = Mechanical Efficiency

J = Mechanical Equivalent of Heat = 778.26 ft. lb/Btu

Preliminary turbine analysis and the IR&D pump test data indicated the following efficiencies to be achievable:

$$\eta_T = 0.70$$

$$\eta_P = 0.65$$

$$\eta_m = 0.90$$

2.4, Design Baseline, cont.

$$\text{or } \bar{\eta} = \eta_T \eta_p \eta_m = 0.41$$

Substituting the assumed values into equations (1) and (2):

$$P_c = \frac{\Delta P_p - 300}{PR_T} - 300 \quad (3)$$

$$PR_T = \left[1 - 0.031 \frac{\Delta P_p}{T_o} \right]^{3.5} \quad (4)$$

The plot of Equations (3) and (4) is shown in Figure 2.4-2. It indicates a very strong effect of turbine inlet temperature on the TPA power balance and the achievable engine chamber pressure.

2.4.2 Design Point and Predicted Performance

The power balance results and TPA design programs were used to develop a TPA design point that would meet the engine requirements. This is given in Table 2.4-1. This assumes a two-stage pump with an inducer section. The inducer design point is given in Table 2.4-2. Some explanation for the first and second stage pump design point values are given in Tables 2.4-3 and 2.4-4. With the design point chosen, pump predicted performance curves could be generated. These curves are given as Figure 2.4-3 and 2.4-4 for the individual stages and for the combined pump output, respectively.

The turbine section design point is:

Flowrate	\dot{W}_p	= 5.5 lbm
Pressure Rise	ΔP_p	= 4600 psid
Inlet Total Pressure,	P_o	= 4315 psia
Inlet Total Temperature,	T_o	= 860°R

O₂ Turbopump

$\eta_T/\rho/\eta_m = 0.41$
 $\Delta P_C, \Delta P_I = 300 \text{ psi}$
 $\dot{W}_p/\dot{W}_T = 1.1$

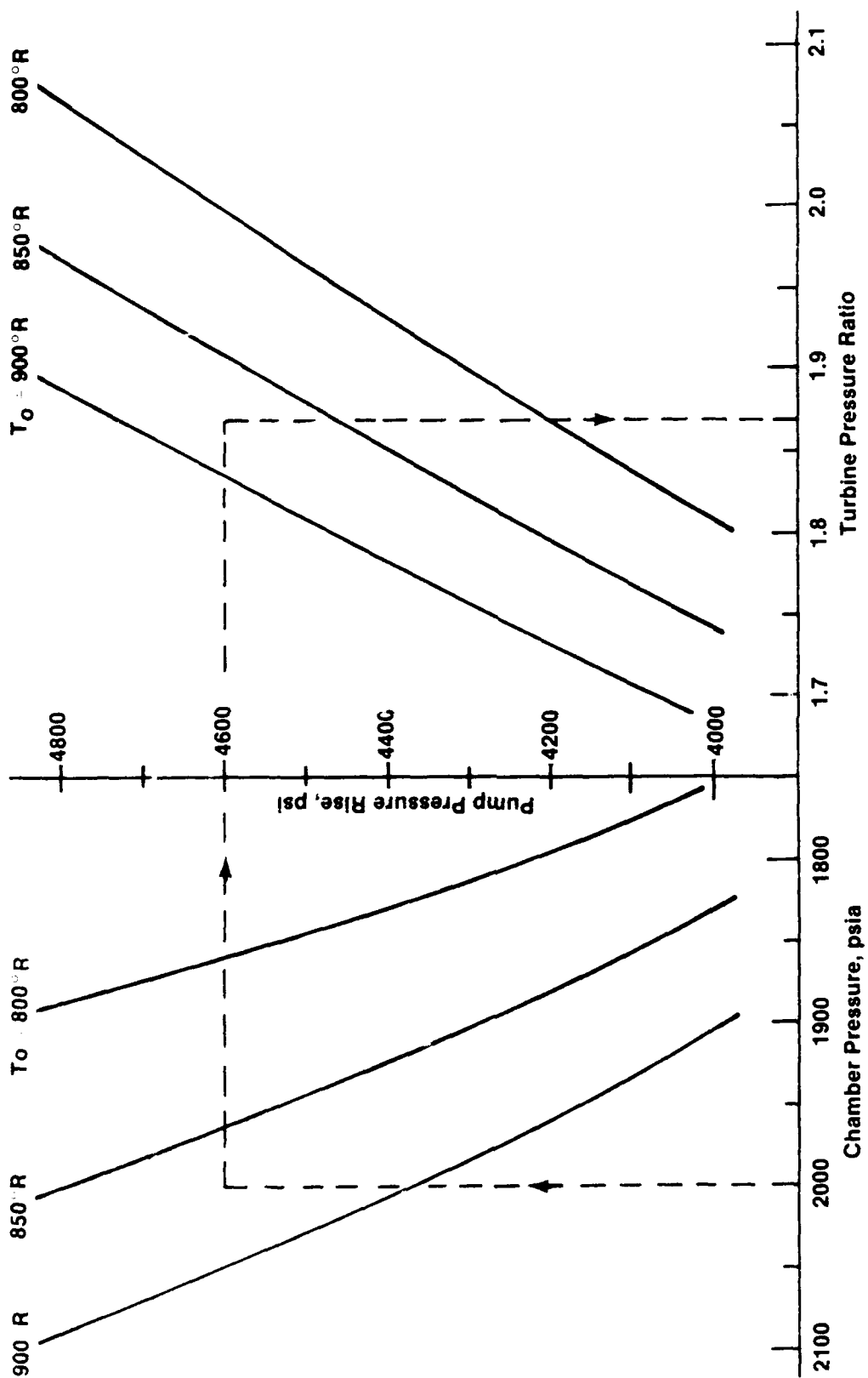


Figure 2.4-2. Power Balance at Maximum Thrust

Table 2.4-1.
OTV LOX Pump Design Point

	BOOST PUMP	HIGH PRESSURE PUMP
NUMBER OF STAGES	1	2
WEIGHT FLOW, LB/SEC	5.5	5.5
VOLUME FLOW RATE - INDUCER, GPM	-	51.4
VOLUME FLOW RATE - IMPELLERS, GPM	34.1	34.1
SUCTION PRESSURE - PSIA	15.0	54.6
DISCHARGE PRESSURE - PSIA	54.6	4654.6
INDUCER HEAD RISE - FT	-	525
HEAD RISE PER STAGE - FT	80.	4575
SPEED, RPM	12,700	75,000
STAGE SPECIFIC SPEED	2,772	787
IMPELLER DISCHARGE DIAMETER - IN.	1.41	1.615
IMPELLER DISCHARGE PORT WIDTH - IN.	.097	0.0774
EFFICIENCY, STAGE ALONE %	65.0	65.
NET POSITIVE SUCTION HEAD - FT	0 (TSH=4.3 FT)	80
SUCTION SPECIFIC SPEED	24,800	20,100

**Table 2.4-2
Inducer Design**

REQUIREMENTS

$$Q = 51.4 \text{ GPM}$$

$$\Delta H = 525 \text{ FT}$$

$$N = 75,000$$

$$\text{NPSH} = 80$$

$$\text{SUCTION SPECIFIC SPEED} = 20,100$$

PROCEDURE

USE SPACECRAFT OXIDIZER INDUCER TO SCALE

$$Q/ND^3 = 9 \times 10^{-4}$$

$$\Delta H/N^2D^2 = 6.85 \times 10^{-4}$$

RESULTS

$$\text{TIP DIAMETER} = 0.913 \text{ INCHES}$$

$$\text{INLET HUB DIAMETER} = 0.457 \text{ INCHES}$$

$$\text{DISCHARGE HUB DIAMETER} = 0.566 \text{ INCHES}$$

$$\text{TIP INCIDENCE TO BLADE ANGLE RATIO} = 0.4$$

$$\text{HEAD RISE} = 520 \text{ FT}$$

**Table 2.4-3.
OTV 1st Stage Pump**

- SCALE FROM IR&D WATER TESTED IMPELLER $N_s = 1050$
- $\frac{Q}{ND_1^3}$ IR&D = 9.8×10^{-4} AT MAXIMUM EFFICIENCY
- Q/N OTV = 4.55×10^{-4}
- D_1 OTV = 0.774 INCHES
- IR&D IMPELLER HAD LEAKAGE LOSS OF 12%
- OTV 1ST STAGE HAS NO LEAKAGE LOSS
- ADJUST D_1 TO GIVE 12% FLOW REDUCTION
 $D_1 = 0.695$ INCHES
- DISCHARGE DIAMETER SET TO GIVE $P = 2300$ PSI AT DESIGN POINT
 $D_T = 1.54$ INCHES
- PROVIDE 10% HEAD MARGIN
 $D_T = 1.615$ INCHES
- STAGE EFFICIENCY = 0.72

**Table 2.4-4.
OTV 2nd Stage Pump**

- SCALE FROM IR&D WATER TESTED IMPELLER $N_s = 1050$
- Q/ND_1^3 IR&D = 9.8×10^{-4}
- Q/N OTV = 4.55×10^{-4}
- D_1 OTV = 0.774 INCHES
- DISCHARGE DIAMETER SET TO GIVE $\Delta P = 2300$ PSI AT DESIGN POINT
 $D_T = 1.54$ INCHES
- PROVIDE 10% HEAD MARGIN
 $D_T = 1.615$ INCHES
- STAGE EFFICIENCY = 0.61

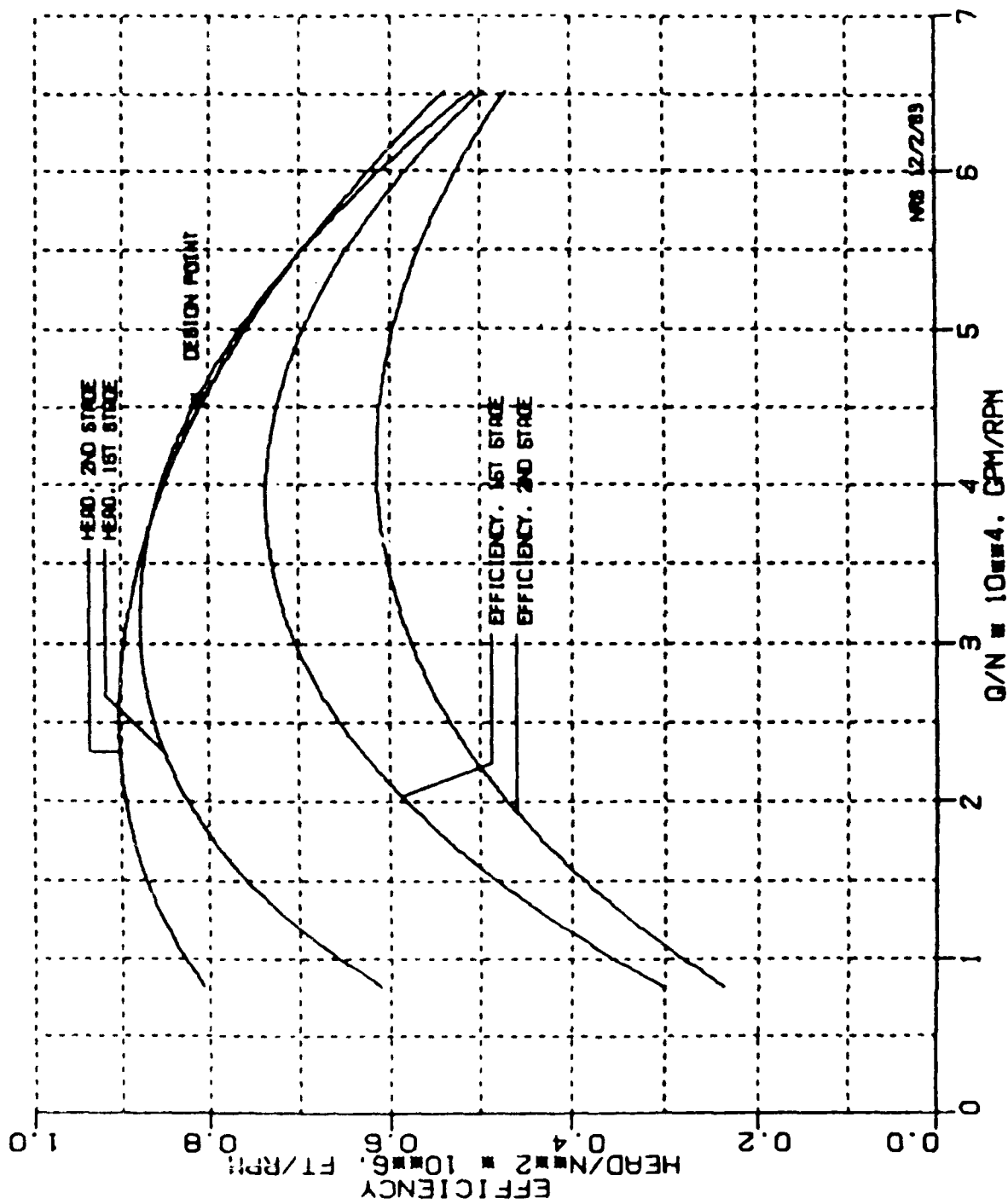


Figure 2.4-3. Predicted OTV Stage Performance

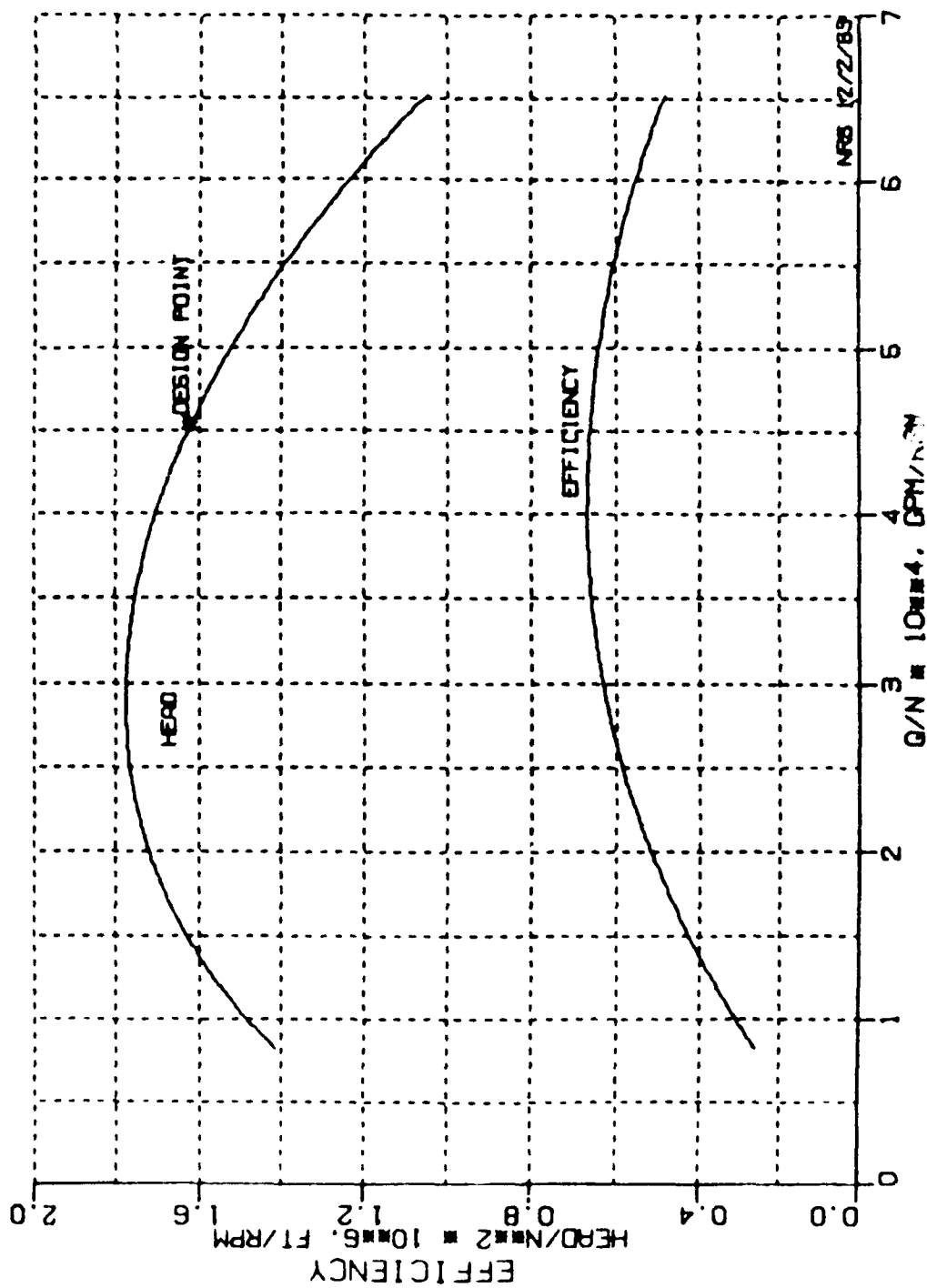


Figure 2.4-4. Predicted OTV Combined Stage Performance

2.4, Design Baseline, cont.

Exit Total Pressure,	P_{o2}	=	2300 psia
Specific Heat at Constant Pressure,	C_p	=	0.22 Btu/lb °R
Specific Heat Ratio	γ	=	1.4
Gas Constant,	R	=	48.29 ft lb/lb °R

2.0, Design, cont.

2.5 DETAIL DESIGN

This section includes results of the various trade studies References 8 & 9 conducted to complete the preliminary design. Actual configurations presented are those at the completion of the detailed design.

2.5.1 Bearing and Seal Design

Design Features and Parameters — The shaft, bearing, and seal system selected after initial analysis and trade studies is shown in Figure 2.5-1. Various features and parts identifications are called out on the figure. This two piece shaft assembly having a high stiffness hydrostatic bearing was selected for subcritical operation at a peak shaft speed of 75,000 rpm. The first critical speed is calculated to be 115,000 rpm. The rotor lumped parameter system is shown in Figure 2.5-2 along with the first three mode shapes. Calculated bearing spring rate is between 0.3 and 0.6 lbf/in $\times 10^{-6}$. The resultant first critical (N_{C1}) speed is well above the 30% margin goal. The first three critical speeds are plotted in Figure 2.5-3 as a function of bearing radial stiffness.

The parameters for the bearing design are:

Lubricant	LO ₂
Shaft Speed	75,000 rpm
Journal Surface Speed	196 ft/sec
Thrust Bearing Surface Seal	530 ft/sec
Bearing Pressure Differential	2000 lbf/in ²

Rotor misalignment clearances with the selected bearing/seal combination are given in Figure 2.5-4. Thrust bearing nominal axial clearance is 0.0012 inch while turbine tip clearance is 0.005 inch.

Bearing Configuration — The pump is a two stage design with impellers arranged back to back. The first stage is outboard with the inlet concentric with the shaft axis, the second stage impeller is located at midspan with a radial flow

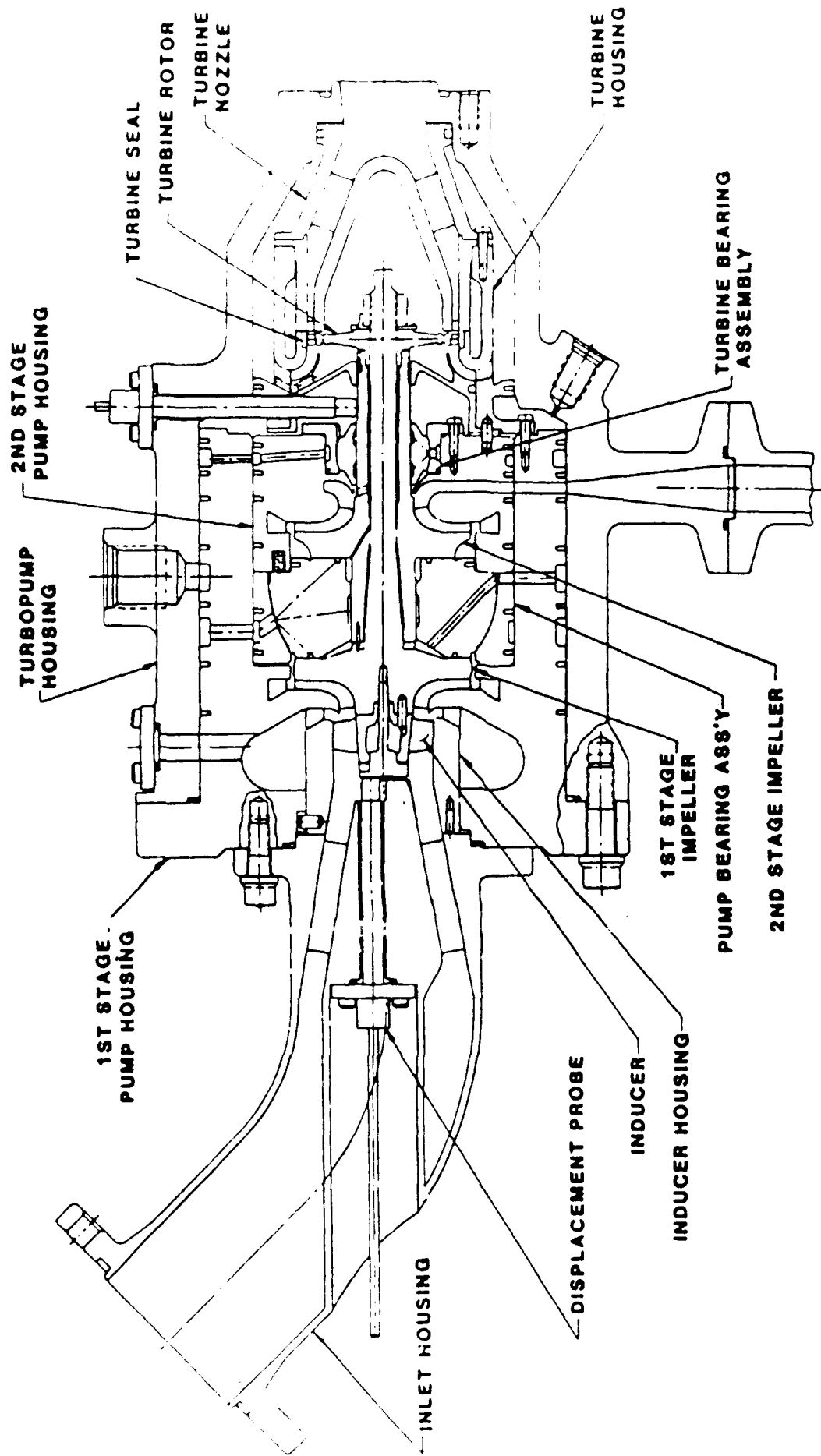
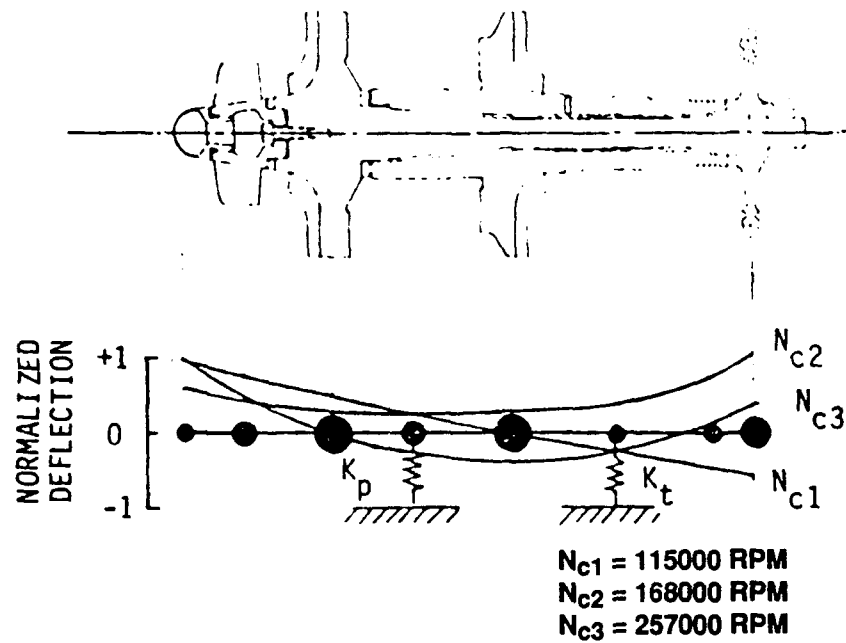


Figure 2.5-1 OTV Oxygen Turbopump Features Ease of Assembly



n	1	2	3	4	5	6	7	8
L (in)	.4	.6	.55	.68	.70	.68	.40	
R_o (in)	.2	.22	.3	.3	.27	.25	.225	
R_i (in)	.19	0	0	0	0	0	0	
W (lb)	.0085	.143			.149		.0375	
J (lb-in-sec ²)		-.000064			-.000056		-.000012	

Figure 2.5-2. Rotating Assembly Mass-Elastic System and Mode Shapes

Turbine Overhang 1.08 in.
 Bearing Span 1.38 in.
 Rotor Density = .319 lb/in.³

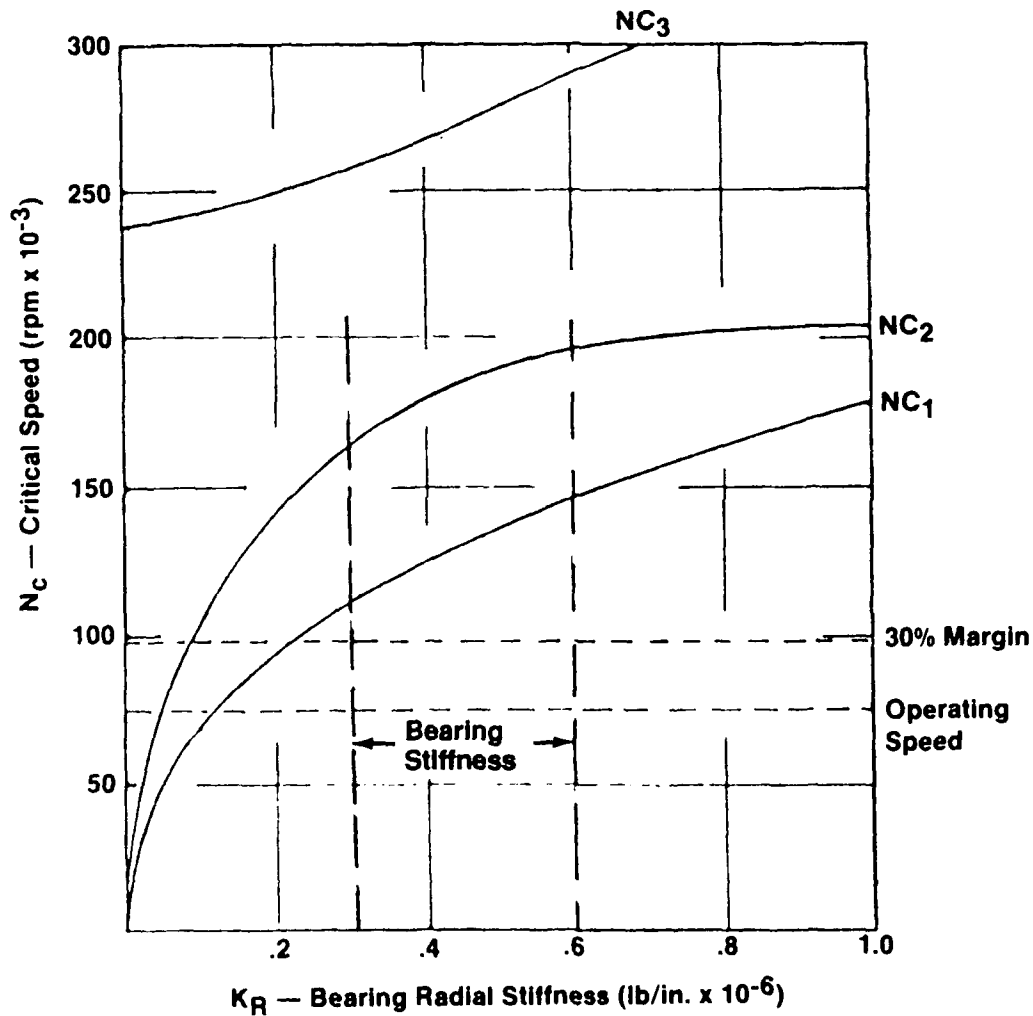


Figure 2.5-3. Critical Speed as a Function of Bearing Stiffness

DOTTED LINES REPRESENT MAXIMUM MISALIGNMENT POSITION WITHOUT THERMAL, HYDRAULIC OR MECHANICAL INDUCED DEFLECTION

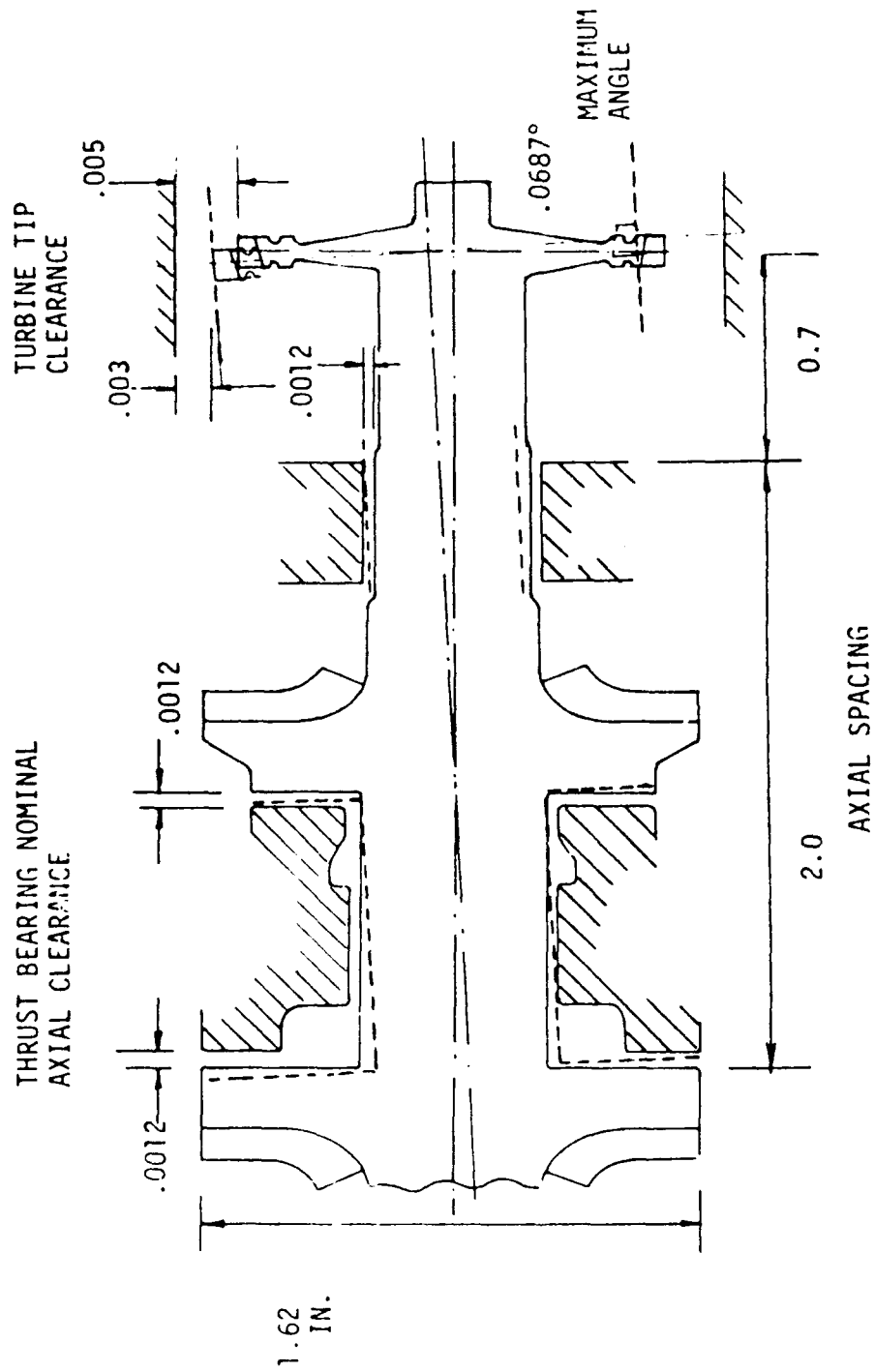


Figure 2.5-4. Rotor Maximum Misalignment

2.5, Detail Design, cont.

inlet. Between the impellers are the double acting hydrostatic thrust bearing and the hydrostatic journal bearing. This bearing assembly is supplied from the second stage pump discharge at 4600 lb/in² when the TPA is operating at 75,000 rpm. The turbine end journal bearing is directly in front of the second stage impeller inlet with an axial space outboard for thermal transition from the cryogenic bearing to the warm turbine. The overhung turbine is spaced at a maximum distance limited by critical speed and a length adequate for the temperature gradient. The pump bearing cartridge and the second stage pump diffuser housing are inserted into the pump discharge housing and are held mainly by hydraulic and aerodynamic pressures. A small set of bolts hold the internal pump assembly together prior to operation. Selective pressure balance causes the pump and turbine components to be loaded on the housing shoulder directly over the first stage impeller.

The rotating assembly loads are shown in Figures 2.5-5 and 2.5-6. Figure 2.5-5 shows the axial thrust situation indicating the high pressure area forces on the rotor and the variable load capacity of the double acting hydrostatic thrust bearing. Figure 2.5-6 gives a summary of radial and axial loads on the rotating assembly.

Thrust and Journal Bearing — The thrust and journal bearing shown in Figure 2.5-7 serves a multifunction purpose. This bearing supports load variation in both axial and radial directions, balances the steady axial thrust and acts as the impeller interstage seal. By combining the functions of bearing and seals into a common part, the maximum efficiency is achieved. Since the hydrostatic bearing operates at a very close clearance (~.001 in.), the parasitic leakage is lower than conventional wear ring seals. Also, the close clearance and orientation of the bearing controls the axial position very accurately and allows the operation of open impellers with close clearances. In order to operate bearings at a close clearance, the hydraulic, thermal, and mechanical deflections and tolerances must be controlled very accurately.

Two basic concepts are employed to achieve these goals. First, a fixed bearing design is used where very tight tolerances are maintained with minimal deviations. This concept requires precise machining of parts and minimal

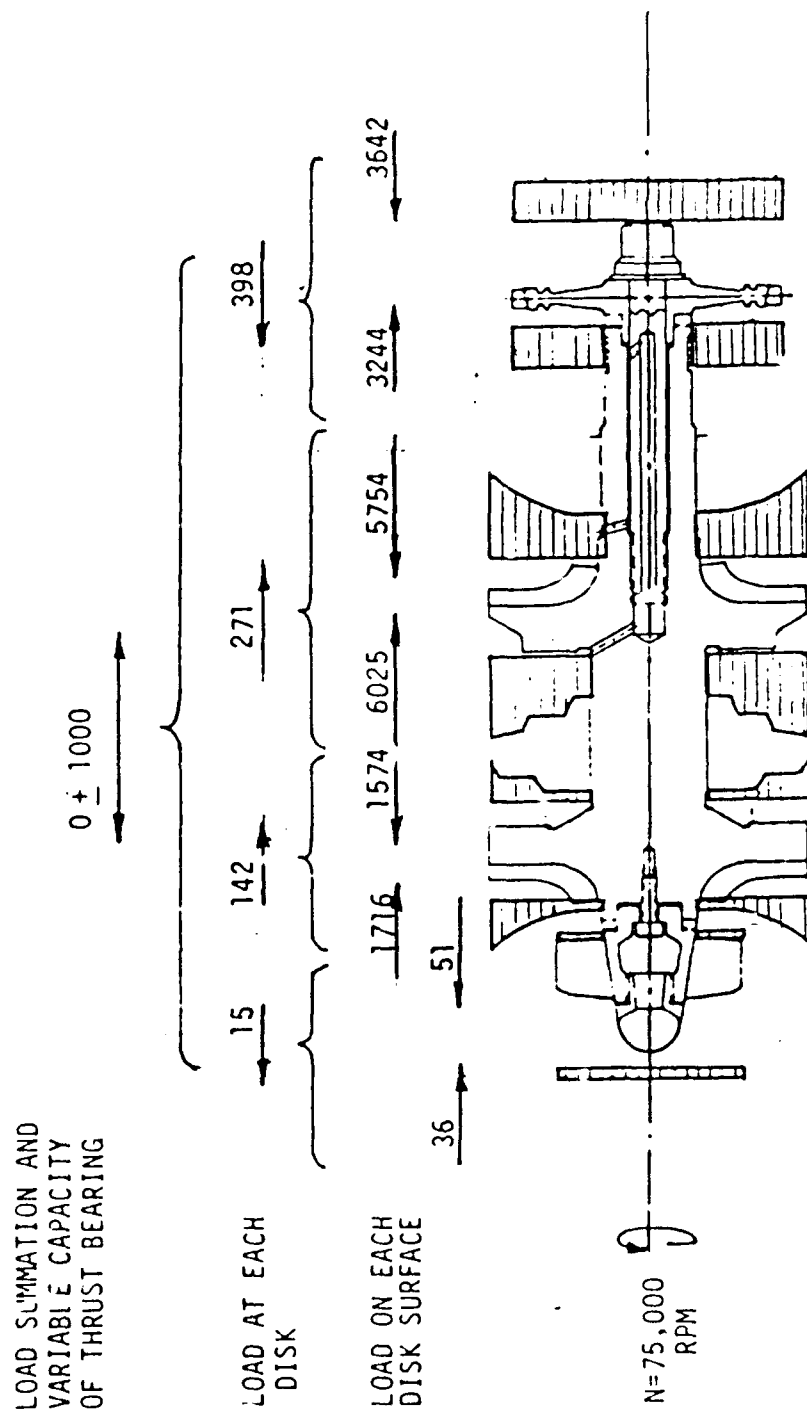


Figure 2.5-5. Rotor Axial Thrust

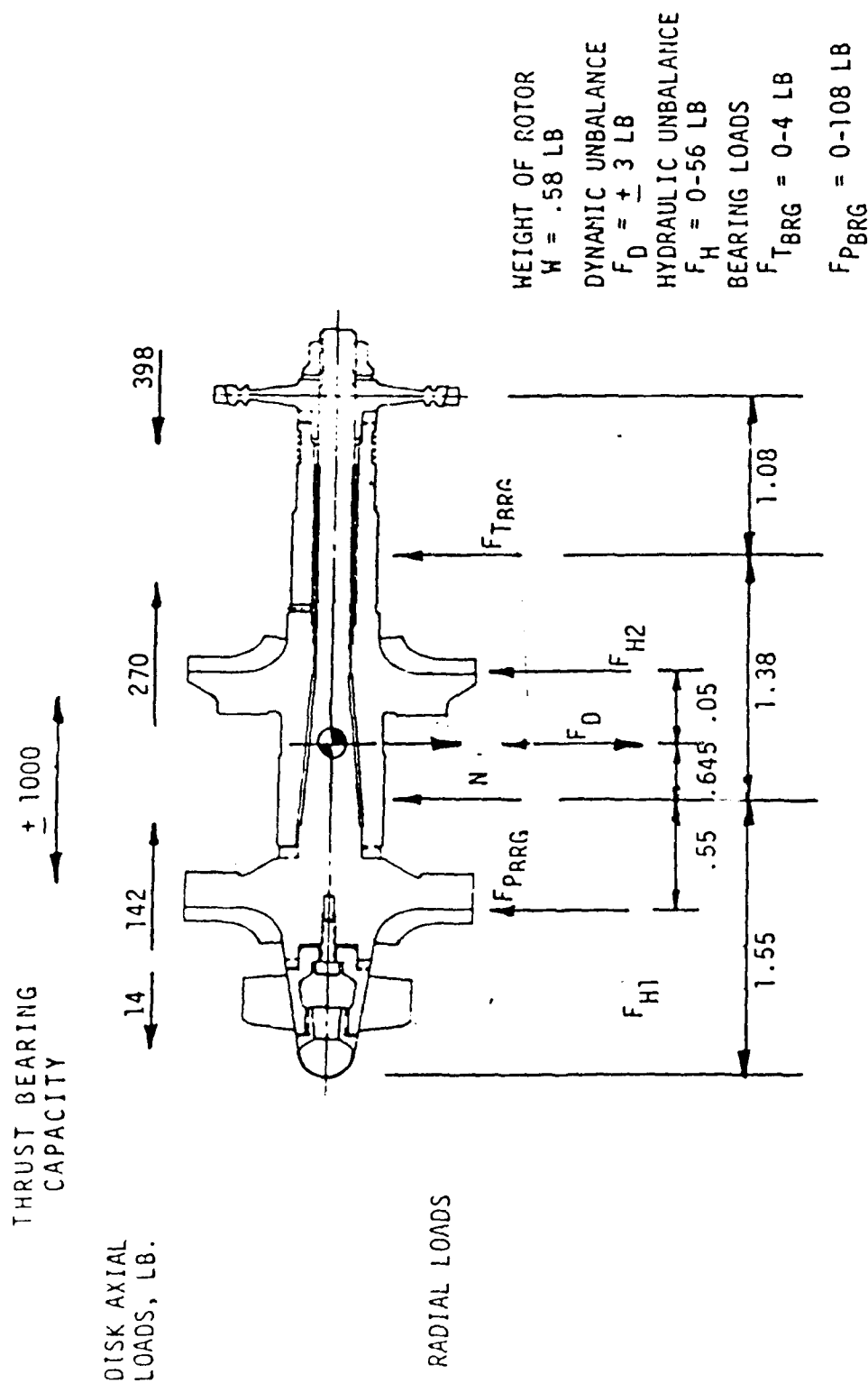


Figure 2.5-6. Summary of Rotor Loads

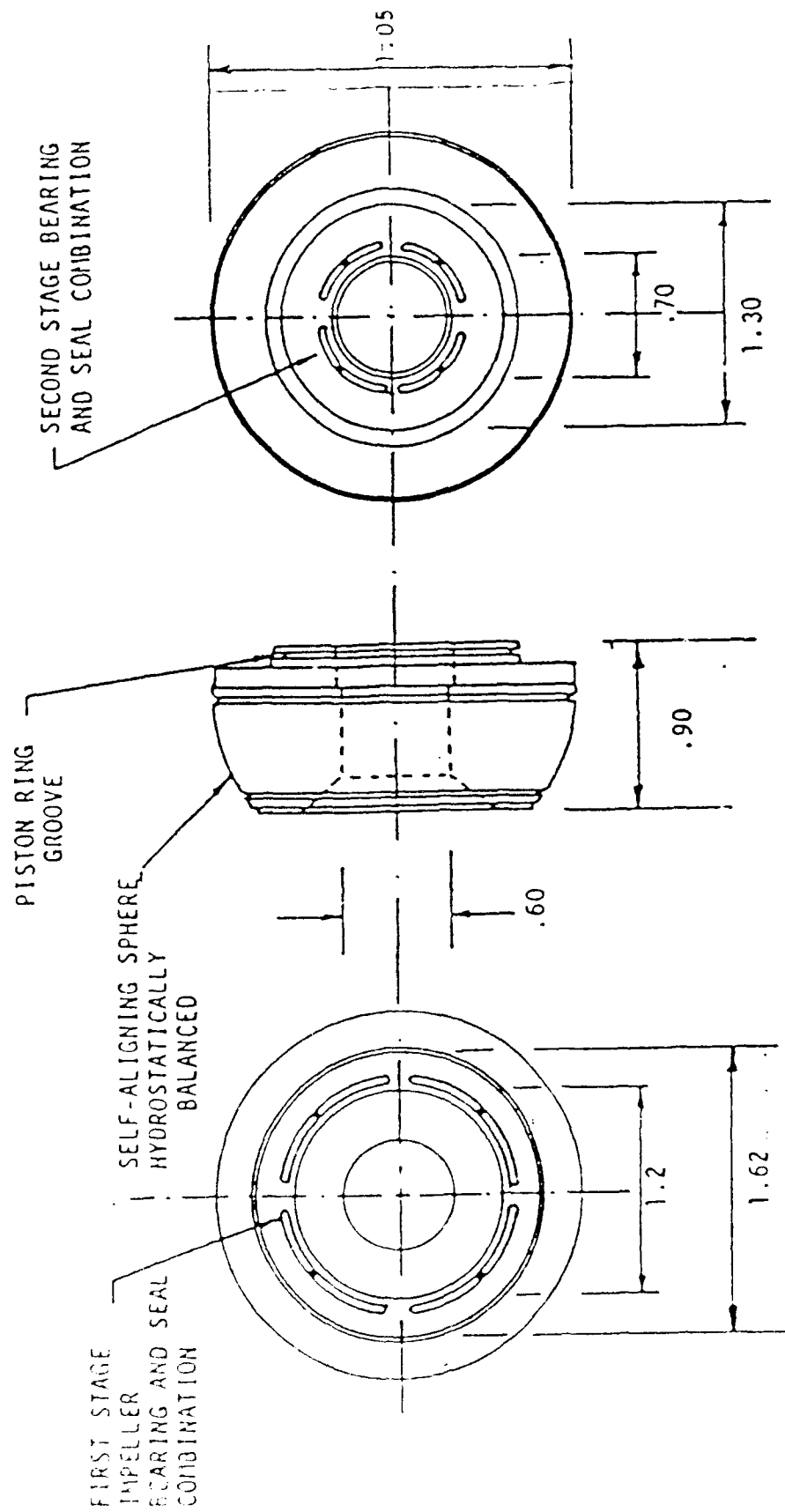


Figure 2.5-7. Pump End Hydrostatic Thrust and Journal Bearing

2.5, Detail Design, cont.

assembly error. The most sensitive area for contact is the thrust bearing. It will most likely be operating at less than .001 in. clearance and with the 1.62 in. dia. turbine wheel contact is possible. The second concept attempts to eliminate this potential by making the bearing self-aligning. By mounting the bearing in a spherical seat housing the effect of tolerances and deflections is eliminated. But the spherical seat must be lubricated to assure ease of alignment. The spherical seat is also a hydrostatic bearing operating at very close clearance ($\sim .000010$ in.). The bearing supply lines cross the sphere joint and the close clearance at these supply lines controls the leakage. A system of grooves on the surface of the sphere fed from the supply lines provide hydraulic compensation for varying axial loads. The clearance at the spherical surface is so small that the effect on radial and axial stiffness is insignificant. Due to the two stage pump arrangement the axial loads on the thrust bearing are always towards the first stage impeller from the second stage impeller. The only way for the load to reverse would be if the second stage impeller were to lose pressure while the first stage was still pressurized, a virtually impossible combination. This situation allows a hemispherical shaped bearing to be used. It is seated initially by three lightly loaded ground end coil springs which are located on a radial face towards the second stage impeller. The axial clearance at this face is controlled to approximately .002 in. to limit axial motion.

This .002 axial clearance allows sufficient self aligning motion and provides a safety feature for unforeseen axial loads. Directly below the coil springs is a pressure reducing piston ring. The cavity of the coil spring is vented to a low pressure (approximately 500 psi) return passage to the inducer discharge. This reduced pressure zone contributes to the axial thrust balance on the spherical bearing surface.

This double acting thrust bearing/seal combination mounted on back-to-back impellers is a unique arrangement. Normally a hydrostatic thrust bearing would be completely supplied and controlled with the inlet orifice. In that situation as the load is reduced and the bearing backs away from the running surface the maximum flowrate is controlled by the compensating orifice. In this situation the axial clearance is not too critical. The typical face seal rubbing contact, hydrodynamic or hydrostatic type, will have a fixed axial load either from hydraulic or

2.5, Detail Design, cont.

spring forces. In that situation the maximum flowrate is controlled by the design clearance at equilibrium balanced load. In the OTV TPA bearing/seal combination, this component must limit the flow and provide thrust bearing variable load capacity. Without the balanced fixed load to control maximum leakage the overall axial clearance of the double acting bearing is set low enough to restrict the maximum leakage to an acceptable level. This clearance is also set large enough to allow variable load compensation by the thrust bearing. This thrust bearing design is analogous to the journal bearing design. It is slightly more difficult to design but the combined function of bearing and seal in one component provide much lower parasitic losses while simplifying the TPA design.

Figures 2.5-8 through 2.5-17 show the performance for the pump end bearing assembly. Figures 2.5-8, 2.5-9, and 2.5-10 show the general characteristics of pressure differentials, surface speeds, and anticipated Reynolds numbers for the operating conditions. Figure 2.5-11 through 2.5-17 show the selected design performance and some of pertinent parametric analysis results. The pump end journal bearing performance shown in Figure 2.5-11 has excess radial load capacity as determined in the load summary and excess radial stiffness as determined from the critical speed requirements. The first stage thrust bearing/seal combination performance is shown in Figure 2.5-12 indicating the high axial load capacity and low flowrate. The following figure indicates the effect of orifice size on the flowrate as being minimal. The important feature controlling flowrate is the axial clearance. Similar characteristics for the second stage thrust bearing/seal combination are shown in the next three figures. As mentioned previously, the spherical outer surface of the bearing assembly is also a hydrostatic bearing to allow self alignment. The performance of this spherical bearing is shown in Figure 2.5-17.

Turbine End Journal Bearing — The turbine end bearing between the inlet of the second stage impeller and the exhaust side of the turbine serves as both a bearing providing radial support for the shaft and as a shaft seal. The turbine exhaust and the impeller inlet pressures are very close, both approximately 2300 lb/in². A pressure differential at this location is acceptable if necessary. The hydrostatic journal bearing is supplied from the second stage pump discharge and exits to both the

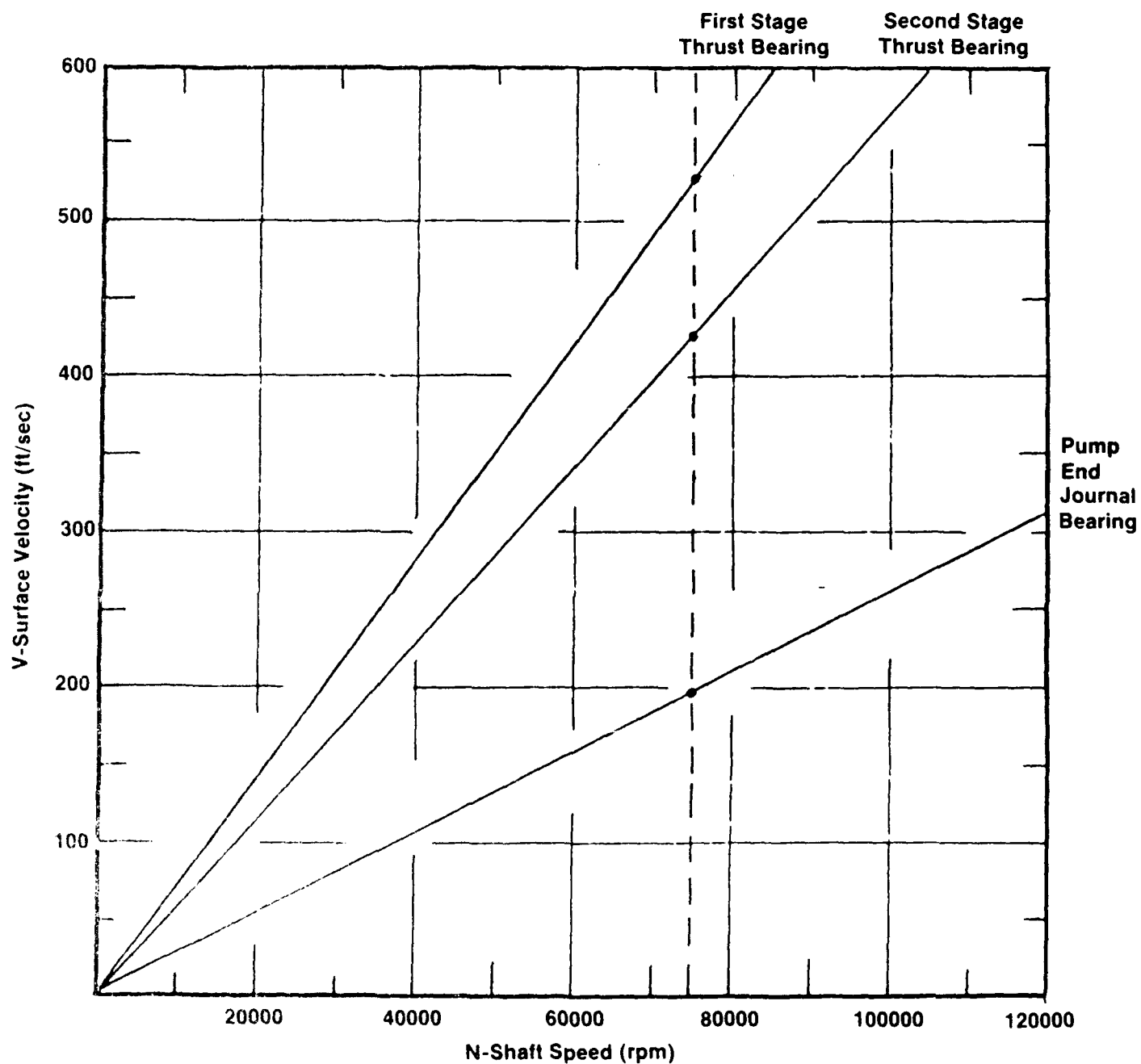
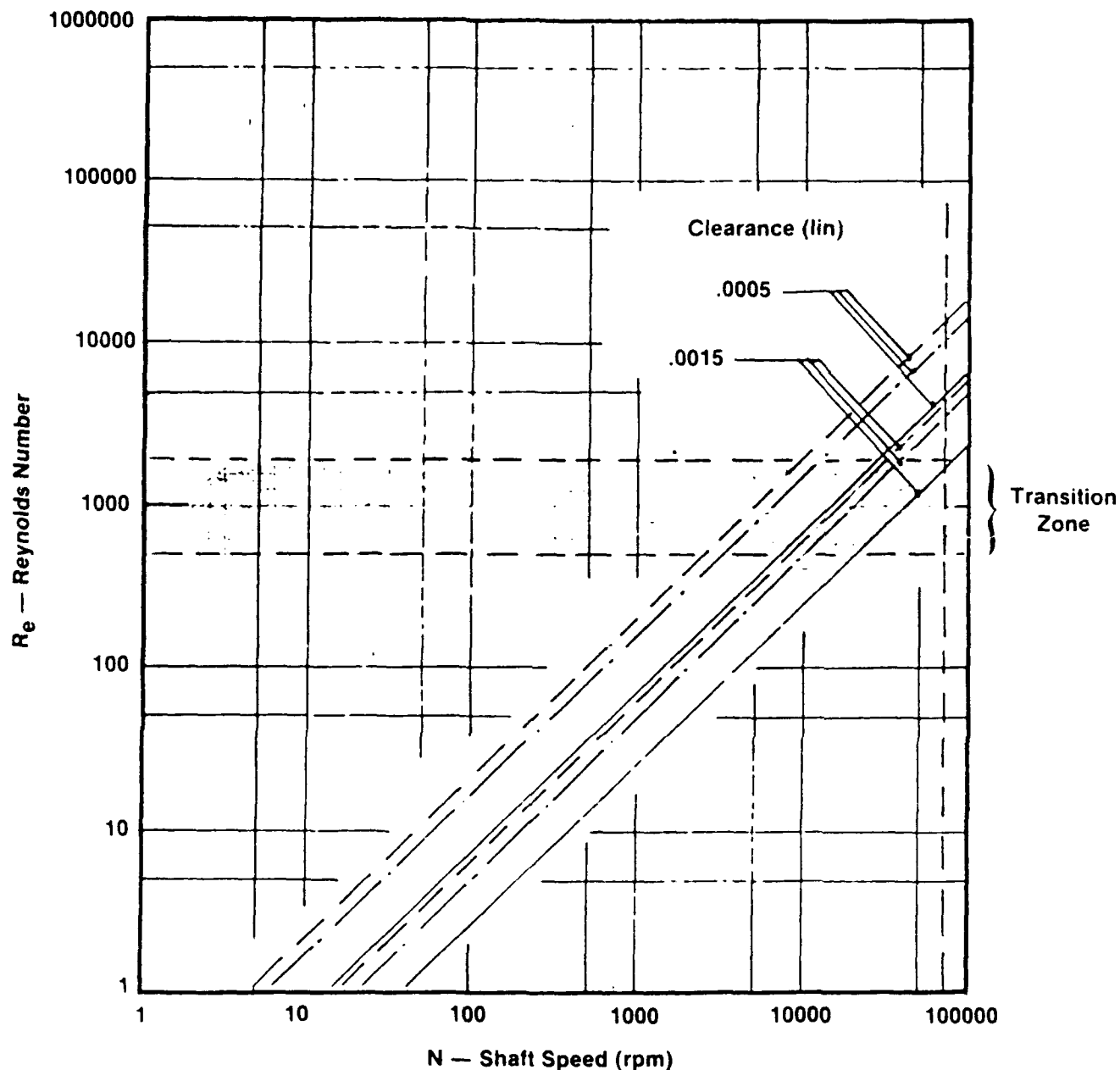


Figure 2.5-8. Bearing Surface Velocity as a Function of Shaft Speed



Notes:

1. Lubricant — LO₂

2. $Re = \frac{\rho V h}{\mu}$

3. $\rho = 1.1 \times 10^{-4} \text{ lb-sec}^2/\text{in}^4$

4. $\mu = 3.8 \times 10^{-8} \text{ lb-sec}/\text{in}^2$

5. $R_{JRNL} = .3 \text{ in.}$

6. $RT_1 = .81 \text{ in.}$

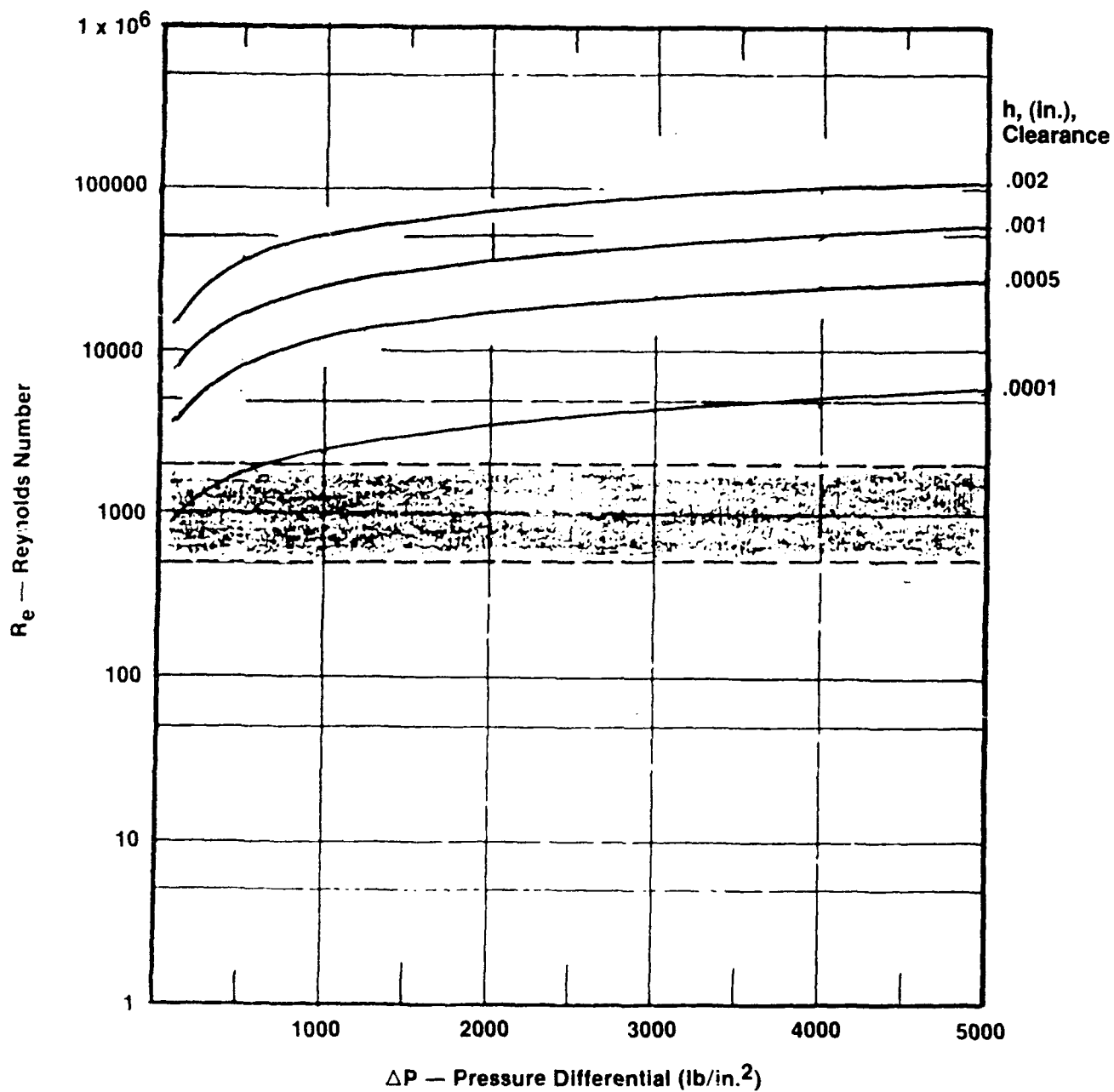
7. $RT_2 = .65 \text{ in.}$

8. R_{JRNL} = Radius of Pump
Journal Bearing (in.)

9. RT_1 = Radius of First Stage
Thrust Bearing

10. RT_2 = Radius of Second Stage
Thrust Bearing

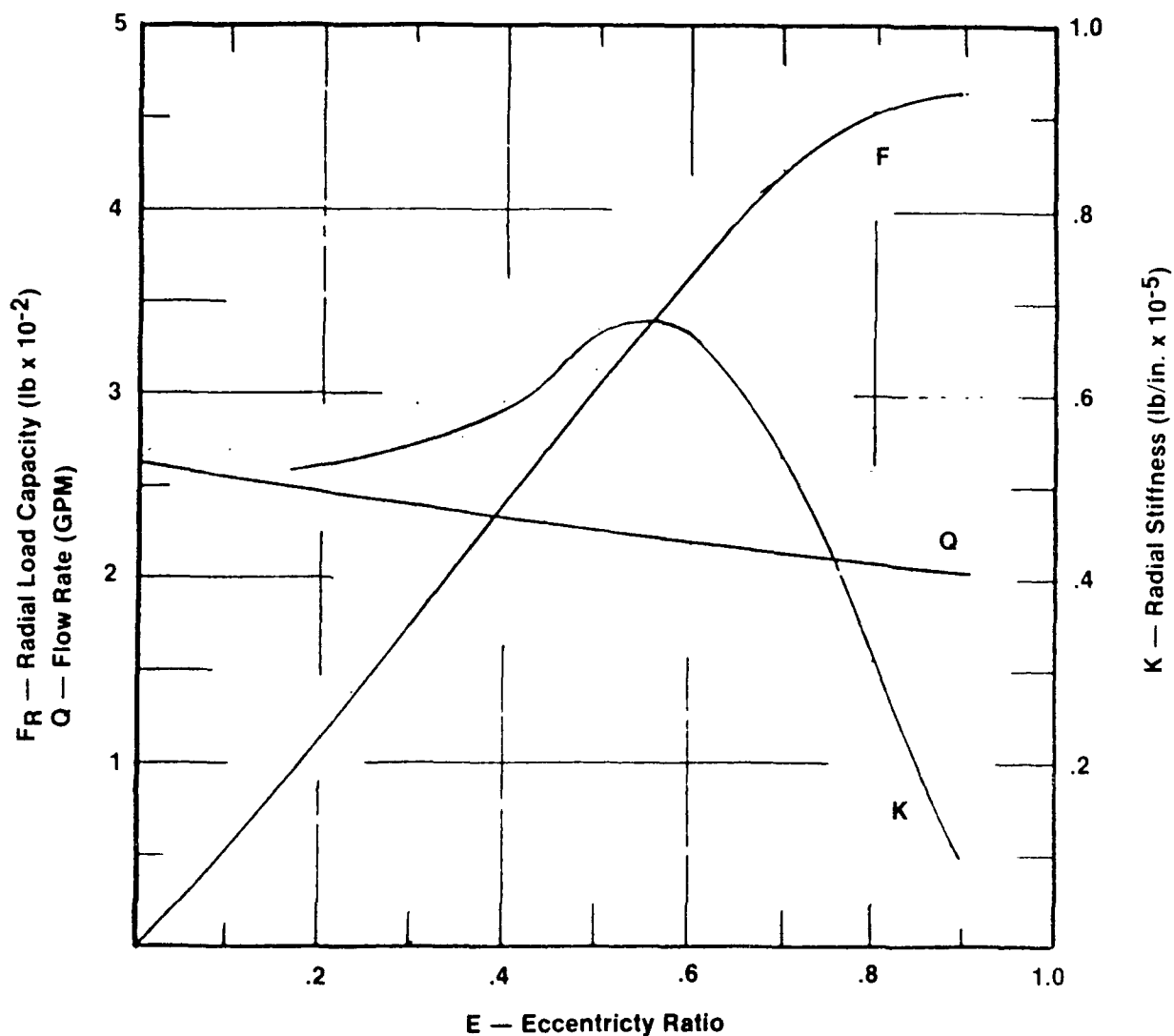
Figure 2.5-9. Fluid Film Reynolds Number Due to Shaft Rotation



Fluid — LO_2
 Density $\rho = 1.1 \times 10^{-4} \text{ lb-sec}^2/\text{in.}^2$
 Viscosity $\mu = 3.8 \times 10^{-8} \text{ lb-sec/in.}^4$

Pump End Journal Bearing

Figure 2.5-10. Reynolds Number Due to Pressure Induced Velocity



Bearing Radius, $R = .30$ in.

Bearing Length, $L = .4$ in.

Recess Width $.24$ in.

No. of Recesses, $N_4 = 4$

Orifice Dia, $D_o = .020$ in.

Shaft Speed, $N = 75000$ rpm

Radial Clearance, $C = .001$ in.

Supply Pressure, $P_s = 4600$ lb/in.²

Exit Pressure, $P_s = 500, 2100$ lbs/in.²

Lubricant — LO₂

Radius at Recesses

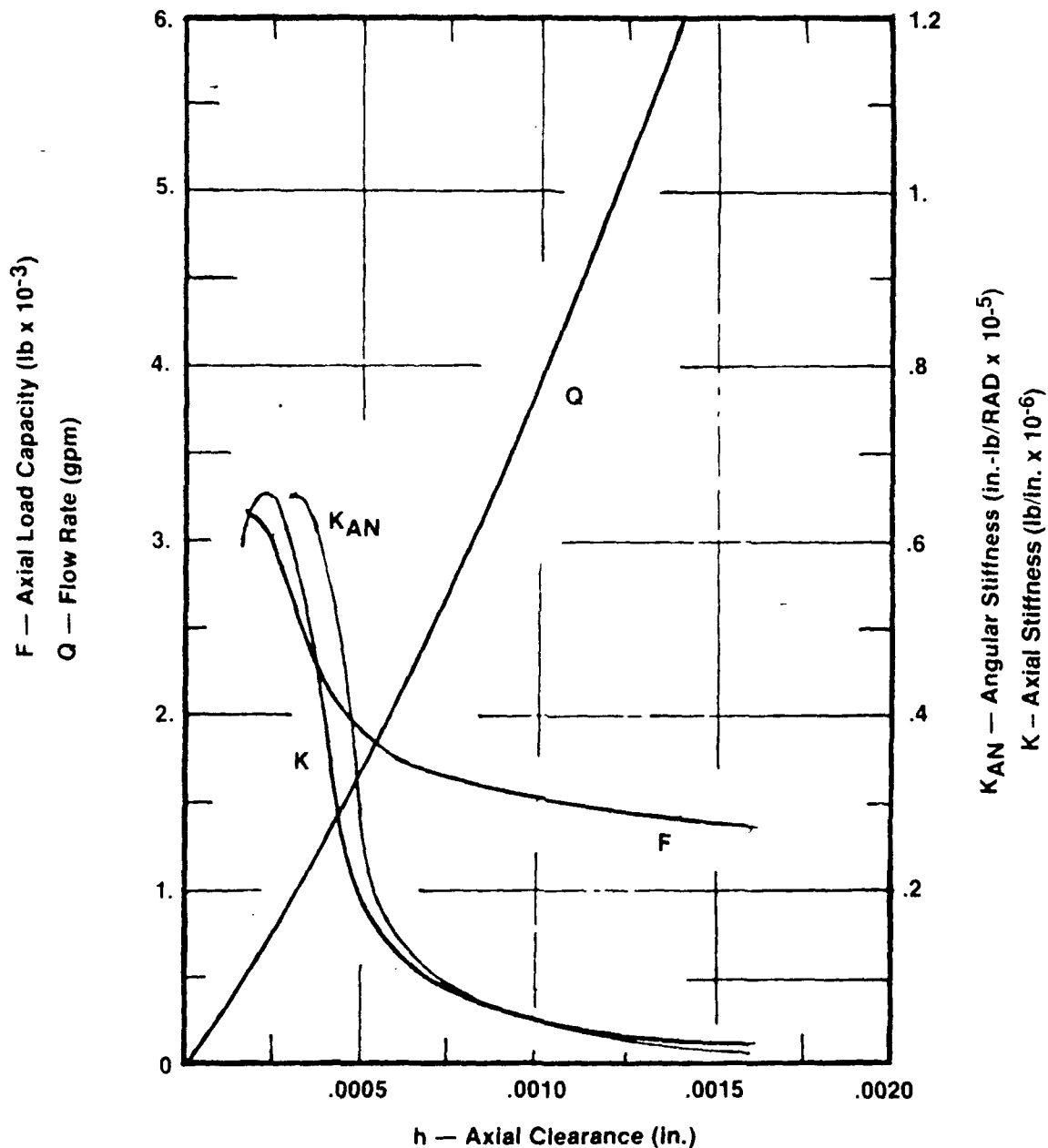
$R_1 = 0.60$ Inch

$R_2 = 0.64$ Inch

$R_3 = 0.69$ Inch

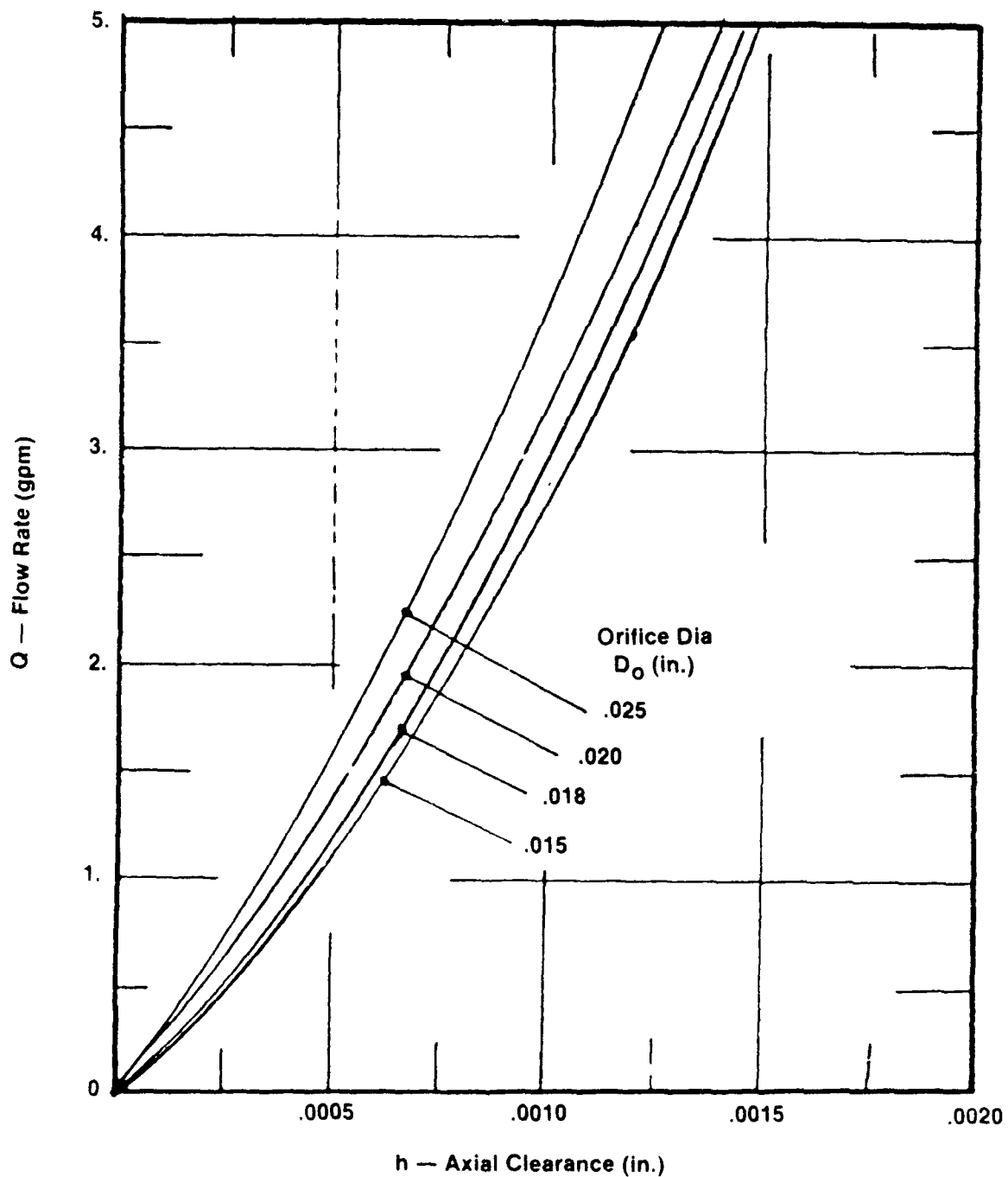
$R_4 = 0.81$ Inch

Figure 2.5-11. Pump End Journal Bearing Performance Prediction



Lubricant LO_2	Radius at Recesses
Supply Pressure, $P_s = 4600 \text{ lb/in.}^2$	$R_1 = .60 \text{ in.}$
Exit Pressure, $P_e = 500 \text{ lb/in.}^2$	$R_2 = .64 \text{ in.}$
Shaft Speed 75000 rpm	$R_3 = .69 \text{ in.}$
No of Recesses 4	$R_4 = .81 \text{ in.}$
Recess Length = .37 in.	$\phi = .020 \text{ in.}$

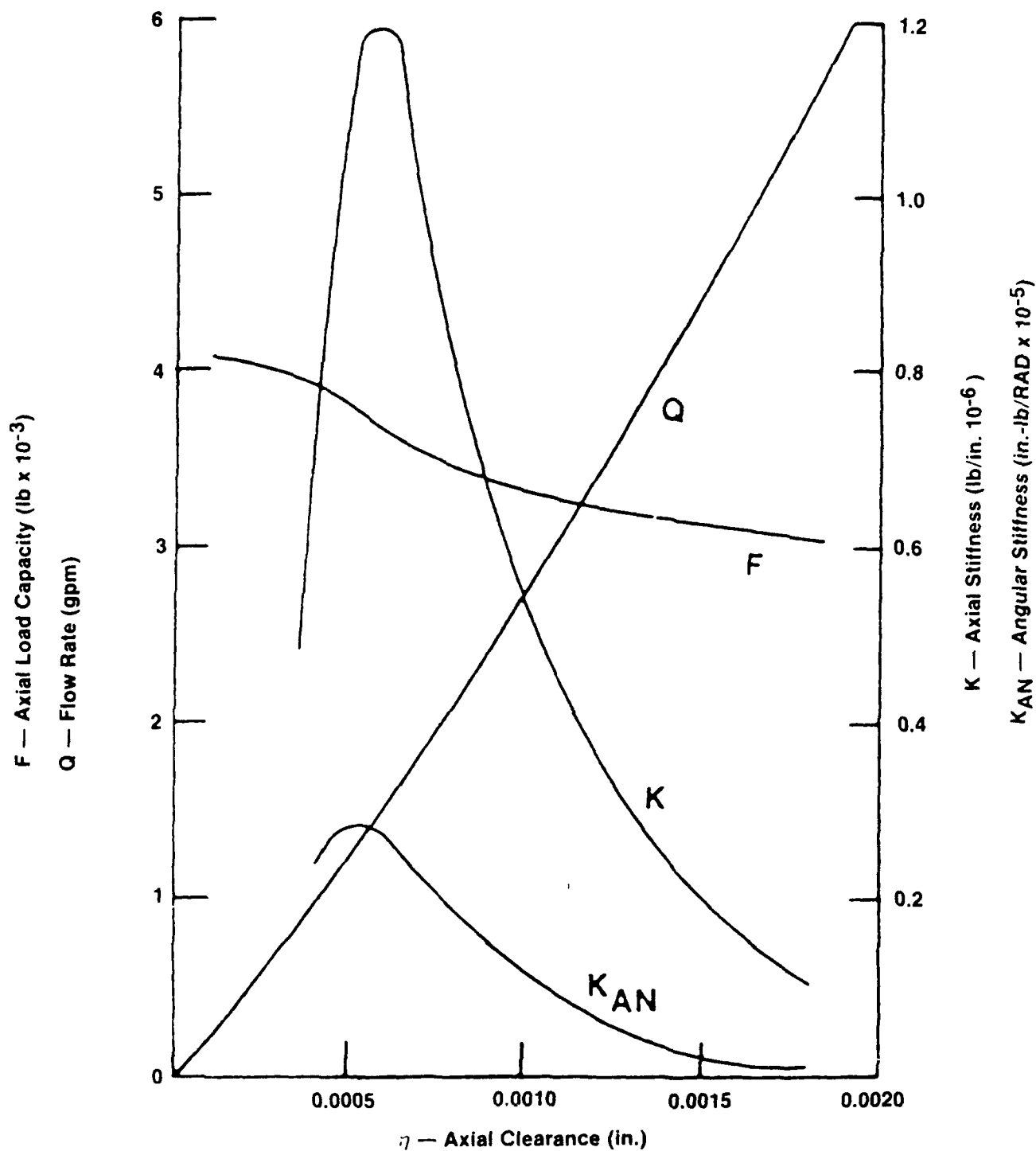
Figure 2.5-12. First Stage Thrust Bearing Performance Prediction



Lubricant LO_2
 Supply Pressure, $P_s = 2200 \text{ lb/in}^2$
 Exit Pressure, $P_e = 500 \text{ lb/in}^2$
 Shaft Speed, $N = 75,000 \text{ rpm}$

Radius at Recess
 $R_1 = .60 \text{ in.}$
 $R_2 = .64 \text{ in.}$
 $R_3 = .69 \text{ in.}$
 $R_4 = .81 \text{ in.}$

Figure 2.5-13. First Stage Thrust Bearing



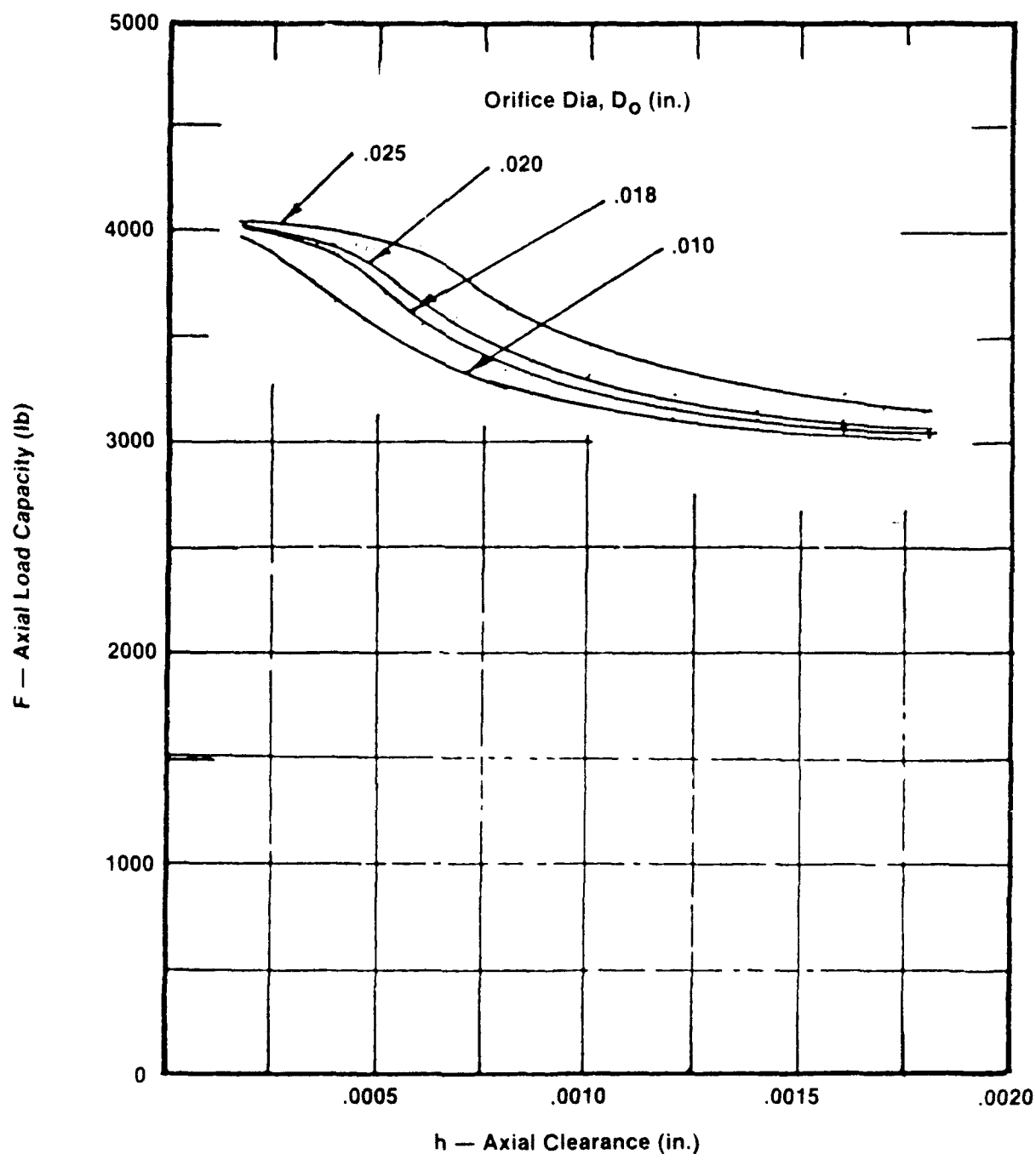
Second Stage Thrust Bearing

Lubricant LO_2
 Supply Pressure,
 $P_s = 4600 \text{ lb/in.}^2$
 Exit Pressure
 $P_e = 2100 \text{ lb/in.}^2$
 Shaft Speed 75,000 rpm

Radius at Recess

$R_1 = .35 \text{ in.}$
 $R_2 = .39 \text{ in.}$
 $R_3 = .45 \text{ in.}$
 $R_4 = .65 \text{ in.}$
 $D_o = .020 \text{ in.}$

Figure 2.5-14. OTV LO_2 TPA Axial Load Capacity vs Axial Clearance

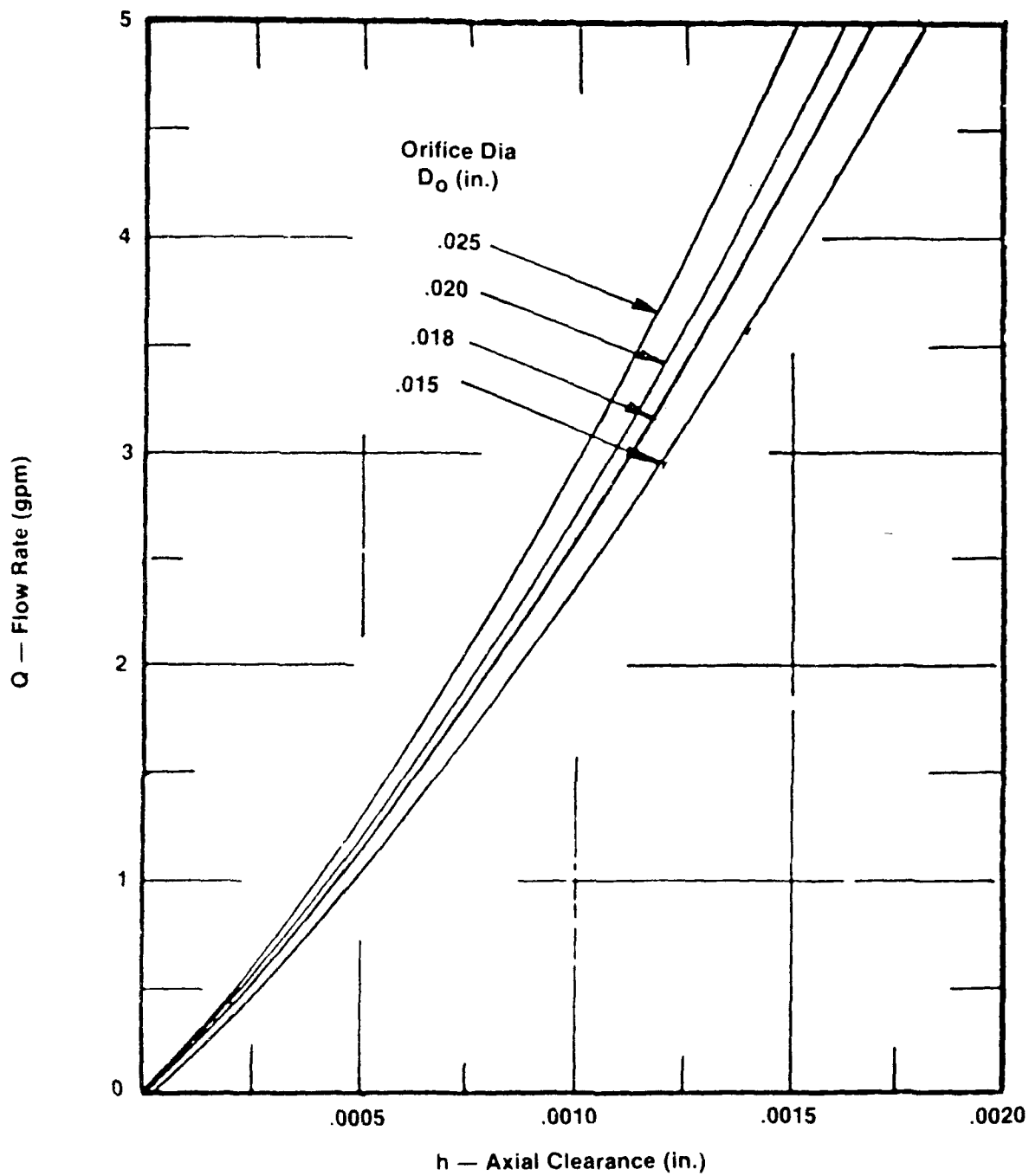


Second Stage Thrust Bearing

Lubricant LO_2
 Supply Pressure,
 $P_s = 4600 \text{ lb/in.}^2$
 Exit Pressure
 $P_c = 2100 \text{ lb/in.}^2$
 Shaft Speed 75,000 rpm

$R_1 = 0.35 \text{ in.}$
 $R_2 = 0.39 \text{ in.}$
 $R_3 = 0.45 \text{ in.}$
 $R_4 = 0.65 \text{ in.}$

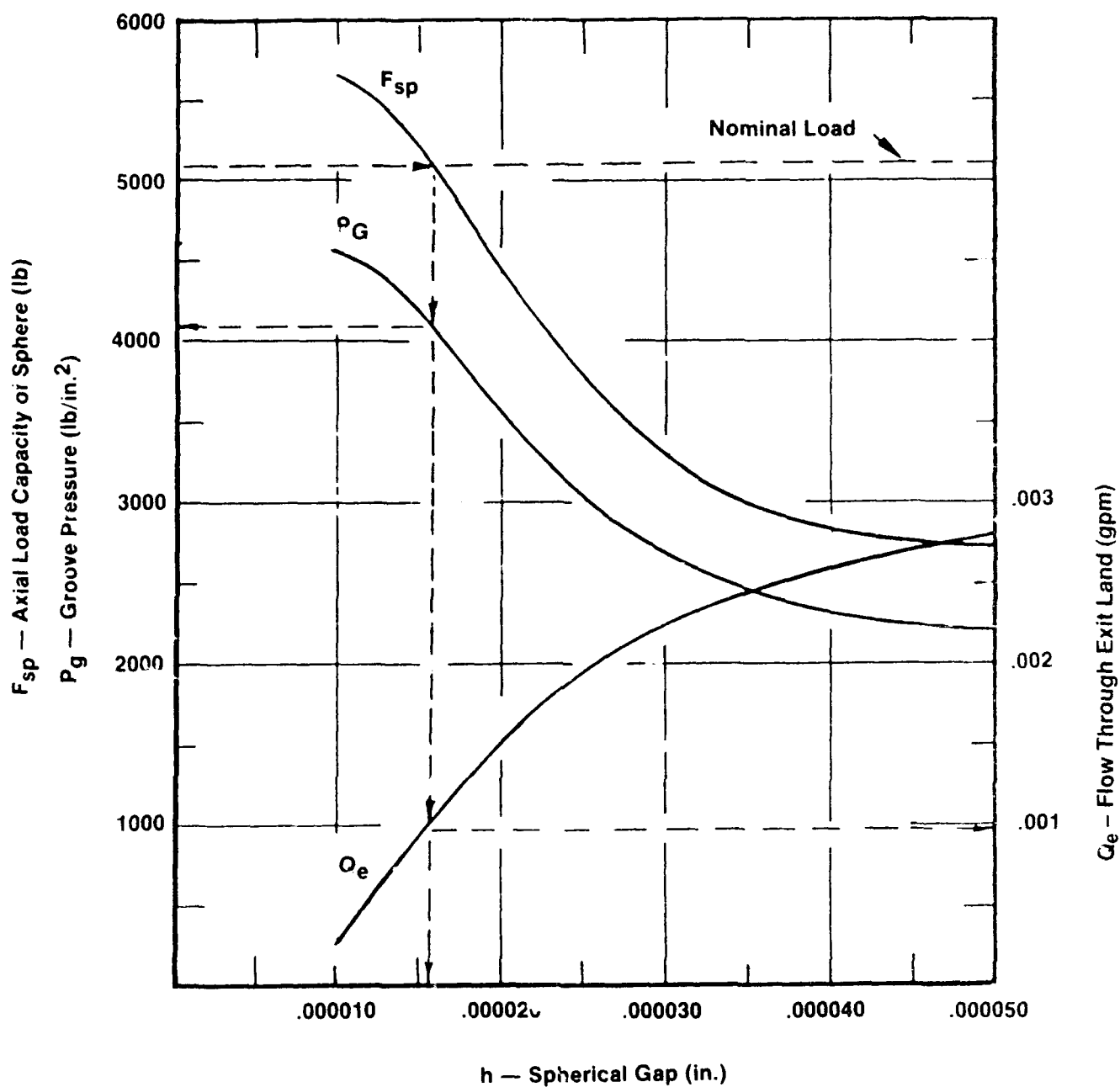
Figure 2.5-15. Second Stage Thrust Bearing



Lubricant LO_2
 Supply Pressure,
 P_s 4600 lb/in.²
 Exit Pressure
 P_c 2100 lb/in.²
 Shaft Speed 75,000 rpm

$R_1 = 0.35$ in.
 $R_2 = 0.39$ in.
 $R_3 = 0.45$ in.
 $R_4 = 0.65$ in.

Figure 2.5-16. Second Stage Thrust Bearing



P_s 4600 lb/in.²
 P_e 2000 lb/in.²

R_o - 1.05 in.
 R_i - .84 in.
 D_o - .015 in.

Figure 2.5-17. Spherical Socket Performance

2.5, Detail Design, cont.

pump inlet and the turbine and provides a high pressure barrier between the pump and turbine sections. The exit flow to the turbine side is used for a thermal isolation barrier between the cryogenic pump and the warm turbine. This exit flow has the option of being returned to the pump inlet or the turbine exhaust ($Q_{ex} \cong 1.0$ GPM). The location of the bearing was based on maximum overhang of the turbine allowed by critical speed consideration and adequate thermal insulation cavity length to get the shaft temperature down to the bearing temperature. This was done to assure proper clearance within the bearing and stable bearing performance. The shorter the bearing span and the more joints in the housing between the two journal bearings the higher the potential angular misalignment of the shaft to bearing.

The consequences of misalignment are reduced bearing load capacity and stiffness. Two basic approaches are used to minimize the effects of bearing misalignment. The first approach is to put maximum effort into deflection analysis, into reducing L/D, reducing the number of joints, and in assuring the highest quality machining. The second method is to design articulated self-aligning bearings that accommodate misalignment and maintain high stiffness. The spherically mounted self aligning hydrostatic journal bearing is shown in Figure 2.5-18. This design is hydrostatically mounted on a spherical surface and is aligned by a restoring moment from the two rows of independently compensated pockets in the bearing bore. This design appears to have the best chance of meeting the design goals of no rubbing contact and high radial stiffness for critical speed control. This bearing is a cartridge design that allows easy bearing sleeve replacement for testing material combinations, geometry or fixed bearing designs.

Selected design bearing performance is shown in Figure 2.5-19. This curve includes the bearing flow rate, load capacity and radial stiffness. Comparing the load capacity to the applied load of this bearing, 0-4 lb, Figure 2.5-6, it is obvious the bearing will have very little eccentricity during operation. This small eccentricity results in minimum motion at the turbine tip seal. The flow rate through the bearing is low, 2 gpm, and fairly constant with eccentricity ratio. One of the key characteristics is the radial stiffness in achieving the subcritical design. The radial stiffness is above 3×10^5 lb/in. in the eccentricity range of operation. The

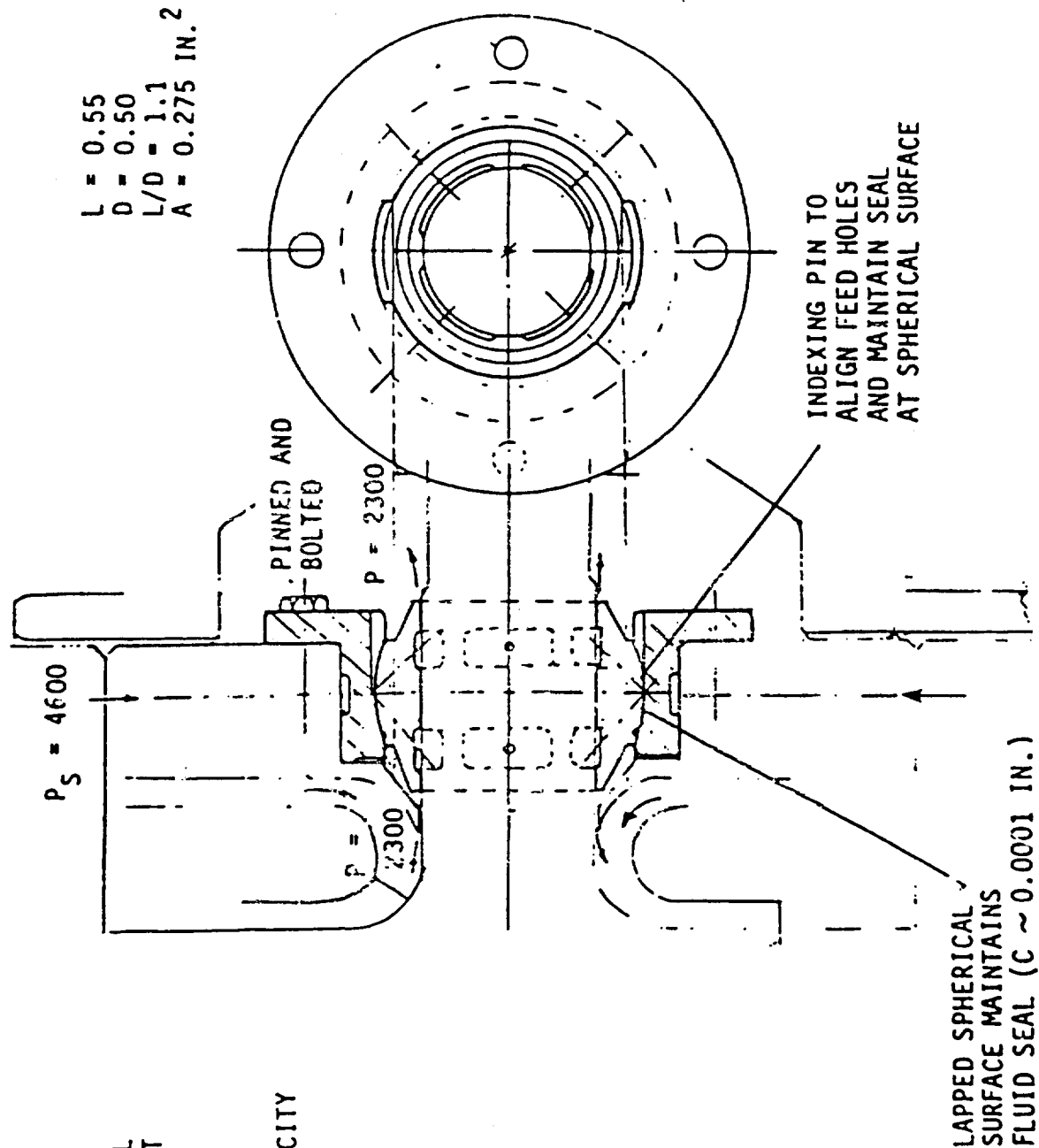
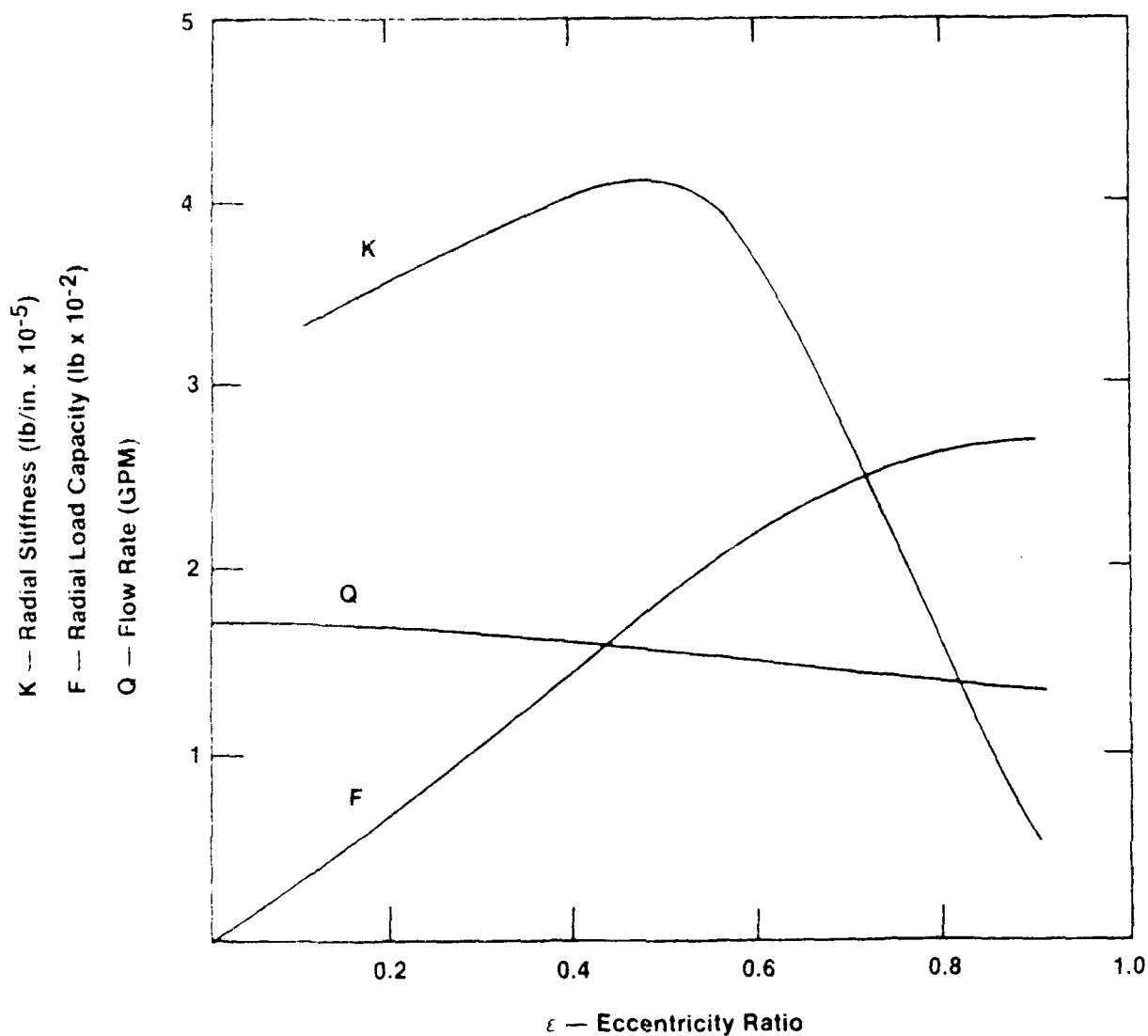


Figure 2.5-18. Turbine End Journal Bearing



Bearing Radius 0.25 in.
 Bearing Length 0.4 in.
 Recess Width 0.24 in.
 No. of Recesses 4
 Orifice Diameter 0.020 in.
 Shaft Speed 75000 rpm
 Supply Pressure 4600 lb/in.²
 Exit Pressure 2300 lb/in.²
 Lubricant — LO₂
 Radial Clearance 0.0010 in.

Figure 2.5-19. OTV LO₂ TPA — Turbine End Journal Bearing

2.5, Detail Design, cont.

shape of these performance curves are a result of the supply pressure and the orifice size, clearance and recess geometry. Parametric bearing performance for geometry variations of clearance and orifice size is shown in Figures 2.5-20, 2.5-21, 2.5-22, and 2.5-23. Figure 2.5-20 shows load capacity as a function of eccentricity ratio for several orifice sizes. The maximum capacity is the same for each orifice size but the shape of the load curve varies at low eccentricity ratio. Small orifice size has low load capacity at low eccentricity. The load curve with .020 orifice diameter has the most linear shape at low eccentricity and was selected for the final design as it has a lower shaft displacement for a given imposed load.

The bearing flowrate variations are shown as a function of orifice size and operating clearance in Figure 2.5-21. The goal was to keep this flowrate as low as possible without compromising the shape of the load capacity or stiffness without incurring excess risk from too close of a bearing clearance. Again the .02 orifice diameter and .001 nominal radial clearance was an acceptable compromise.

Figures 2.5-22 and 2.5-23 are variations of radial stiffness with orifice size and radial clearance. The smaller orifice areas shown in Figure 2.5-23 results in low radial stiffness at low eccentricity ratio while having high stiffness at high eccentricity. This is unacceptable for operating at low eccentricity ratio. Figure 2.5-22 shows the stiffness with the 0.020 and 0.025 inch diameter orifices for 0.0008 to 0.0012 inch clearance tolerance. Orifices of these sizes are the better compromise for high stiffness starting at low eccentricity and extending into the higher eccentricity range. The bearing with the 0.020 inch diameter orifice was the best performance compromise for the flowrate, load capacity and stiffness. It was, therefore, selected as the final design.

2.5.2 Pump Section and Crossovers

2.5.2.1 Introduction

The performance of small, low specific speed turbopumps similar to the OTV OX TPA had been investigated by Aerojet in an IR&D technology program. During the IR&D program, impellers with specific speeds of 350, 565, and 1050 (gpm, rpm, ft. units) were tested with volute housings. The specific speed of the

Fluid — Liquid Oxygen
 $P_s = 4600 \text{ lb/in}^2$
 $P_e = 2300 \text{ lb/in}^2$
 Radius 0.25 in.

Number of Recesses = 4
 P_s = Supply Pressure
 P_e = Exit Pressure

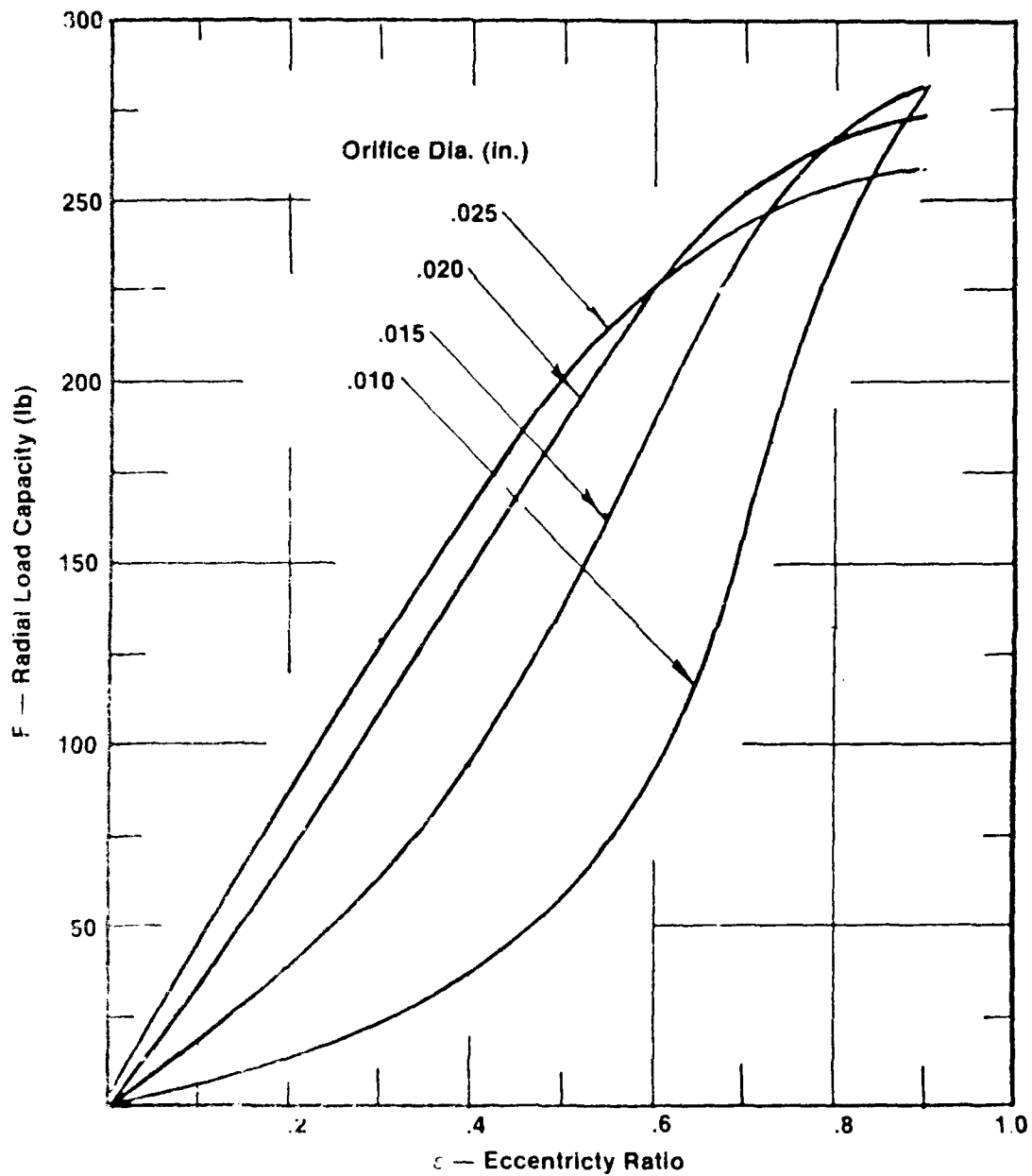


Figure 2.5-20. Turbine End Journal Bearing

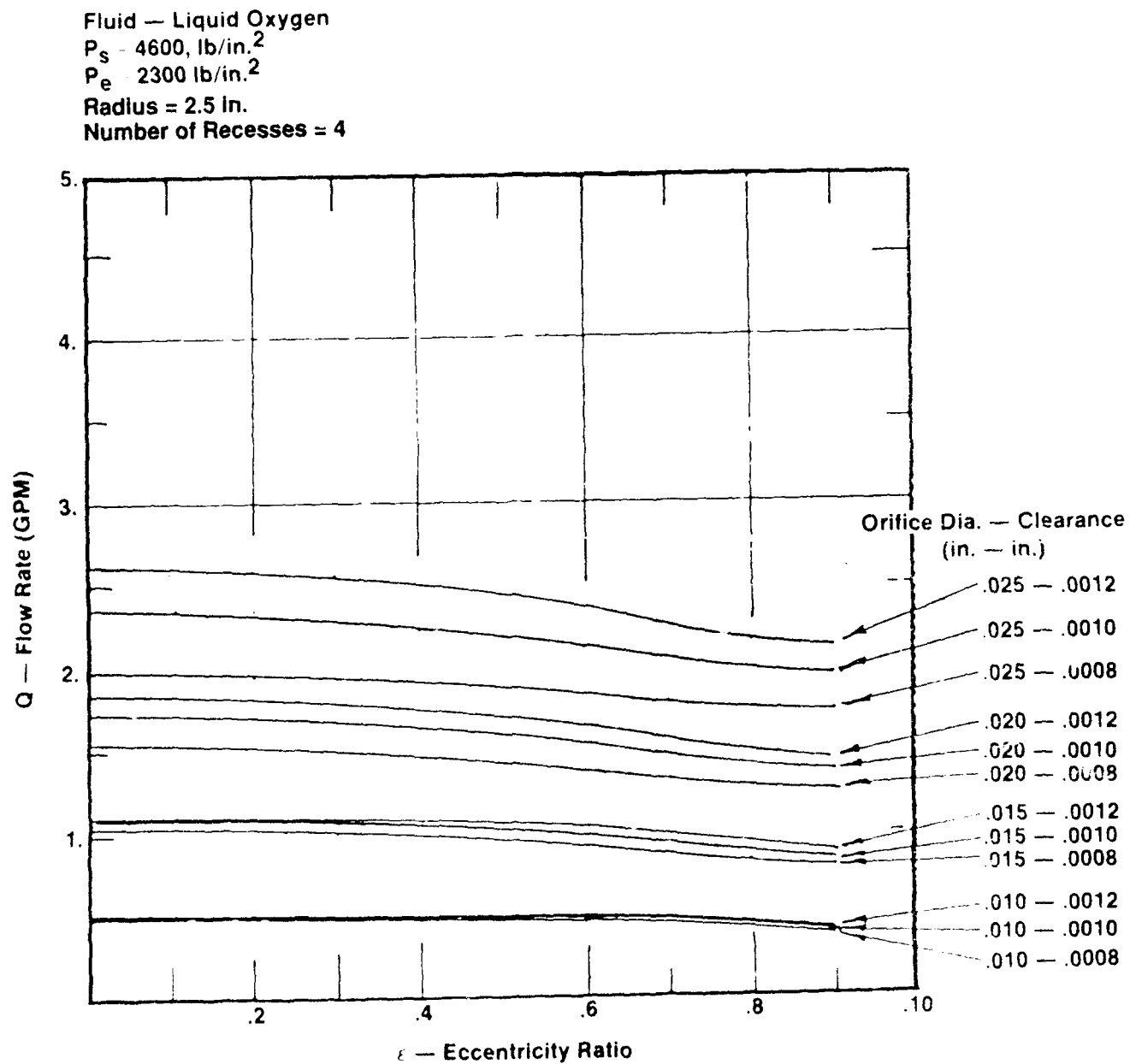


Figure 2.5-21. Turbine End Journal Bearing

Fluid Liquid Oxygen
 $P_s = 4600 \text{ lb/in.}^2$
 $P_e = 2300 \text{ lb/in.}^2$
 Radius — .25 in.

Number of Recesses = 4

Orifice Diameter = 0.025 ———

Orifice Diameter = 0.020 - - -

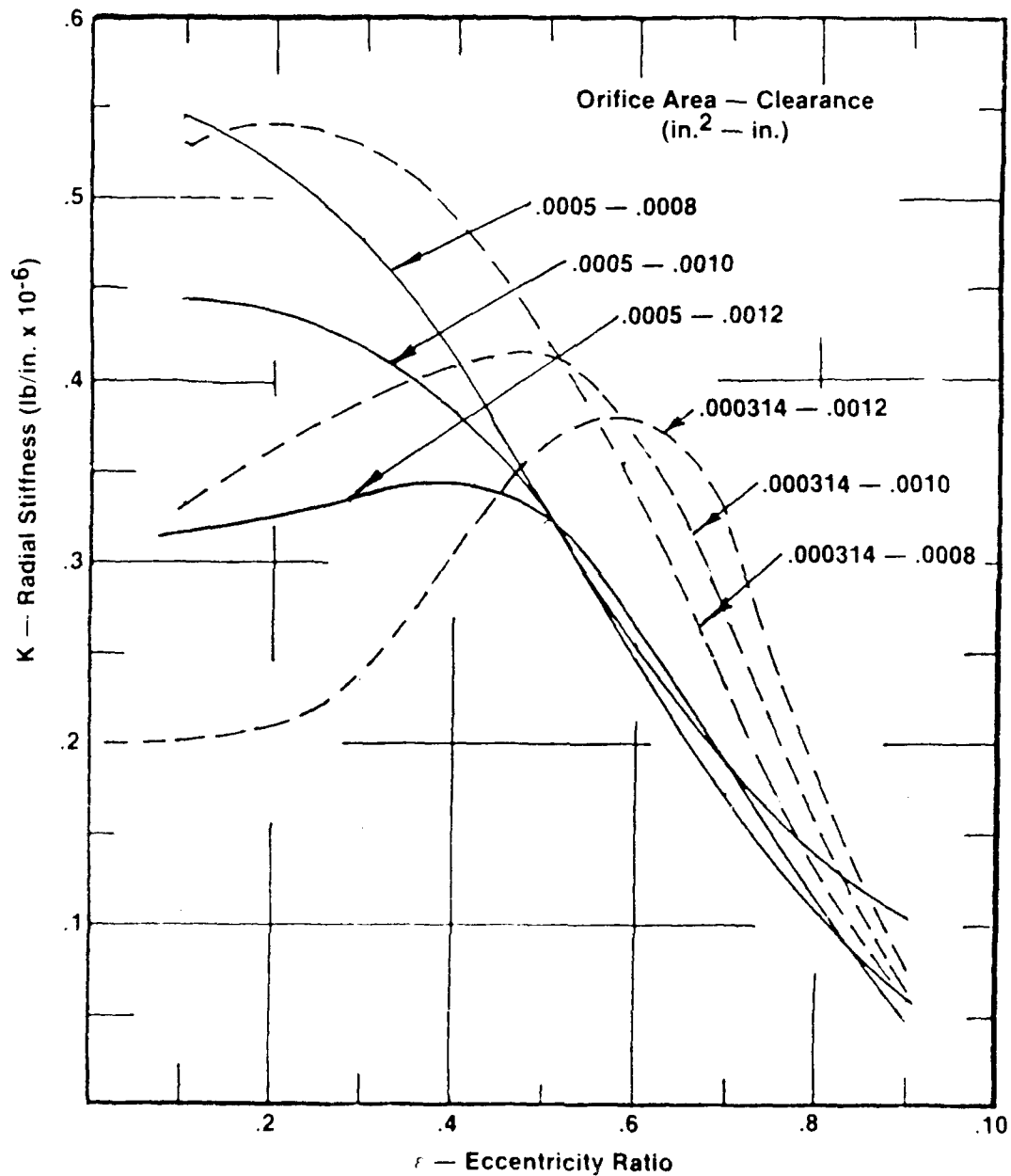


Figure 2.5-22. Turbine End Journal Bearing

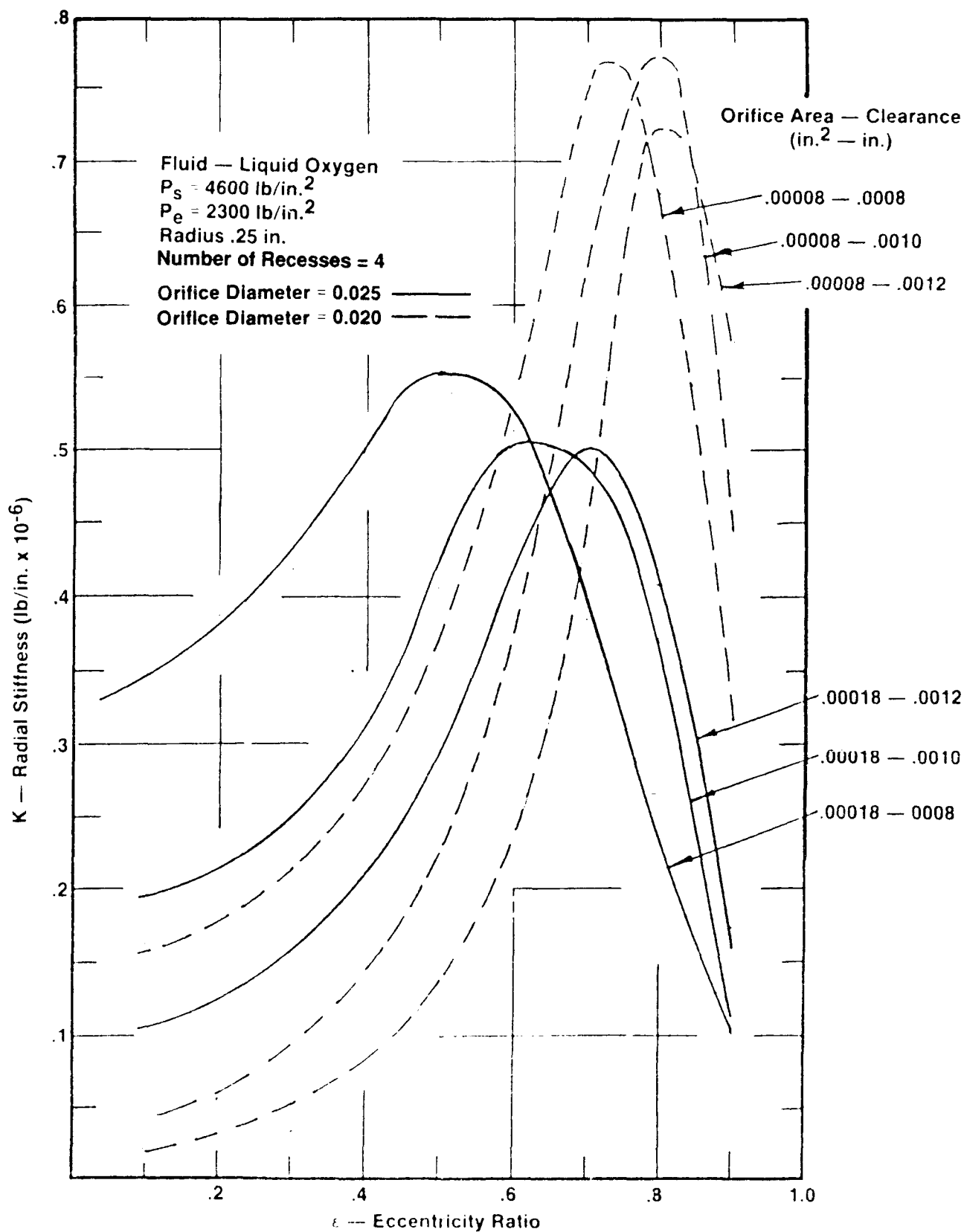


Figure 2.5-23. Turbine End Journal Bearing

2.5, Detail Design, cont.

impellers was varied by trimming the impeller tip diameter from 3.44 inches to 1.7 inches; neither the vane shape nor the vane discharge angle were changed. The test data from this program was used to develop an analytical model to predict the performance of these impellers. The correlation between the analytical model and the test data was excellent. The hydraulic design of the impellers and inducer used on the OTV LOX pump was scaled from that used in the IR&D technology program. Since the specific speed of the impellers on the OTV program falls in the range of specific speeds tested during the IR&D program, the performance risk associated with the impeller and volute designs is small.

With this established hydraulic design and analytical model, the design approach was readily chosen. The pump is two stages with an inducer. A separate low pressure boost pump is proposed to more efficiently solve the problem of very low pressure propellant tanks. The low pressure boost pump was given a preliminary design in Task D.5, Engine Preliminary Design, but was not within the scope of the tasks covered in this report. Its design point is given in Table 2.4-1 along with the detailed design point for the high pressure pump. An axial flow inducer receives flow from the boost pump. At the inducer discharge, 20 percent of the flow is tapped off to drive the boost pump hydraulic turbine. The remaining flow enters the first stage impeller. The first and second stage impellers are identical centrifugal impellers. The impellers are arranged in a back-to-back configuration due to mechanical design considerations. Two options are presented for the transfer of fluid from the first stage impeller discharge to the second stage impeller inlet: conventional external crossovers or a volute with external plumbing and internal crossover passages. In the original 3K engine design, internal crossover passages were needed as the TPA was designed for installation in a centerbody within the thrust chamber (see Figure 1.1-1). As the design evolved this configuration was no longer desired, and external crossover passages are planned for the flight engine. The test unit was designed with the external crossovers. For either of the interstage flow passage designs, the fluid must be turned sharply at the entrance to the second stage impeller. To counteract flow distortions caused by the curvature of the second stage inlet, inlet guide vanes were considered. Inlet guide vanes were not incorporated in the turbopump design; however, as their expected benefits were of

2.5, Detail Design, cont.

less value than the complexity they would add to the fabrication. As in the case of the interstage fluid passages, two options are presented for transfer of the fluid from the second stage impeller discharge to the cooled centerbody. The volute option was used on the test unit while an internal vaned diffuser was considered as a development goal until the changes in the engine design under the 7.5K lbf thrust engine design task rendered it unnecessary.

2.5.2.2 Inducer Design

The hydraulic design of the inducer is scaled from that of the inducer used in the IR&D technology program. The measured suction specific speed of the IR&D inducer at two percent head loss varied from 27,000 to 32,000 depending on the configuration being tested. In all cases, the performance of this inducer proved more than adequate to meet the requirements of the OTV program.

The OTV inducer was scaled from the IR&D inducer using the similarity relations.

$$\frac{Q}{ND^3} = \text{constant},$$

and

$$\frac{\Delta H}{N^2 D^2} = \text{constant}$$

where D is inducer tip diameter. Using these relations, the inducer can be scaled to satisfy either the design head or the design flow requirement, but not both. A tip diameter of 0.913 inches results if the design flow is used in conjunction with the first relation. Fortuitously, a head rise of 520 feet is calculated using a diameter of 0.913 and the second relation. A design description of this inducer is given in Table 2.5-1.

Table 2.5.1.
Inducer Design Parameters

Flow	= 51.4 gpm
Head Rise	= 520 ft
Speed	= 75,000 rpm
Minimum NPSH	= 80 ft
Required Suction Specific Speed	= 20,100
Minimum Measured Suction Specific Speed	= 27,000
Tip Diameter	= 0.913 inches
Inlet Hub Diameter	= 0.457 inches
Discharge Hub Diameter	= 0.566 inches
Hub Slope	= 8.5 degrees
Number of Blades	= 4
Tip Inlet Blade Angle	= 10.6 degrees
Tip Inlet Fluid Angle	= 6.4 degrees
Tip Incidence to Blade Angle Ratio	= 0.40
Mean Wrap	= 100 degrees
Mean Discharge Blade Angle	= 22.5 degrees

2.5, Detail Design, cont.

2.5.2.3 Impeller Design Approach

The LOX OTV high pressure pump is a two stage pump with each stage contributing one half the head rise. The rotors used in each stage are identical. The hydraulic design of the OTV impellers is based on the impeller design tested during the IR&D technology program. The OTV impeller is derived by scaling the IR&D impeller design based on the flow rate requirements and by trimming the re-sulting impeller to meet the pressure rise requirements. In small, low specific speed pumps, the effect of leakage flows on impeller performance is important. All the impellers tested during the IR&D program were single stage pumps. The leakage flows in a two stage pump like the OTV can vary significantly from the leakage flows in single stage pumps. The impeller flow rate and the through flow plus the leakage flow, were used to scale the IR&D design for the OTV application. The OTV flow rates, determined from analysis of bearing and seal leakage paths, are:

Thru Flow - 34.1 gpm

First Stage Impeller Flow - 41.6 gpm

Second Stage Impeller Flow - 44.1 gpm

Since the first and second stage rotors are to be identical, a flow rate of 44.1 gpm was used in equation 1 to calculate the impeller inlet tip diameter. The resulting tip diameter was 0.812 inches. This impeller was trimmed to give 2300 psi pressure rise by applying equation 2 with D equal to the impeller discharge diameter. The nominal impeller discharge diameter is 1.52 inches. The nominal diameter was increased to 1.615 inches to provide 10 percent head margin. The design parameters of the OTV impellers are shown in Table 2.5-2.

2.5.2.4 Interstage Flow Path

The test OTV unit uses volutes to collect the first stage impeller discharge flow and deliver it to external lines. The external lines carry the flow to the second stage inlet. Since the design and analysis of volutes is well understood at Aerojet, this approach has little performance risk. Another approach is to use

Table 2.5-2.
Impeller Design Parameters

Discharge Flow	= 34.1 gpm
First Stage Impeller Flow	= 41.6 gpm
Second Stage Impeller Flow	= 44.1 gpm
Head Rise per Stage	= 4575 ft.
Speed	= 75,000 rpm
Stage Specific Speed	= 787
Nominal Impeller Discharge Diameter	= 1.512 inches
Maximum Impeller Discharge Diameter	= 1.615 inches
Impeller Discharge Port Width	= 0.0812 inches
Impeller Inlet Tip Diameter	= 0.812 inches
Impeller Inlet Hub Diameter	= 0.546 inches
Number of Blades	= 8
Blade Inlet Angle	
Tip	16.9 degrees
Mean	20 degrees
Hub	24.5 degrees
Discharge Blade Angle	30 degrees

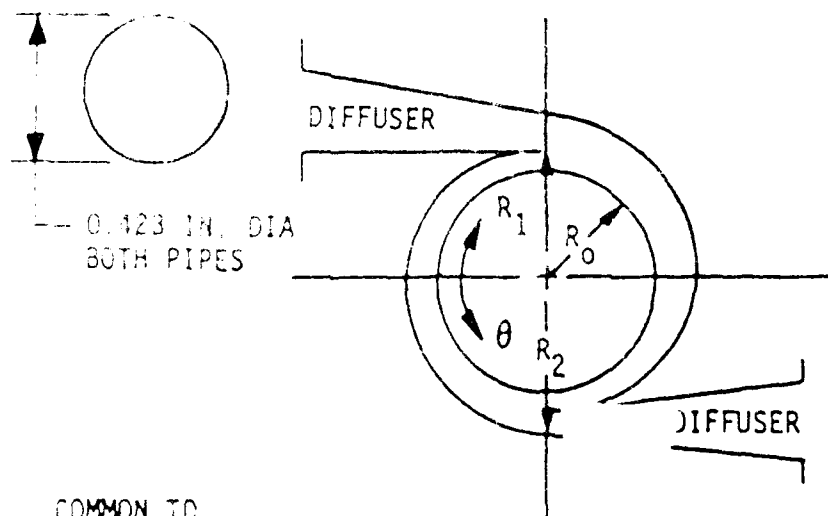
2.5, Detail Design, cont.

internal crossover passages to collect flow from the first stage impeller discharge and deliver it to the second stage inlet.

2.5.2.5 Volute Interstage Passage Design

The volute interstage passage consists of three components. The volute-diffuser collects the impeller discharge flow, diffuses it, and directs it to two external interstage lines. The external interstage lines carry the flow axially to the second stage inlet. The second stage inlet carries the flow radially to the second stage impeller inlet and distributes the flow tangentially.

The volute-diffuser design for the OTV is based on Stepanoff's constant velocity concept (Reference 10). All the volutes used on the IR&D technology program were single tongue volutes designed using the constant velocity concept. Due to the high pressure in the OTV pump, the double tongue volute was chosen to minimize radial loads. The design procedure and the chosen volute design parameters are illustrated in Figure 2.5-24. The volute diffusers were successfully used on the IR&D program with area ratios of five. No problems are expected on the OTV volute diffusers with an inlet velocity of 250 feet per second and an exit velocity of 50 feet per second. The two volute diffusers each connect to a constant diameter pipe. These pipes, which run outside of the pump housing, carry the fluid to the second stage inlet depicted in Figure 2.5-25. The design goal of this inlet is to accept flow from the two external pipes and distribute the flow uniformly in the tangential plane. The inlet design begins with a constant velocity transition from the external pipe circular cross-section to the rectangular cross-section. The width of this cross-section in the meridional plane is set by mechanical design consideration. The width in the tangential plane is calculated using the constant velocity assumption. To distribute the flow uniformly around the periphery, the flow area must vary linearly with the angle, θ . Therefore, it is assumed that $1/8$ of the flow crosses the boundary shown in Figure 2.5-25. The area of the shaded section is reduced linearly with θ as the flow enters the annulus.



COMMON TO
ALL VOLUTES

$$\alpha = 30^\circ$$

$$b_0 = 0.0812 \text{ IN.}$$

$$R_1 = 1.1 R_0$$

$$b_1 = 0.101 \text{ IN.}$$

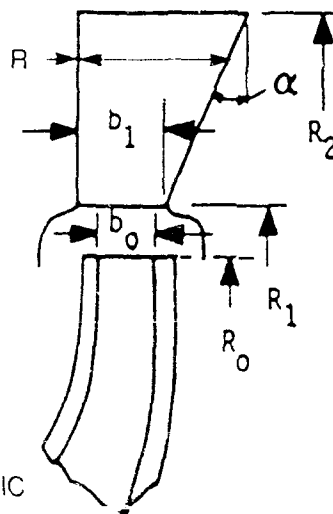
$$R_1 = 0.8825 \text{ IN.}$$

$$R_0 = 0.8075 \text{ IN.}$$

$$A_2 = 0.0268 \text{ IN.}^2$$

$$R_2 = 1.0647 \text{ IN.}$$

$$\theta = \text{TOTAL VOLUMETRIC FLOW RATE}$$



DOUBLE TONGUE APPROACH
CHOSEN TO MINIMIZE RADIAL LOADS

Figure 2.5-24. Volute Configuration Based on Constant Velocity Concept

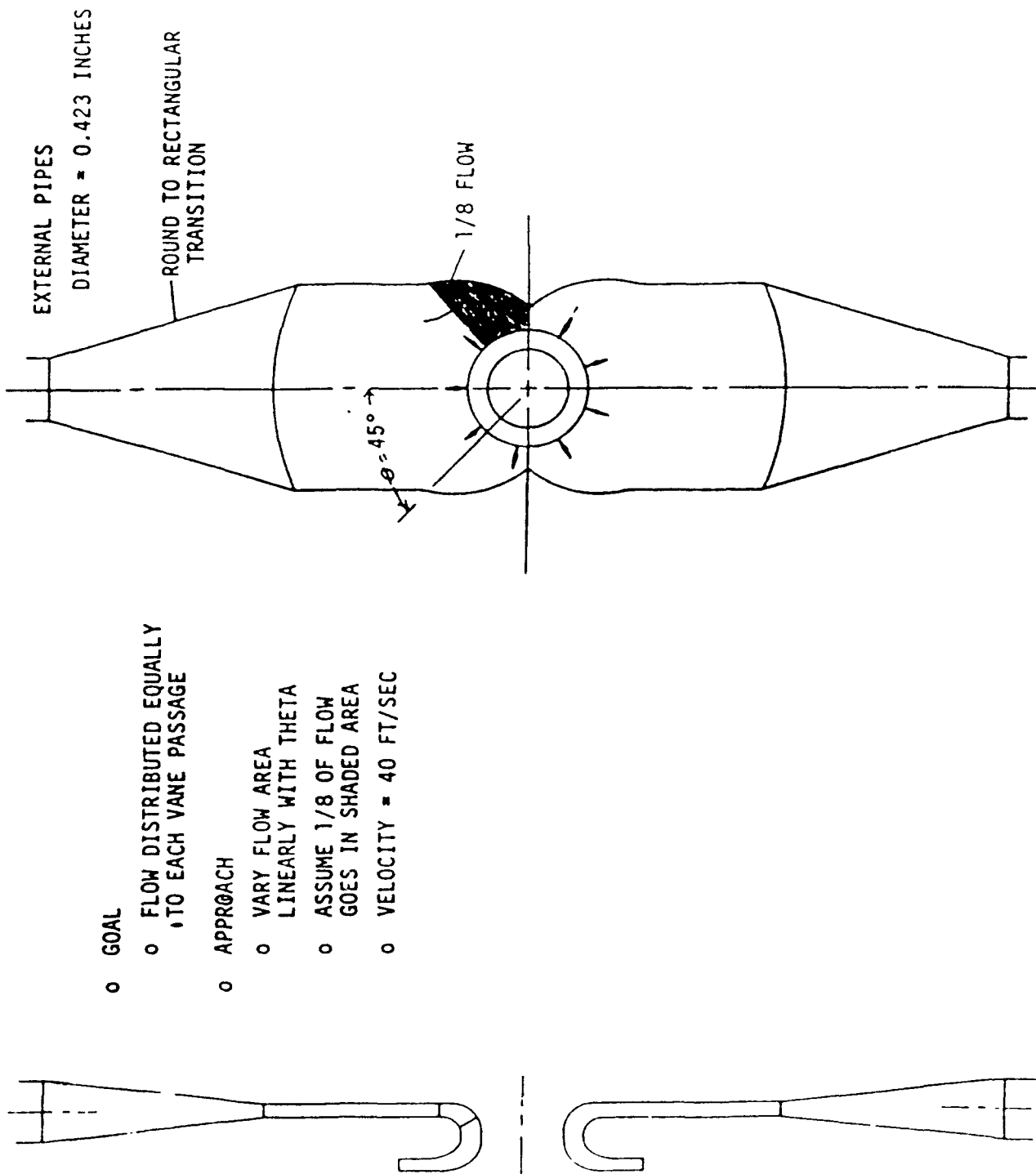


Figure 2.5-25 Second Stage Inlet for External Interstage Passages

2.5, Detail Design, cont.

2.5.2.6 Second Stage Inlet Guide Vanes

The second stage inlet guide vanes are designed to reduce the incidence angle of the second stage impeller. The second stage impeller does not require an inducer. However, the impeller was designed to accept flow from an inducer whose discharge flow had a uniform (hub-to-tip) meridional velocity with a tangential swirl component. The curvature of the second stage inlet, shown in Figure 2.5-26 distorts the meridional velocity. With no inlet guide vanes, the impeller inlet velocity at the tip would be 2.3 times that at the hub. The variation in meridional velocity would cause unacceptable impeller incidence angles.

The swirl component from hub to tip necessary to provide uniform meridional velocity was calculated using streamline curvature techniques. A proprietary Aerojet computer program, NOZZLE, was used iteratively to find the swirl components which result in acceptable impeller incidence angles. The results are shown in Table 2.5-3. The impeller incidence angle with guide vanes is a uniform 2 degrees from the hub to the tip. IMPACT, a standard Aerojet computer procedure for turbomachinery design, was used to define a blade shape which will generate the required swirl. Figure 2.5-27 shows the inlet guide vane meridional profile and Figure 2.5-28 shows an unwrapped blade shape along the mean streamline.

2.5.2.7 Second Stage Discharge

The volute-diffuser used at the second stage discharge is the same as that used at the first stage discharge. The design parameters of the volute-diffuser are shown in Figure 2.5-24.

2.5.2.8 Performance Prediction

The design and off-design performance of the OTV pump has been predicted using an analytical model developed during the IR&D Technology program. The performance was predicted for the internal crossover configuration. Performance for the external crossover configuration should be similar. The efficiency of the internal diffuser passages was set equal to 88 percent at the design

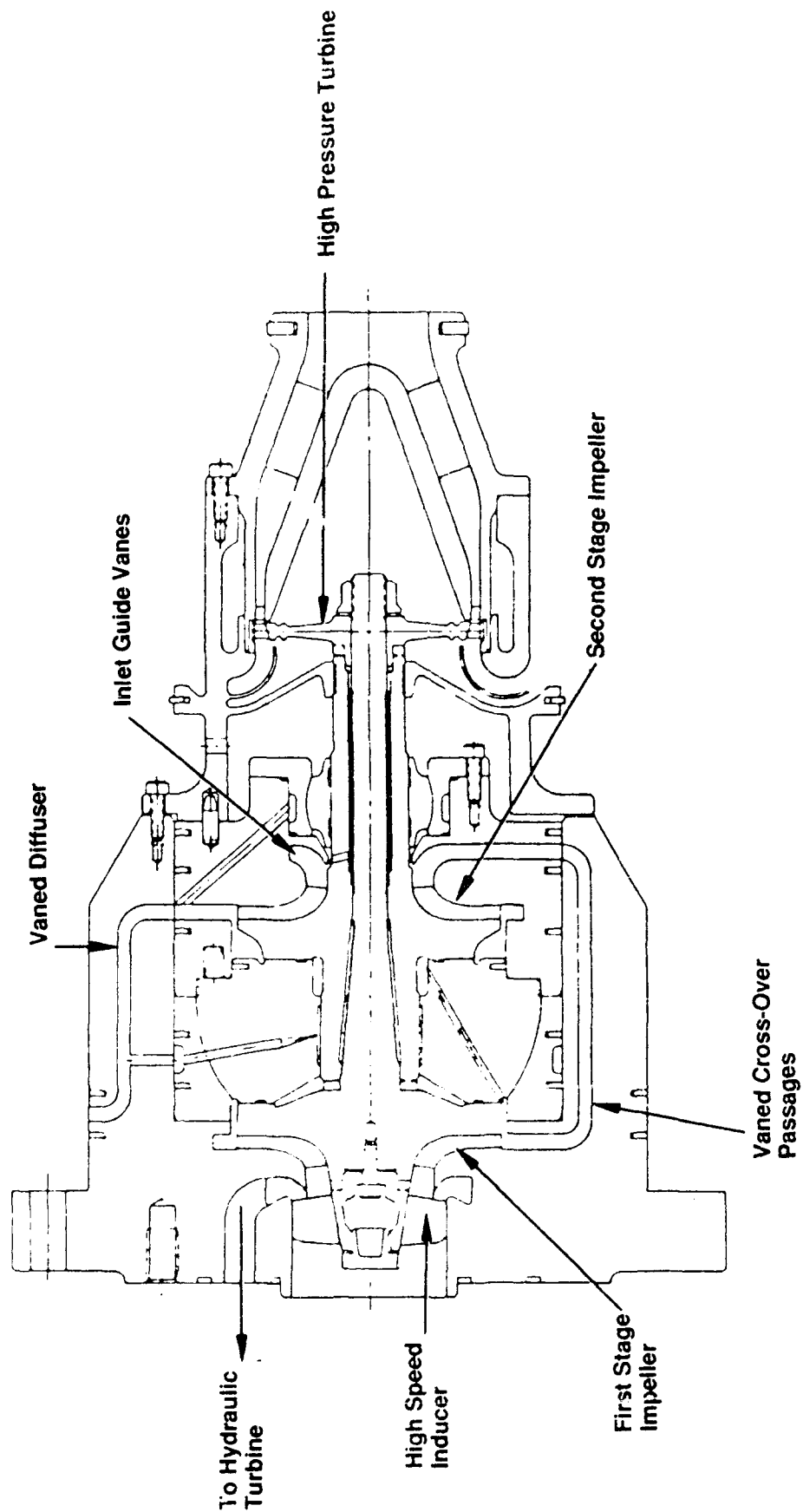


Figure 2.5-26. OTV LOX Turbopump Flight Configuration

TABLE 2.5-3
SECOND STAGE INLET GUIDE VANES
Meridional View

Design Parameters

- Calculate Velocities at the Discharge

	<u>Hub</u>	<u>Mean</u>	<u>Tip</u>
Impeller Blade Angle	24.5	20.0	16.9
Meridional Velocity	57.0	56.5	51.5
Tangential Velocity	40.0	59.0	73.5
Relative Fluid Angle	22.0	18.6	14.9

- Mean Blade Shape
 - Inlet Radius = 0.55 Inches
 - Outlet Radius = 0.34 Inches
 - Meridional Length = 0.31 Inches
 - Wrap = 26.7 Degrees

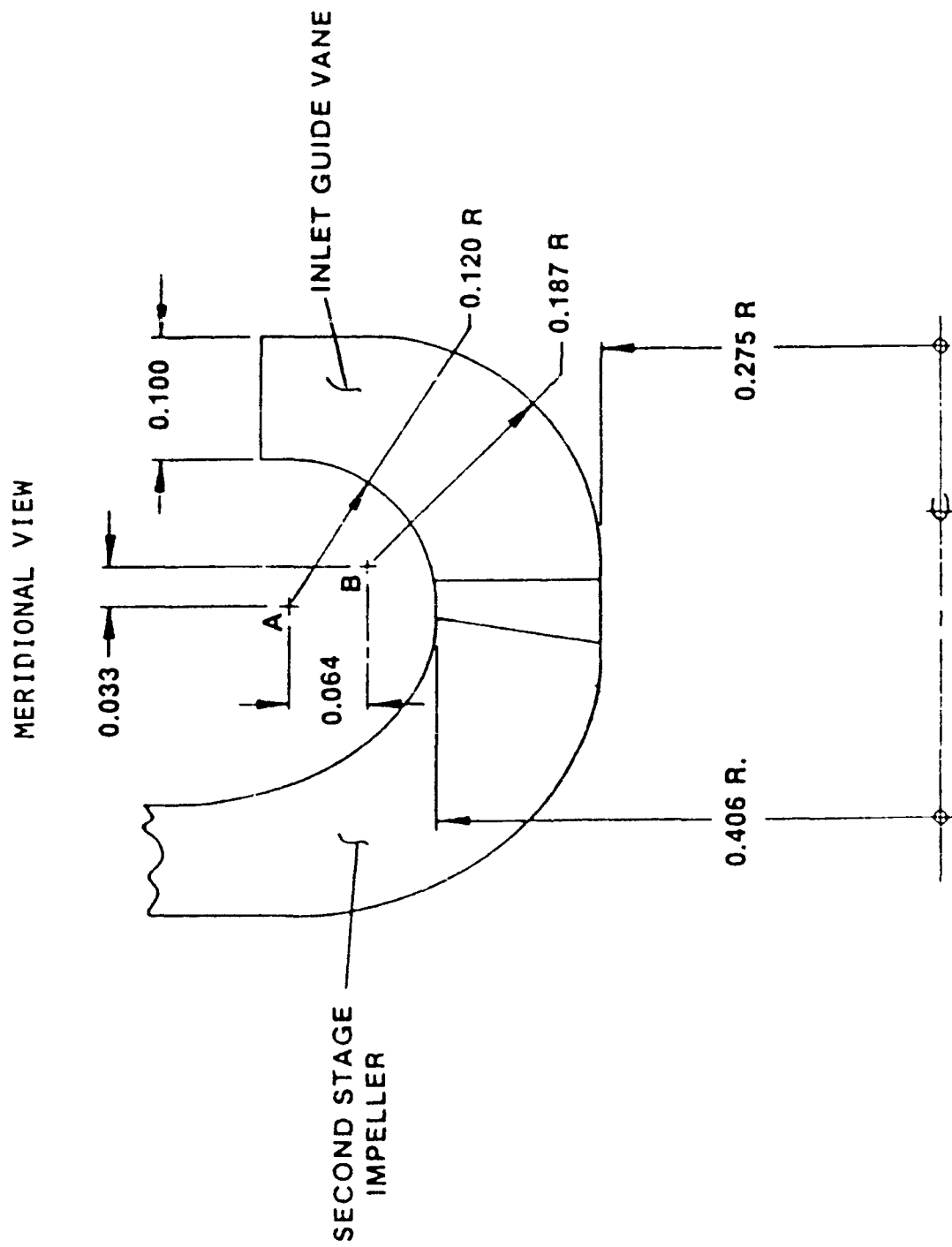


Figure 2.5-27. Second Stage Inlet Guide Vane

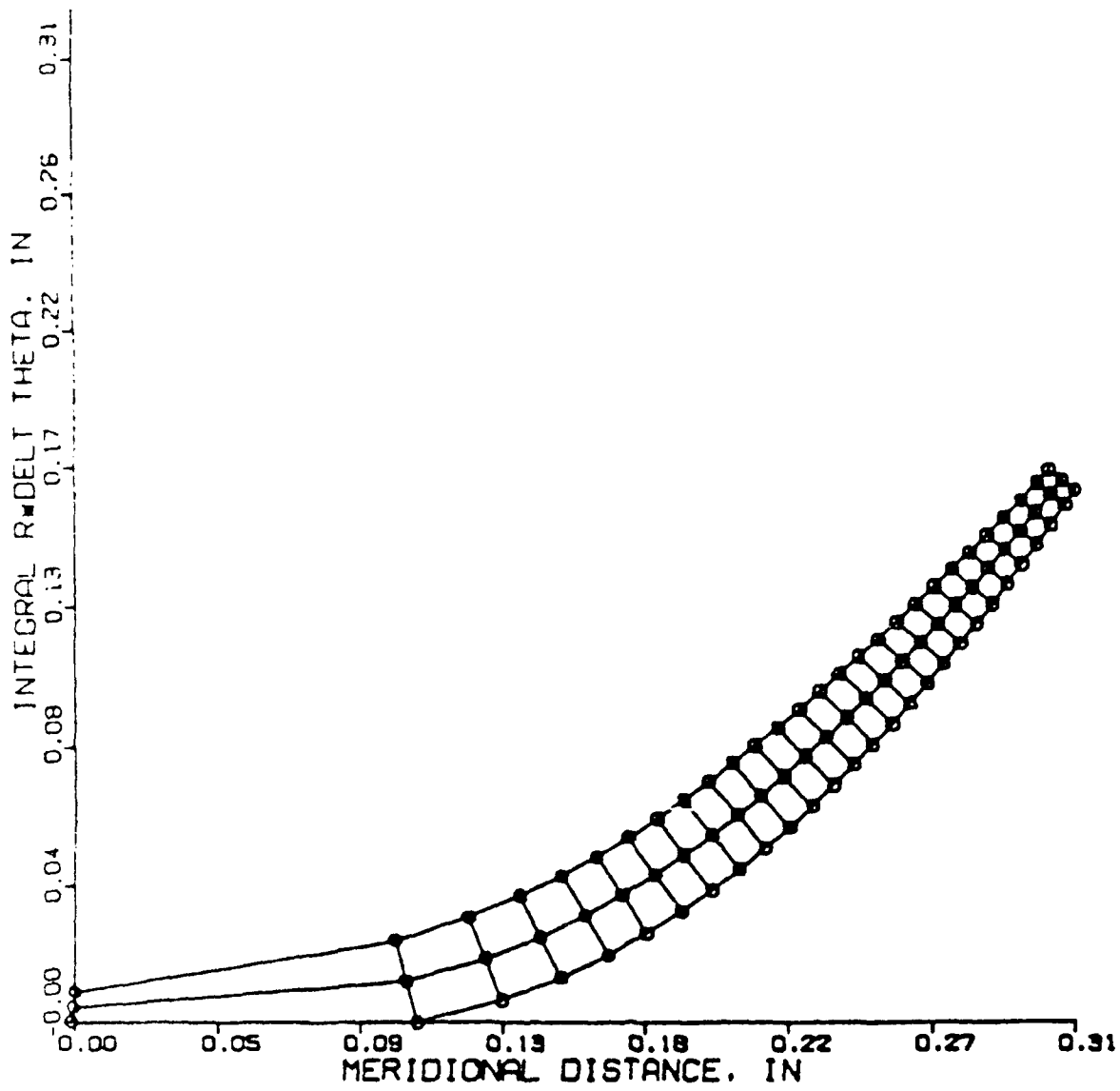


Figure 2.5-28. Second Stage Inlet Guide Vanes Mean Streamline
Unwrapped View

2.5, Detail Design, cont.

point. The derivation of this performance level is based on the NERVA engine TPA designs with a correction for dumping loss.

Based on the IR&D technology results, a four percent efficiency loss was used to correct for a 0.002 inch tip clearance. The predicted head capacity curve for the OTV LOX pump is based on the performance obtained during the IR&D program with unshrouded impellers and volutes. These head capacity curves have a slightly positive slope at low flow rates. Since stable pump operation is possible only in regions of negative slope, the throttling range of the engine could be affected. The slope of the head capacity curve can be changed by a change in the volute or diffuser configuration. A major design goal of the vaned diffuser passages was to eliminate the region of positive slope on the head-capacity curve. The predicted overall performance for the OTV LOX pump is shown in Figure 2.5-29. At the design point, the predicted overall efficiency is 58 percent.

2.5.3 Turbine Section Design

2.5.3.1 Turbine Design Point

The design point was selected from the preliminary engine power balance. The power balance program allows various turbine parameters to be varied from run-to-run so that an optimum design point can be selected. Pump pressure rise and turbine inlet pressure were the principal variables used in the analysis. A baseline for the power balance work was a chamber pressure of 2000 psia. Trade studies were also conducted to select turbine speed, blade reaction, and number of stages, the selected concept design point is given in Table 2.5-4.

2.5.3.2 Turbine Trade Studies

Using pump and turbine point specifications, various trade studies were conducted to determine the type of turbine that is best suited to the LOX TPA requirements. Specifically, the following parameters were examined:

- a. Blade Reaction
- b. Number of Stages
- c. Rotational Speed
- d. Pitch Diameter

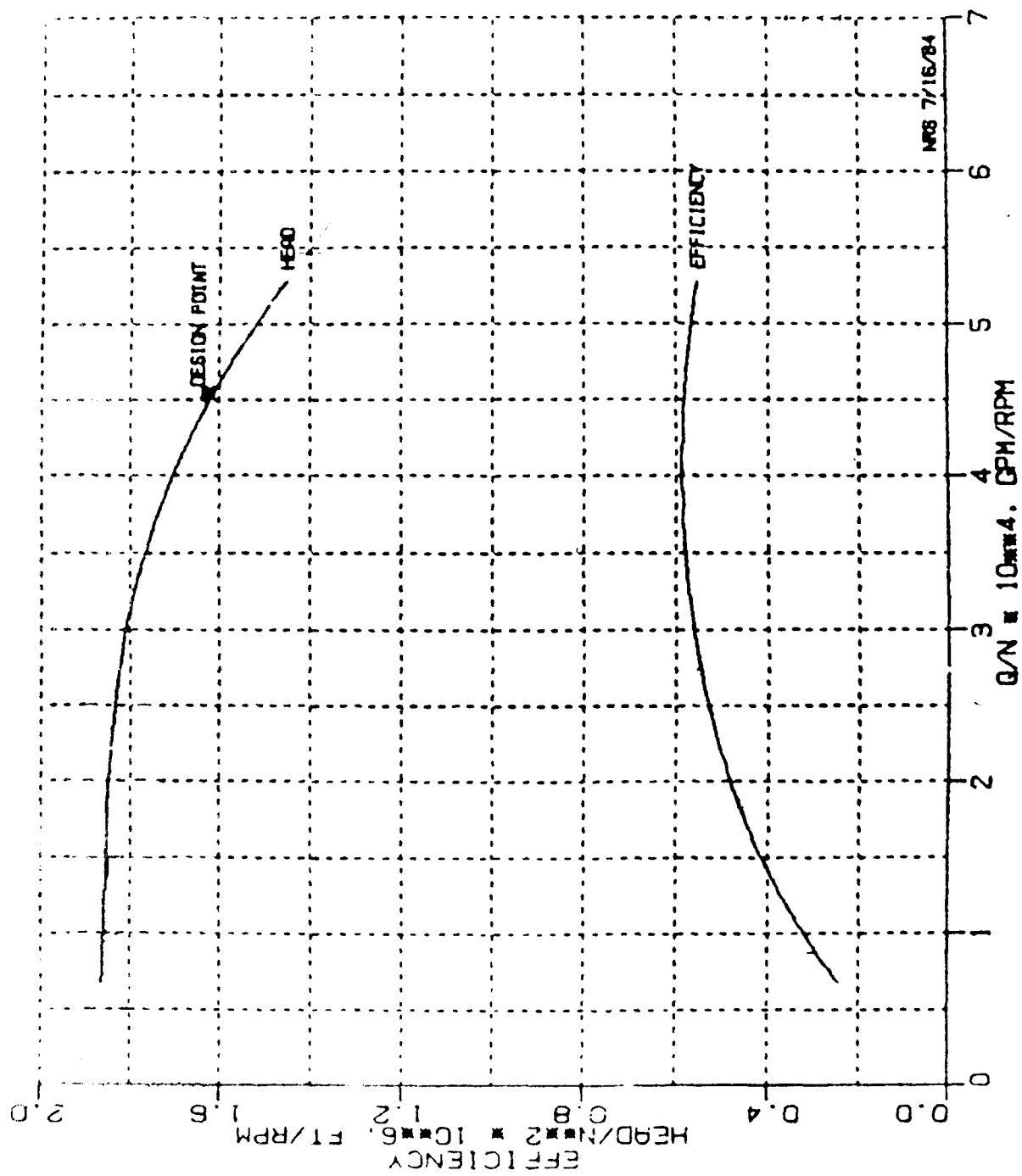


Figure 2.5-29. Predicted OTV Performance Overall Performance

TABLE 2.5-4
TURBINE SECTION DESIGN POINT

<u>Item</u>	<u>Design Value</u>
Engine Maximum Thrust, F	3000 lbf
Engine Chamber Pressure, P_c	2000 psia
Engine Chamber Cooling System Pressure Rise, ΔP_c	300 psi
Injector Pressure Drop, ΔP_i	300 psi
Turbine Speed	75,000 RPM
Number of Turbine Stages	1
Turbine Type	Full Admission, Impulse, Overhung Rotor
Pitch Diameter	1.333 inch
Inlet	Axial
Nozzle Vanes	60
Blades	71
Horsepower	156.4
GO ₂ Flow Rate	5.1 lbm/sec
Efficiency, η_T	70%
Engine Throttling Range	15:1
Inlet Total Pressure, P_0	4315 psia
Inlet Total Temperature, T_0	860°R
Exit Total Pressure, P_{O2}	2300 psia
Specific Heat, C_p	0.22 Btu/lb°R
Specific Heat Ratio, γ	1.4
Gas Constant, R	48.29 Ft-lb/lb°R

2.5, Detail Design, cont.

Blade Reaction

Turbine blade performance is a function of:

- | | | |
|---------------------------------|-------|---------------------------|
| • Velocity Ratio, U/C_0 | where | U = Mean blade speed |
| | | C_0 = Spouting velocity |
| • Clearance Ratio, δ_T/h | | h = Blade height |
| | | δ_T = Clearance |
| • Aspect Ratio, h/c | | c = Blade chord |
| • Reaction (no symbol) | | |

The velocity ratio for this turbine will be about 0.35 which is less than required for optimum efficiency of a single stage impulse turbine and more than needed for optimum efficiency of a reaction turbine. To minimize ignition potential due to rubbing friction in the oxygen environment, a large tip clearance ratio, $\delta_T/h \geq 0.04$, might be desired. The expected low aspect ratio, $h/c < 1.0$, would also favor an impulse turbine.

Since an impulse turbine requires lower U/C_0 and its performance is less affected by the large tip clearance and low aspect ratio (Reference 11), it was selected for this application.

Number of Stages

The performance advantage of a two-stage turbine over a single stage is substantially reduced for low aspect ratio blading with large tip clearances. Two-stage turbine blading requires four leak paths compared to one in the single-stage design (see Figure 2.5-30). Also, the ignition hazards of the two-stage turbine would be higher due to more potential rubbing surfaces. The lower mach number, however, (Figure 2.5-31) would tend to reduce these hazards.

A single-stage design would also be simpler and lighter allowing a larger critical speed margin than the more expensive two-stage configuration. In view of these considerations, a single-stage turbine was selected.

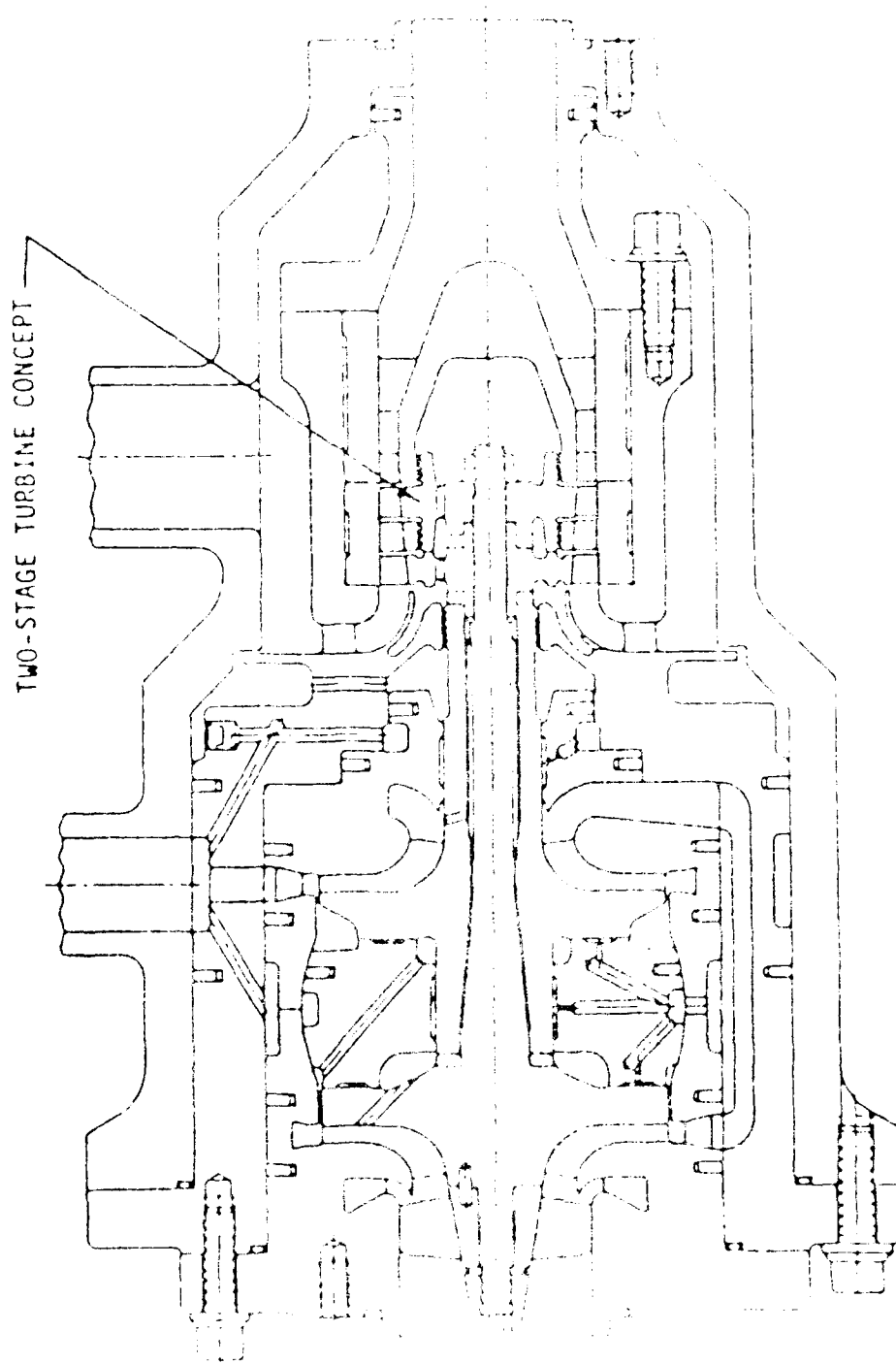


Figure 2.5-30. OTV LOX Turbopump

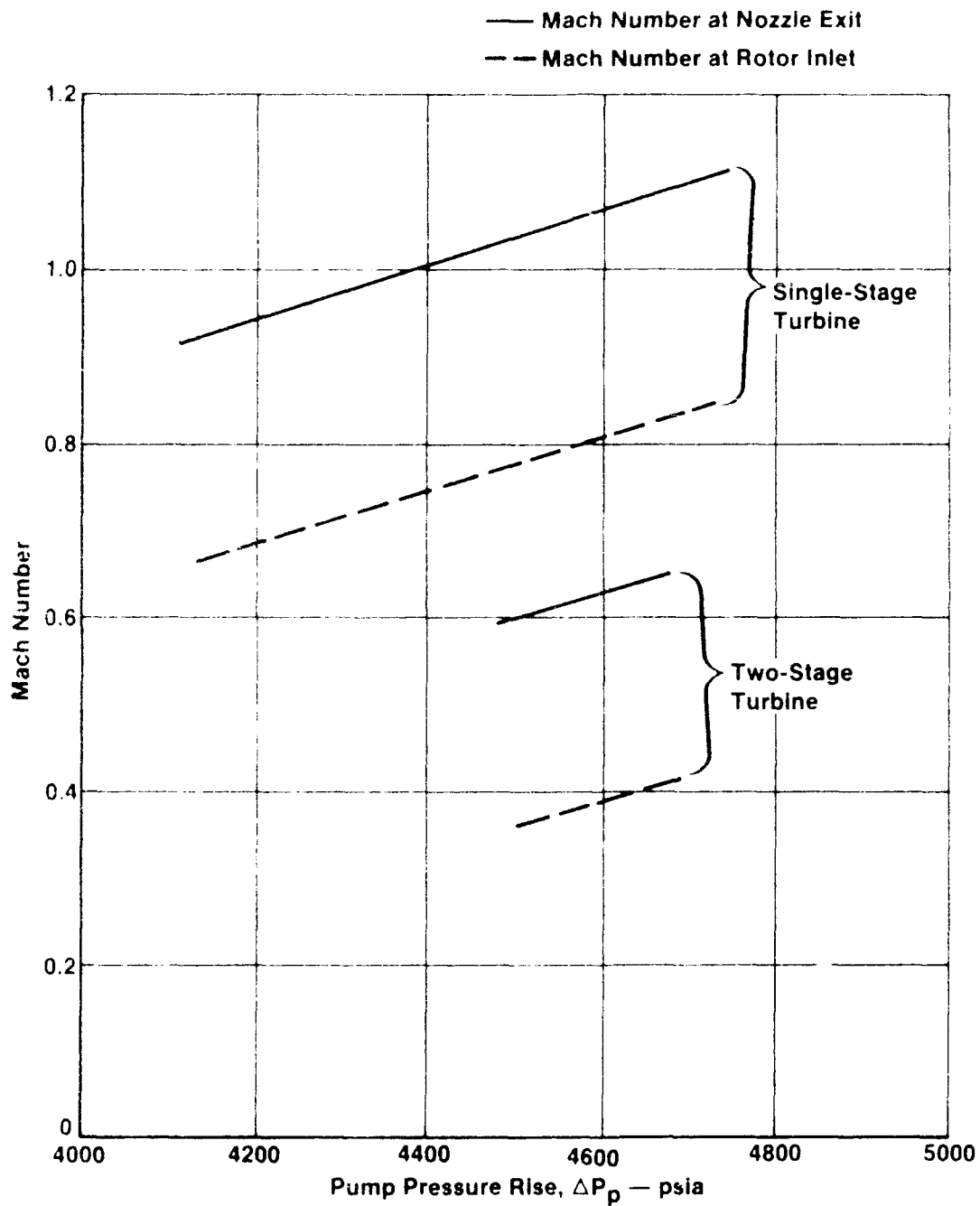


Figure 2.5-31. LOX Turbine Maximum Thrust Point Turbine Mach Numbers

2.5, Detail Design, cont.

Rotational Speed

Turbine speed selection involves a compromise of parameters effecting TPA design, fabrication and performance. Pump performance is commonly given as a function of speed. As the speed is increased, the impeller size becomes smaller and more difficult to fabricate. Also the shaft size, thrust balance and critical speed margin requirements become difficult to satisfy.

The effect of speed and pitch diameter can be seen in Table 2.5-5 where the speed is varied from 75K to 100K rpm. At 75K rpm, the increase in pitch diameter from 1.0 in. to 1.333 in. increased turbine efficiency by 3.4 points mainly due to an increase in the velocity ratio. At 100K rpm, the critical speed margin would not allow the pitch diameter to be larger than one inch. The estimated 72 percent efficiency for the 100K rpm turbine is probably too optimistic as it does not include the leakage through the stator labyrinth.

In conclusion, considering the performance, fabrication and critical speed aspects of the TPA, a 75K rpm was chosen.

Pitch Diameter

Pitch diameter selection effects:

- a. Velocity Ratio, U/C_o
- b. Blade Aspect Ratio, h/c
- c. Admission (Full or partial)
- d. Rotor Weight

Turbine admission, velocity ratio and aspect ratio influence turbine performance while the rotor weight relates to the critical speed margin. The compromise choice was a full admission, 1.333 in. pitch diameter turbine.

2.5.3.3 Turbine Loss Analysis

The losses in a full admission axial flow turbine are commonly divided into the following categories:

Table 2.5-5.
LOX Turbopump Speed Selection

Pump Design Point

Flow Rate,	\dot{W}_p	=	5.5 lb/sec
Pressure Rise,	ΔP_p	=	4600 psi
Efficiency,	η_p	=	0.65
Mechanical Efficiency,	η_m	=	0.90
Horsepower,	HP	=	156.4

Turbine Design Point

Speed, RPM	75K	80K	100K
Pitch Diameter, in	1.0	1.333	1.0
Inlet Total Pressure, psia	4315	4315	4315
Inlet Total Temperature, °R	860	860	860
Rotor Blade Height, in.	0.095	0.071	0.093
Tip Clearance, in.	0.005	0.003	0.005
Velocity Ratio, U/C_o	0.260	0.340	0.278
Total Efficiency	66.6	70.0	68.4
Bypass Flow, %	2.7	7.4	4.7

2.5, Detail Design, cont.

- a. Blade Profile Loss
- b. Blade Secondary Loss
- c. Tip Clearance Loss
- d. Disc Friction Loss
- e. Inlet and Exhaust Manifold Losses

The blade profile loss is a function of the following variables:

Aerodynamic Loading

Solidity, c/p

Max. thickness-to-chord ratio, t_{\max}/c

Reynolds number, Re

The profile loss coefficient is given by (Reference 12):

$$Y'_p = \left\{ Y_{p\alpha_0=0} + \left| \frac{\alpha_0}{\alpha_1} \right| \left(\frac{\alpha_0}{\alpha_1} \right) [Y_{p\alpha_0=\alpha_1} - Y_{p\alpha_0=0}] \right\} \left(\frac{t_{\max}/c}{0.2} \right) \frac{\alpha_0}{\alpha_1} \quad (1)$$

where α_0 = Inlet Flow angle, degrees

t_{\max} = maximum blade thickness

α_1 = Exit Flow Angle, degrees

κ = Trailing Edge Thickness Correction

$$= 1 + 7 \left(\frac{t_T}{p} - 0.02 \right) \quad (2)$$

where t_T = trailing edge thickness

$$Y_p = Y'_p + \kappa \quad (3)$$

2.5, Detail Design, cont.

The secondary loss coefficient, Y_s , depends on:

Aerodynamic loading
Blade Aspect Ratio, h/c
Reynold's Number

$$Y_s = 0.0334 \times \frac{\cos \alpha_1}{\cos \alpha_0} \times Z \times f_{AR} \quad (4)$$

$$\text{where } Z = \left(\frac{C_L}{P/C} \right)^2 \frac{\cos^2 \alpha_1}{\cos^3 \alpha_m} \quad (5)$$

$$\alpha_m = \tan^{-1} \left\{ 1/2 \left(\tan \alpha_0 + \tan \alpha_1 \right) \right\} \quad (6)$$

$$C_L = 2 \left(\frac{P}{C} \right) \left[\tan \alpha_0 - \tan \alpha_1 \right] \cos \alpha_m \quad (7)$$

$$f_{AR} = \frac{1 - 0.25 \sqrt{2 - h/c}}{h/c} \quad (8)$$

and the total loss coefficient (excluding tip clearance) is

$$Y = (Y_p + Y_s) f(Re) \quad (9)$$

$$\begin{aligned} \text{where } f(Re) &= \left(\frac{Re}{2 \times 10^5} \right)^{-0.4} && \text{For } Re \leq 2 \times 10^5 \\ &= 1.0 && \text{For } 2 \times 10^5 < Re < 10^6 \\ &= \left(\frac{Re}{10^6} \right)^{-0.2} && \text{For } Re > 10^6 \end{aligned} \quad (10)$$

The total loss coefficient, Y , can be converted to the Enthalpy loss coefficient, ξ , by the relation:

$$\xi = \frac{Y}{Y + F} \quad (11)$$

2.5, Detail Design, cont.

The factor F is a function of exit mach (M_2) and Gamma (γ) (Reference 13) and is plotted in Figure 2.5-32. In this report, velocity coefficients (ψ) will be used.

$$\psi = \sqrt{1 - \xi} \quad (12)$$

The tip leakage is

$$C_L = 1 - \frac{(D+h) \delta_T}{D(h + \delta_T)} \quad (13)$$

and the disc friction loss is

$$HP_D = 0.0083 p_1 \left(\frac{N}{1000} \right)^3 \left(\frac{D_T}{12} \right)^5 \left(1 - \frac{h}{D} \right)^{4.5} \quad (14)$$

where N = shaft speed h = blade height
 D_T = diameter at trailing edge D = pitch diameter

Inlet and exit duct losses are assumed to be included in the 300 psi cooling jacket loss and the turbine efficiency is based on nozzle inlet and rotor exit conditions.

The isentropic enthalpy drop is

$$\Delta H_i = C_p T_o \left[1 - \left(\frac{1}{PR_s} \right)^{\frac{\gamma-1}{\gamma}} \right] \quad (15)$$

where C_p = specific heat at control pressure
 γ = ratio of specific heats
 H_i = Isentropic enthalpy
 R_s = gas constant
 P = pressure
 T_o = inlet temperature

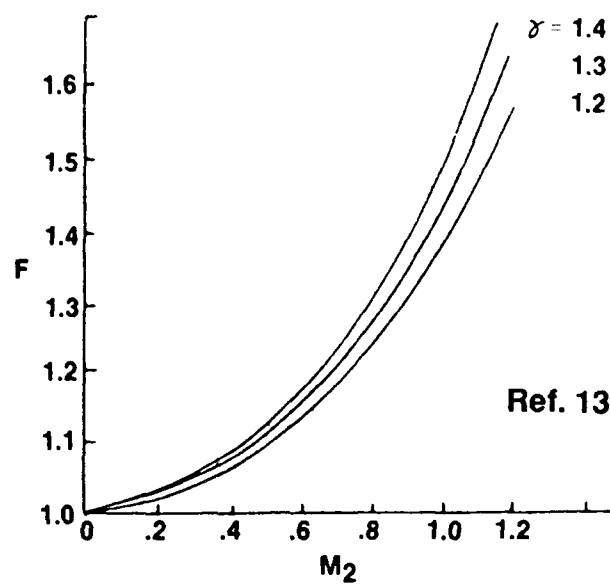


Figure 2.5-32. Relation Between Factor F and Exit Mach Number

2.5, Detail Design, cont.

and the spouting velocity is

$$C_0 = 223.78 \sqrt{\Delta H_i} \quad (16)$$

The blade velocity is

$$U = \frac{I I D N}{720} \quad (17)$$

and the velocity ratio is U/C_0

The blade efficiency is given by

$$\eta_B = 2 \frac{U}{C_0} (1 + \psi_R) \left(\psi_N \sin \alpha_1 - \frac{U}{C_0} \right) \quad (18)$$

where ψ_R = rotor velocity coefficient
 ψ_N = nozzle velocity coefficient

The horsepower is

$$HP = \left[\frac{\dot{W}_T \Delta H_i \eta_B J}{550} \times C_L \right] - HP_D \quad (19)$$

and the total efficiency is

$$\eta_T = \frac{550 HP}{\dot{W}_T \Delta H_i J} \quad (20)$$

2.5.3.4 Turbine Thermodynamic Analysis

As mentioned earlier, the turbine was designed to drive the LOX pump at 75,000 RPM with gaseous oxygen as the working fluid. The design point values are listed in Table 2.5-5 and 2.5-6.

Table 2.5-6.
Turbine Design Values

Total-To-Total Pressure Ratio, P_o/P_{o2}	1.868
Total-To-Total Isentropic Enthalpy Drop, ΔH_I , BTU/Lb	30.93
Rotational Speed, N - RPM	75,000
Blade Mean Diameter (Pitch Diameter) D-in.	1.333
Flow Rate, W_T - Lb/Sec	5.095
Torque, τ - Ft.Lb.	11.0
Horsepower, HP	156.4

Stage Parameters

Nozzle

Inlet Total Pressure, P_o - psia	4315.0
Inlet Total Temperature, T_o - °R	860.0
Inlet Flow Angle, α_o - Degrees	0.0
Velocity Coefficient, Ψ_N	0.957
Exit Static Pressure, P_1 - psia	2235.8
Exit Total Pressure, P_{o1} - psia	4062.2
Exit Flow Angle, α_1 - Degrees	75.0

Rotor

Inlet Relative Total Pressure, P_{o1R} - psia	2938.8
Inlet Relative Total Temperature, T_{o1R} - °R	724.0
Inlet Relative Flow Angle, β_1 - Degrees	66.9
Velocity Coefficient, Ψ_R	0.766
Exit Static Pressure, P_2 - psia	2235.8
Exit Relative Total Pressure, P_{o2R} - psia	2310.2
Exit Total Temperature, T_{o2} - °R	756.7
Exit Relative Flow Angle, β_2 - Degrees	66.9

2.5, Detail Design, cont.

A turbine velocity diagram is shown in Figure 2.5-33. It can be seen that the nozzle ($M_1 = 0.97$) and the rotor ($M_{1R} = 0.64$) are subsonic. The gas is leaving the rotor with a 30 degree swirl.

2.5.3.5 Design Point Performance Prediction

Performance analysis begins by assuming velocity coefficients and then conducting a detail blade loss analysis as shown in Table 2.5-7. Usually, several iterations are required to complete the analysis. The results are summarized in Table 2.5-8 resulting in a total efficiency of 70 percent at the U/C_o of 0.348.

The effect of rotor tip clearance on efficiency of an impulse turbine is shown in Table 2.5-9 (Reference 14). This effect varies with the size and the type of the tip clearance. Increasing tip clearance from 0.003 to 0.005 in. will reduce efficiency by two points for a simple clearance type, one point for a recessed housing type and only 0.4 points for shrouded blades.

2.5.3.6 Off-Design Performance Estimate

Figures 2.5-34 and 2.5-35 show the estimated turbine off-design characteristics. Total efficiency, η_T , versus velocity ratio, U/C_o , is plotted in Figure 2.5-34 while the flow parameter, $\dot{W}_T \sqrt{T_o/P_o}$, is plotted in Figure 2.5-35. These plots are used to analyze the TPA power balance at the minimum thrust point.

2.5.3.7 Nozzle Vane Profile Design

The construction of the nozzle vane profiles is shown in Figure 2.5-36. a parabolic camber line and a 50 degree stagger angle are used for the construction. The leading and trailing edges are 0.012 and 0.003, respectively. The solidity, c/P , and aspect ratio, h/c , are 1.66 and 0.52. Nozzle profile parameters are given in Table 2.5-10.

Pitch Diameter = 1.333 in.
 Speed = 75,000 rpm
 Inlet Total Pressure = 4315 psia
 Inlet Total Temperature = 860°R
 Total Pressure Ratio = 1.868

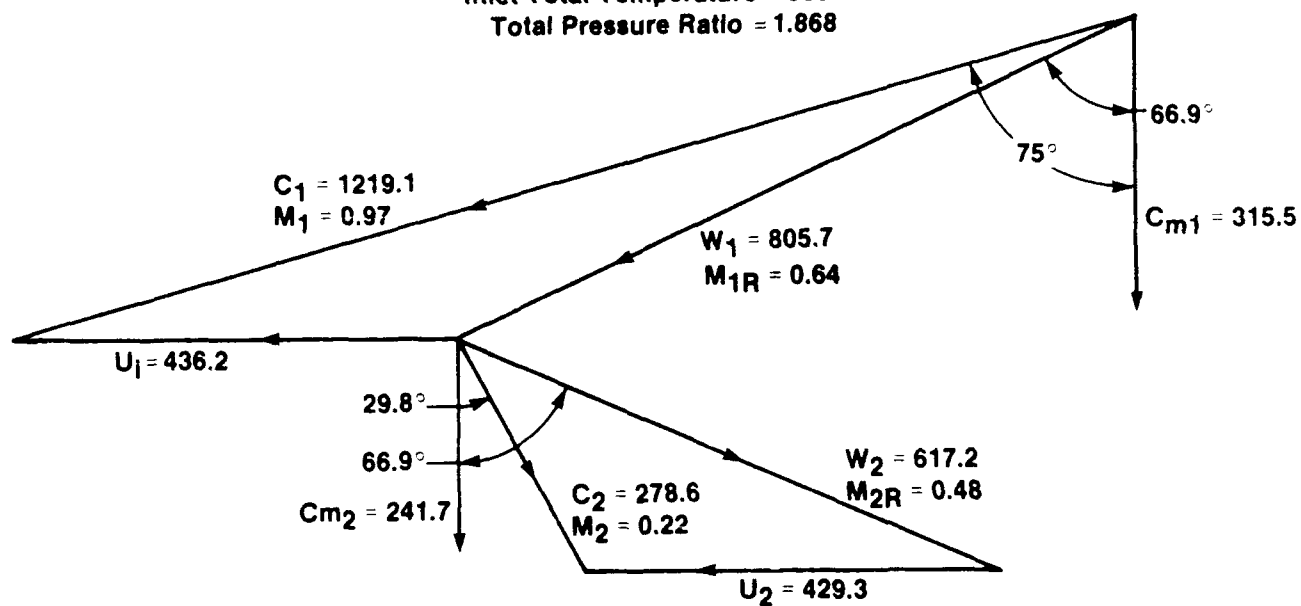


Figure 2.5-33. OTV LOX Turbine Velocity Diagram

Table 2.5-7.
Nozzle and Rotor Blade Loss Analysis

$N = 75,000 \text{ RPM}; D = 1.333 \text{ in.}$

	<u>Nozzle</u>	<u>Rotor</u>
Number of Blades	60	71
Blade Pitch, p - in.	0.0698	0.0590
Pitch/Chord, P/C	0.6017	0.602
Chord, c - in.	0.116	0.098
Blade Height, h - in.	0.0604	0.071
Aspect Ratio, h/c	0.521	0.724
Throat Opening, inches	0.0181	0.0231
Throat Opening/Pitch, O/P	0.259	0.392
Trailing Edge Thickness, t_T - in.	0.003	0.005
t_T/p	0.043	0.085
Thickness/Chord, t_{\max}/c	0.18	0.366
Y'_p (Equation 1)	0.043	0.240
k (Equation 2)	1.16	1.45
Profile Loss, $Y_p = Y'_p \times k$ (Equation 3)	0.050	0.349
Lift Coefficient, C_L (Equation 7)	2.122	5.656
Z (Equation 5)	7.902	13.545
α_m (Equation 6), degrees	61.8	0°
f_{AR} (Equation 8)	1.336	0.991
Secondary Loss Coefficient, Y_s (Equation 4)	0.091	0.448
Reynold's Number, $Re = \frac{CC_1}{\nu}$	4.93×10^6	2.04×10^6
$f(Re) = (Re/10^6)^{-0.2}$	0.727	0.867
Total Loss Coefficient, $Y = (Y_p + Y_s)f(Re)$	0.103	0.691
F (from Figure 2.5-32)	1.47	1.11
$\xi = \frac{Y}{Y+F}$	0.066	0.384
Velocity Coefficient, $\psi = \sqrt{1-\xi}$	0.967	0.785

Table 2.5-8.
Design Point Performance Prediction

Blade Velocity, u - Ft/Sec	432.76
Spouting Velocity, C_0 - Ft/Sec	1244.55
Velocity Ratio, U/C_0	0.348
Tip Clearance, δ_T - in	0.003
Tip Clearance Loss Coefficient, C_L	0.958
Disc Friction Loss, HP_D	0.53
Static Efficiency, η_s	0.67
Total Efficiency, η_T	0.70

Table 2.5-9.
Effect of Rotor Tip Clearance on Efficiency

	Reduced Blade Height		Recessed Housing		Shrouded Blades	
Tip Clearance, δ_T - in.	0.003	0.005	0.003	0.005	0.003	0.005
Total Efficiency, η_T - %	70.0	68.0	71.8	70.7	73.2	72.8

(Preliminary)

η_t vs U/C_0

Pitch Diameter = 1.333 in.

Rotational Speed = 75K RPM

Total Pressure Ratio = 1.868

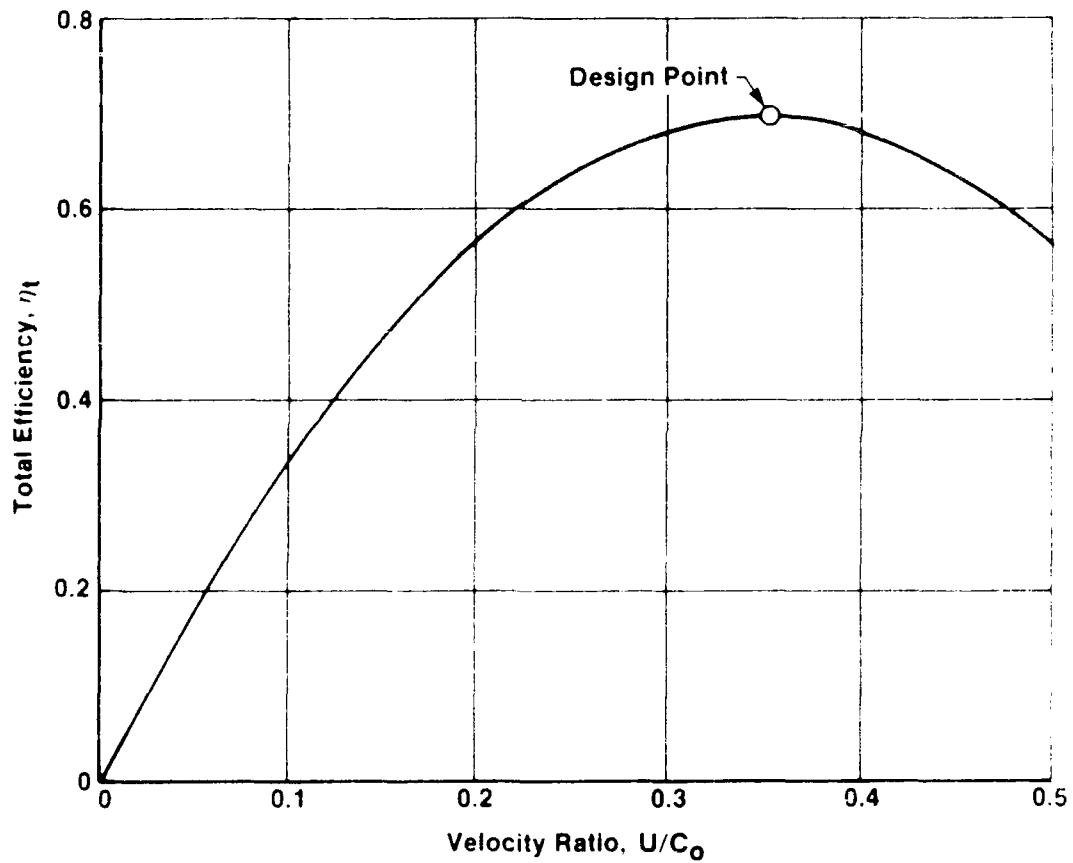


Figure 2.5-34. Turbine Performance Characteristics

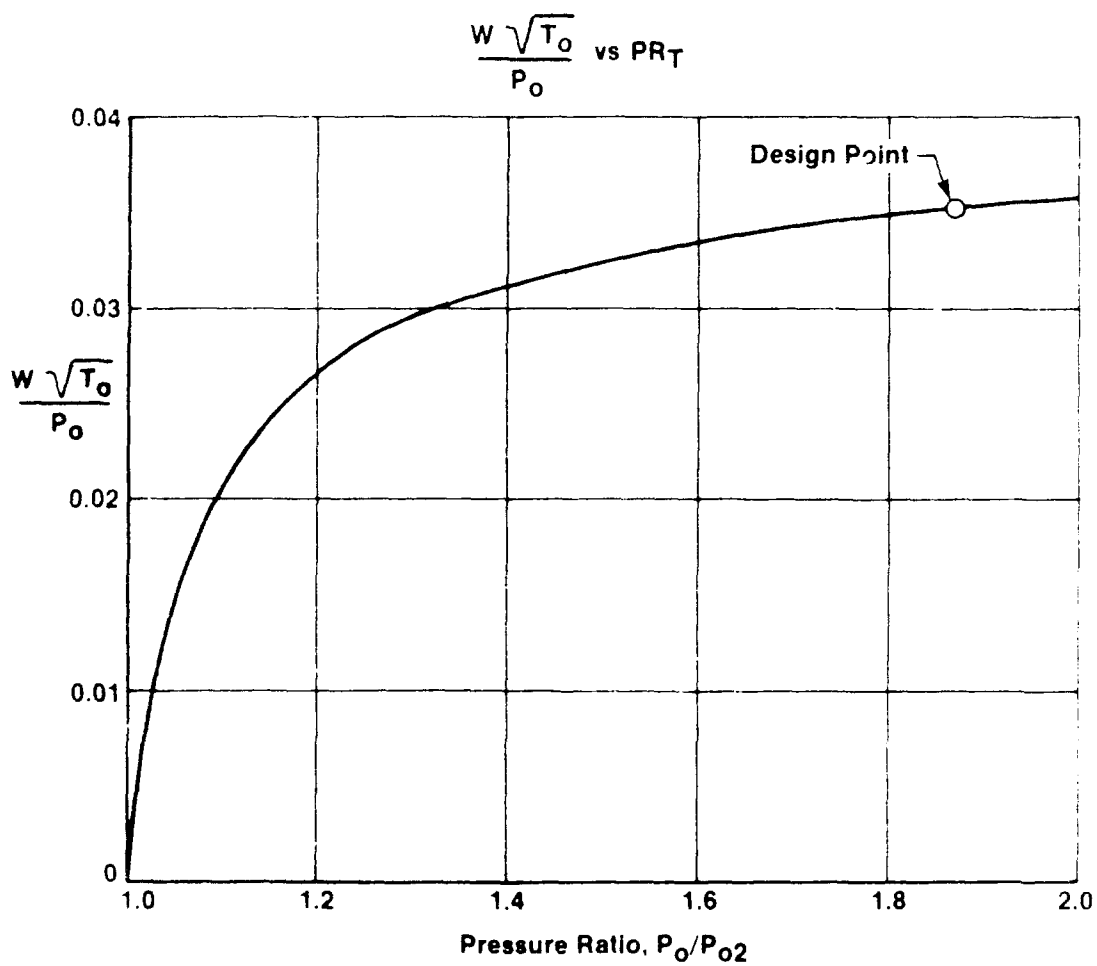
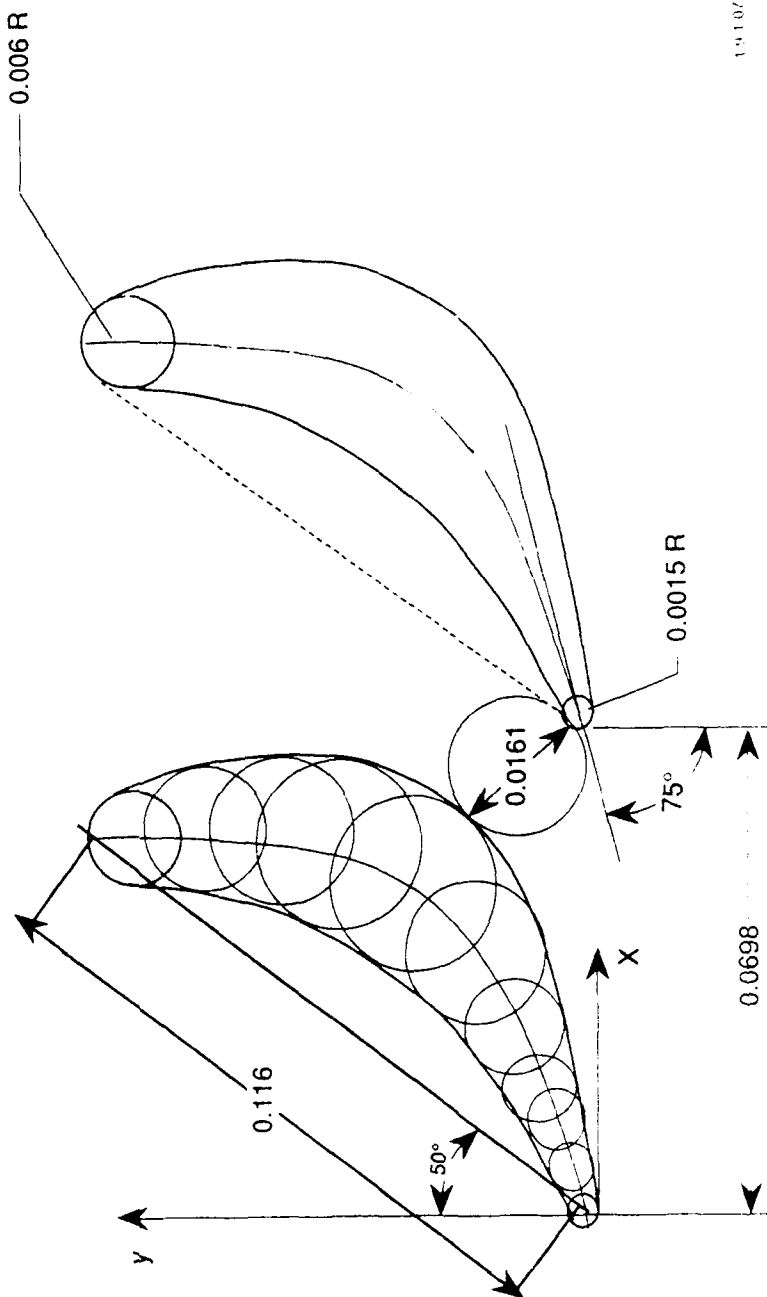


Figure 2.5-35. Turbine Performance Characteristics

X, In	Y _P , In	Y _S , In
0	0	0
0.02	0.0105	0.0029
0.03	0.0154	0.0055
0.04	0.0210	0.0086
0.05	0.0277	0.0123
0.06	0.0376	0.0165
0.07	0.0500	0.0220
0.08	0.0654	0.0296
0.0899	0.0	0.0
0.096		0.0600

Nozzle Pitch Diameter = 1.333 In
 Number of Vanes = 60
 Solidity, C/P = 1.662
 Aspect Ratio, h/c = 0.52



1-5107

Figure 2.5-36. OTV LOX Turbine Nozzle Contour

Table 2.5-10.
Nozzle Vane Profile Parameters

Number of Vanes,	60
Inlet Angle, α_0 - Degrees	0
Leading Edge Radius, R_L - in.	0.006
Chord, c - in.	0.116
Pitch, p - in.	0.0698
Solidity, c/p	1.66
Thickness/Chord, t_{max}/c	0.18
Height, h - in.	0.0604
Aspect Ratio, h/c	0.52
Throat Opening, "O" - in.	0.0181
Stagger Angle, γ_N - Degrees	50.0
Exit Angle, α_1 - Degrees	75.0
Trailing Edge Radius, R_T - in.	0.0015

Table 2.5-11.
Rotor Blade Profile Parameters

Number of Blades	71
Inlet Angle, β_1 - Degrees	66.9
Leading Edge Radius, R_L - in.	0.0025
Chord, c - in.	0.098
Pitch, p - in.	0.059
Solidity, c/p	1.66
Thickness/Chord, t_{max}/c	0.366
Height at Inlet, L_1 - in.	0.0604
Height at Exit, h_2 - in.	0.0815
Aspect Ratio, h/C	0.724
Stagger Angle, γ_R - Degrees	0.0
Exit Angle, β_2 - Degrees	66.9
Trailing Edge Radius, R_T - in.	0.0025

2.5, Detail Design, cont.

2.5.3.8 Rotor Blade Profile Design

A symmetrical rotor blade profile is constructed using arcs for the suction and pressure surfaces. Seventy-one untwisted blades having 0.005 in. thick leading and trailing edges and the solidity, c/P , of 1.66 are specified. Table 2.5-7 lists all rotor blade parameters. Rotor blade contour is shown in Figure 2.5-37.

2.5.3.9 Turbine Flow Passages

Figure 2.5-38 shows the turbine flow passage. The nozzle vane height is constant while the rotor flow passage is flared at the hub to allow for blade losses and a change in the gas density. The rotor tip clearance in hot running conditions is assumed to be 0.003 in. Gaseous oxygen enters turbine nozzles through an axisymmetric inlet and leaves the rotor in a radially outward direction. The final design turbine configuration can be seen in Figure 2.5-39.

2.5.3.10 Turbopump Power Balance at Minimum Thrust Point

The minimum thrust point is obtained by throttling the LOX pump from the design $Q/N \times 10^4 = 4.5$ to $Q/N \times 10^4 = 0.85$. The corresponding pump head and efficiency are,

$$\frac{H}{N^2} \times 10^6 = 1.865$$

$$\eta_p = 0.29$$

If the pump pressure rise of 800 psi is assumed (above critical), the estimated turbine exit temperature is 1316°R at a mixture ratio of 5. The pump head is,

$$H = \frac{144 \Delta P_p}{\rho_p} = \frac{144 \times 800}{72.4}$$

$$H = 1591.16 \text{ Ft.}$$

ROTOR BLADE CONTOUR

BLADE PITCH DIAMETER = 1.333 in.

NUMBER OF BLADES = 71

SOLIDITY, $C/P = 1.66$

ASPECT RATIO, $h/c = 0.724$

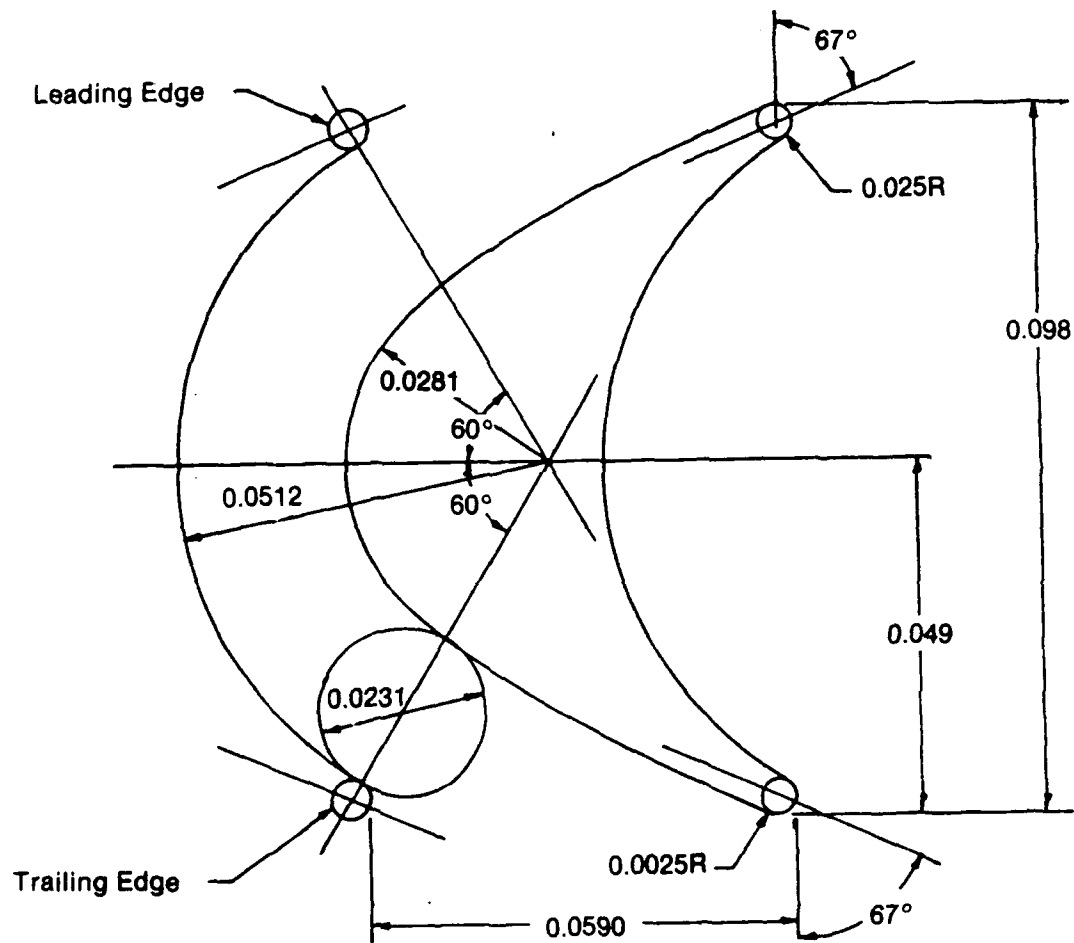


Figure 2.5-37. Preliminary Sketch of Rotor Blade Contour

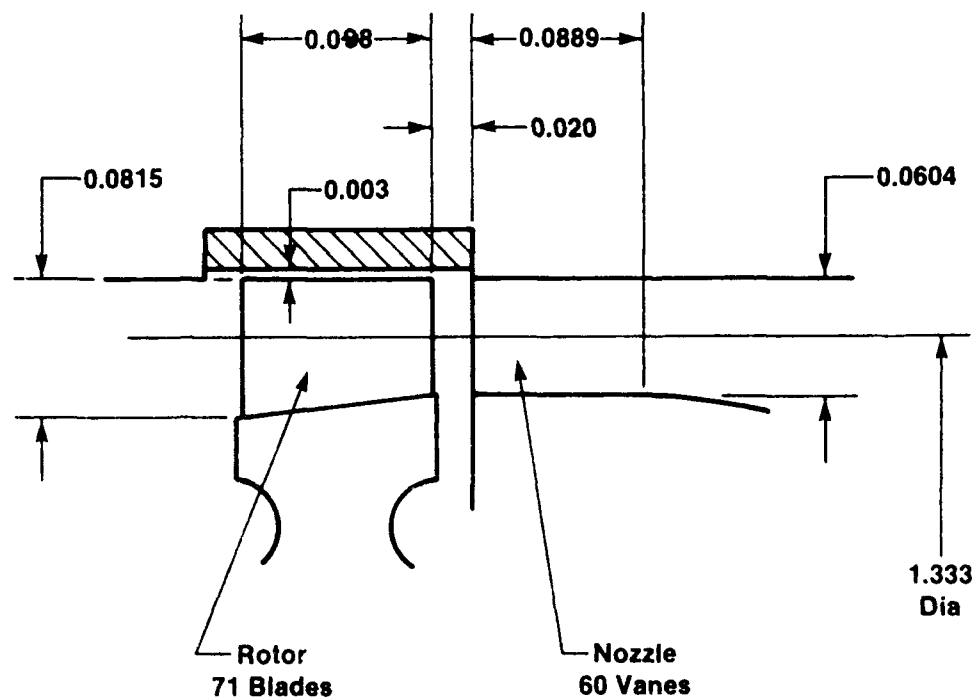


Figure 2.5-38. OTV LOX Turbine Flow Passage

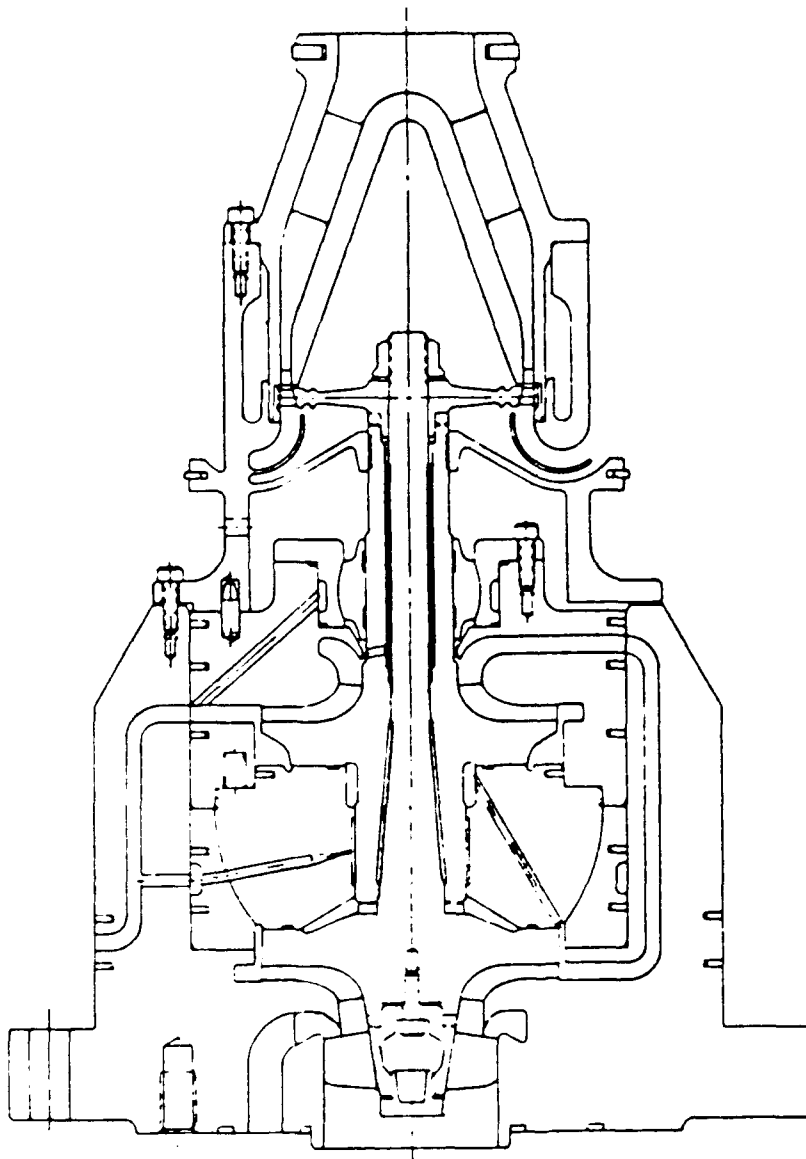


Figure 2.5-39. OTV LOX Turbopump

2.5, Detail Design, cont.

and the pump speed is

$$N = \sqrt{\frac{H \times 10^6}{1.865}} = \sqrt{\frac{1591.16 \times 10^6}{1.865}}$$

$$N = \underline{29,209 \text{ RPM}}$$

The pump flow is

$$\dot{W}_p = \frac{Q}{N} \times \text{C.F.} \times \rho_p \times N = \frac{0.85 \times 2.228}{10^7} \times 72.4 \times 29,209 = 0.40 \text{ lbm/sec}$$

$$\text{where C.F.} = \text{conversion factor} = \frac{\text{ft}^3 \times \text{minute}}{7.48 \text{ gal} \times 60 \text{ sec}}$$

and 0.85×2.228 are from the pump $Q/N \times 10^4$ curve at minimum thrust

and the horsepower is

$$\text{HP} = \frac{\dot{W}_p H}{550 \eta_p \eta_m}$$

$$\eta_m = 0.9 \text{ (assumed)}$$

$$\text{HP} = \frac{0.40 \times 1591.16}{550 \times 0.29 \times 0.9} = \underline{4.43}$$

Knowing TPA horsepower and speed, the turbine power balance point can be calculated assuming turbine pressure ratio and using Figures 2.5-34 and 2.5-35. The results of the analysis are presented in Table 2.5-12 and Figure 2.5-40.

Examination of Figure 2.5-40 shows there is excess pressure available to drive the turbine. A turbine bypass valve is required in parallel with the turbine for control. The power to drive the pump can be provided with a low turbine pressure ratio of 1.51, flow rate of 0.228 lb/sec and efficiency of 0.428.

Table 2.5-12.
Turbine Power Balance at Minimum Thrust Point

PR_T	1.4	1.5	1.6	1.7
ΔH_i , BTU/Lb	26.562	31.70	36.415	40.766
C_0 , Ft/Sec.	1153.33	1259.95	1350.40	1428.80
U , Ft/Sec.	169.89	169.89	169.89	169.89
U/C_0	0.147	0.135	0.126	0.119
η_T	0.460	0.430	0.410	0.390
$W_T \sqrt{T_0}/P_0$	0.0312	0.0325	0.0335	0.0343
W_T , Lb/Sec.	0.256	0.230	0.210	0.197
P_0 , psia	297.66	256.73	227.41	208.35
P_{02} , psia	212.61	171.15	142.13	122.56
WB.P. %	36.0	42.5	47.5	50.8

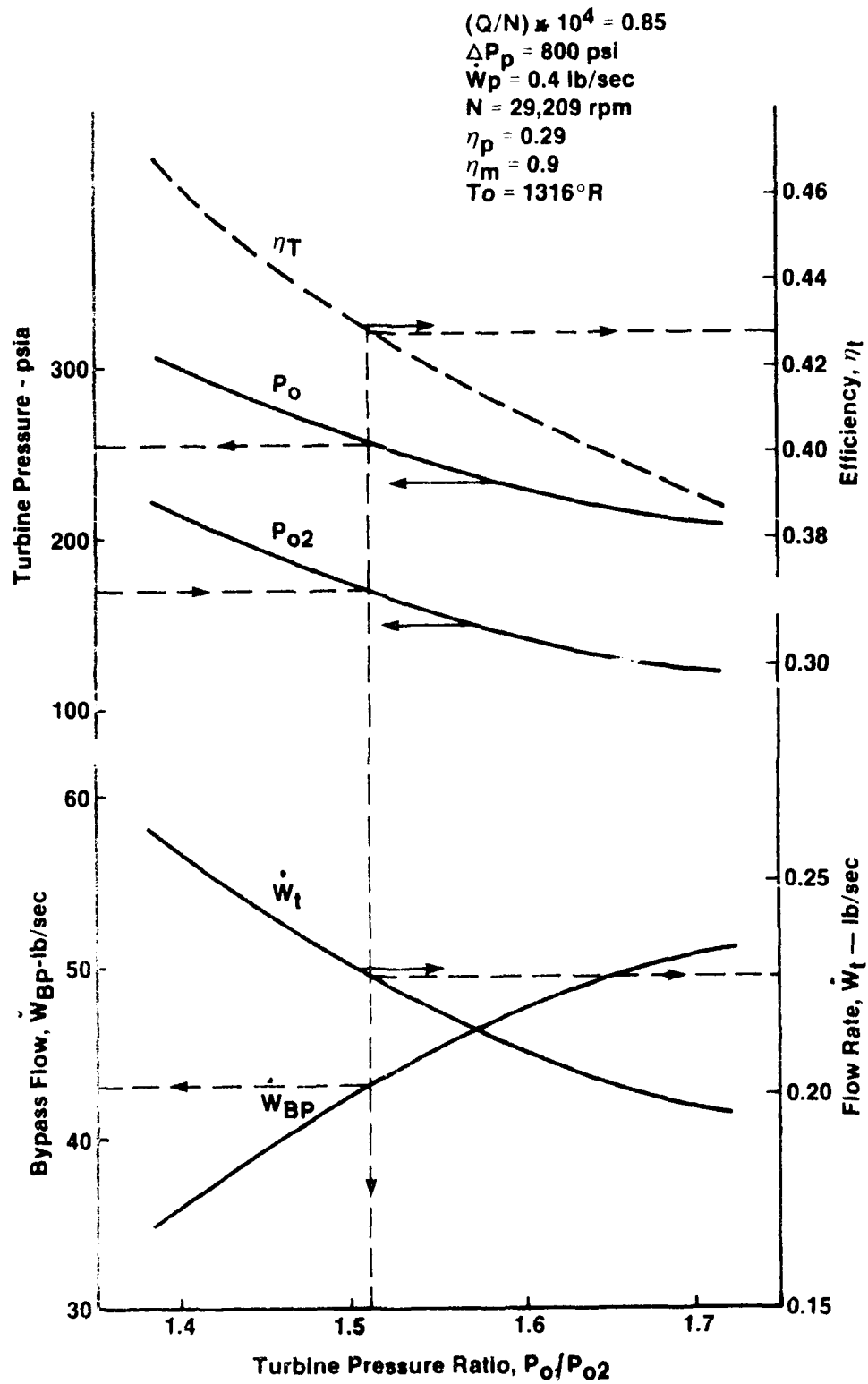


Figure 2.5-40. O₂ Turbopump Power Balance at Minimum Thrust

2.5, Detail Design, cont.

2.5.3.11 Conclusions

The turbine was designed to meet the OTV LOX turbopump requirements with the following results:

- a. A simplified engine power balance at the maximum thrust point (3750 lbf) was used to select the turbopump design point (pump: $\Delta P_p = 4600$ psi., $\dot{W}_p = 5.5$ lb/sec; turbine $P_o = 4315$ psia, $T_o = 860^\circ\text{R}$, $P_{o2} = 2300$ psia).
- b. Trade studies were performed to select the type of turbine best suited to the OTV LOX turbopump requirements. The selected concept is a single-stage, full admission, impulse turbine having 1.333 inch pitch diameter and operating at 75,000 RPM.
- c. At the engine nominal operating point of 3000 lb thrust, the predicted turbine gaseous oxygen consumption and efficiency are 5.1 lb/sec and 70 percent, respectively.
- d. A simplified power balance at the minimum thrust point indicates that the engine thrust can be throttled by a factor of 15.

2.5.3.12 List of Symbols

c	Chord	in
C_p	Specific Heat at Constant Pressure	Btu/Lb. $^\circ\text{R}$
C	Absolute Velocity	Ft/Sec
C_L	Lift Coefficient or Tip Leakage Loss Coefficient	—
C_o	Spouting Velocity	Ft/Sec
D	Pitch Diameter	in
f_{AR}	Aspect Ratio Function	—
F	Equation (11) or Fuel	—
h	Blade Height	in
H	Head	Ft.
ΔH	Enthalpy Drop	Btu/Lb.

2.5, Detail Design, cont.

List of Symbols (cont)

HP	Horsepower	—
J	Mechanical Equivalent of Heat	Ft Lb/Btu
κ	Trailing Edge Thickness Correction	—
M	Mach Number	—
N	Speed	RPM
o	Throat Opening	in
O	Oxidizer	—
p	Pitch	in
P	Static Pressure	psia
P_o	Total Pressure	psia
ΔP	Total Pressure Drop	psi
PR	Pressure Ratio	—
Q	Propellant Flow	GPM
r	Radius	in
R	Gas Constant	Ft Lb/Lb°R
Re	Reynolds Number	—
T	Static Temperature	°R
T_o	Total Temperature	°R
U	Blade Pitch Velocity	Ft/Sec
W	Relative Velocity	Ft/Sec
W	Flow Rate	Lb/Sec
Y	Pressure Loss Coefficient	—
Z	Equation (9)	—
α	Absolute Flow Angle	Degrees
β	Relative Flow Angle	Degrees
γ	Stagger Angle	Degrees
γ	Specific Heat Ratio	—
δ	Clearance	in
ψ	Velocity Coefficient	—
ρ	Density	Lb/Ft ³

2.5, Detail Design, cont.

List of Symbols (cont)

η	Efficiency	—
$\bar{\eta}$	$\eta_p \eta_T \eta_m$	—
ξ	Enthalpy Loss Coefficient	—
τ	Torque	Ft. Lb.
ν	Kinematic Viscosity	Ft. ² /sec.

Subscripts

B	Blade
BP	Bypass
c	Chamber or Cooling System
D	Disc
i	Injector or Isentropic
L	Leading Edge
m	Axial Direction, Mean or Mechanical
N	Nozzle
p	Pump or Profile
R	Rotor or Relative
S	Rotor or Relative
T	Trailing Edge or Total
o	Nozzle Inlet
1	Nozzle Exit or Rotor Inlet
2	Rotor Exit

2.5, Detail Design, cont.

2.5.4 Housing Design

The turbopump housing, as can be seen in the photo in Figure 2.5-41, has considerable design complexity. The initial drawing package was reviewed with several fabricators in a series of meetings in September 1984. These vendors suggested several changes to simplify the fabrication. The final package of 32 drawings incorporated most of the suggested changes to ease fabrication.

The four major sections of the housing are the first and second stage pump housings, the turbine housing, and the main turbopump housing. Figure 2.5-42 is ATC 11975114 sheet 1, which is the drawing showing the TPA housing end views. Figure 2.5-43 is ATC 1197514 sheet 2. It shows a cross section of the TPA housing. The final Figure 2.5-44, is ATC 1197514 sheet 3. It shows a top external view of the main housing depicting the four pump and two canted extended turbine exit flanges.

The materials selected for the bearing test unit are shown in Figure 2.3-1. Note that the major structure of the housing is Monel 400. Important properties of candidate materials are listed in Table 2.5-13.

The bolted flanges and accessible instrumentation ports are typical of a test article where mechanical connections and ready changeout of instrumentation are needed. A flight type turbopump housing would not require this outer housing and would be considerably lighter, less complex, and have a reduced number of seals, see Figure 2.5-26.

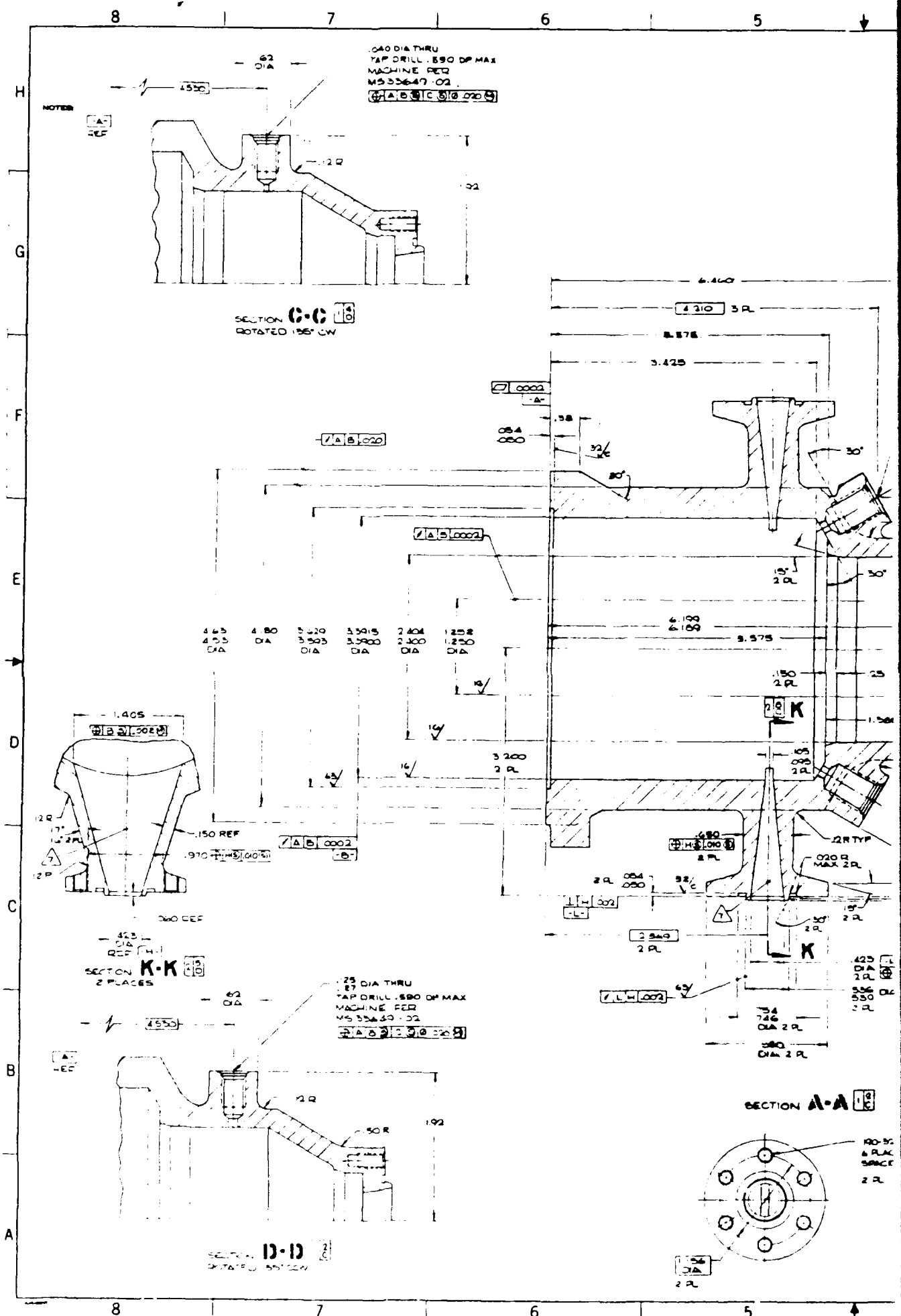
This housing configuration represented the inner contour of a thrust chamber centerbody in its geometry. It served as a pressure vessel for the turbopump. A requirement for this turbopump design was a large radial temperature gradient. The mechanical design was configured to accommodate radial growth without affecting seals or rotor to stator alignment.

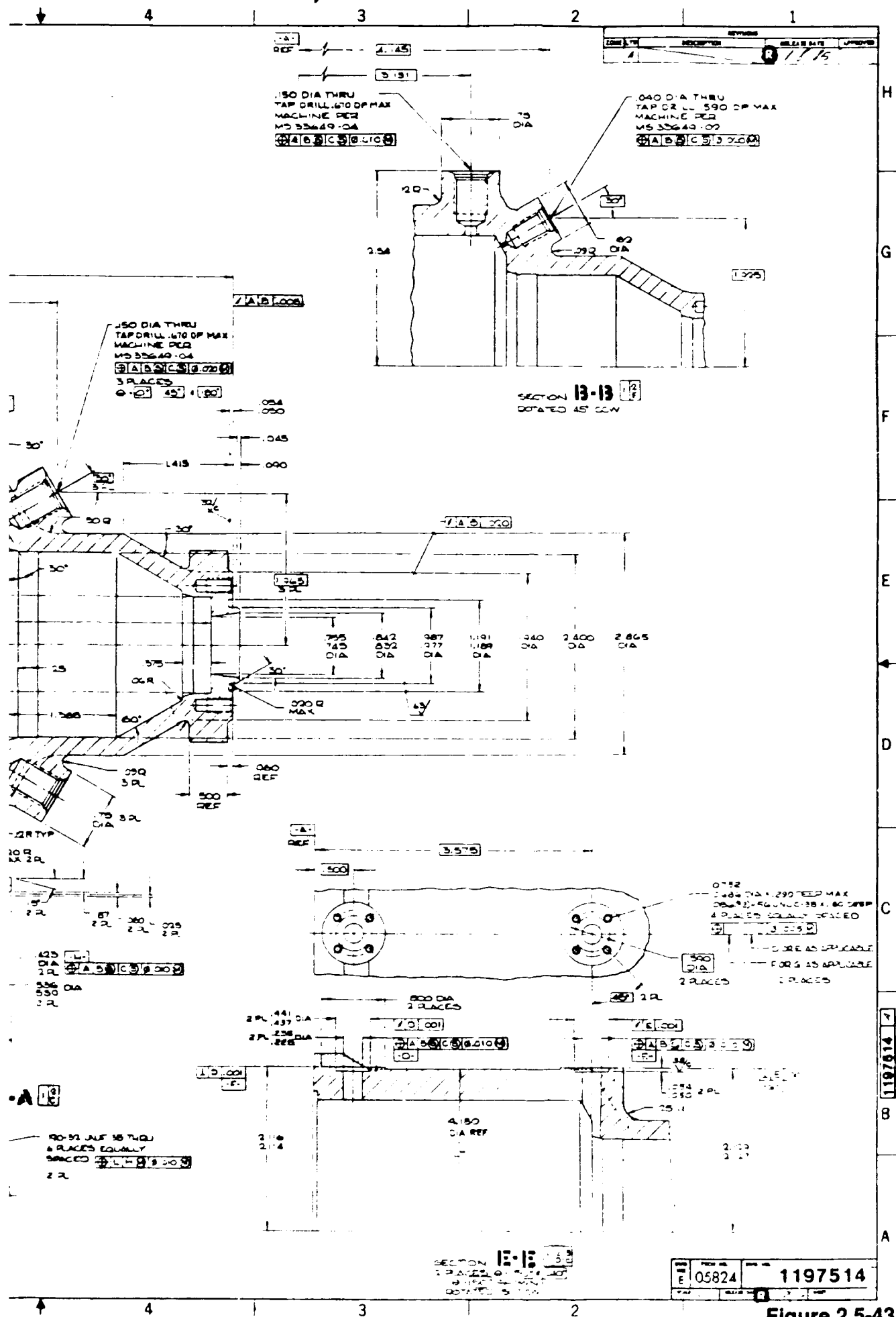


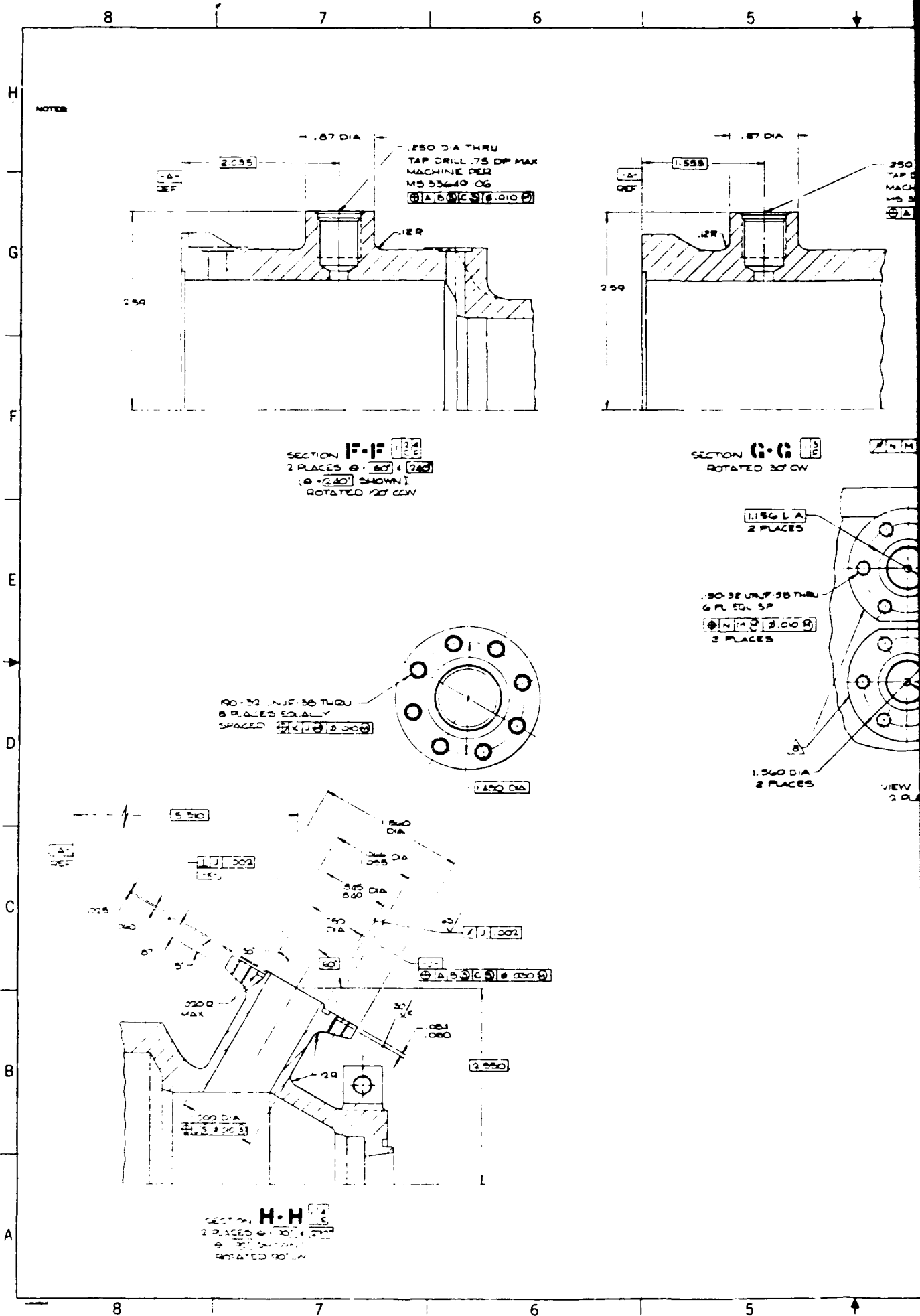
Figure 2.5-41. Bearing Tester Initial Installation

TABLE 2.5-13
IMPORTANT PROPERTIES OF CANDIDATE MATERIALS

Material	Density (lb/in. ³)	Yield Strength lb/in. ²	Modulus lb/in. ²	Thermal Conductivity BTU-ft/hr-ft ² °F	Thermal Expansion Coefficient in./in.°F	Burn Factor CAL-s/g-cm ²
Inco 718	0.296	147,000	30.4 x 10 ⁶	7.25	7.8 x 10 ⁻⁶	4600
Silver	0.379	8000	12 x 10 ⁶	242	10.9 x 10 ⁻⁶	2
Monel 400	0.319	70,000	26 x 10 ⁶	12.6	7.7 x 10 ⁻⁶	1390
K Morel	0.306	100,000	26 x 10 ⁶	10.1	8.7 x 10 ⁻⁶	2462
Nickel 201	0.321	10,600	29.6 x 10 ⁶	44	8.5 x 10 ⁻⁶	35
Zirconium Copper	0.323	38,000	18.7 x 10 ⁶	212	9.8 x 10 ⁻⁶	550
Silicon Carbide	.114	20,000T 5000,000C	60 x 10 ⁶	33	2.2 x 10 ⁻⁶	1145







2.5, Detail Design, cont.

2.5.5 Tester Drive Unit Design

In a related IR&D activity, Aerojet designed and fabricated a generic 100,000 rpm, 100 hp turbine drive with an integral shaft torque measurement capability. This workhorse driver, shown in Figure 2.5-45 will be utilized in several different programs to conduct life testing on hydrostatic bearings and rolling contact bearings. The driver was available in early 1985 as a replacement for an existing 40,000 rpm machine.

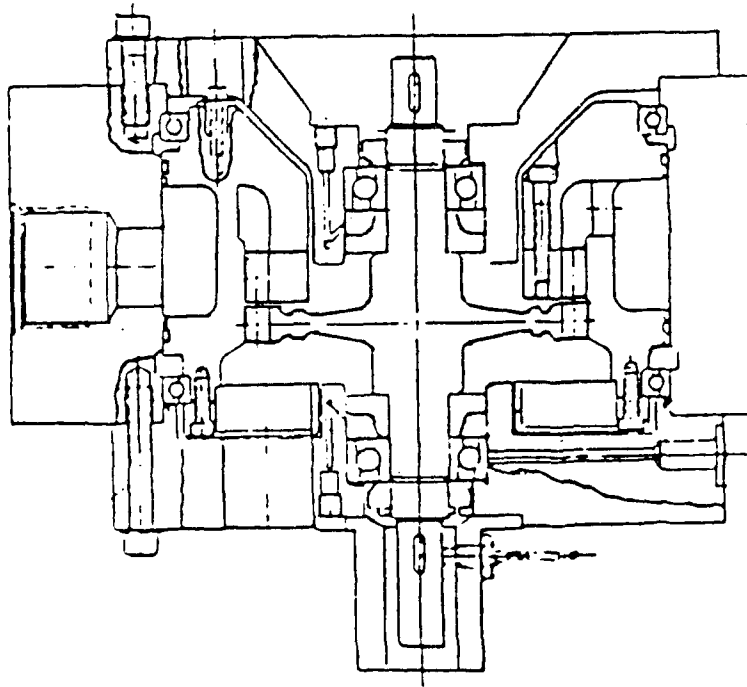
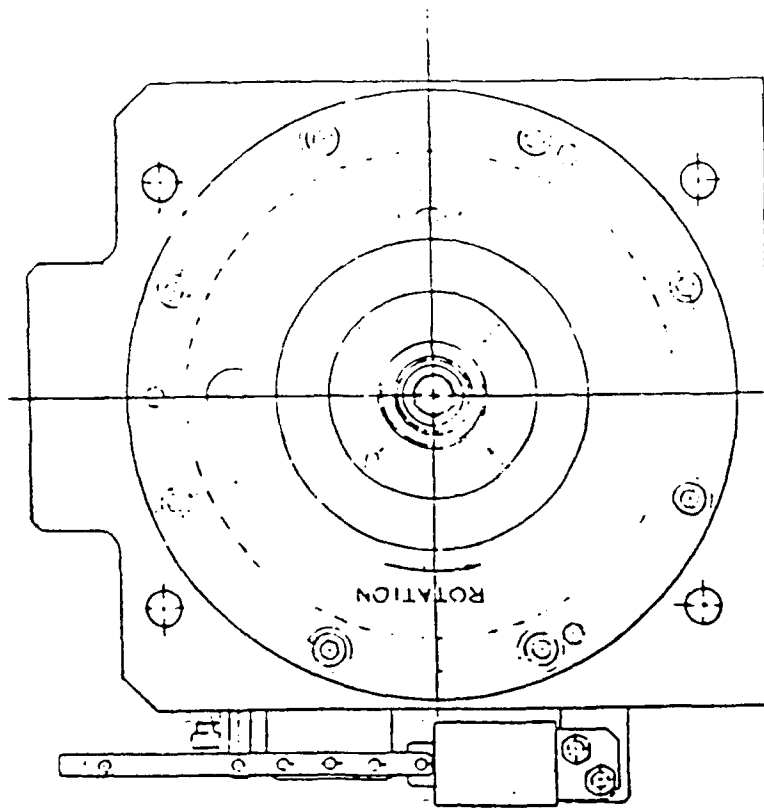
This turbine drive is powered by high pressure gaseous nitrogen. Connection to the actual bearing tester is via a quill drive shaft which is splined onto the rotating assembly at the turbine end. Figure 2.5-46 shows the drive unit and bearing tester when coupled. Figure 2.5-47 shows the quill shaft with the floating ring seal in the foreground and the other bearing and rotating elements in the background. The complexity of the actual tester installation can be judged by Figures 2.5-48 and 2.5-49 which show the tester as installed, instrumented, and with lines insulated.

2.5.6 Thermal and Stress Analysis

The amount of thermal and stress analysis done during the design was less than desired as limited program resources had to be prioritized to complete the drawing package. Emphasis was placed on analyzing the deflections in the pump and turbine housing, pressure induced effects and resulting deflections on the impeller and rotor assembly, stress levels in the turbine disc and adjacent shaft parts, and turbine blade bending. A thermal analysis was completed to map the temperature distribution for the operating condition where 400°F oxygen turbine drive gas is used while pumping liquid oxygen in the pump section on the same shaft. This last analysis included pressure and speed as well as thermal effects. Each of these analyses is discussed in one of the sub-sections that follow.

2.5.6.1 Rotating Assembly Analysis

A critical speed analysis of the shaft system is given in Figure 2.5.3. Critical speed, N_c , is shown plotted against bearing stiffness, K_R . There is at least



		TEST DRIVE TURBINE AND TORQUEMETER ASSY	
Part No. 05824	Rev. 1	Qty. 1	Lot No. 1197321
Date 11/11/84		By J. H. H.	
Checked J. H. H.		Approved J. H. H.	
Description Torque Meter Assembly		Material 303 Stainless Steel	
Quantity 1		Unit Cost \$119.73	
Total Cost \$119.73		Remarks 1.000	

Figure 2.5-45. Turbine Drive Assembly

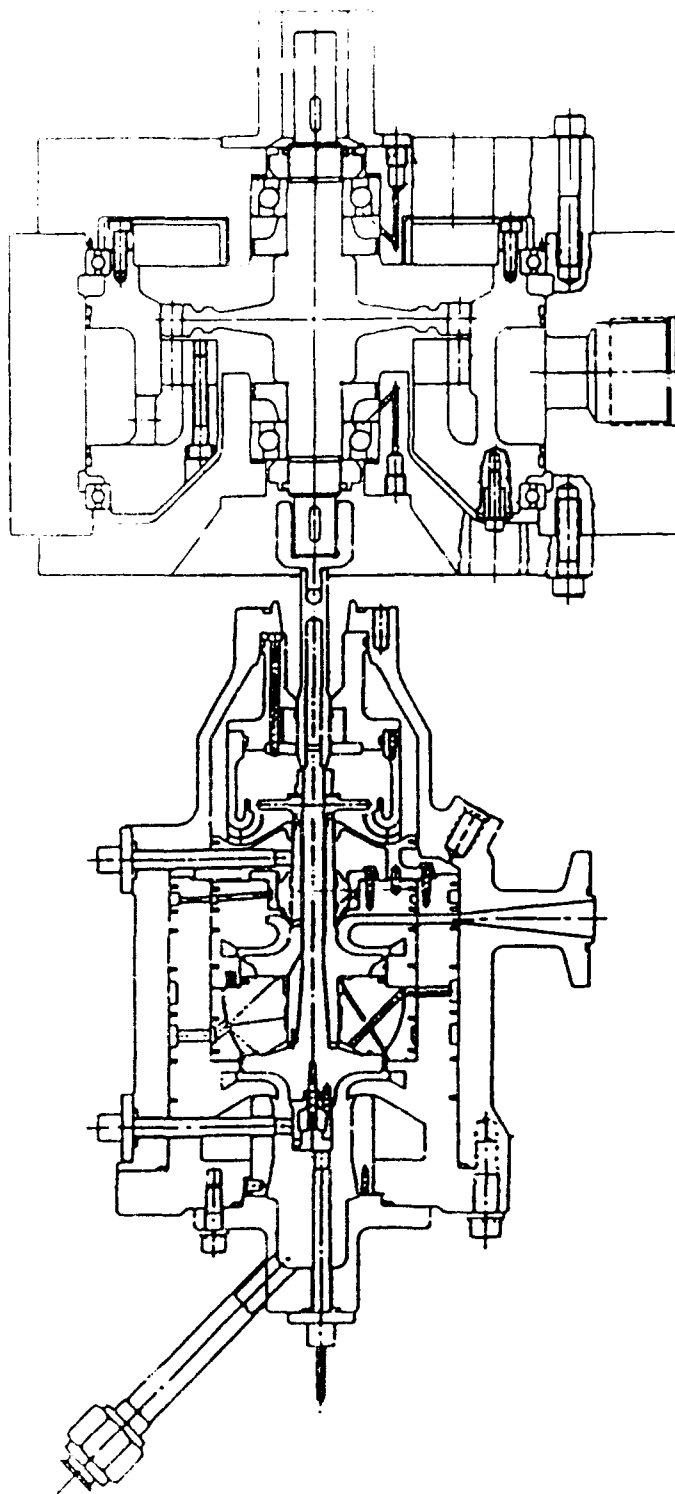


Figure 2.5-46. Drive Turbine and Torquemeter Assembly

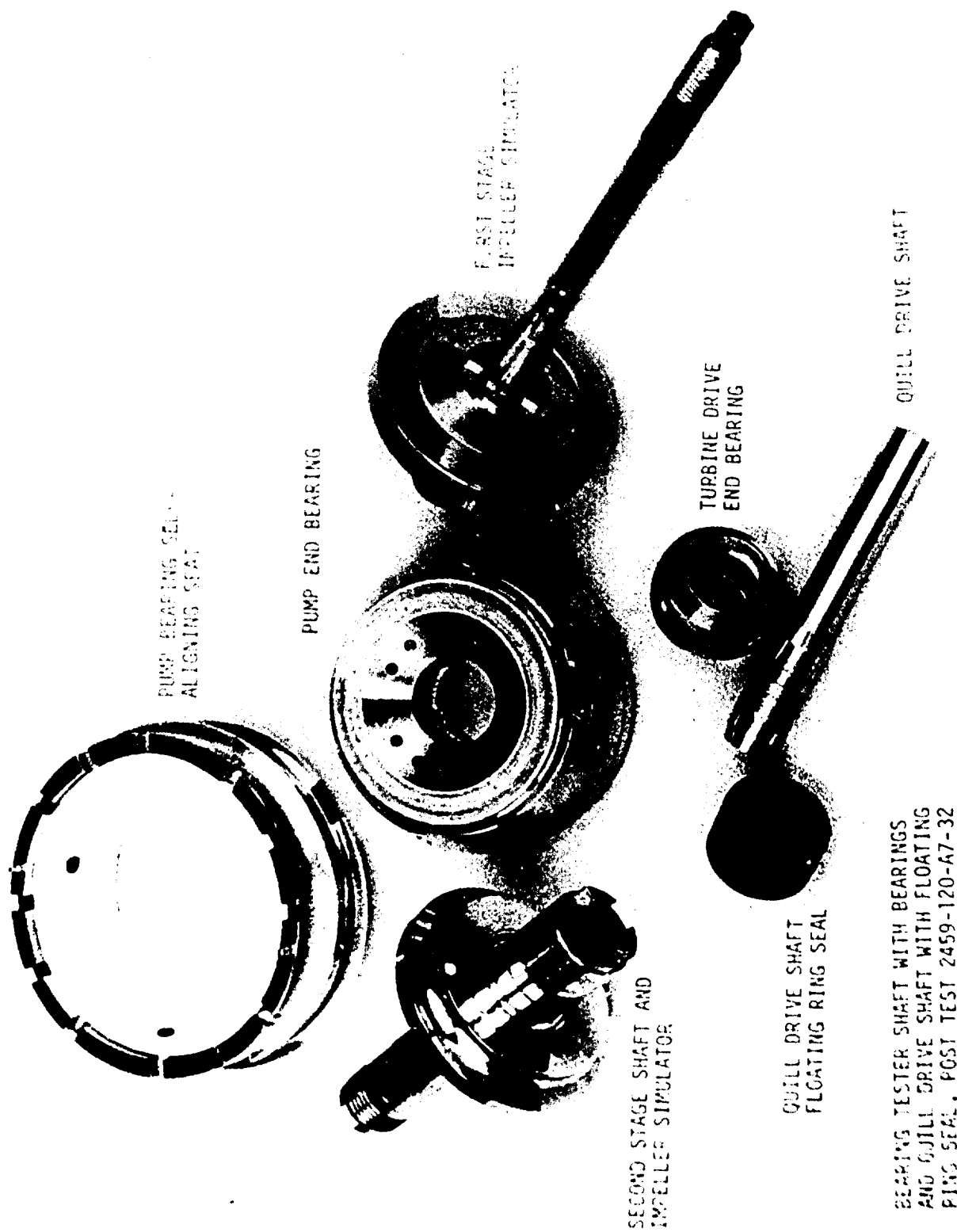


Figure 2.5-47. Bearing Tester Shaft and Quill Drive Shaft With Floating Ring Seal, Post Test 2459-120-A7-32



Figure 2.5-48. Post View of Test Setup Looking Obliquely at the Bearing Tester End

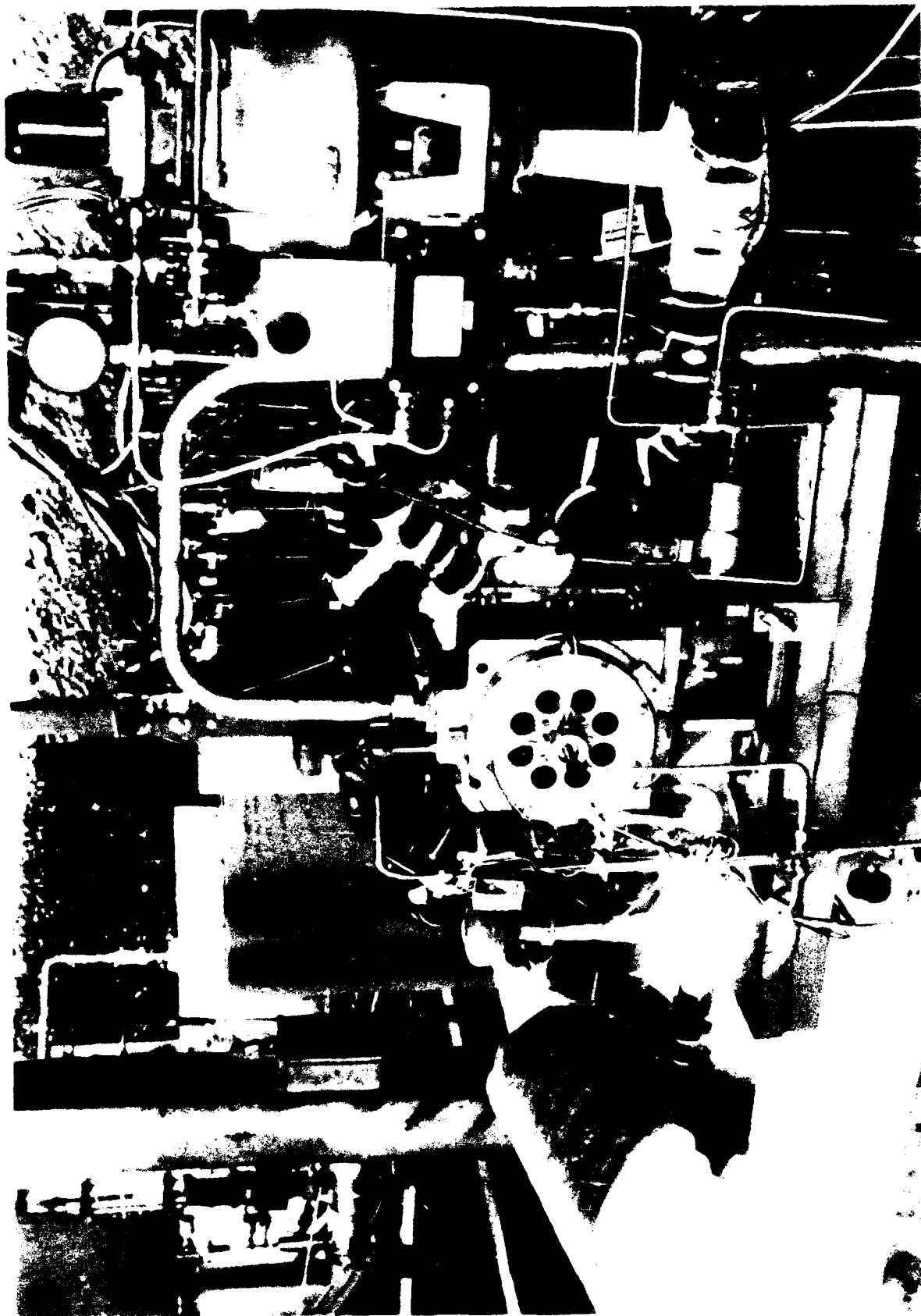


Figure 2.5-49. Post Test View of Test Setup Looking at the Test Drive Turbine Exhaust End

2.5, Detail Design, cont.

a 30% margin of the first critical speed above the operating speed. With this design the TPA will never operate close to shaft/bearing critical speeds over the entire operating speed range. This also avoids any problems of sub-synchronous whirl.

The initial material selection for turbine blades was Nickel 200. A finite element analysis showed a stress of 15.4 psi at the blade root. This yielded a negative margin of safety. The next design iteration included a Monel 400 tip shroud brazed to the nickel blades. The hub was also Monel 400. This left only the actual blade sections as Nickel 200. The turbine construction was becoming very complex in an effort to preserve the good oxygen compatibility of Nickel 200 blades. After re-evaluating the need for Nickel 200 as a turbine blade material, a decision was made to eliminate the tip shroud and fabricate the entire turbine out of Monel K-500. This would greatly reduce the cost of the turbine manufacture at some slight loss in oxygen compatibility and turbine efficiency. The turbine blade bending stresses are shown in Figure 2.5-50.

The analysis of the rotating assembly including pressure effects and the resulting deflections is given in Figure 2.5-51. Note that the impeller outer tips move further apart (by 0.00024 inch) resulting in a slight increase in impeller axial clearance. Turbine rotor deflection due to the combination of thermal, pressure, and speed effects is shown in Figure 2.5-52. (the displacement of the blades is exaggerated to show the direction of the effects). The combined radial displacement at the turbine rotor outer diameter is 0.00146 inch in a radial direction and 0.00317 inch in the axial direction.

Figure 2.5-53 shows the stress levels in the turbine disc and adjacent shaft parts due to clamping forces and rotational effects. At the hub the maximum stress level is 39,319 psi. This precludes the use of a Nickel 200 hub although Monel K-500 is acceptable.

2.5.6.2 Housing Assembly Analysis

The deflections under pressure for the first stage housing are summarized in Figure 2.5-54. The deformed shape summary for both first and

• LOADING — ΔP ACROSS THE BLADE

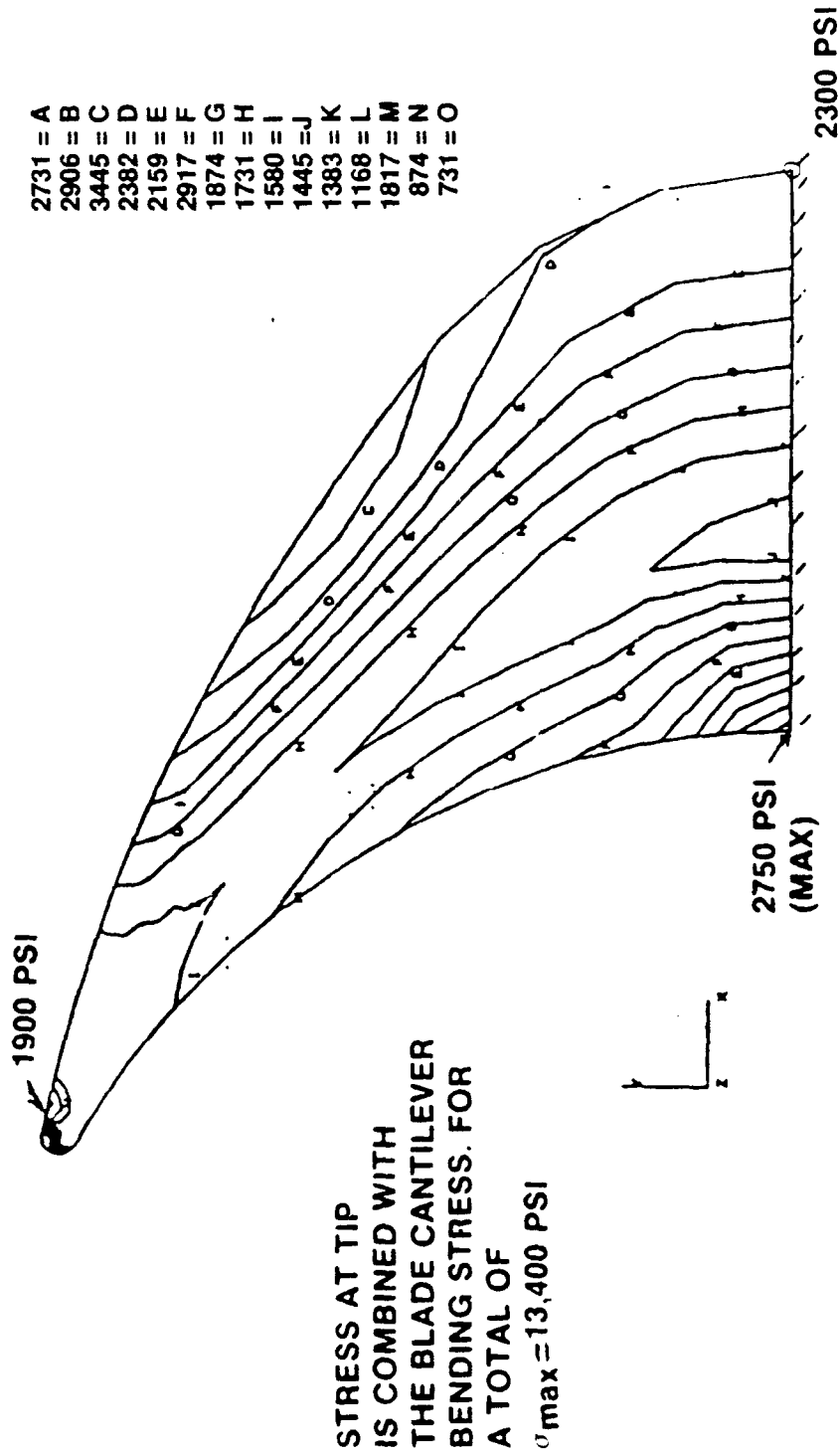


Figure 2.5-50. Turbine Blade In-Plane Bending Stress

1000 lb Bolt Preload
 N = 75,000 rpm
 Steady-State Pressure

Cavity Opening

$\Delta Z \ 1/3 = .00025$

$\Delta Z \ 2/4 = .00007$

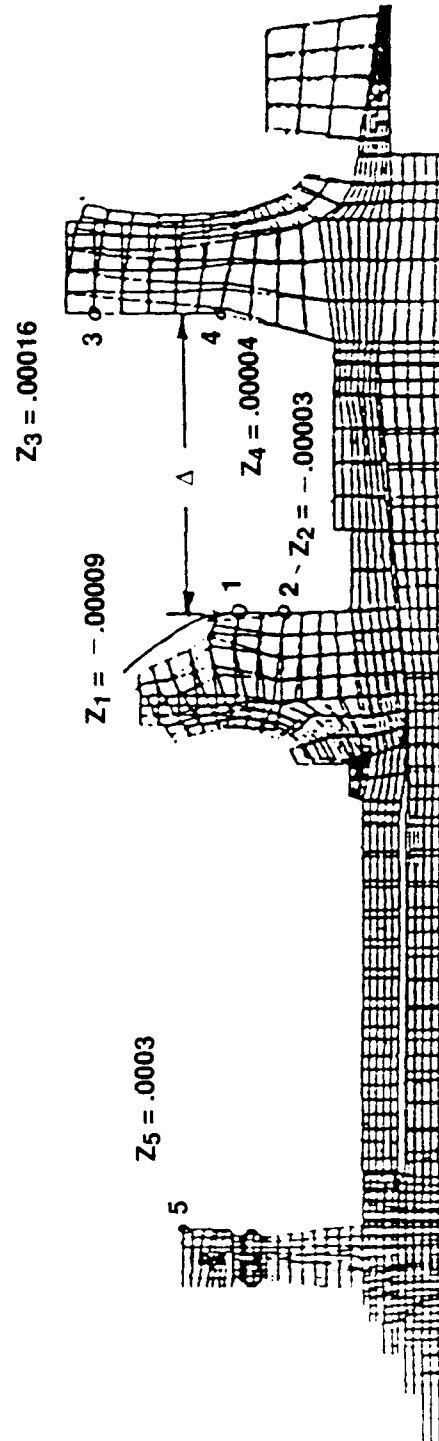


Figure 2.5-51. OTV TPA Shaft and Impellers – Deformed Shape

(75,000 rpm)

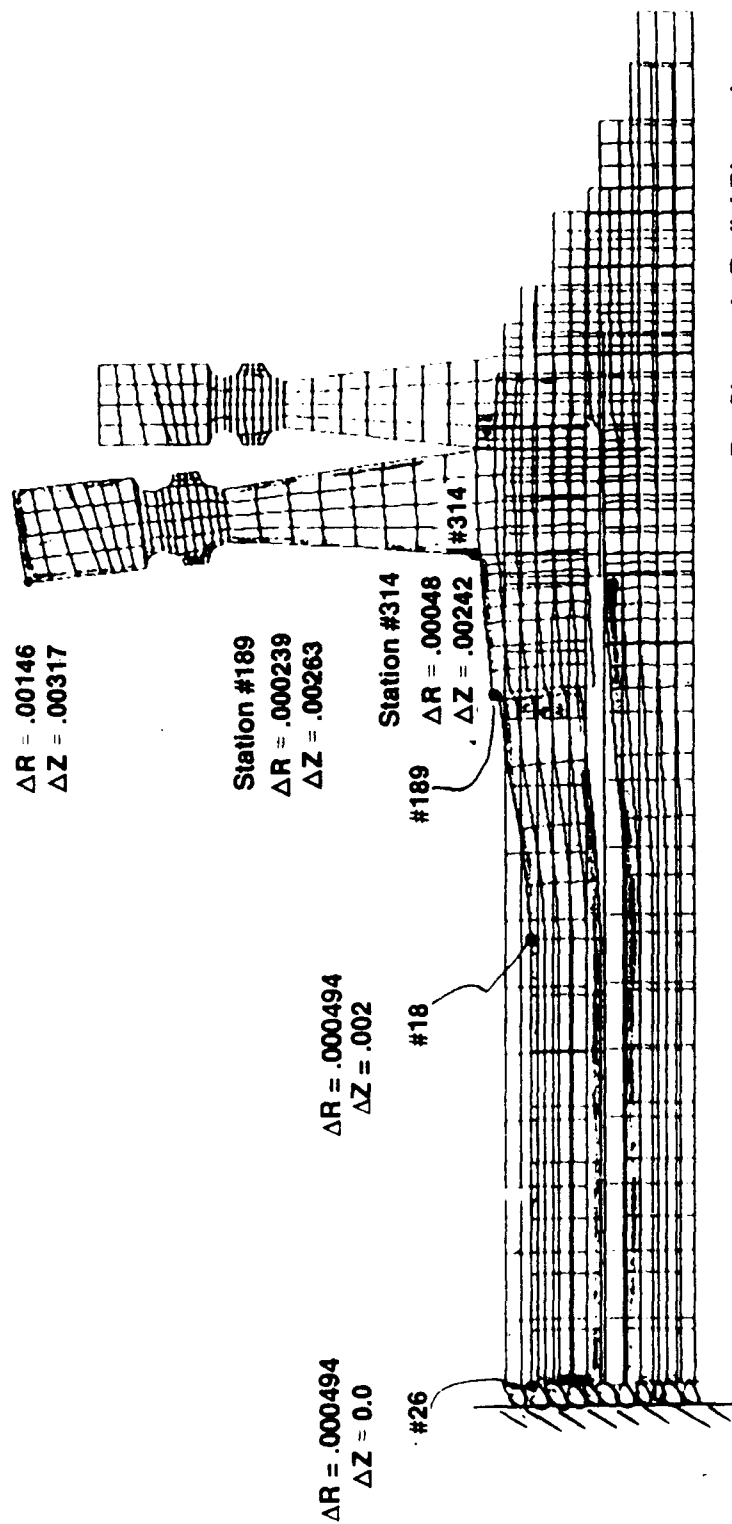


Figure 2.5-52. OTV Rotor w/Bolt, Deformed Shape, Steady State - Full Thrust Thermal Pressure and Speed Effects (75,000 rpm)

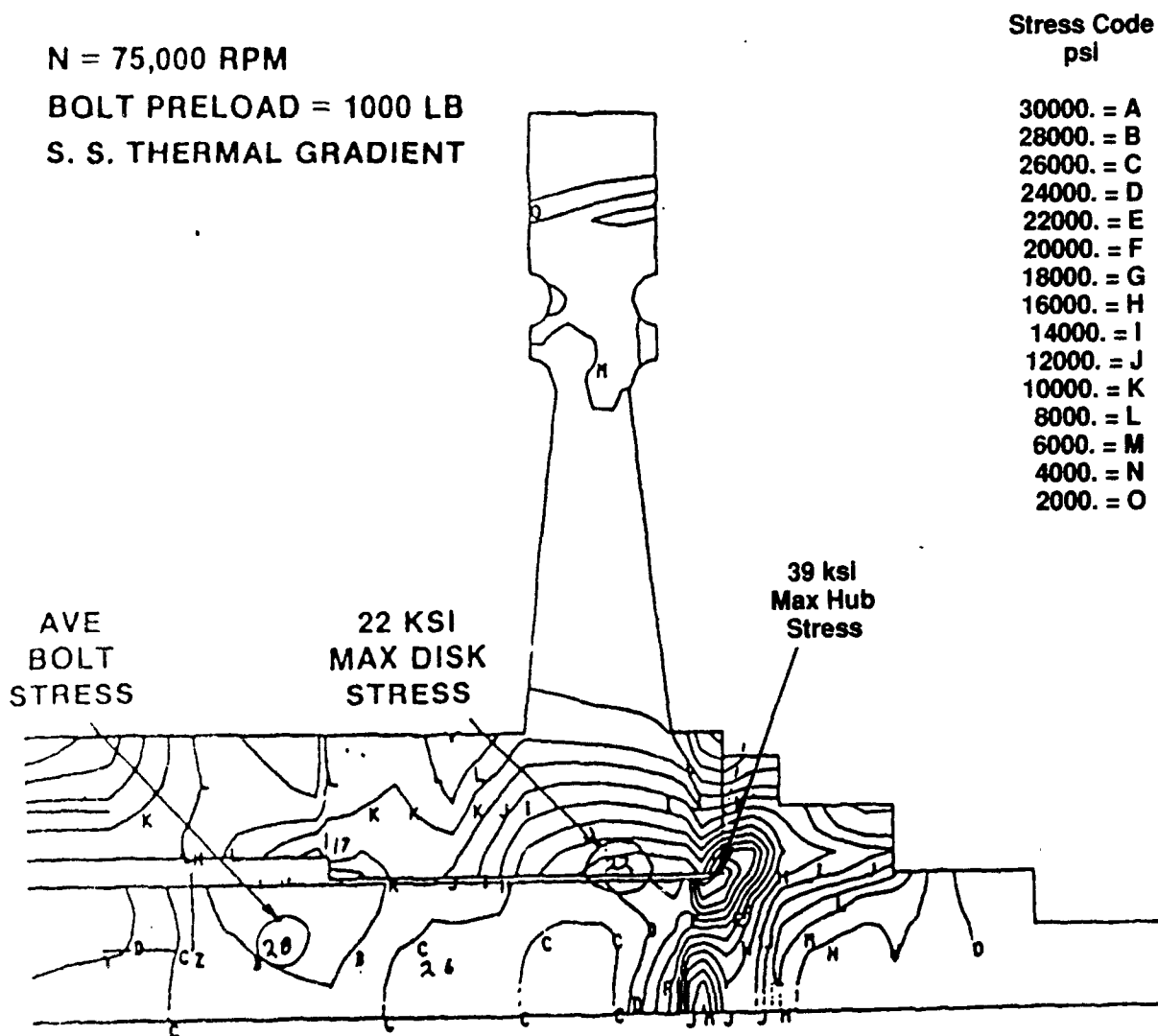


Figure 2.5-53. Turbine Disk Effective Stress Due to Clamping and Rotating Loads

• PRESSURE LOADING

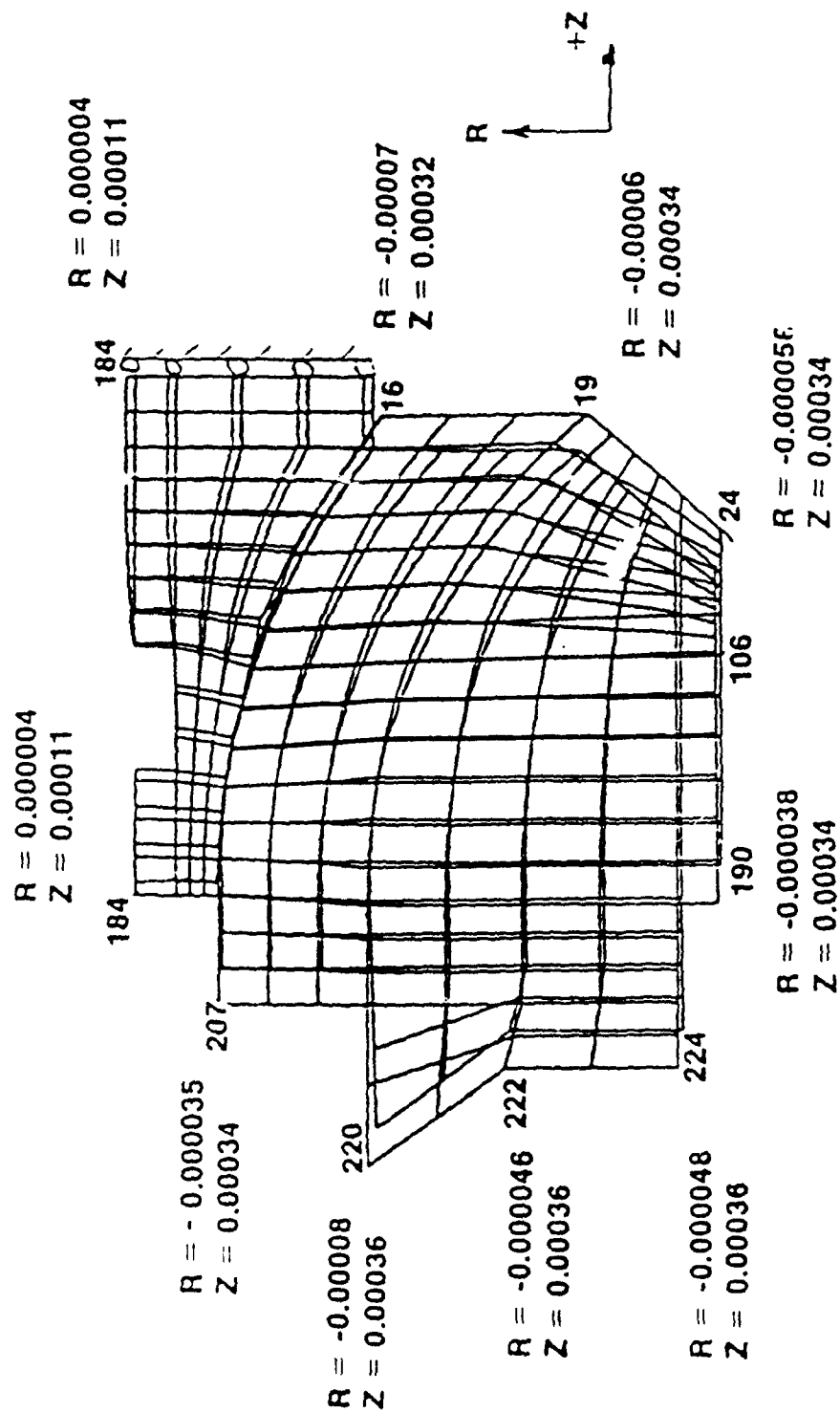


Figure 2.5-54. Pump End Bearing and Spherical Seal

2.5, Detail Design, cont.

second stage pump housings is given in Figure 2.5-55. The turbine housing effective stress through a representative section is given in Figure 2.5-56.

2.5.6.3 Thermal Analysis

All rotating parts are attached to a metal shaft. This provides a conductive heat path from the hot ($\sim 400^{\circ}\text{F}$) turbine blade section to the cold (-300°F) pump section. Even with a relatively low thermal conductivity material like the Monel K-500, the close separation of the two sections would allow an excessive thermal gradient to develop unless active cooling were used. The turbine shaft coolant path is shown in Figure 2.5-57. The turbine blade itself is not shown, but the thermal analysis assumed it would be at 400°F . The coolant flow is tapped off from the second stage pump inlet, and, because of the coolant circuit pressure drop, is returned to the first stage impeller. It constitutes an efficiency loss, but is needed to maintain the bearing at liquid oxygen temperature. This temperature sets the clearance for the hydrostatic bearing design. Any significant increase or decrease will change the bearing losses and pump efficiency. There is also a concern that cavitation could be induced under some operating conditions if the heat conduction is not controlled. A temperature map at steady-state design conditions of the turbine/shaft system is given in Figure 2.5-58.

2.5.6.4 Stress Summary

A summary of the TPA stress analysis is given in Table 2.5-14 for the critical design points/parts. Note that all margins are positive. A design survey of other structural parts and potential stress points concluded that margins should be very high due to the workhorse nature of the housing and flanges. A flight-weight design would require a more extensive structural analysis.

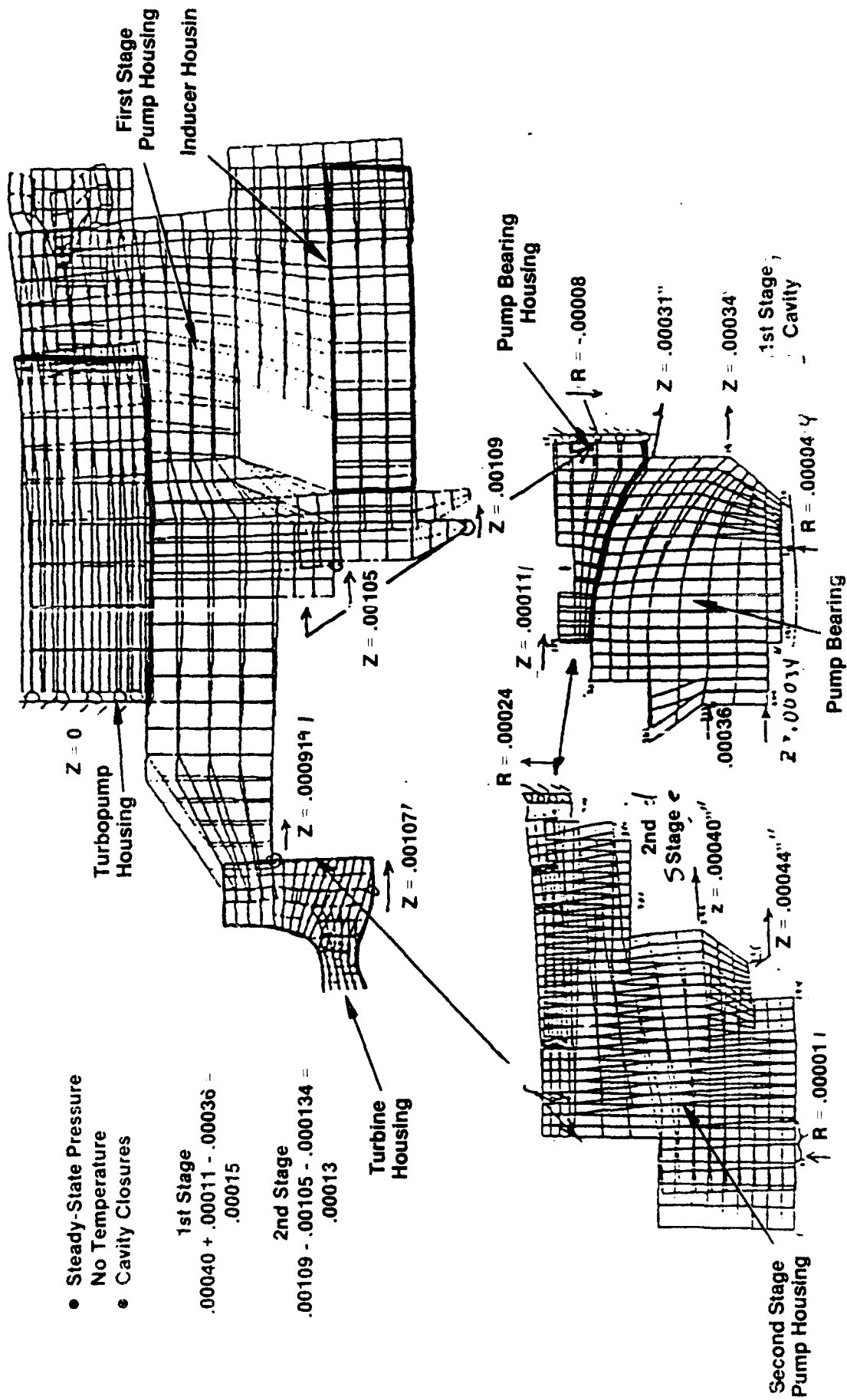


Figure 2.5-55. Pump Housings – Deformed Shape Summary

Stress Code
psi

30000 = A
28000 = B
26000 = C
24000 = D
22000 = E
20000 = F
18000 = G
16000 = H
14000 = I
12000 = J
10000 = K
8000 = L
6000 = M
4000 = N
2000 = O

- PRESSURE
- TEMPERATURE — STEADY-STATE

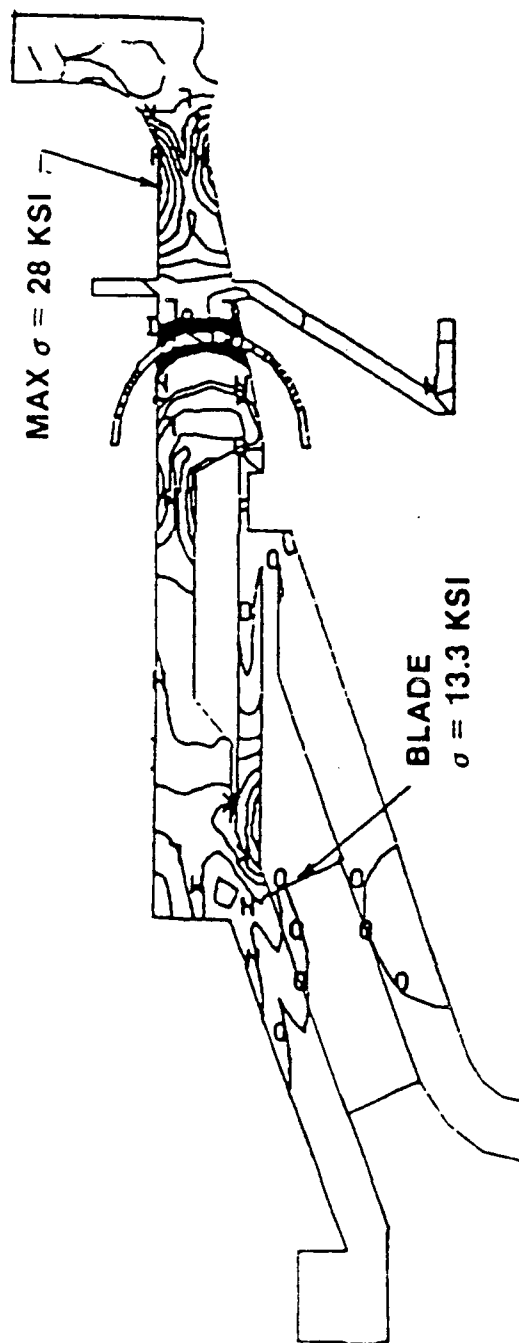


Figure 2.5-56. Turbine Housing Effective Stress

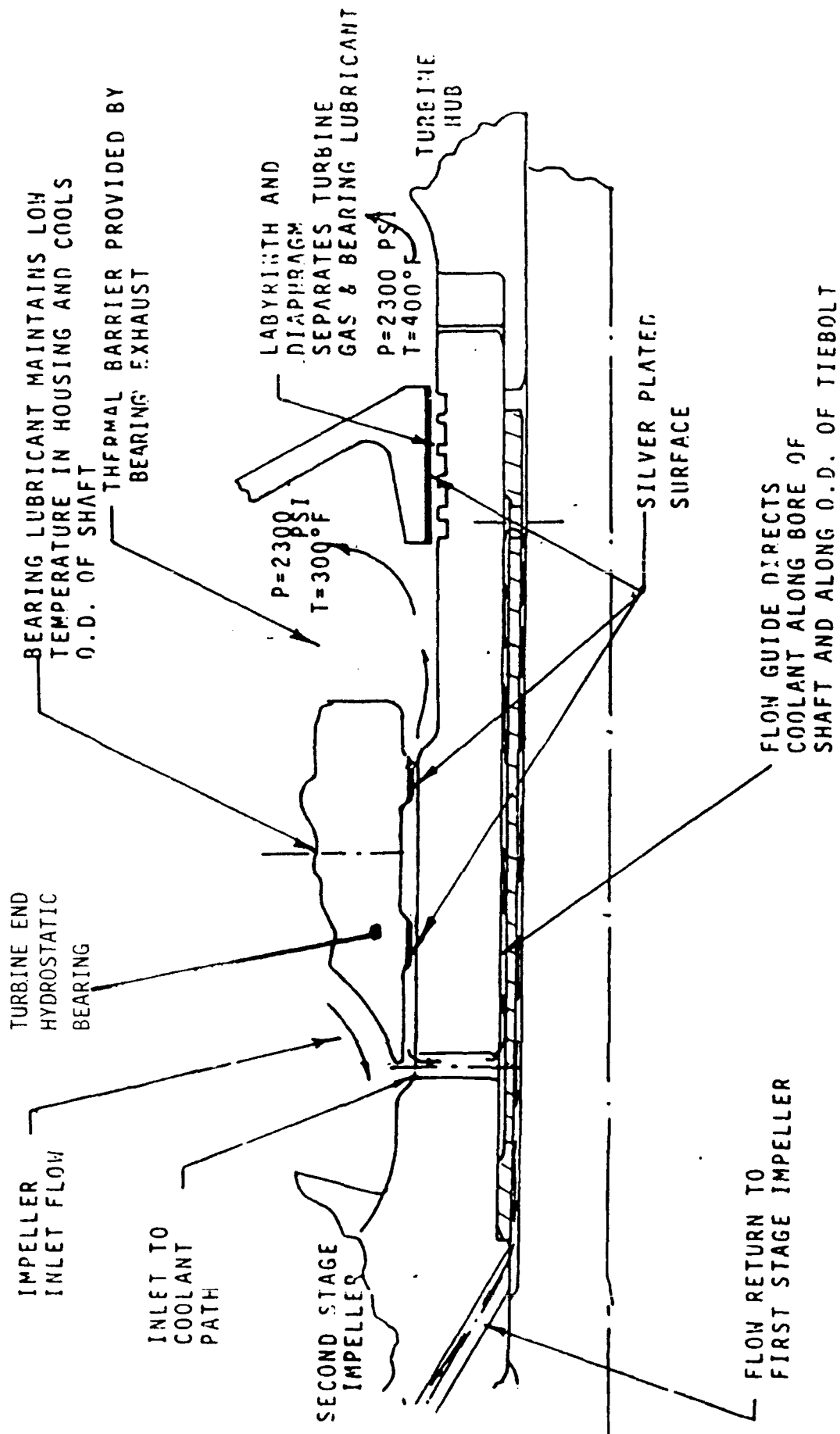
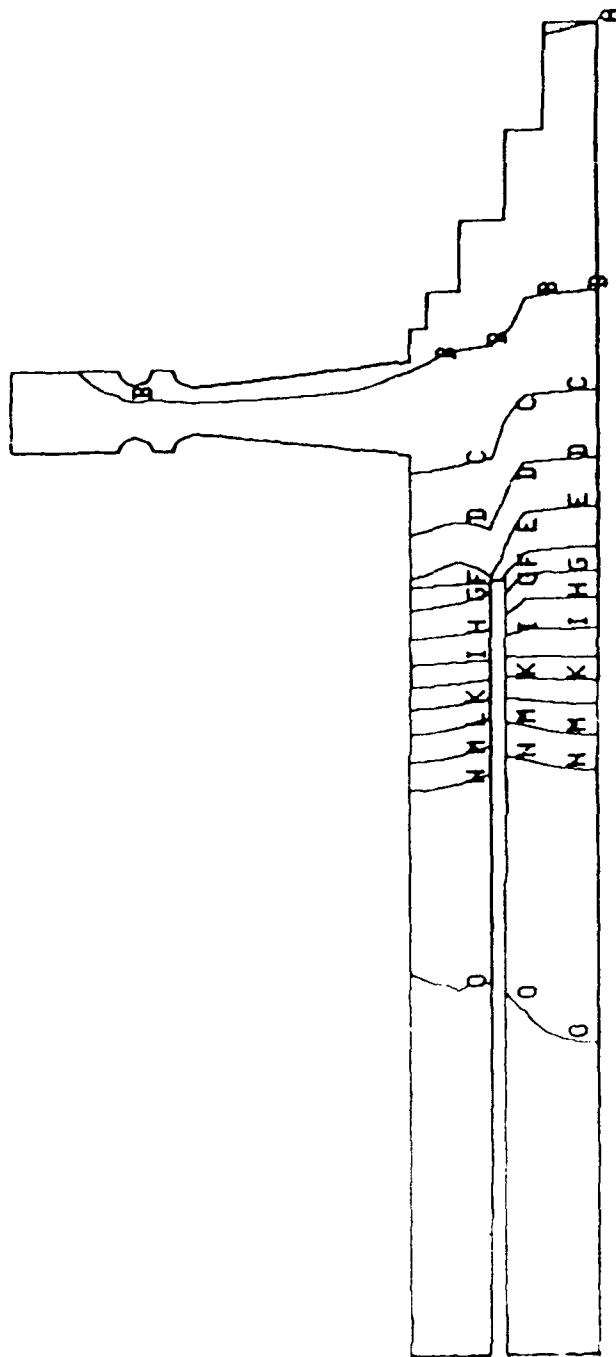


Figure 2.5-57. Turbine Shaft Coolant Path

390. =A
 350. =B
 300. =C
 250. =D
 200. =E
 150. =F
 100. =G
 50.0 =H
 0. =I
 -50.0 =J
 -100. =K
 -150. =L
 -200. =M
 -250. =N
 -300. =O



OTV OX IPA ROTOR WITH SHAFT AND BOLT
 TEMPERATURE, DEG F
 STEADY STATE - FULL THRUST

Figure 2.5-58. Steady State Temperature Map at Turbine End
 and Adjacent Parts

Table 2.5-14.
OTV TPA Stress Summary

	TYPE OF LOAD	MATERIAL	F _{ty} KSI	STRESS KSI	SAFETY FACTOR
TURBINE DISK	CENTRIFUGAL/THERMAL PRESSURE	K MONEL (400°)	106	22.0	4.8
BLADE	CENTRIFUGAL	K MONEL (400°)	106	3.8	2.8
1ST IMPELLER VANE	CENTRIFUGAL	K MONEL (-300°)	125	30	4.1
2ND IMPELLER VANE	CENTRIFUGAL	K MONEL (-300°)	125	50	2.5
SH/FT	TORQUE/COMPRESSION THERMAL	K MONEL (200°)	108	11.3	9.5
DRIVE CLUTCH	BEARING STRESS	K MONEL (200°)	106	47	2.2
TIE BOLT	TENSION	K MONEL (200°)	106	28	3.8
PUMP HOUSING	PRESSURE	K MONEL (-300°)	125	12	10.4
FLANGE BOLTS	PRESSURE/PRELOAD	A286	100	25	4.0
TURBINE HOUSING	PRESSURE/400°/-350°F	K MONEL (400°F)	106	28	3.78

3.0 FABRICATION

3.1 VENDOR SURVEY AND SELECTION

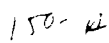
Nearly all parts' purchase orders were written in the late October through early December 1984 period. Orders were placed for the simpler parts in January through March of 1985. It also became evident at that time that the pump and turbine bearing assemblies were being "no bid" by competent fabricators. Over the next year AT (Aerojet) procurement and engineering staff discussed the bearing fabrication requirements with many vendors, often well outside of the geographic area where most of our vendors are located. The common difficulty was the very tight tolerances specified for the bearing geometry. Where possible the requirements were loosened, but the designer considered that the very tight clearances required for a hydrostatic bearing demanded the clearances specified. A specialty precision machining shop in Campbell, California, finally took the order and delivered parts to specification in March of 1986. Drawings of the two bearings are given in Figures 3.1-1, 3.1-2, and 3.1-3.

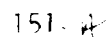
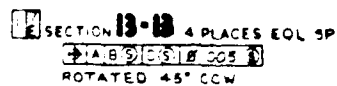
3.2 VENDOR CAPABILITY/PRODUCIBILITY

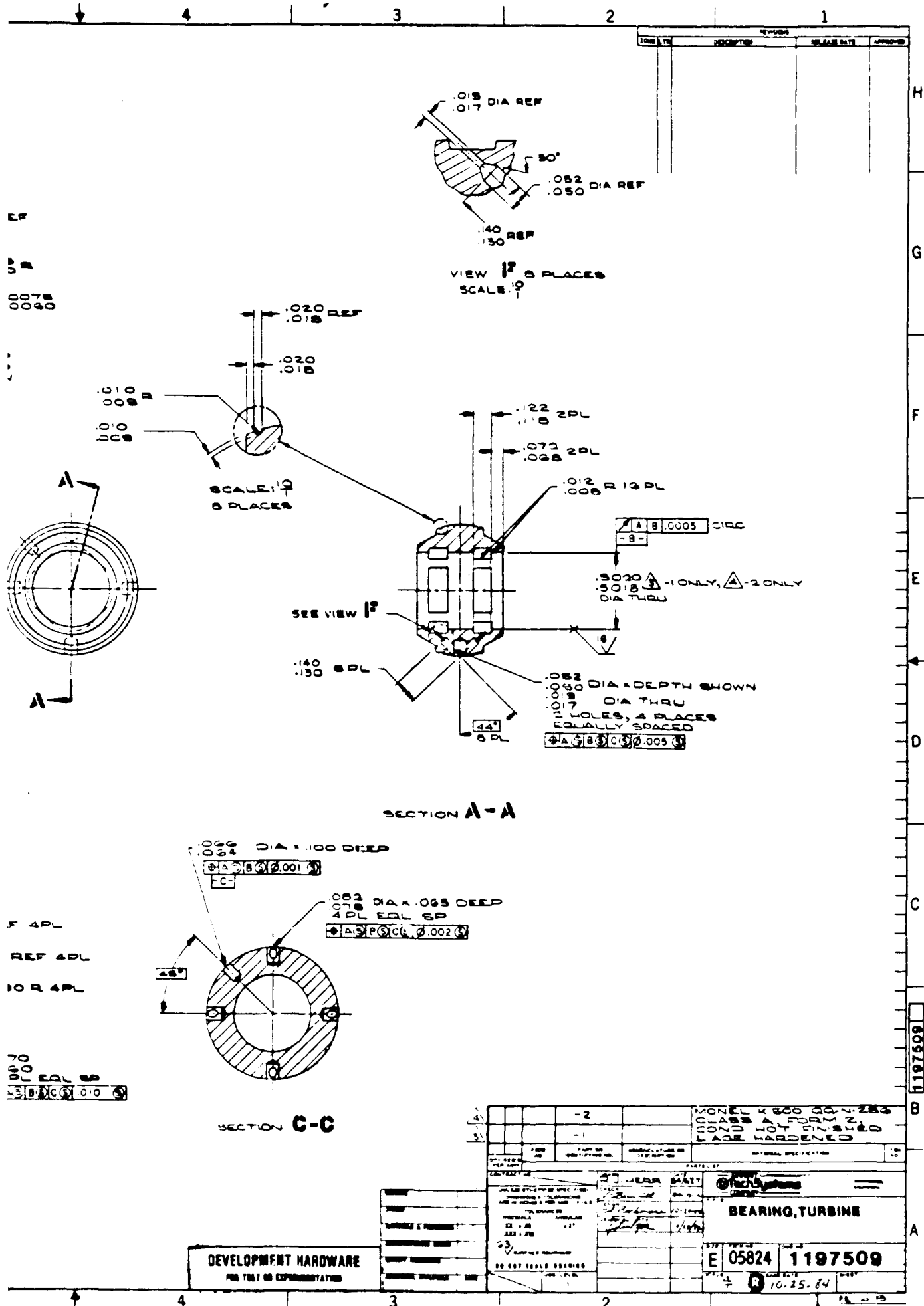
The combination of a complicated geometry, Silver, K500 material, and tight tolerances make the pump and turbine bearings a demanding fabrication job. The reluctance of vendors to bid the work raises the question of "is this a producible design?" The fact that they were fabricated to the drawings shows that they are. It also demonstrated that in 1986 only a very few specialty vendors had both the capability and interest to bid a demanding job like this. This has changed. Several shops, both new and well-established, have acquired the machines and the trained operators to handle this level of precision. AT is also using specialized producibility engineers and early vendor contacts as a routine part of the design process at the present time.

One other item of concern was the turbine rotor blade machining. Several potential fabricators were contacted and it was decided that manufacturing experiments should be done using a four blade sample quadrant in three different materials to verify both the blade design and the material selection. During the

THIS FEATURE TO BE SUBSEQUENTLY MACHINED.







3.2, Vendor Capability/Productibility, cont.

bearing test this was not a problem as a disc without blades was used in place of a turbine. Actual manufacturing experiments were conducted in 1986. The actual finished turbine wheel was not needed until 1987.

The K-500 surfaces were, in contact areas, to be plated with a low ignition hazard material. The early candidates were gold and silver. Silver was finally selected for its mechanical properties in rubbing contact with the hard electroless chrome plated rotor parts. Gold is used on the surface of the turbine rotor tip seal for its immunity to oxidation. These platings were tested under repeated cyclings to the operating cryogenic temperatures on monel test articles. Adherence was not impaired under the repeated thermal cycling.

The dimensional stability of Monel K-500 was demonstrated under repeated cryocycles using ball shaped test articles. A drilled and carefully measured hole in some of the balls was used to generate data on dimensional stability under cryocycling for K-500 articles resembling the spherical bearings. In all cases the material proved stable.

Most other parts for the tester were delivered in 3 to 6 months. The housings, very complicated parts, were delivered in September 1986. Vendors, for the most part, did competent, acceptable work. This TPA is producible.

3.3 FABRICATED ITEMS

An emphasis on conserving the limited program resources is reflected in the very minimal amount of spare parts produced in the program. The TPA housing performed double duty as the housing for the bearing tester used in Test Series A and B, and, with finish machining, as the housing for the actual test unit used in all subsequent TPA tests. The wisdom of this skimping on test hardware is questionable as the hiatus between Test Series B and Test Series C was over 1 1/2 years due to problems in getting the partially finished case machined to the TPA configuration. Similar though less severe problems were experienced with the finish machining of the impeller and turbine blades. Again, spares for these critical parts would have saved a great deal of time and, very likely, some program cost.

3.3, Fabricated Items, cont.

A total of fifty-six different parts were fabricated for the TPA. This does not count tester drive unit parts and test stand parts external to the tester. Table 3.3-1 is the listing as of 10 March 1986.

All parts were machined from bar stock; no castings or forgings were used. Conventional metal cutting tools were used as well as EDM for the flow passages. The pump housing (Figures 2.5-43, -44, and -45) was the most challenging fabrication task from the standpoint of complexity. After the 8 inch bar stock was turned to the maximum external dimensions, the piece was drilled, milled, and ground to the final configuration. The vendor elected to form the flanges of the parent metal rather than taking the easier method of fashioning weldable stubouts for welding on separately finished flange pieces. This used some additional machining time but avoided problems with thermal distortion and property changes in a heat affected zone (HAZ). Final dimensions were set by carefully finishing the rough flange faces. The interior of the piece was finished by conventional lathe turning. Monel 400 was selected for this piece for both good oxygen compatibility and weldability should a repair be needed. The work was completed without incident, and no weld repair was needed.

The two bearing sets were fabricated from Monel K-500. The fabrication was delayed as vendor after vendor "no-bid" this fabrication. Discussion with the various precision machine shops confirmed that the vendor reluctance was due to the monel metal, silver, and the tight tolerances. A number of shops had done very little or no work with K-500 and were reluctant to bid fixed price where they were unfamiliar with the machining properties of the metal. Other vendors did not have numerically controlled machines of the necessary precision. A personal contact by the TPA project engineer with the owner of Wacker Engineering in Campbell, California, led to a bid and the successful fabrication of the two bearings. The fabrication sequence required machining the spherical bearings to final dimensions of less than 3 to 8 mils tolerance. The bearings were then sent to another vendor for silver electroplating. The silver plated bearings were then machined to final dimensions with tolerances of 0.0001 to 0.0002 inch typical.

TABLE 3.3-1
OTV OXYGEN TPA FABRICATED PARTS LIST

Title	Duty Type	Document Number	Item No.	Quantity per Assembly	Quantity Ordered
OTV LO ₂ Turbopump-Hydrostatic Brg Tester		1197493			
Inlet Housing	N W	1197494	1	1	1
Spinner	L	1197495	2	1	2
Inducer Simulator	N W	1197496	3	1	1
Sleeve	N W	1197498	4	1	1
First Stage Impeller Simulator	W	1197574	5	1	1
Second Stage Impeller Simulator	W	1197502	6	1	1
Rotor Turbine Simulator	N W	1197504	7	1	1
Bearing Housing Pump		1197506 see 1197515			
Bearing, Pump		1197507 " "			
Bearing, Housing Turbine		1197508 see 1197577			
Bearing, Turbine		1197509 " "			
Pump Housing, 1st Stage	N W	1197510	12	1	1
Pump Housing 2nd Stage	N W	1197511	13	1	1
Turbine Housing	N W	1197512	14	1	1
Housing Turbopump	N W	1197514	15	1	1
Pump Bearing Assembly	W	1197515	16	1	1
Balance Assembly		1197517			1
Lock Washer, Turbine	E	1197519	18	1	18
Seal, Ring Cylindrical, Housing		1197520	19	1/7/7	8
Seal Housing	N W	1197522	25	1	1
Cover Seal	N W	1197523	26	1	1
Seal	W	1197524	27	1	2

TABLE 3.3-1
OTV OXYGEN TPA FABRICATED PARTS LIST (CONT)

Title	Duty Type	Document Number	Item No.	Quantity per Assembly	Quantity Ordered
Quill Shaft	W	1197525	28	1	2
Probe	L	1197571	29	5	6
Coupling	W	1197572	30	1	2
Lock Washer, Inducer	E	1197573	31	1	18
Nut, Turbine	L	1197576	34	1	4
Turbine Bearing Assembly	W	1197577	35	1	1
Seal Ring Turbine Bearing Housing		1197580	24	1	8
Seal, Crush, Turbine Housing		OTV-2		1	10
Ball 11/64 Inch Diameter Grade 100			37	1	20
"O" Ring Teflon	E	AS8040E1-024	38	1	18
"O" Ring	E	AS8040E1-0.	39	1	18
"K" Seals FSCN 08199	E	12100A A 2	40	3	4
"K" Seals	E	12100A A 4	41	4	5
"K" Seals	E	12100A A 6	42	3	4
Nipple	NW	MB 24302-J2, K2 or S2	43	2	4
Nipple	NW	K4 or S4 -J4,	44	4	5
Nipple	NW	K6 or S6 J6,	45	3	4
Screw, SOC HD Cap 2-56 UNJC		1197581 304SS	46	3	6
Screw, Torque-Set A-286 "B"	L	NAS 1101 E02-5	17	12	15
Screw A-286 "E"	L	NAS 1101 E02-4	48	20	24
Bolt 12 Pt FSCN 56878 Inconel 718	L	72991-3-3	49	8	48
Bolt 12 Pt FSCN 56878 Inconel 718	L	72991-4-7	50	12	52

TABLE 3.3-1
OTV OXYGEN TPA FABRICATED PARTS LIST (CONT)

Title	Duty Type	Document Number	Item No.	Quantity per Assembly	Quantity Ordered
Spring LC-022A-188	L		51	3	54
Fitting Large HEX FSCN 02570	N W	M-200-6-2AN	52	1	2
Lubricant Dry TFE	AR	ATC 44159	53	AR	2
Seal "O" Ring Teflon	E	AS3040 E1-011	54	5	45
Seal "O" Ring Teflon	E	AS3040-E1-031	55	1	9
Seal "O" Ring Teflon	E	AS3040-E1-043	56	1	9
Seal Metallic "V" Inconel 718-Gold		TVR-011-08-05	54	5	30
Seal Metallic "V" Inconel 718-Gold		TVR-031-08-05	55	1	6
Seal Metallic "V" Inconel 718-Gold		TBR-043-08-05	56	1	6
Balls Cryo-Test Solid/Hollow			57	—	6/2

Symbols:

AR - As Required
E - Expendable
L - Losable
N W - Non-wearing
W - Wearing

3.3, Fabricated Items, cont.

The shaft sections adjacent to the silver plated bearing surfaces were surfaced with electrolyzed chrome (not a wet plating process), and turned to final dimensions. The pump end bearing shaft was chrome surfaced but the turbine bearing end was left uncoated. This was done deliberately to allow an evaluation of the effectiveness of the chrome surface versus the uncoated monel at potential rub points. No problems were encountered with either surface so no clear conclusions can be drawn at this point in the testing as to the merit of the chrome surface compared to uncoated monel.

4.0 OXYGEN TURBOPUMP TESTING

4.1 FACILITY AND HARDWARE DESCRIPTION

The oxygen TPA testing was conducted at the Aerojet 'A Zone' test facility. The test complex includes a central control room adjoining a laboratory experimental facility. An earth embankment separates the control room from the complex of seven test bays. The OX TPA testing was done in Bay 7. Figure 4.1-1 shows the bearing tester in the foreground with the turbine drive unit to the rear at the start of installation. Note the crossover pipes and the various pressure taps. When ready for test these articles are obscured by the many wires, plumbed lines, and insulation. All valves and controls are actuated through electrical lines with direct connection to the control room through the bay box (electrical panel). Propellants are plumbed to the bay from large storage tanks on the other side of the earth embankment. As the only fluids used are nitrogen and helium, discharge from the tester is directly to the atmosphere. Testing is done remotely from the control room with monitoring by TV cameras and video displayed data.

The OTV Bearing Tester consists of a turbopump housing and bearing parts with an unbladed shaft assembly driven by an external drive through a quill shaft. The Bearing Tester and its external drive are mounted to a common bed plate as can be seen in Figure 4.1-1. The bed plate has a rigid mount on the turbine (driven) end of the Bearing Tester. A sliding crowned HEX drive coupling at the Bearing Tester end of the quill shaft allows for axial movement between the Bearing Tester and the external drive unit. Also this external drive unit was designed to absorb the 150 lb axial load from quill shaft pressure area force.

The actual testing is concerned with the contact and interaction of the shaft and bearing system. The disassembled pump is shown in Figure 1.3-2. The disassembled bearings are shown in Figure 1.3-3. The tester is shown in longitudinal section in Figure 4.1-2 with callouts for the various parts.

The external drive turbine has a floating nozzle instrumented to read turbine torque applied to the Bearing Tester. Referring to Figure 4.1-2, the bearing tester shaft is driven by male hex coupling (30) * that in turn drives the quill

* See balloons of Figure 4.1-6 for identification and location.

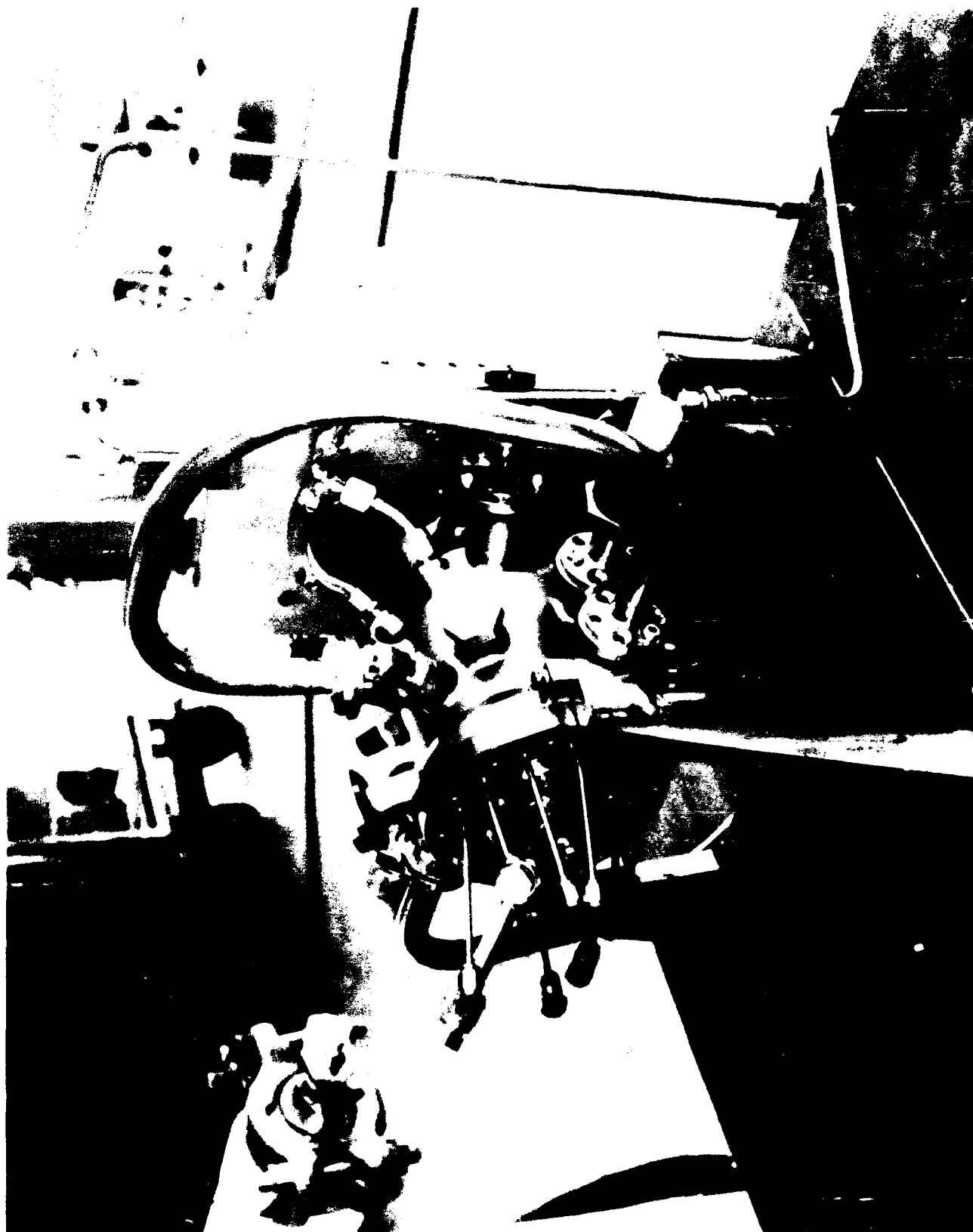


Figure 4.1-1. Bearing Tester and Test Drive Turbine Assemblies at Mockup Installation in Test Bay A7

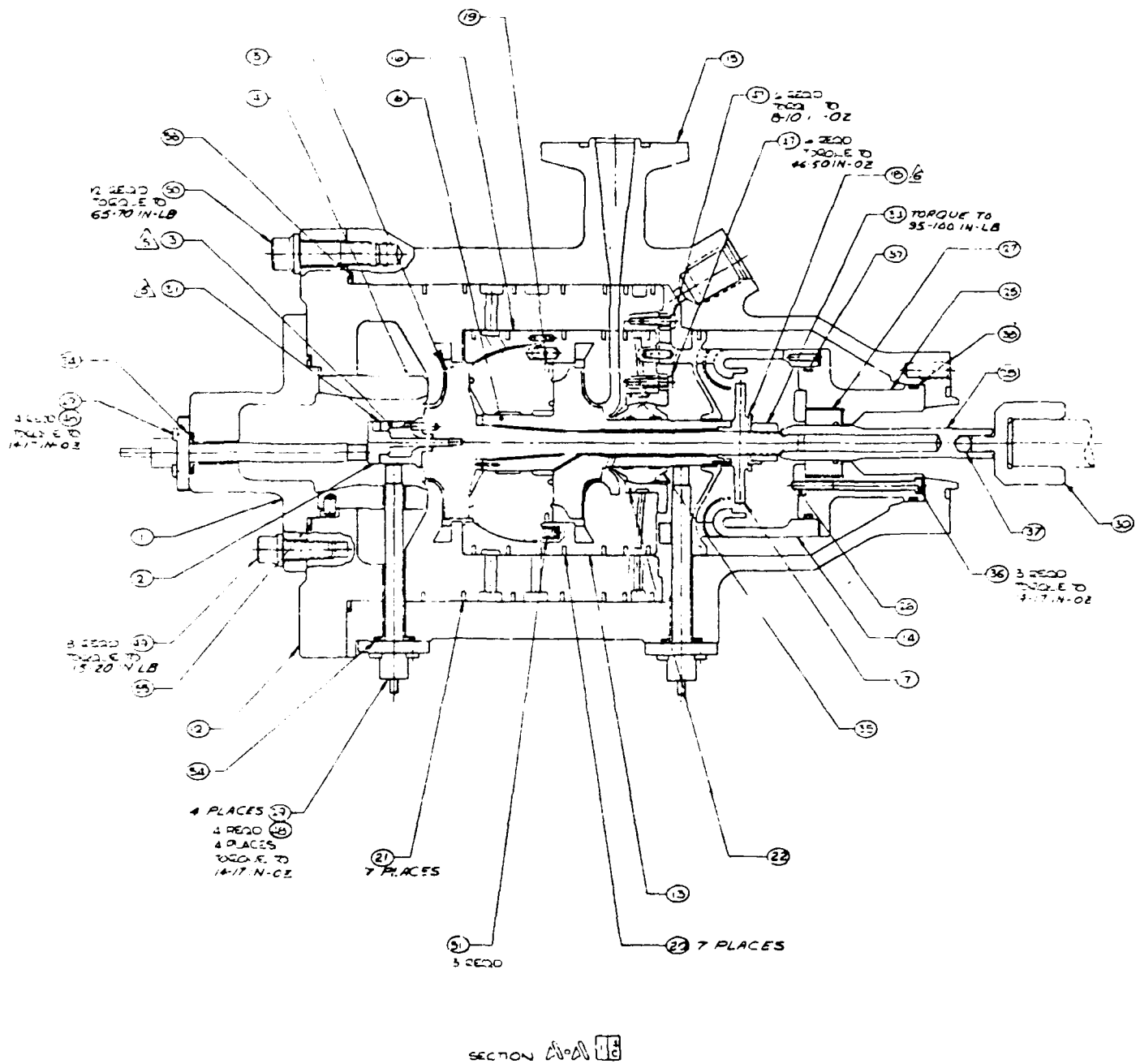


Figure 4.1-2. LOX Bearing Tester — OTV Turbopump

4.1, Facility and Hardware Description, cont.

shaft (28) . A high pressure (2500 psi) floating shaft seal (27) provides a flow limiting seal between the quill shaft seal and quill shaft. These parts are shown at the bottom of Figure 4.1-3. The seal housing is shown above the quill shaft.

A second hex drive coupling connects the quill shaft to the bearing tester shaft assembly (5) and (6) . The shaft assembly includes an inducer hub (3) and spinner (2) that are recessed to provide a known step change in the radial and axial surfaces, respectively, for deflection and speed measurements.

The pump bearing is a combination hydrostatic double acting thrust bearing and journal bearing (16) . It is placed between the impeller hubs, (5) and (6) . The turbine end bearing (35) is placed between the second stage impeller and the turbine rotor. It reacts to radial movement only. The two assembled bearings are shown in Figure 4.1-4 and shown disassembled in Figure 1.3-3. The turbine rotor is replaced by a bladeless disk (7) for the external drive tests to reduce rotor drag and simulate mass.

The major housing parts are shown in Figure 1.3-2. The major three housings in the center are the 1st stage pump housing (12) , 2nd stage pump housing (13) , and turbine housing (14) . Flow limiting sealing rings of five sizes are shown in Figure 4.1-5.

4.2 TEST APPROACH AND RATIONALE

The primary purpose of operating the turbopump shaft/bearing system in a bearing tester is to confirm the stability of the rotor/bearing system in a low or unloaded environment over the full speed range. The bearing testing was done with liquid nitrogen as the bearing fluid. Liquid nitrogen simulates liquid oxygen without the risk of ignition. Secondary purposes of the Test Series "A" and "B" are to demonstrate articulation of the spherical mounts, chill down time, and to confirm that no distortion of metal parts exists to the point of impairing bearing clearance or alignment.

In theory a bearing test program allows for low cost design iterations or multiple design comparisons without the wastage of hardware and resources that

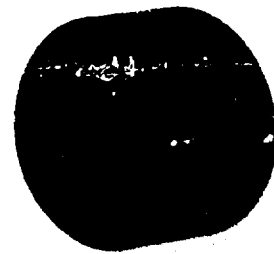
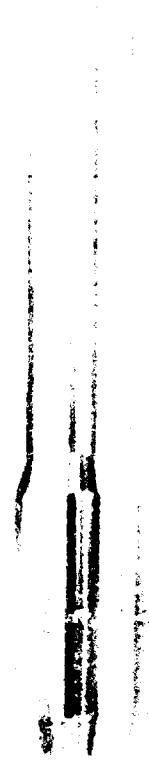
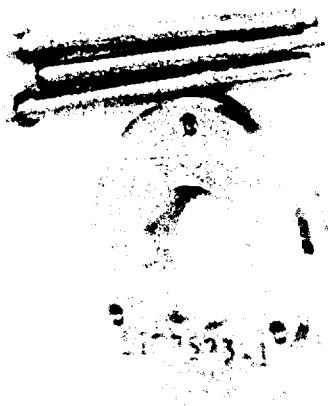
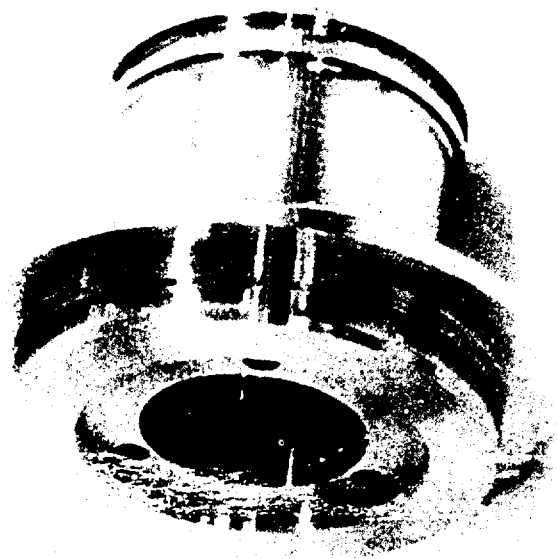


Figure 4.1-3. Floating Shaft Seal and Quill Shaft With Seal Housing

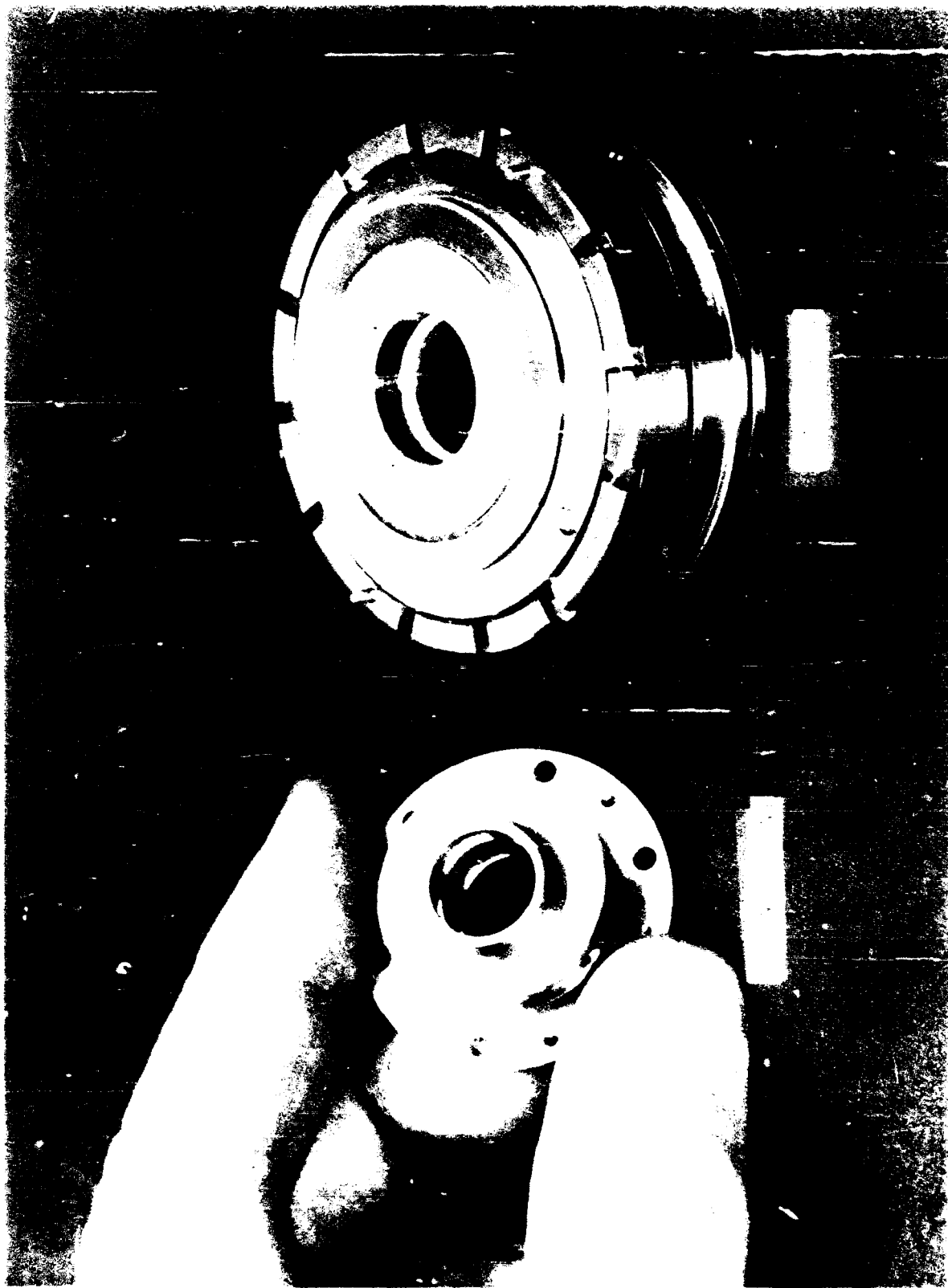


Figure 4.1-4. Assembled Turbine and Pump Bearings

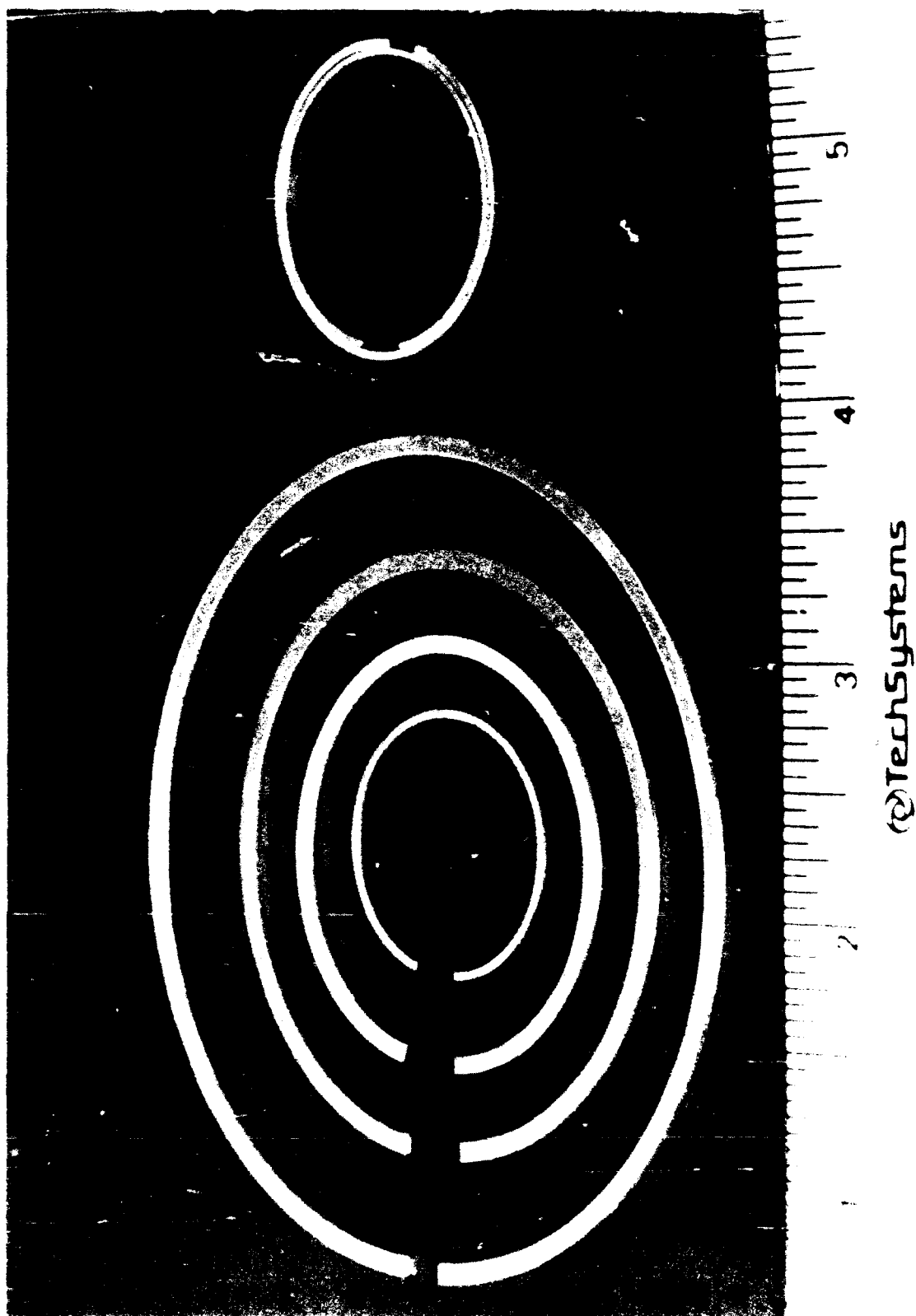


Figure 4.1-5. Turbopump Housing Seal Split Rings

4.2, Test Approach and Rationale, cont.

accompany a major design change after the design is reduced to a complete test unit. If results are not as desired the design change can be made with the benefit of test results and prior to the fabrication of all other hardware. Two or three variants of a design can be compared in a short period of time and the best selected. This program did not have any alternate designs, and there were insufficient resources to do any significant design iteration if the design was faulty. The major result of the test program was confirmation that the bearing worked as expected without significant clearance or alignment problems.

4.3 FACILITY BUILDUP

4.3.1 Facility Schematic and Flow Loop Description

The facility schematic is given in Figure 4.3-1. The bearing tester flow loop is a once through system that used pressurized tanks to supply bearing fluid, housing coolant and turbine drive gas. Exiting nitrogen liquid/gases are vented to the atmosphere.

The hydraulic design of the flow system was modeled using the Aerojet simulant code, NETSIM. The nodes and branches for the model are shown in Figure 4.3-2. This simulation was used to predict pressures and flow rates at various points in the system.

4.3.2 Facility Instrumentation

The details of facility instrumentation are given in Appendices A and B.

One item not covered in the appendices is the speed and proximeter probe installation used for turbopump speed and shaft motion detection. A flat of 0.002 inch is machined on the rotating assembly shaft directly below the tip of a proximeter probe. This step is used to calculate speed. The signals are sensed by special probes made by the Bently-Nevada Co. The tips are a ceramic material selected for compatibility with oxygen. A picture of the probe and a signal conditioning unit are given in Figure 4.3-3.

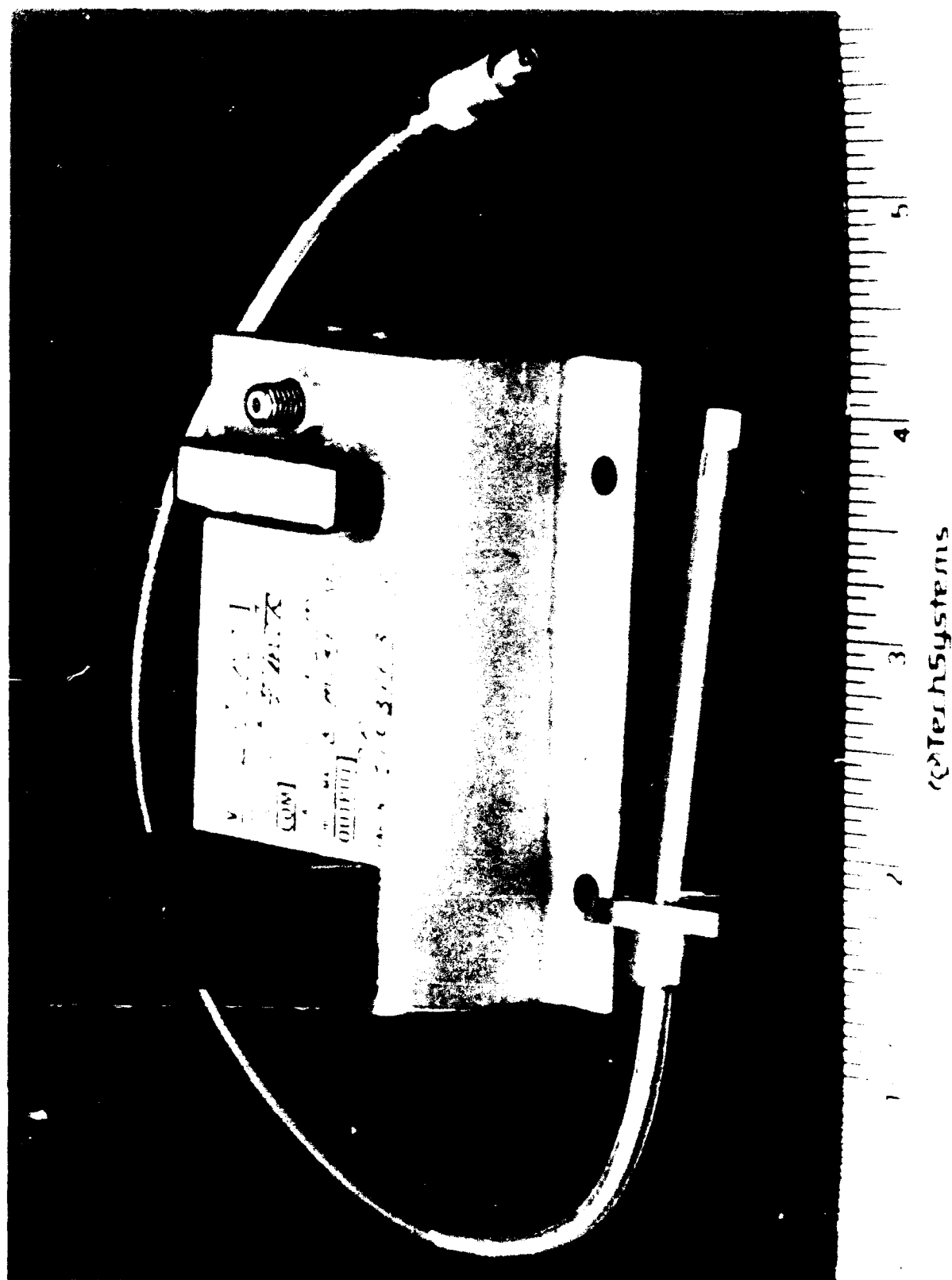


Figure 4.3-3. Inductance Distance Probe with Signal Conditioning Box

4.3, Facility Buildup, cont.

This signal change caused by the known step is divided into the signal strength at any other location to obtain the multiplier based on the known step distance to calculate the shaft radial or axial movement. Two probes in each axial position are 90° apart in order to produce orbit plots of shaft movement. A third probe senses axial movement. In all, five probes are used to read shaft motion: two in the planes at each end of the shaft assembly, (total 4), and one to read axial motion. Figure 4.3-4 shows the axial distance detector flange face at the pump suction elbow. The exit from the elbow is shown in Figure 4.3-5 where the probe tip can be seen slightly offset from the center of the housing. The radial support struts are clearly seen in the photo.

Instrumentation for the bearing tester and drive turbine is listed in detail in Appendix A, location/identification, and Appendix B for function and type of instrument.

4.4 TEST PROCEDURES

4.4.1 Test Plan Requirements

The original oxygen TPA test plan divided the testing into seven series, A through G, with series A and B comprising the bearing test phase of the program. Table 4.4-1 gives a summary of the test objectives and verification goals. The formal test plan was prepared as a separate document with NASA-LeRC review and concurrence. It contains details on data requirements, photographic requirements, and safety.

4.4.2 Test Conduct

The testing is initiated when the lines through the bearing tester have been tested to confirm that water contamination is <50 ppm of water. The 50 gallon-5500 psi tank is chilled and filled with liquid nitrogen from the 1800 gallon-50 psi storage vessel, Figure 4.3-1. The 50 gallon run tank is then pressurized to ~5000 psi by the 10,000 psi cascade. The flow control valve is then opened and regulated to the prescribed bearing inlet pressure for pressurized tank supply. Flow is directed to the turbine and pump bearing inlet ports and the pump suction cavity. The shaft



Figure 1-10 Inlet Housing -- Distance Probe Port, P/N 1197575



Figure 4.3-5. Inlet Housing — Distance Probe Tip End, P/N 1197575

TABLE 4.4-1.
Oxygen Turbopump Test Plan Highlights

A. LOW SPEED LOW PRESSURE BEARING POWER CONSUMPTION FLOW NITROGEN

<u>PURPOSE</u>	<u>OUTPUT</u>	<u>DECISION</u>	<u>CONFIGURATION</u>	<u>MODEL</u>
Checkout test. Confirm bearing flow coefficients. Record bearing cooldown rates. Record bearing torque as a function of flow rate and speed. Record bearing clearance and dynamics.	Torque vs. speed vs. flow rate. Temperature vs. time vs. flow rate. Bearing clearance and dynamics of shaft orbit.	Test system is functioning satisfactorily. Bearing flow coefficients are satisfactory. Shaft assembly is dynamically stable at low speeds.	Unbladed pump and turning rotors to isolate bearing and shaft drag power. Externally pressurized bearings. Powered by external torque measuring turbine assembly.	"CRSP," "AXTH," "HJBRG" and "HJIBRG" - Verify bearing flow load, capacity, stiffness, torque and rotor dynamics at low speed.

B. MAXIMUM SPEED HIGH PRESSURE BEARING POWER CONSUMPTION AND DYNAMICS FLOWING NITROGEN

<u>PURPOSE</u>	<u>OUTPUT</u>	<u>DECISION</u>	<u>CONFIGURATION</u>	<u>MODEL</u>
Confirm the same functions as Series "A" at full pressures and maximum speed.	Torque vs. speed vs. flow rate. Temperature vs. time vs. flow rate. Bearing clearance and dynamics.	Shaft system is stable at maximum speed that it is safe to operate up to full speed.	Same as "A."	Same as "A" series but extended to high speed.

C. LOW SPEED PUMP PERFORMANCE WITH BEARINGS FLOWING NITROGEN

<u>PURPOSE</u>	<u>OUTPUT</u>	<u>DECISION</u>	<u>CONFIGURATION</u>	<u>MODEL</u>
Pump hydraulic performance and efficiency at partial speed.	Head rise vs flow rate vs speed. Efficiency vs flow rate vs shaft speed.	Pump characteristic and efficiency determined using tare bearing torque from Series "B."	Complete pump and bearing system powered by external torque measuring turbine drive assembly. Turbine in tester unbladed. Bearings externally pressurized for start cycle. Bearings pump fed for remaining cycle.	"HEAD" - Verify head/flow coefficients, efficiency and suction specific speed to impeller clearance.

D. TURBINE PERFORMANCE AT RATED SPEED FLOWING NITROGEN FOLLOWED BY FIRST LOX IN PUMP AND BEARINGS

<u>PURPOSE</u>	<u>OUTPUT</u>	<u>DECISION</u>	<u>CONFIGURATION</u>	<u>MODEL</u>
Turbine performance and efficiency to full speed with nitrogen in pump and turbine. First LOX in pump and bearings driven by nitrogen in turbine.	Torque and efficiency vs. speed. First LOX experience in bearings.	Turbine performance and efficiency satisfactory at initially selected clearance. Bearings demonstrate reliable steady state operation in LOX.	Complete turbopump comprising of inducer, two stage pump and integral turbine. Bearings fed by integral pump with externally pressurized start. GN ₂ turbine gas.	"TM 0021" and "TM0022" - Verify torque-pressure ratio. Speed relations vs. clearance to blade height ratio.

TABLE 4.4-1. (Cont)
Oxygen Turbopump Test Plan Highlights

E. PUMP/BEARING TANKHEAD START TRANSIENT IN OXYGEN			
<u>PURPOSE</u>	<u>OUTPUT</u>	<u>DECISION</u>	<u>CONFIGURATION</u>
Confirmation of tankhead bearing start transient. Determine cooldown time required before rotating shaft assembly.	Temperature vs. time history. Conform acceptable wear levels of shaft to bearings.	Bearing has acceptable wear rate during start transient.	Complete turbopump with bearings internally pressurized by pump. GN ₂ turbine gas.
			<u>MODEL</u>
			"Engine performance dynamic model" utilizing "TUTSIM." Heat transfer coefficients determined for turbopump.
F. EFFECT OF TURBINE TIP CLEARANCE ON TURBINE EFFICIENCY			
<u>PURPOSE</u>	<u>OUTPUT</u>	<u>DECISION</u>	<u>CONFIGURATION</u>
Obtain the performance of turbine as a function of tip clearance.	Torque and efficiency as a function of pressure ratio and speed.	Tip clearance to achieve adequate turbine power for a given pressure ratio.	Same as "E."
			<u>MODEL</u>
			"TM0021" and "TM0022" - Torque - pressure ratio - speed - relations to clearance/blade weight ratios.
G. DEMONSTRATE GASEOUS OXYGEN DRIVEN TURBINE			
<u>PURPOSE</u>	<u>OUTPUT</u>	<u>DECISION</u>	<u>CONFIGURATION</u>
Demonstrate gaseous oxygen driven axial flow turbine. Demonstrate 100 start/stop cycles. Demonstrate 5 hours total accumulated life.	Turbopump pressure, flow speed and fluid temperatures. Shaft clearance and orbit.	Gaseous oxygen driven turbines are feasible. Hydrostatic bearings in oxygen are feasible. Turbopump assembly has a 5 hour, 100 start/stop cycle life.	Complete turbopump with bearings internally pressurized by pump. Gaseous oxygen in turbine.
			<u>MODEL</u>
			Additional data to confirm data obtained in all previous test series.

4.4, Test Procedures, cont.

assembly is lifted by the radial and axial bearing pockets before rotation starts to avoid the chance of rubbing during the first few revolutions. Bearing flow is discharged through ports provided in the turbopump housing. When liquid is sensed leaving the bearings, the drive turbine torquemeter assembly is powered by gaseous nitrogen. The drive turbine torquemeter/bearing tester is then uniformly accelerated to the desired speed.

4.5 TESTING

4.5.1 Facility Checkout and Tester Chillydown

All lines and the tester were thoroughly purged with dry nitrogen until dew point tests showed less than 50 ppm of water per liter. In September 1986 testing commenced with a series of runs (A1, A2, A3-1, A3-2, and A3-3) to determine the bearing circuit flow characteristics and the chillydown time. Bearing flow circuit orifices were resized based on the chillydown flow data.

The temperature of the turbopump is important for at least two reasons. First, adverse temperature gradients may cause adverse deflections of close clearance components. Second, two phase flow in hydrostatic bearings and pump inlets will promote unstable bearing performance and pump cavitation. This rotor-bearing tester was tested for chillydown characteristics with flow to the bearings and pump inlet simultaneously. This is a very restricted flow path relative to the real turbopump with impeller vanes and pump discharge passages. The data for a chillydown test is shown in Figure 4.5-1. The data includes one metal surface temperature on the turbine seal diaphragm. Eleven thermocouples give fluid temperatures for such locations as the bearing inlet, the pump bearing exit cavity and the pump inlet. Supply pressure to the turbopump was from a low pressure tank at approximately 56 lb/in². After about 1000 seconds the low pressure tank valve was closed and a second tank with 120 lb/in² supply pressure was used for approximately 500 seconds. The end temperatures were about the same for the two pressures. The bearing inlet temperature came down immediately but the other two fluid temperatures, pump inlet and bearing exit, took several minutes. The turbine seal

TEMPERATURE AS A FUNCTION OF TIME

- △ TEMPERATURE PUMP SIDE OF DIAPHRAM INSIDE DIAMETER
- TEMPERATURE BEARING INLET
- TEMPERATURE SUCTION EXR
- ▽ TEMPERATURE PUMP BEARING EXIT CAVITY

TEST NO. 2459 - 120 - A7 - 15

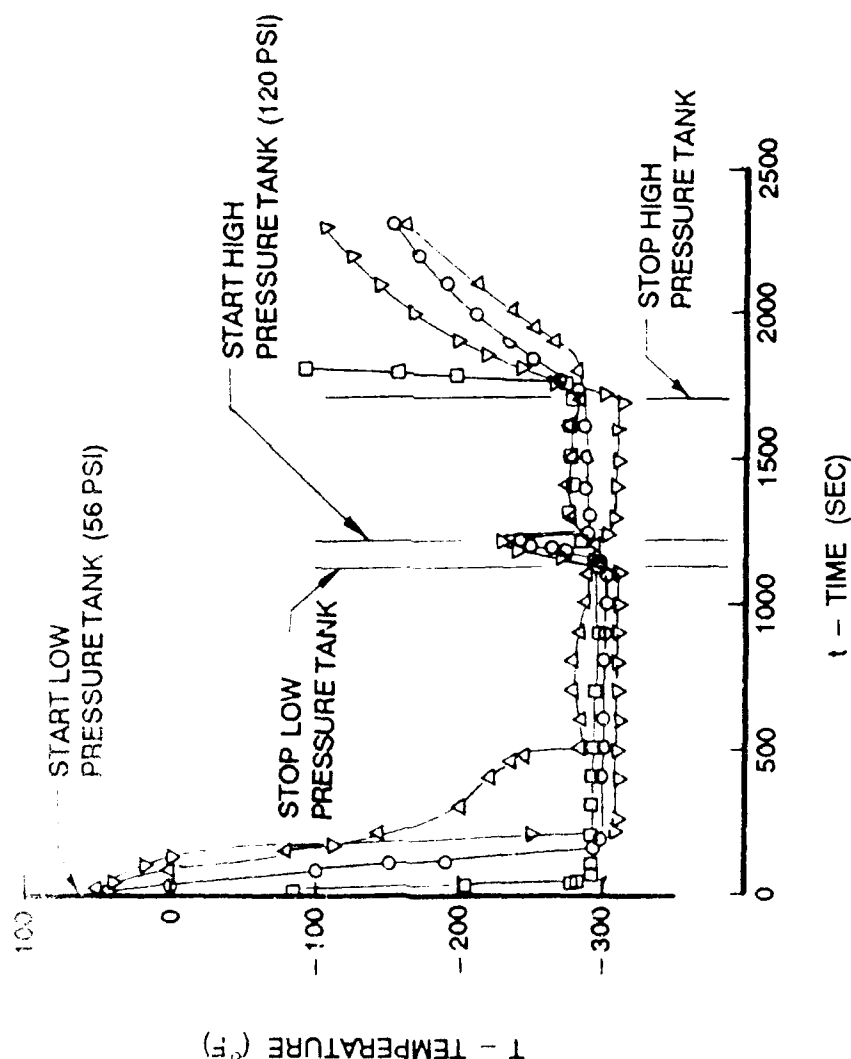


Figure 4.5-1. Temperature as a Function of Time

4.5, Testing, cont.

diaphragm took approximately 500 seconds. The turbopump is designed to accommodate thermal gradients, the two phase fluid in the pump and bearing is undesirable. This chilldown time was considerably reduced in the complete TPA due to the improved liquid access.

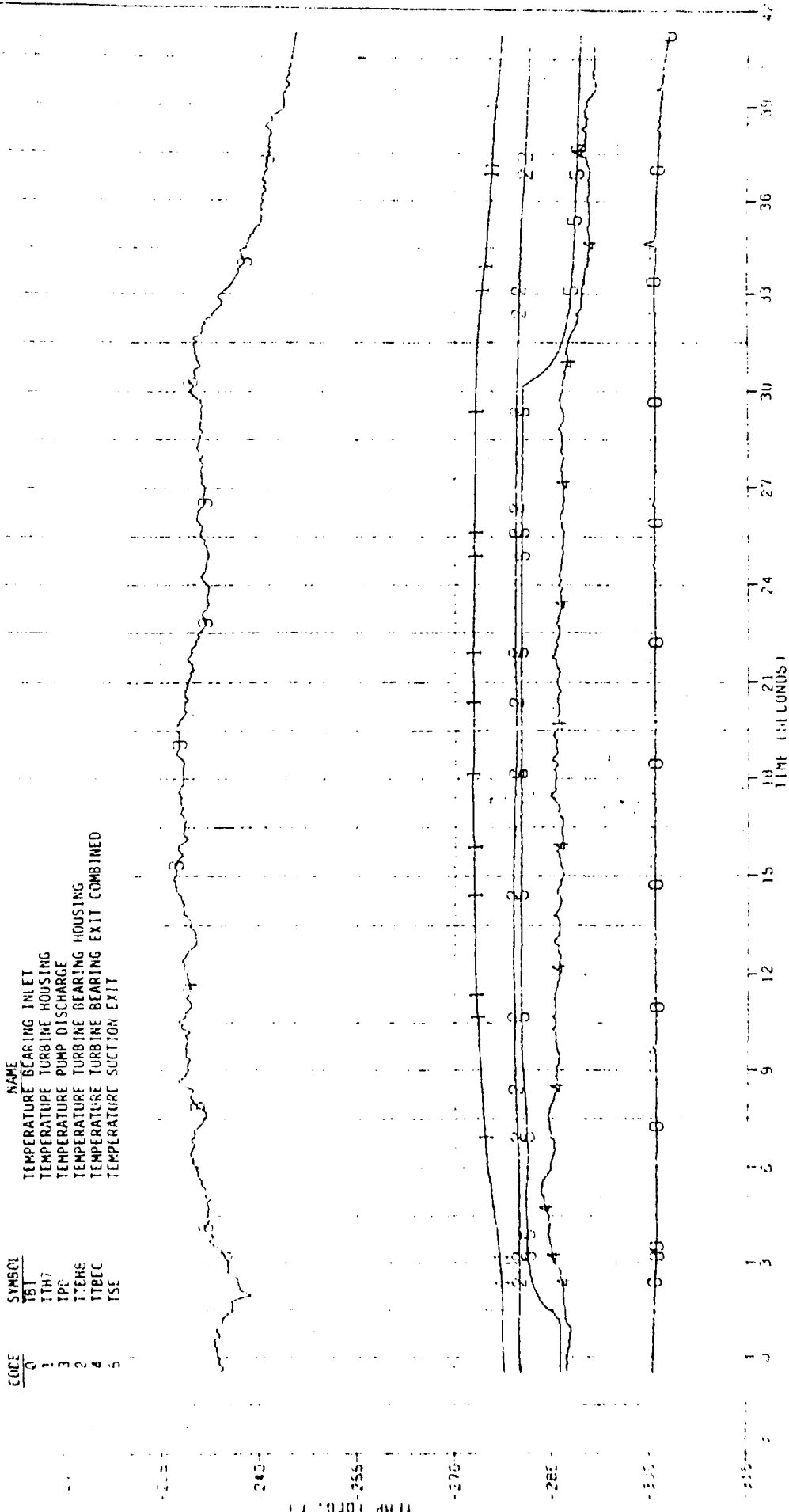
Actual data plots for test No. A7-042 are given as Figures 4.5-2 and 4.5-3. These plots are typical of the successful TPA chilldown runs.

Tests A3-4 and A4 were conducted in November 1986. Revised orificing had not brought the pressure loading on the shaft assembly to the design direction. Repeats of Series A4 were required to insure safe loads before going on to higher pressure tests in Series A5. The torque readings, following the re-orificing, showed that the pressure imbalance could be corrected to pressure load the shaft in the design direction. The problems encountered were attributed to the fact that the test hardware uses a mechanical driver instead of an actual turbine assembly. This was one of many instances where time and energy had to be expended on solving a tester problem not related to the bearing performance.

Four tests were conducted in December 1986. The first test, Run #12, was conducted to confirm the accuracy of the high pressure range transducers used at their lower range. Gaseous nitrogen was used to pressurize the Bearing Tester Assembly with all exit ports sealed. All transducers sensed within their typical error tolerance at the low pressures being used in the initial tests.

Chilldown tests 13, 14 and 15, were directed toward controlling the back pressure in the bearing tester cavities which control the rotor thrust and the bearing pressure differentials. With high rotor thrust and low bearing pressure differential, the rotating assembly experiences excessive drag torque. Excessive torque is defined as 30 in. oz or greater. Adjusting the back pressure orifices did not result in predictable back pressure based on liquid flow. Flow and back pressure measurements indicated various degrees of two phase flow at several locations within the tester cavities.

PREPARED BY: J. A. B. 10/27/87
 DRAWING NO. 2459-120-A7-042



FLUID AND HOUSING EXTERIOR-TEMP. VS. TIME
 TEST NO. 2459-120-A7-042 PLOT NO. 1
 TEST STAND A287 TEST DATE 06-03-87

AEROJET
@TechSystems
 COMPANY

Figure 4.5-2. Fluid and Housing Exterior-Temp. vs. Time Test No. 2459-120-A7-042
 Plot No. 1 Test Stand A287 Test Date 06-03-87



4.5, Testing, cont.

Test #15 also was started by flowing from the low pressure chill-down supply tank and then switching over to the high pressure run tank at about 115 psi in an attempt to suppress the two phase flow. It produced a greater back pressure than tests 13 and 14. The drag torque on the rotor was a natural result of improper pressure differentials within the tester with very little pressure differential across the bearing. With the termination of flow and the resulting pressure decay at the end of the test, torque slowly declined to zero with time. A residual torque persists for a few minutes as the tester warms. These conditions may exist due to a cocked bearing. The lack of sufficient pressure drop across the bearing can leave it misaligned. The pressure-temperature measured near or in the exit lines indicate two phase conditions at some exit orifices.

The Bently proximeter probes were returned to the manufacturer prior to the Christmas break in the testing. Lack of comparable readings made it necessary that they be calibrated. Two were found to be inoperative. A fifth signal conditioning unit was ordered as one of those in use was not compatible with the probe at cryogenic temperatures.

Testing was resumed in January 1987 with five tests. Continued conflict with other programs prevented more tests being run. Ambient temperature nitrogen was used in the tests to eliminate temperatures as a cause of the high static drag torque encountered in earlier tests. A synopsis of the tests follows:

Test #16

The purpose of flowing ambient temperature nitrogen is to eliminate temperatures as a variable. The ambient temperature gaseous nitrogen was supplied at pressures up to 115 psia. The torque remained low, (2 in. oz) up to 100 psia. The torque increased above 100 psia to a maximum of 30 in. oz. It was limited to less than a 90° arc of a full revolution.

The first stage inlet pressure was too high for correct simulation of turbopump pressures and loads. The turbine bearing did not develop sufficient pressure drop. This could have contributed to the drag torque by not having sufficient restoring pressure to float the bearing free.

4.5, Testing, cont.

Test #17

A second ambient temperature gaseous nitrogen test was conducted at pressures up to 500 psia to see if the shaft assembly would float free or self align. Static breakaway torque was very low until the load shifted at about 120 psi supply pressure. The cause is thought to be the inability to control pump suction pressure (PSE) which is the predominate pressure-area force controlling rotor thrust. At about 120 psi the thrust load opened the pump bearing sphere and first stage suction pressure increased due to the additional flow. Torque also increased at the same time.

Test #18

A hand operated valve was installed to allow the suction cavity exit line resistance to be varied.

The turbine cavity exit line orifice diameter was increased to reduce the turbine cavity back pressure. These two changes did reduce the bearing back pressures but not as much as desired. Valve area was not quite large enough. Very low torque values were achieved over full pressure rise.

Test #19

A larger cryogenic hand valve was installed in the suction cavity exit line to replace the initial valve. In addition to being larger it is insulated for later tests in liquid nitrogen. The bearing turbine side cavity exit line orifice was further increased. These changes allowing the suction exit line resistance to be controlled at the tester caused the shaft rotating assembly to float free of solid contact. This test allowed the proper pressure ratios through the tester to simulate turbopump pressures and resulted in very low torques to 500 psi. In addition with this larger hand valve it was possible to vary the first stage inlet pressure (PSE), to determine the limits for binding the shaft.

4.5, Testing, cont.

Test #20

Test #19 showed the bearing system workable in ambient temperature gaseous nitrogen. Test #20 was conducted by chilling the Bearing Tester Assembly with the low pressure (50 psi) storage tank followed by the smaller high pressure tank for pressures above 50 psi. Within 10 seconds of the initiation of the high pressure tank flow there developed an increasing resistance between the run tank and bearing inlet lines. The high resistance remained until it quickly decayed at a feed pressure of 500 psia. Post test examination of the system revealed a ruptured metal 10 micron filter in the main feed line. The prime potential cause of the filter resistance is thought to be water or freon ice. An investigation was conducted to determine the source. The system had been used without incident in previous tests.

The investigation of the high pressure flow line and tank (upstream of the ruptured 10 micron filter) found some Freon like fluid in drain stub teeing off the bottom of the tank. This could also have been the source of the material causing the filter blockage and rupture. The entire circuit was cleaned and rechecked for contaminated fluid. The cleaning continued until the 200 to 250 ppm of moisture content was brought down to 1.5 to 8.5 ppm. The secondary filters were examined and found free of solids contamination. The final conclusions as to the cause of the upstream full flow filter collapse is that it was probably Freon vapor snow produced when the cold liquid nitrogen cooled the vapor in the system. Source of the Freon was not determined. Contamination checks were conducted before each test from then on.

Spin testing of the assembly was initiated in March 1987 to begin the actual Series A testing.

4.5.2 Series A Testing

Series A testing started in March 1987. To limit the possible overspeed of the rotor systems, a short bypass line with two valves was connected

4.5, Testing, cont.

around the main GN₂ flow control valve. This allowed about 8 cubic inches of turbine drive gas to be locked up in the line. Release of this gas to the turbine permitted a limited flow to the turbine to allow rotation without overspeeding. The first two attempts at 100 psia and 500 psia were insufficient to overcome the static torque and cause rotation. The 500 psia lockup pressure yielded a leak at turbine inlet pressure of 20 psia. The third attempt at 1800 psi yielded 63 psia inlet pressure and drove the rotors to 2700 rpm. Bearing liquid nitrogen inlet pressures were 1000 psia. Indicated tare torque of 11 in.-lbs suggested there could be rubbing in either the drive turbine assembly or the bearing tester. The bearing tester was disassembled to make the first inspection of the internal parts since testing started. No wear or signs of rubbing were found. The bearing tester was reassembled with high pressure metallic "V" seals replacing the teflon "O" rings.

As the bearing tester inspection revealed no evidence of the source of the high torque, the test drive turbine/torquemeter assembly was investigated. A temperature (bearing outer race) versus time history test was conducted employing various means of keeping the assembly warm. Gaseous nitrogen flow from the bearing tester quill shaft seal discharges toward the test drive turbine/torquemeter assembly. Active and passive means were employed to impede the resulting cooling. Warmed gaseous nitrogen is directed at the interconnecting quill shaft and a mechanical deflector is placed between the drive turbine and the bearing tester with felt material used to fit closely around the quill shaft.

Chill testing with and without the afore described methods revealed that as much as an in.-lb of torque can be developed by the test drive turbine being cooled to an outer race bearing temperature of 36°F. As much as 1 in.-lb of torque is developed when the housing cooling chills the bearing race to -47°F, and 4 in.-lb at -90°F. With the source of at least some of the drag torque established as coming from a cooled test drive turbine, a barrier cold gas deflector with a quill shaft seal was used in subsequent tests along with a warm GN₂ purge gas flow to the test drive unit.

Dynamic testing continued in April 1987 with the object of increasing the shaft speed. Runs 29-31 took the shafting to 10,000 rpm but stand

4.5, Testing, cont.

equipment failure limited pressurization. Run 32 did drive the shaft assembly to 29,000 rpm with bearing inlet pressures of 2000 psia. The speed signal was inaccurately digitalized during a portion of the test due to the equipment limitations in counting the speed sensor pulses, see Figure 4.5-4. The maximum speed was verified by making a visual count of pulses off of the high speed strip chart.

A decline of turbine cavity pressure after 28 seconds into the run suggested wear of the quill shaft floating ring seal. A disassembly of the bearing tester confirmed abnormal unidirectional wear of the carbon ring internal diameter and axial face. The quill shaft outside diameter exhibited corresponding scoring, Figure 4.5-5. On examination, the turbopump bearings were found to be in excellent condition. No wear or marking was visible.

The distance sensing probes mounted in the bearing tester did not give readable signals. In order to enhance their signal, the clearance gap was reduced from a nominal 0.015 inches to 0.010 inches. This was based on advice of the manufacturer. Recalibration data had resulted in the best sensing gap at 0.010 inch.

The bearing tester was reassembled with the spare quill shaft and seal.

The test drive turbine/torquemeter (TDT/TM) assembly was disassembled to assess that it had sufficient bearing preload (it has oil lubricated ball bearings). The shaft calibration notch was also investigated to confirm its depth and good signal generating capability. Runs 33 through 40 were conducted with the TDT/TM to recalibrate the speed sensing probes and demonstrate that operation above 60,000 rpm was smooth and not promoting the quill shaft seal wear. With the completion of these TDT/TM checkouts the test stand was made ready to realign the reassembled bearing tester.

4.5.3 Series B Testing

The final testing was completed in May of 1987 with successful completion of test Series B. A summary of the testing follows.

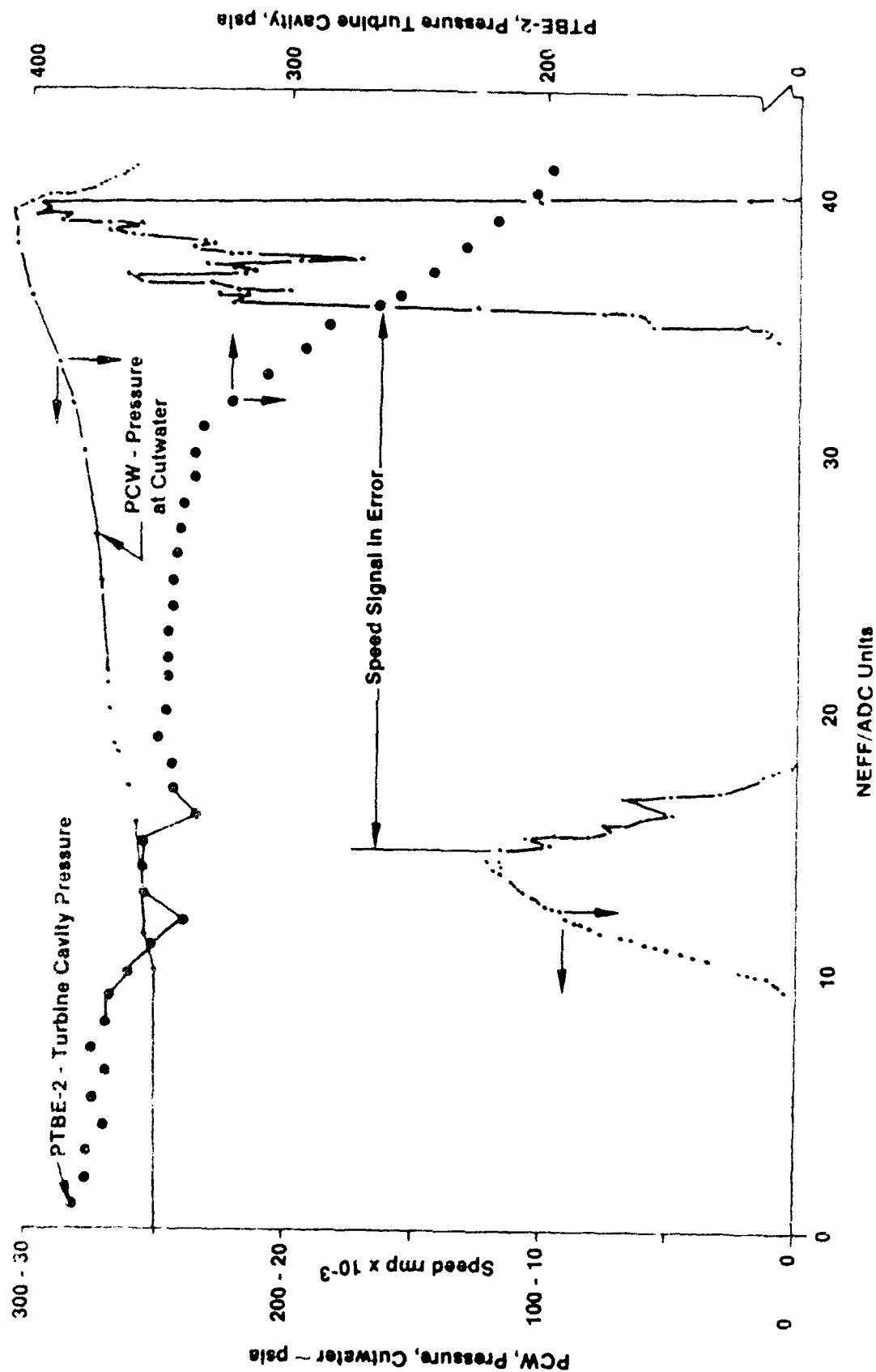


Figure 4.5-4. Test No. 2459-120-A7-32 OTV Bearing Tester Digitized Data

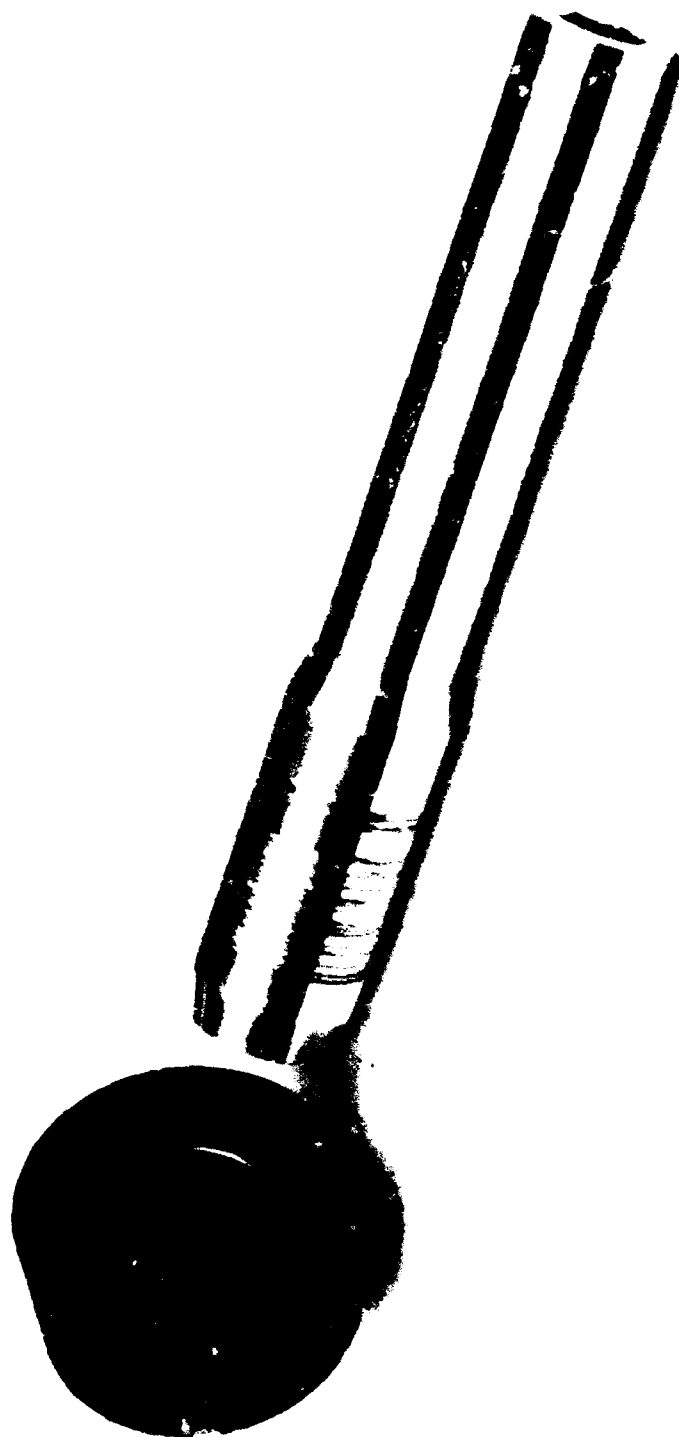


Figure 4.5-5. Quill Shaft

4.5, Testing, cont.

Test #41 was aborted when the turbine block valve did not fully open. Test #42 was conducted with greater actuation pressures permitting full turbine valve opening and 72,000 rpm speed to be reached. Bearing inlet pressures ranged from 3400 to 3100 psia over the 30 second run.

Ninety-six percent of design speed was reached with stable operation at no load conditions (the shaft was unbladed). No wear due to the test is in evidence. The four cryogenic distance detectors did deliver a signal in the liquid nitrogen environment but with no uniformity.

The following five figures have been excerpted from the analogue strip charts to illustrate the following comments. Figure 4.5-6 shows the first four revolutions of the start transient. The upper three traces are from the cryogenic distance detectors (DDTX, DDTY and DDPY). It is noted that no two are similar although all three are sensing the bearing tester shaft at the turbine or pump end. The shaft location being read is round except for a calibration undercut 0.25 inch wide by 0.002 inch deep used to reference any shaft movement. There seems to be a scaling factor difference and perhaps an induced signal. The pump end location (DDPY) for instance, has a 3800 cps output before there is any shaft rotation. There is no known 3800 cps source used in the signal processing.

The top trace (DDTX) has its upper value limited by an intermediate signal conditioner that reads zero if it exceeds a limit value. The flat dash between the broken trace is due to this process.

As the probes are identical it was expected their outputs would be similar. The lower two traces are of the two speed sensing probes that are mounted on the Test Drive Turbine Torquemeter. They operate at ambient temperature in air. Timing marks at the bottom of the trace are milliseconds.

Figure 4.5-7 and 4.5-8 are the same distance and speed sensor traces at 5000, 10,000, 20,000, 40,000, 60,000, and 72,000 rev./min. The interesting phenomenon illustrated is that DDTY output voltage seems to vary with speed. In all sensors the shaft appears to be running smoothly.

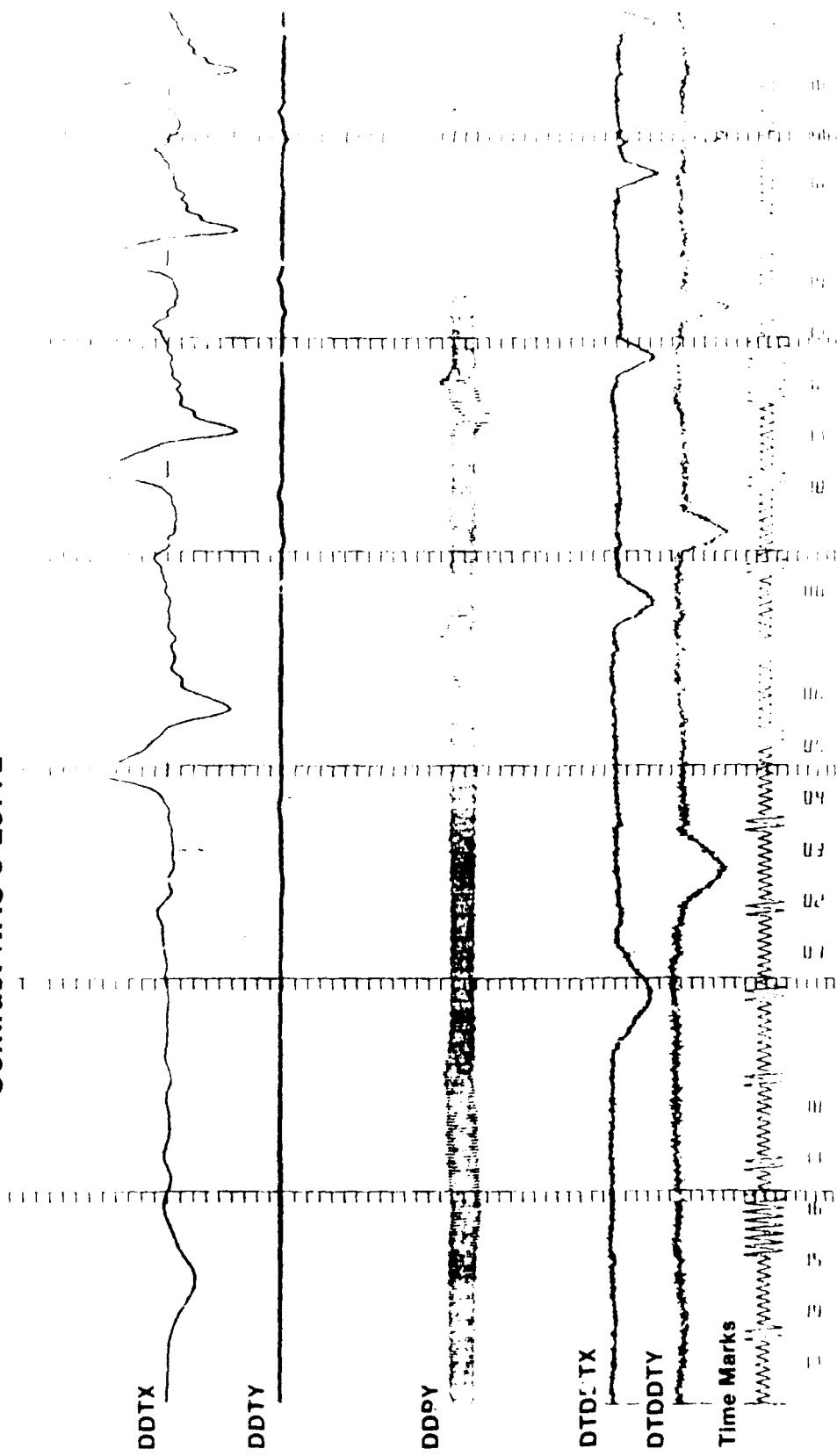


Figure 4.5-6. Cryogenic and Ambient Temperature Distance Sensors — Start Transient

Test 2459-120-A7-42
Contract NAS 3-23772

OTV Bearing Tester

5/6/87

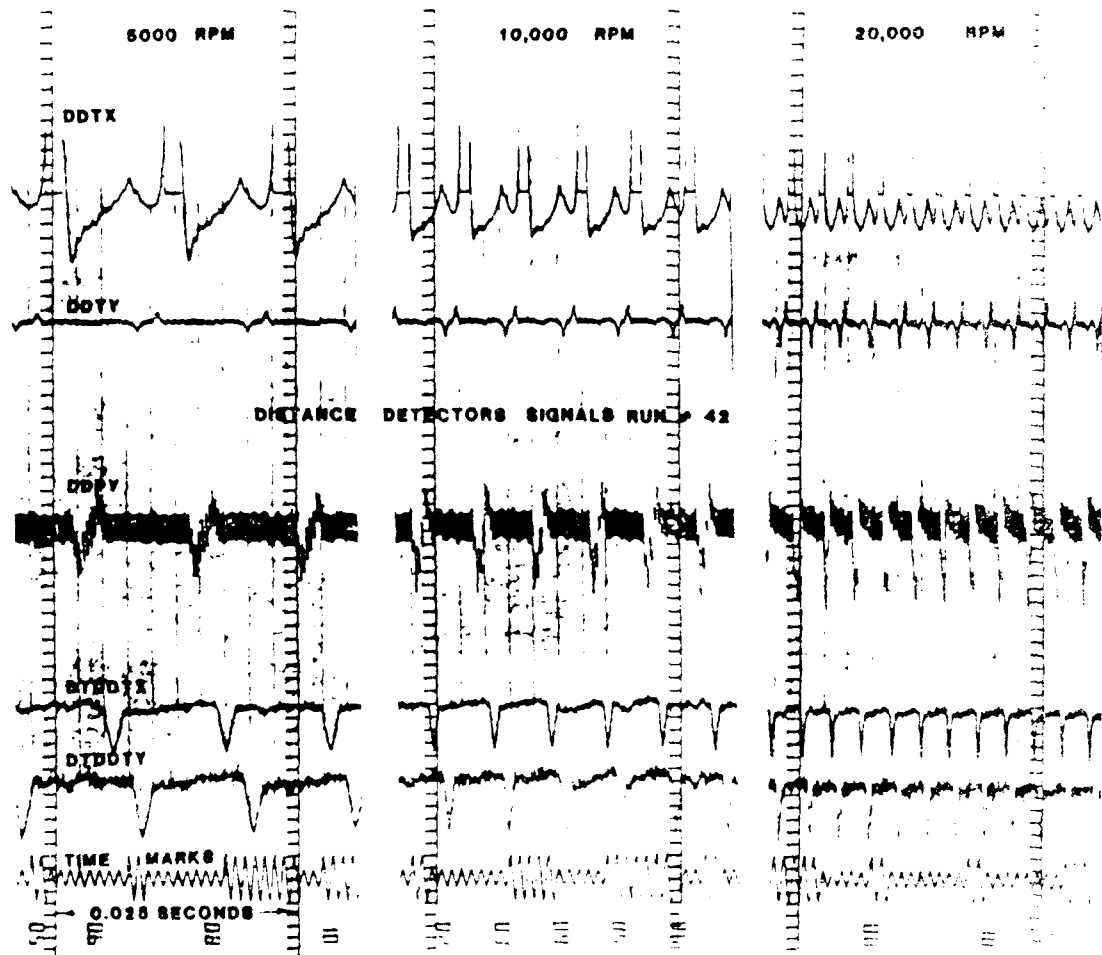


Figure 4.5-7. Distance Sensor Signal as a Function of Speed

Test 2459-120-A7-42
Contract NAS 3-23772

OTV Bearing Tester

5/6/87

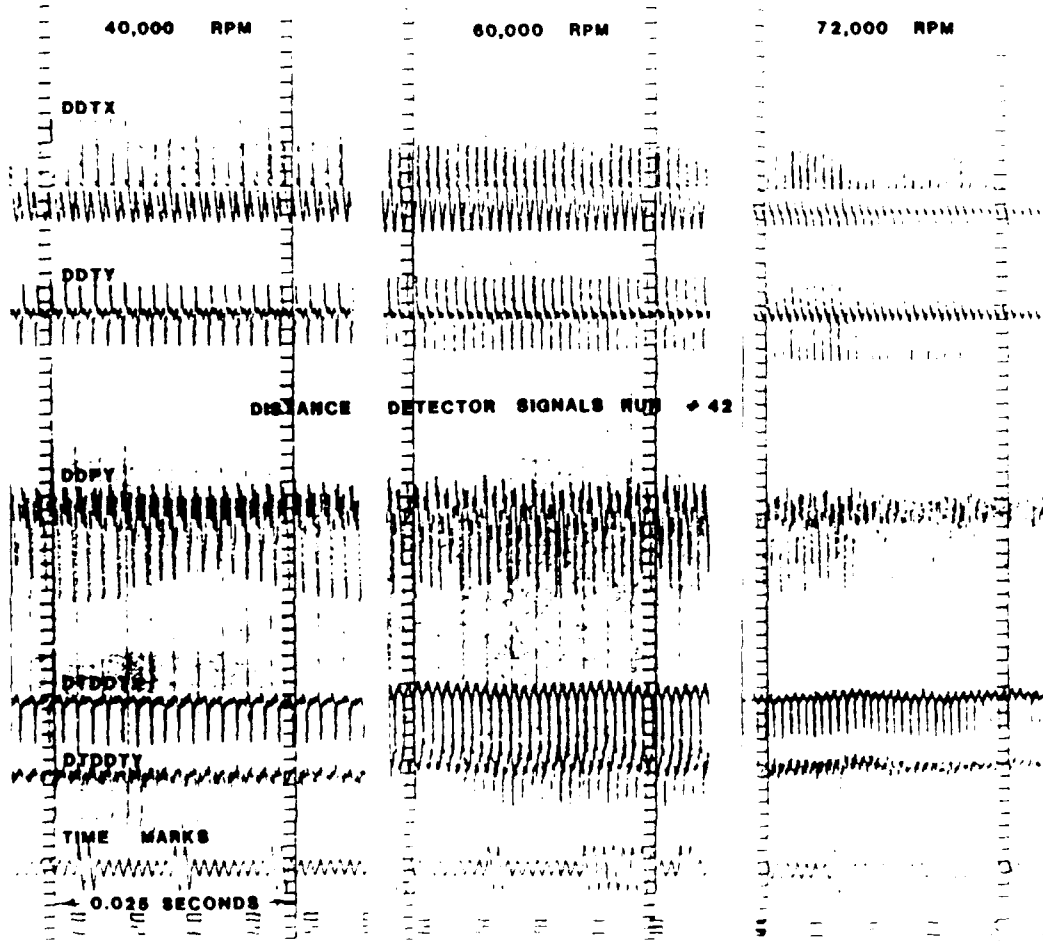


Figure 4.5-8. Distance Sensor Signal as a Function of Speed

4.5, Testing, cont.

Figure 4.5-9 gives an expanded trace of the same distance and speed sensors of the previous figures at the maximum test speed, 72,000 rev./min. They illustrate the same variation between sensors is also present at maximum speed. Timing marks are milliseconds per cycle.

Speed, displacement and flow data through the start transient of run 42 is displayed in Figure 4.5-10. all four cryogenic probes (DDTX, DDTY, and DDPY and DDPZ) produced a signal. Turbine "X" plane probe, DDTX, shows a strong signal that varies with speed. The phenomenon is evident in the raw signal of NTRAW but not at all in DDPZ. NTRAW probe is at ambient temperature. DDPZ is the axial probe submerged in liquid nitrogen. DDTX which shows the similar halving of the signal at the right side of the trace is also in liquid nitrogen. Temperature does not appear to be the cause of this phenomenon. Speed is 33,000 rev./min. at the right side of the data displayed. It is to be noted that the pump bearing flow, FMPBI, generated an irregular signal. This data indicates an under flow condition that is not believed to have existed. Either the meter rotor was slowed or the signal processor was malfunctioning. The turbine bearing meter, FMTBI, and suction cavity inlet flow, FMSI, yield the expected flow rates for the pressure drops imposed across the bearings.

A summary chart of the Series B testing is included as Table 4.5-1.

Computer processed data for run number 42 is given in Figures 4.5-11 through 4.5-14 for the full rotation duration.

4.5.4 Teardown Inspection

The disassembled bearing hardware in the post test condition is shown in Figure 4.5-15, after the high speed test. The rotating bearing surfaces are shown on the first stage impeller and the second stage impeller and shaft. The mating bearing surfaces can be seen on the pump end bearing and on the turbine end bearing. In all cases on post test examination the hard thrust and journal bearing surfaces on the rotating parts and the soft bearing surfaces on the stationary bearing parts were in excellent condition. Only minor scratches, the type expected

Test 2459-120-A7-42 OTV Bearing Tester 5/6/87
 Contract NAS 3-23772

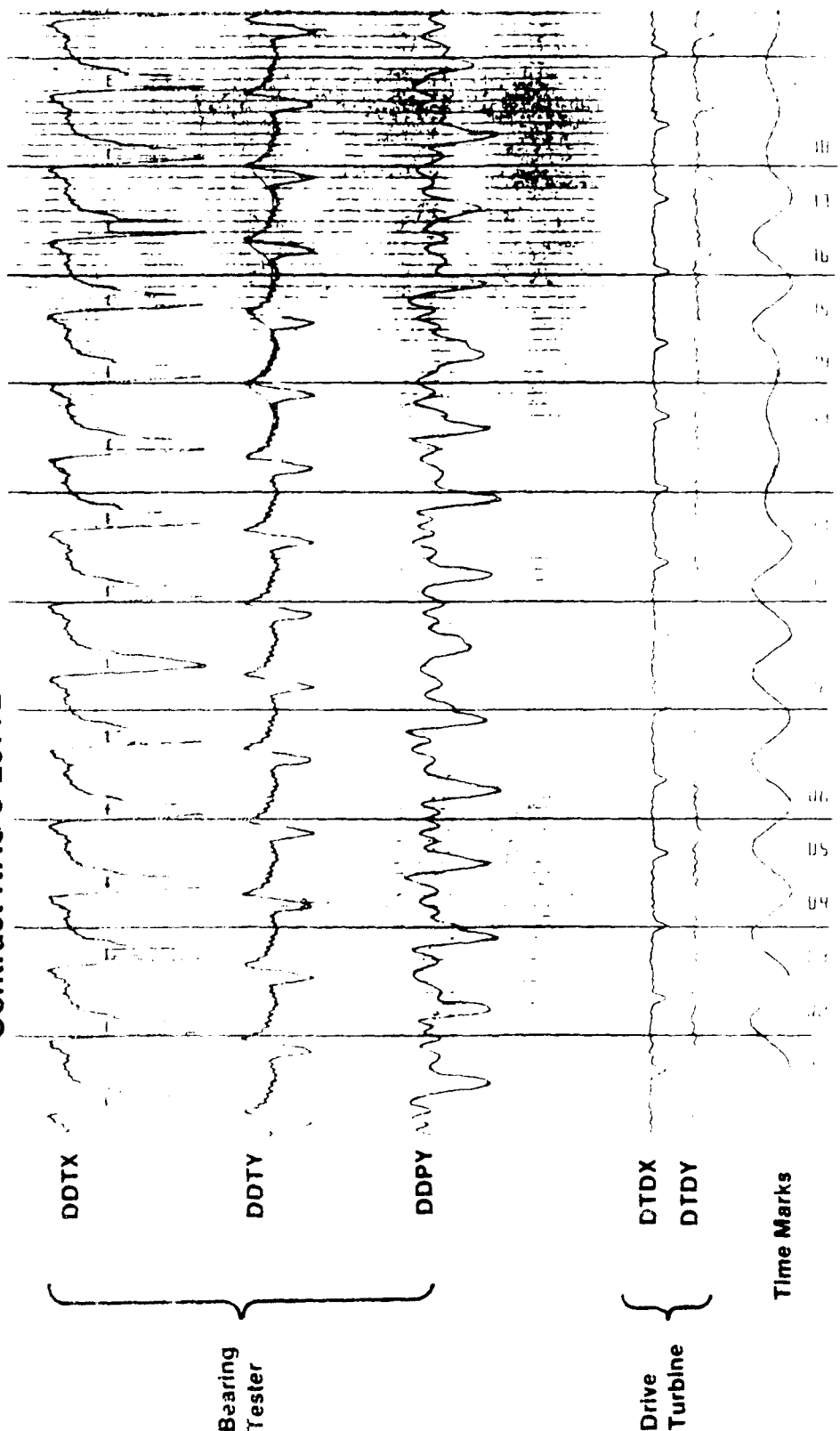


Figure 4.5-9. Cryogenic Operation of Distance Sensors at 72,000 RPM Steady State

Test 2459-120-A7-42 OTV Bearing Tester 5/6/87
 Contract NAS 3-23772

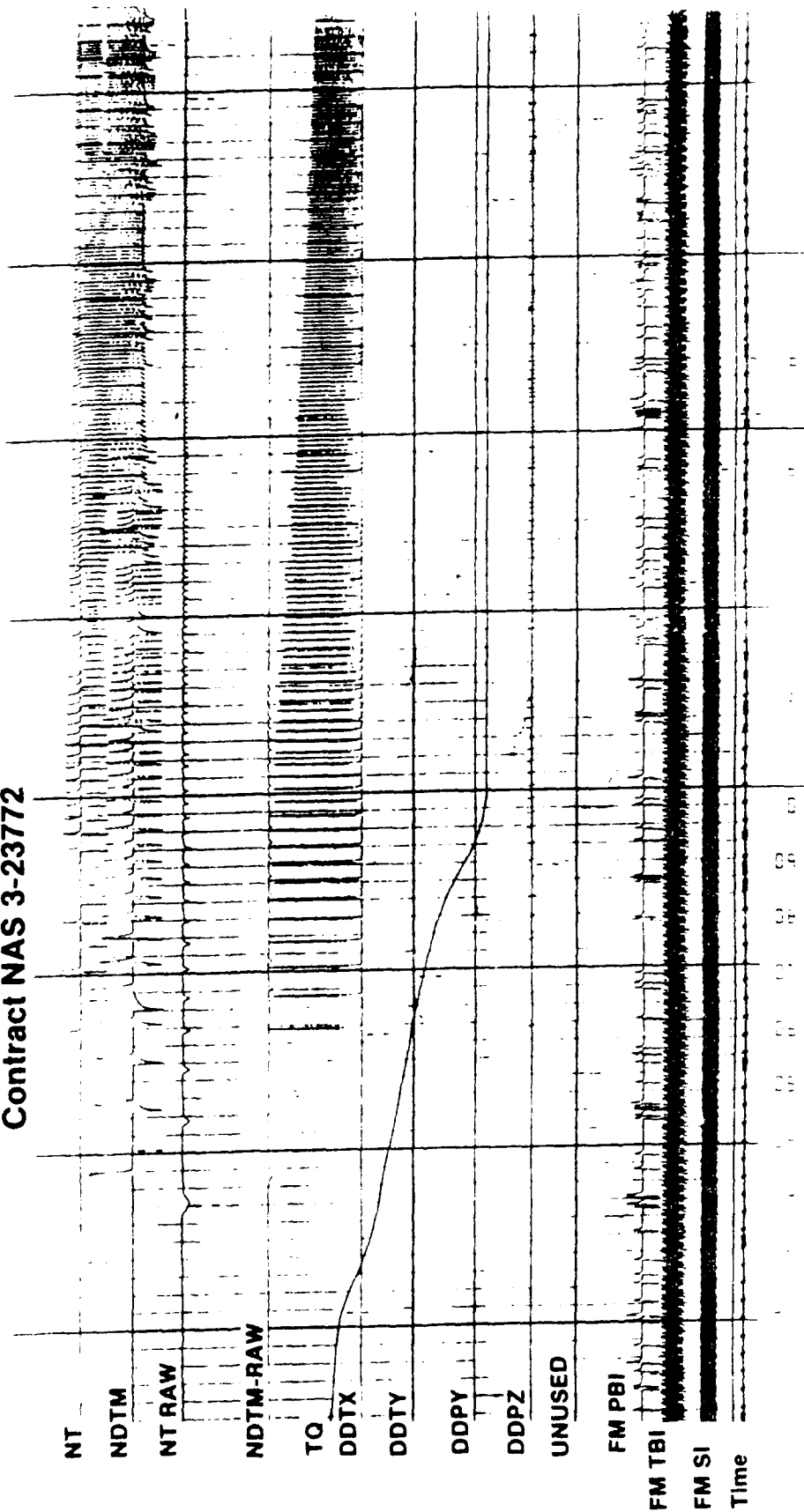
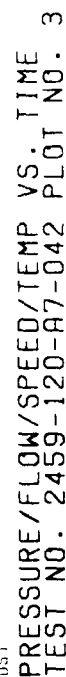


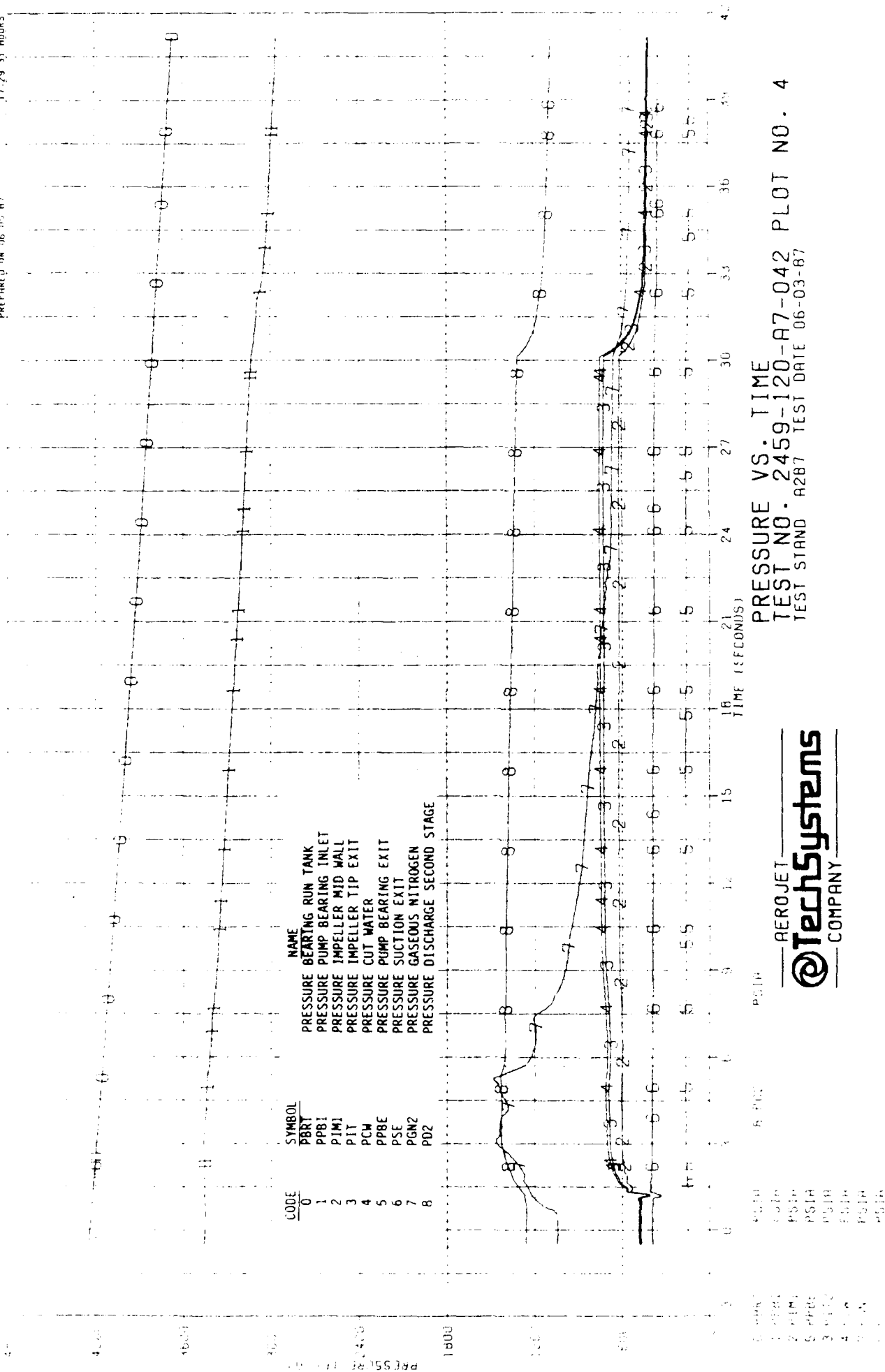
Figure 4.5-10. Cryogenic Operation of Distance Sensors Through Start Transient, Speed and Flow Meters

**TABLE 7.3-1.
Test Series "B" Summary**

		Pressure, PSIA	Speed, RPM
• Series "B" Four Runs	Gaseous Nitrogen Pressure Balance	115 to 500	---
• Series "B" Three Runs	Liquid Nitrogen Thermal Conditioning and Pressure Balance	500 to 1000	---
• Series "B" Three Runs	Liquid Nitrogen with Rotation	1000	2700
• Series "B" Four Runs	Liquid Nitrogen with Rotation	1600 to 2100	10,000
• Series "B" Three Runs	Liquid Nitrogen with Rotation	2050	30,000
• Series "B" Eight Runs	Drive Turbine Valve Checkout	---	---
• Series "B" Two Runs	Liquid Nitrogen Full Speed and Pressure	3400	72,000



AEROJET
Technics
COMPANY



PRESSURE VS. TIME
TEST NO. 2459-120-A7-042 PLOT NO. 4
TEST STAND A287 TEST DATE 06-03-87

— AEROJET —
@TechSystems
— COMPANY —

Figure 4.5-12. Pressure Vs. Time Test No. 2459-120-A7-042 Plot No. 4 Test Stand A287
Test Date 06-03-87

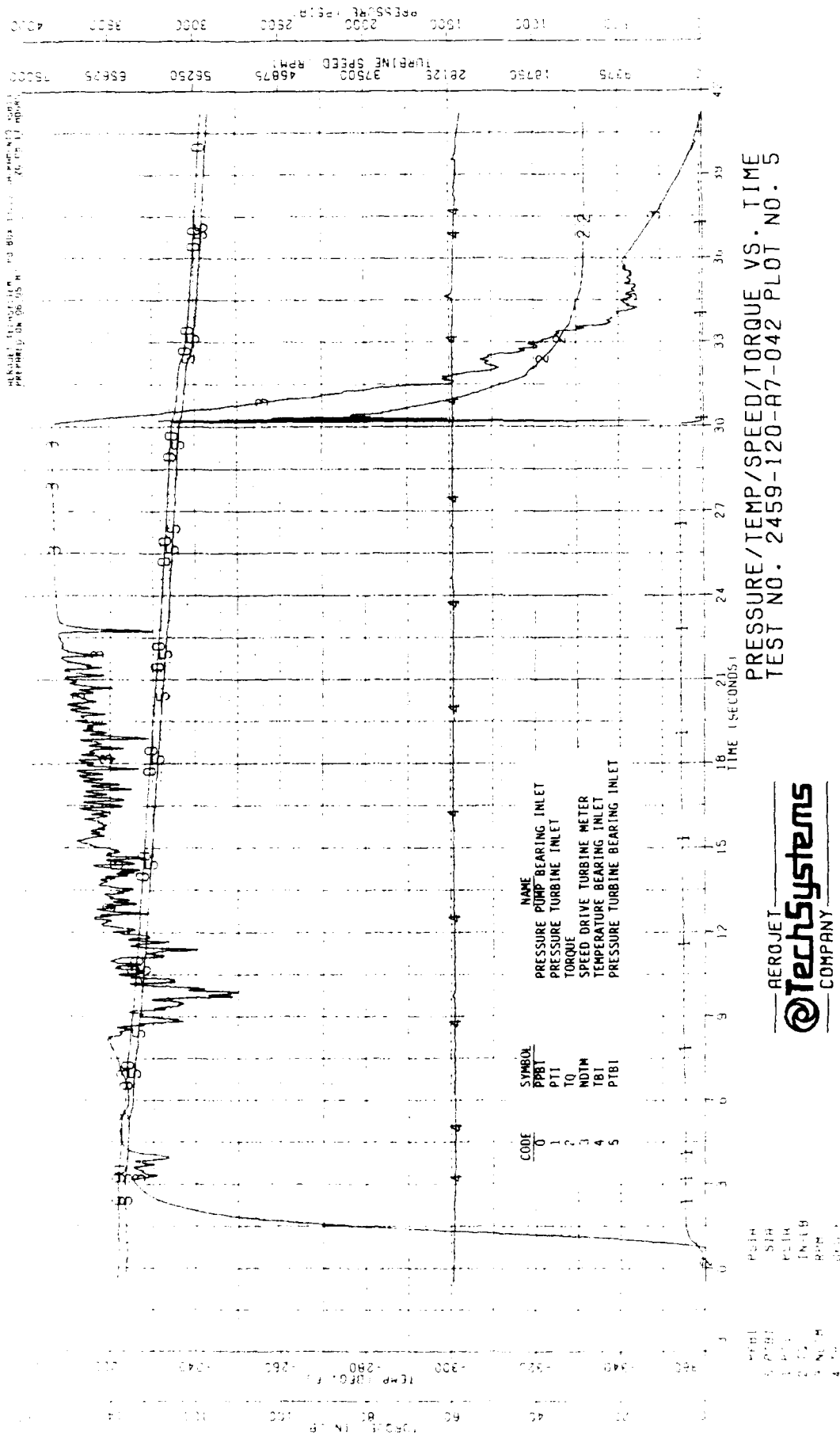
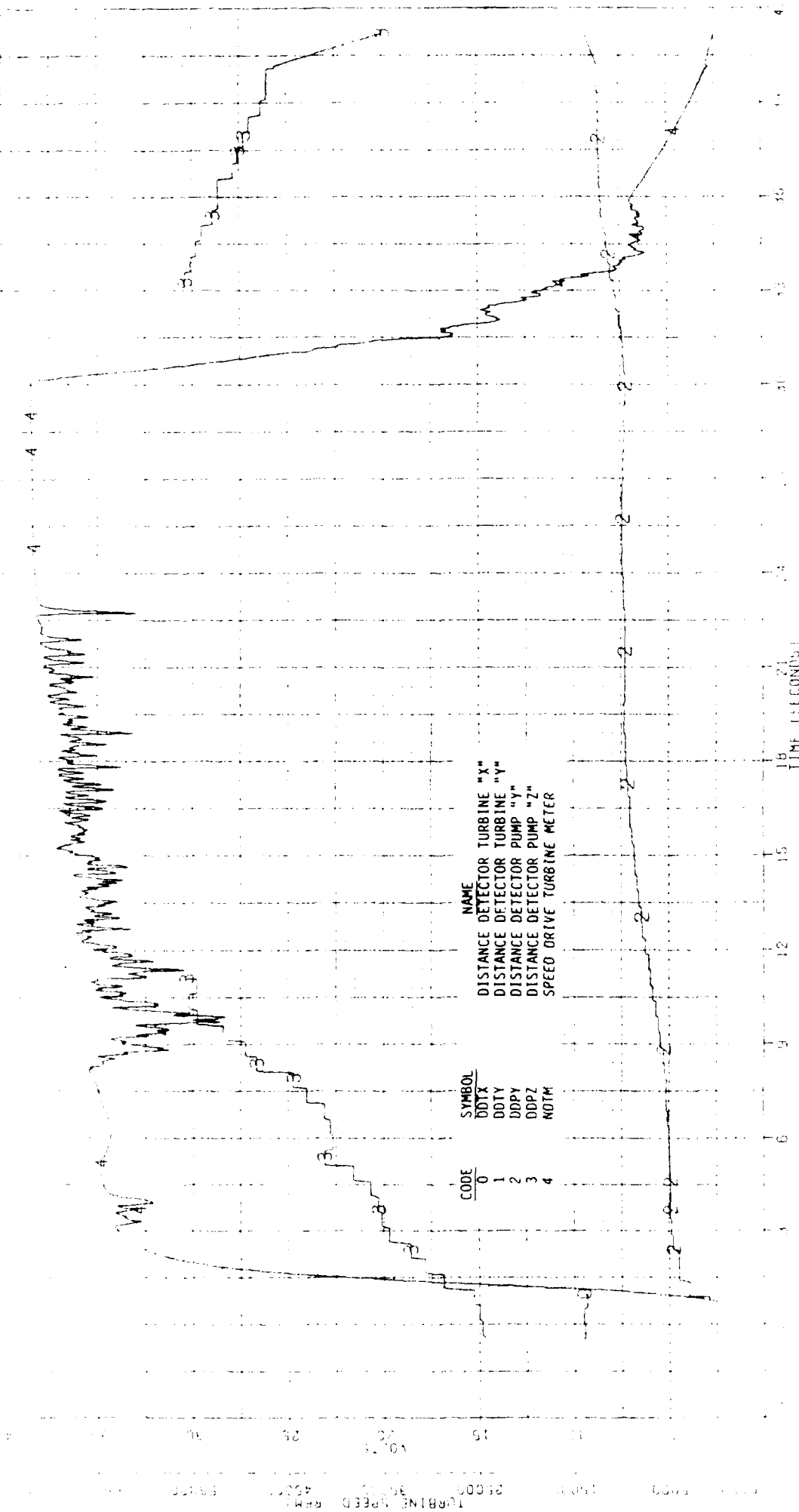


Figure 4.5-13. Pressure/Temp/Speed/Torque Vs. Time Test No. 2459-120-A7-042 Plot No. 5



AEROJET
@TechSystems
 COMPANY

VOLTAGE/SPEED VS. TIME
 TEST NO. 2459-120-A7-042 PLOT NO. 6
 TEST STAND A287 TEST DATE 06-03-87

Figure 4.5-14. Voltage/Speed Vs. Time Test No. 2459-120-A7-042 Plot No. 6
 Test Stand A287 Test Date 06-03-87

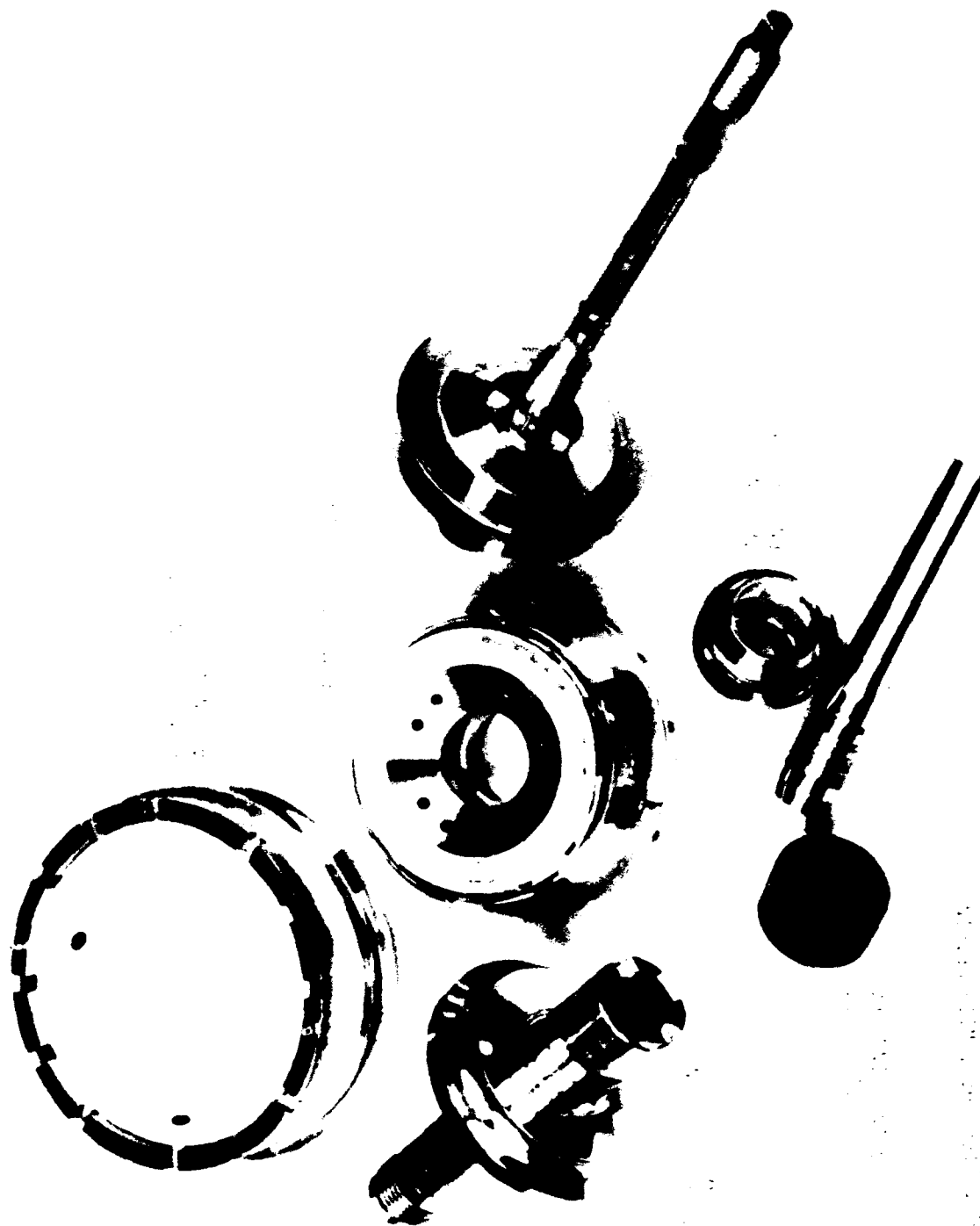


Figure 4.5-15. Bearing Tester Shaft With Bearings and Quill Drive Shaft with Floating Ring Seal, Post Test 2459-120-A7-32

4.5, Testing, cont.

from assembly by hand without lubrication to the bearing were evident. Circumferential wear was experienced on the quill shaft drive seal surface. The wear on this surface was caused by a unidirectional misalignment of the quill shaft within the seal bore. This was diagnosed as being vertical misalignment of the drive turbine with the bearing tester shaft caused by thermal differential.

The excellent condition of the bearing surfaces coupled with the operational speed and pressures at cryogenic temperature has demonstrated the feasibility of this self-aligning fluid film bearing design. The self-aligning capability allows the bearing to align itself with the rotating surfaces under deflections caused by high pressure and thermal gradients so that very close operating clearances in the bearings can be accommodated. Based on operating conditions and the excellent bearing condition after test it appears that this feature is performing as designed.

5.0 DISCUSSION OF RESULTS AND CONCLUSIONS

5.1 DISCUSSION

The final high pressure high speed test bearing parameters are shown below.

Bearing Parameters

Lubricant	LN ₂
Shaft Speed	72,000 RPM
Journal Surface Speed	188. ft/sec
Thrust Bearing Surface Speed	508. ft/sec
Bearing Pressure Differential	
Pump End	2486. lb/in ²
Turbine End	2150. lb/in ²

The LOX turbopump bearing system test program completed Test Series "A" and "B" using unmachined impeller disks. Also, the system is driven by an external turbine through a quill shaft assembly. This added apparatus and the additional mass of the solid impeller disks is a more severe rotor-bearing dynamics test than will occur with the bladed rotating assembly. A significant amount of weight was removed with the machining of the two sets of impeller vanes. The weight and friction effects of the quill shaft were also eliminated in subsequent turbopump testing. The additional disk weight has the effect of reducing the critical speed margin at the maximum operating speed. The design has a very stiff bearing and a rigid shaft design that results in a subcritical rotor with about 50% critical speed margin. Even with the additional rotor weight and overhung quill shaft the rotor bearing system operated subcritical at maximum speed. This is a significant feature for a throttleable turbopump allowing operation over the full speed range without "redline" zones. Post test examination showed the bearing system in excellent condition.

The bearings operate at very close clearances with a short bearing span. Small tolerance and unsymmetrical loading effects make a self-aligning feature a necessity to avoid loss of bearing performance due to misalignment within the fluid film. The tests demonstrated this particular self aligning design functioned as intended. The self aligning feature allows the close bearing clearance of a subcritical

5.1, Discussion, cont.

rotor assembly and very accurate axial rotor positioning. This stiff axial positioning feature provides close impeller front vane clearance leading to high pump efficiency and the open impeller leads to lower fabrication costs. The design configuration has proven to be very simple and easy to assemble.

Some fabrication difficulty was experienced in obtaining accurate tight tolerance surfaces with the low burn factor materials (K-Monel). The turbopump is designed to accommodate radial and axial thermal gradients and pressure deflections without affecting the rotor-bearing system performance. Again, these features appear to function as intended in the concluded test series.

The bearing test assembly encountered problems in two areas. The first problem was with instrumentation. The second is the inability of completely simulating the internal turbopump environment. Two types of instrumentation proved difficult: the torque measurement and shaft movement sensing. The torque measuring device is a torque transducer on the trunnion mounted turbine. There is sufficient friction in the torque measurement system that low torque readings are inaccurate.

Reluctance clearance gap sensors (proximeter probes) are used to determine shaft movement. The clearance sensors were subjected to liquid nitrogen temperatures. The sensor output signal is strongly dependent upon temperature. Both the sensing probe and the signal processing electronics box showed evidence of temperature dependence. The influence of temperature is believed to be the major contributor to the variation between sensing probe output signals. In some cases, however, the probes gave no detectable signal at all. In spite of these disappointments, sufficient data were obtained to document that the bearing system is stable over the full speed range with normal axial loads and very light radial loads. The probe tip cover was made from a low "burn factor" material that inhibited the sensitivity of the distance detectors by requiring a thicker case wall and therefore a greater space between the coil and the shaft. An advanced design is being pursued for this application to be used on subsequent tests.

The other area of difficulty was in simulating the pressure and temperature environment of the turbopump. The rotor simulator did not have vanes and

5.1, Discussion, cont.




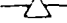
therefore did not generate its own pressure environment. A substitute uniform pressure for each pump stage and turbine area was necessary to achieve proper thrust balance on the rotating assembly with unbladed impellers. The small fluid volume within the test rig and low flow rates required by balancing orifices, made chilldown with a low pressure tank (50 psi) long and variable. The chilldown and pressure environment will improve significantly with the parts machined to actual TPA configuration. Bearing fluid supply will be proportional to pump impeller loads as they will be supplied by the pump.

Discharge pressures of these pumps are 2300, first stage, and 4600 psia for second stage. As a consequence, the pumps generate very high axial loads relative to the bearing size. In order to measure the load, pressure taps are provided at strategic locations around the turbopump. One large force is the pressure on the front of the impeller disk. The first stage impeller housing has pressure taps to determine the radial pressure gradient and the circumferential pressure variation. As expected the inlet pressure remains fairly constant and the pressure on the face of the disk increases by a factor of the speed squared. The pressure gradient as a function of speed is shown in Figure 5.1-1

A major feature of this design is combining the function of the bearings and seals. In order to achieve the proper function the axial loads on the rotating assembly must be controlled and understood. There are three major components on the rotating assembly (1) first stage impeller, (2) second stage impeller and (3) turbine. Due to the high pressures involved, high net axial loads are generated at each component. Pressure profiles at each of these components were measured to assess the net bearing loads. The resulting loads of each component are shown in Figure 5.1-2. The net force on the first impeller, neglecting the thrust bearing area, is shown in the figure by triangles and acts towards the turbine end of the rotor. The second stage impeller force neglecting the bearing area acts toward the pump end of the rotor and is identified by the squares. The turbine net force acts towards the pump end of the rotor also. The impeller forces are large values, approximately 1000 lb and 1500 lb for first and second stage impeller, respectively. The turbine force is lower than that for the impellers, approximately 500 lb. The turbine force decayed

FIRST STAGE IMPELLER DISK PRESSURE

PRESSURE GRADIENT

- N = 72,000 RPM
- PRESSURE AT CUTWATER 
- PRESSURE AT .765 R 
- PRESSURE AT .580 R 
- PRESSURE AT INLET 

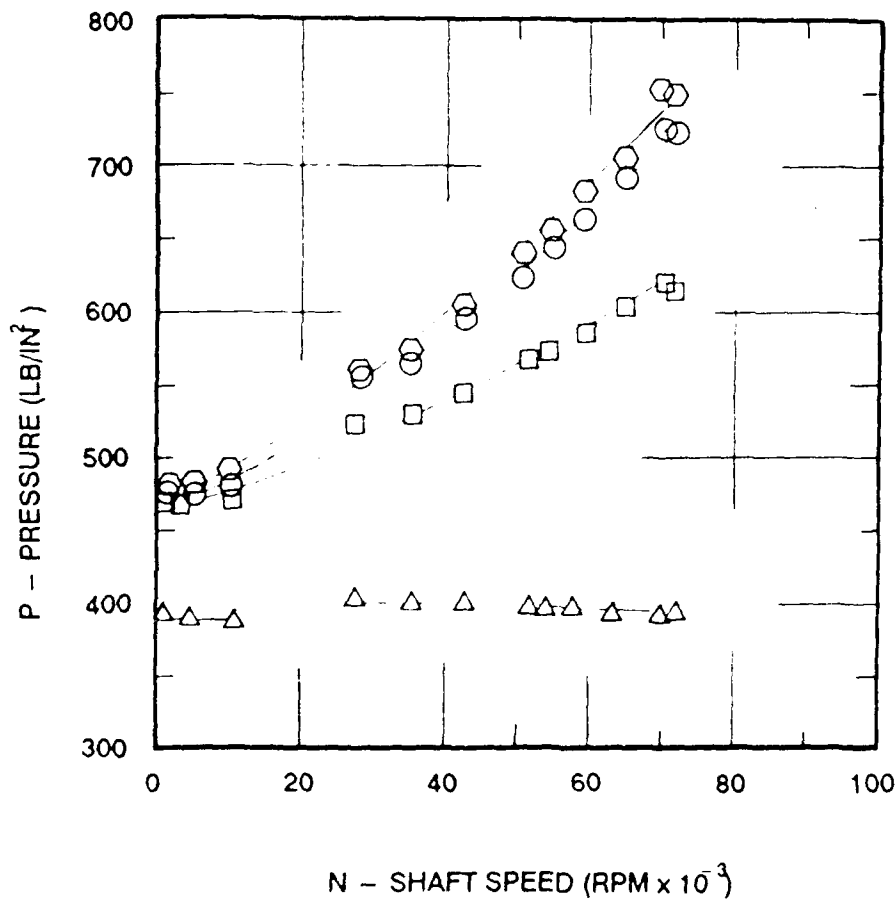


Figure 5.1-1. First Stage Impeller Disk Pressure

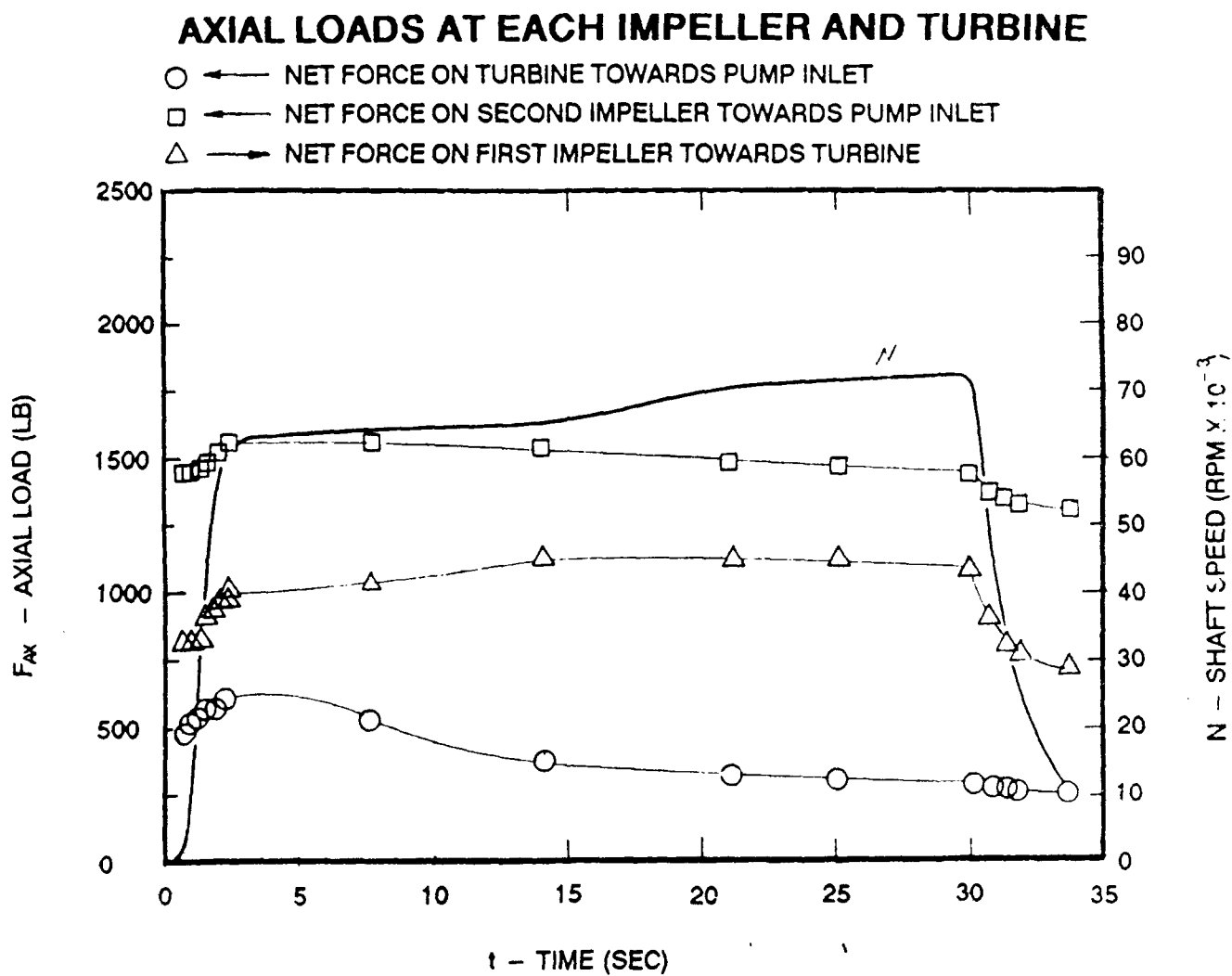


Figure 5.1-2. Axial Loads at Each Impeller and Turbine

5.1, Discussion, cont.

with time due to a decay in the turbine cavity pressure. The pressure started at about 1200 psi and dropped to about 500 psi by the end of the test run. This reduction in pressure was due to a journal seal on the quill shaft drive that suffered significant wear. The additional flow through the worn seal was more than the pressure regulator could accommodate. This wear was attributed to vertical shaft misalignment due to thermal differential between the ambient temperature drive turbine and the cryogenic temperature test unit. Also shown in the figure is the shaft speed versus test run time. The centrifugal pressure gradient effect is evident on the first and second stage impeller net axial force.

The net load on the double acting hydrostatic thrust bearing/seal combination is shown in Figure 5.1-3. The axial load is approximately 1200 lb initially and drops to around 700 lb by the end of the test. The axial load reduction is the result of the quill shaft seal flow rate plus the reduction in the supply pressure to the test fixture as time passes. These two characteristics combined to reduce the net load in the bearing about 500 lb during the test. This was not intentional although it did demonstrate the bearings capability to accommodate a large thrust load variation without bearing contact. Unfortunately, the axial distance detector malfunctioned and axial deflection was not obtained. The applied load is significant relative to the size of this bearing.

Both the pump end and turbine end bearings are self-aligning for operating at close clearance without causing a rub. Both bearings are spherically mounted with a restoring moment applied to align the bearing surfaces. The pump bearing spherical surface is biased for high axial load towards the pump. In the turbopump environment pressure loads maintain the spherical surface in close proximity to the bearing socket. One of the issues in running this rotor-bearing simulator test was to duplicate the turbopump pressure environment and maintain a positive load on the bearing sphere. The axial force on the spherical socket is shown in Figure 5.1-4 for the high speed test. Even with a reduced turbine end pressure

NET LOAD ON PUMP HYDROSTATIC BEARING

• NET LOAD TOWARDS PUMP END

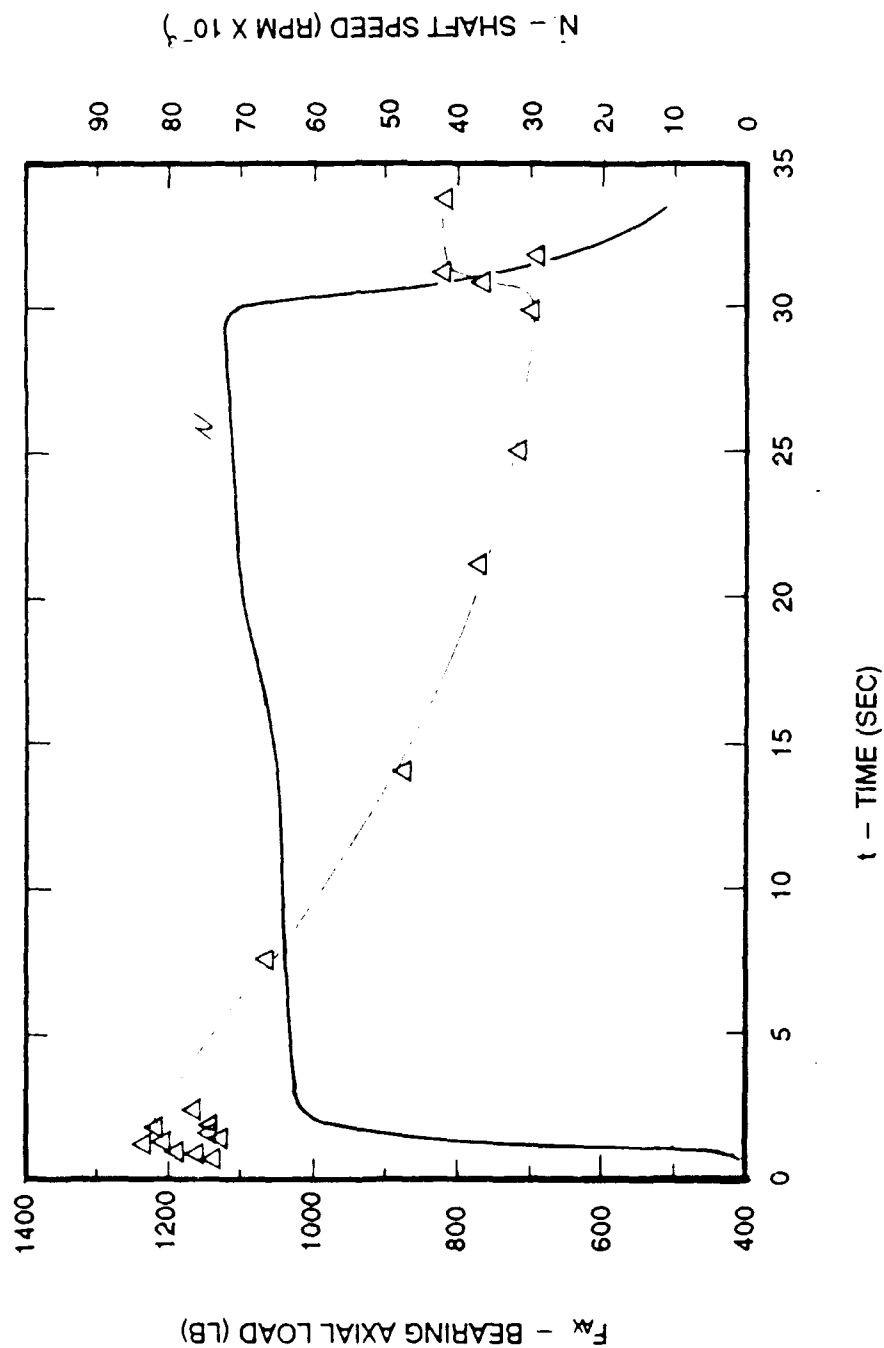


Figure 5.1-3. Net Load on Pump Hydrostatic Bearing

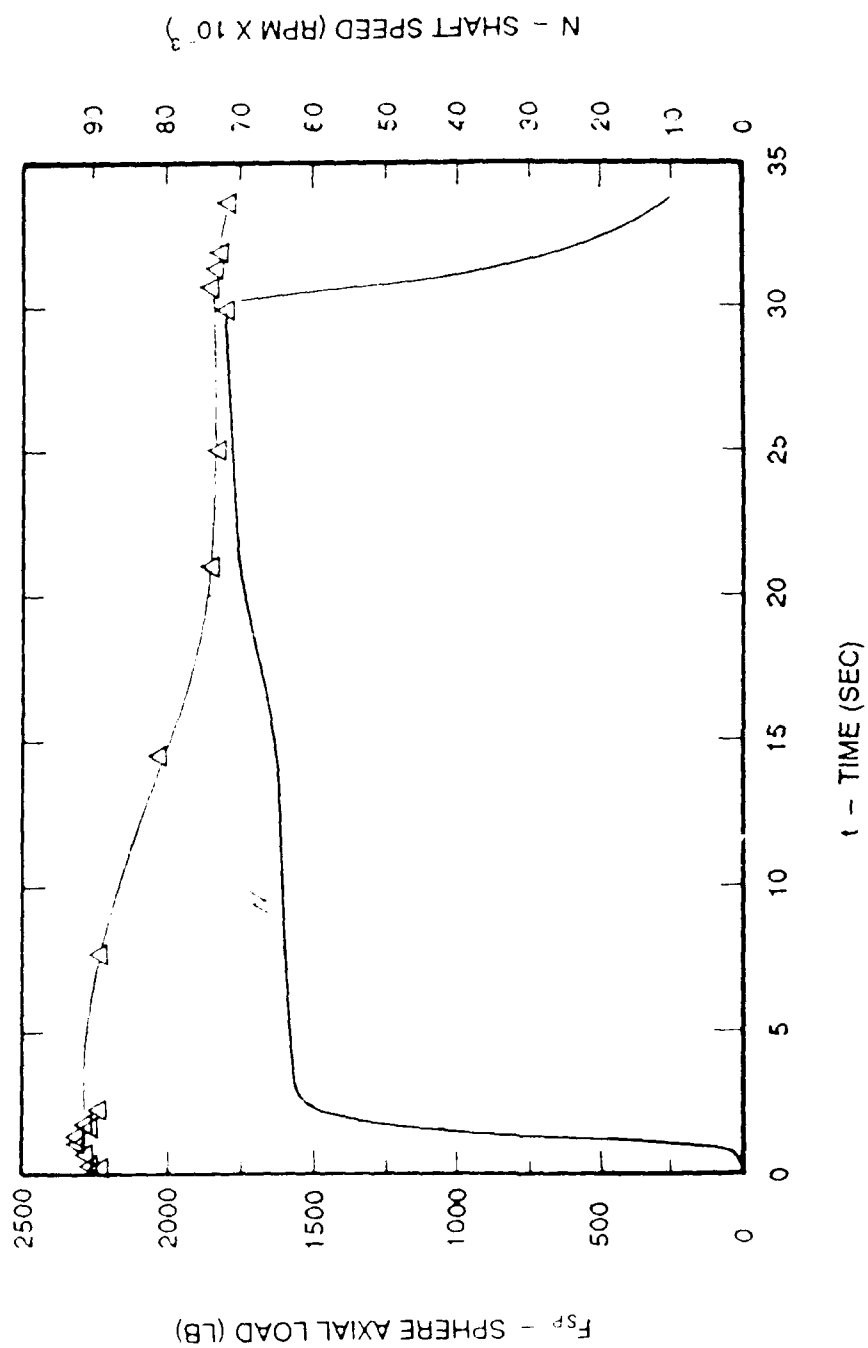


Figure 5.1-4. Net Load on Spherical Socket

5.1, Discussion, cont.

load acting on the stationary parts the socket axial load was maintained above 1800 lb which is equivalent to about 1500 lb/in² unit loading on the socket. The load on the socket starts out around 2300 lb and decays with time due to a reduction in the turbine cavity pressure.

Pump end bearing flow rate is shown in Figure 5.1-5 as a function of pressure. This is the flow rate supplied to three bearing faces, the pump journal, the first stage thrust face and the second stage thrust face. The data shown is for rotating and non-rotating tests. The solid curve is the predicted flow rate for the bearing only while the data points include any leakage the piston rings may allow. This bearing operating environment is similar to the turbopump, but not exact. The pressures simulate the pump loads, but not the exact pressure gradients. This difference is due to the smooth impeller disks used in the tester in place of the real impeller blades. Due to this difference in the pressure gradient for the hydrostatic thrust bearing, flow is radially outward as well as inward through the bearing clearance. In the actual turbopump the bearing flow will be unidirectional, radially inward only. For this reason the flow in this bearing is larger than will be experienced in the turbopump.

The flow rate to the turbine end bearing is shown in Figure 5.1-6. The measured flow and predicted flow differ considerably. The predicted maximum flow is approximately 2 gpm while the measured flow was approximately 8 gpm, or 4 times what was anticipated. This test flow appears to follow a square root of pressure differential curve for a fixed seal flow area. There were no anomalies in the bearing where this amount flow could escape at the test pressure, but the supply line had some potential leak paths. The bearing supply is fed through the housing across two circumferential joints sealed by piston rings. One of the four piston rings was stuck in the groove on disassembly which could have accounted for the excessive flow rate for this flow circuit. This piston ring seal is a 3.4 inch diameter, almost 7 times the circumference of the .500 diameter journal bearing. The housing radial gap at the piston ring is similar to the bearing clearance of .001 inch, and is exposed to the same pressure differential as the bearing (7 times the flow area). A small mismatch of the piston ring with the bore will easily allow the leakage experienced.

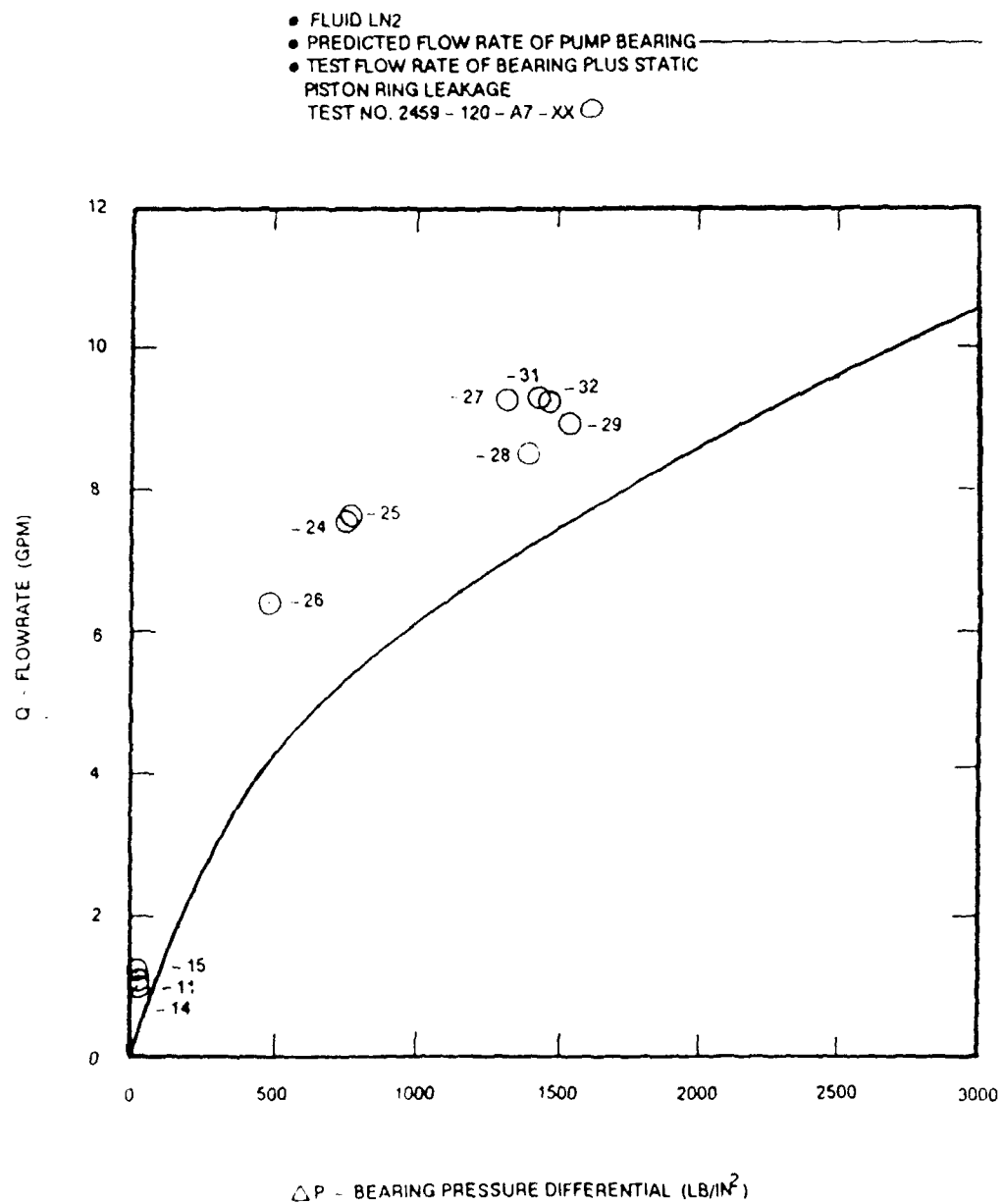


Figure 5.1-5. OTV LOX Pump End Self-Aligning Hydrostatic Bearing Flow Rate

- FLUID LN2
 - PREDICTED FLOW RATE OF TURBINE BEARING
 - TEST FLOW RATE OF BEARING PLUS STATIC PISTON RING LEAKAGE
- TEST NO. 2459 - 120 - A7 - XX ○

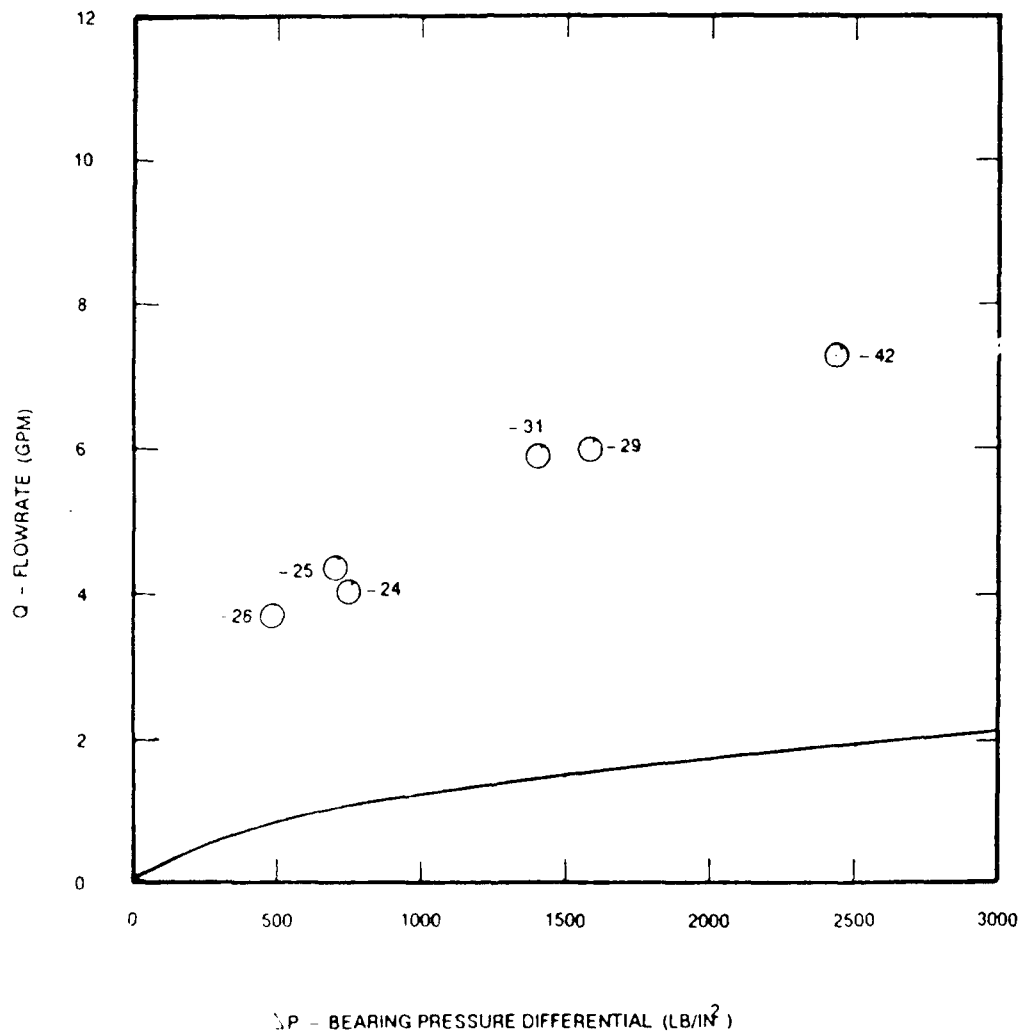


Figure 5.1-6. OTV LOX Turbine End Self-Aligning Hydrostatic Bearing Flow Rate

5.1, Discussion, cont.

It might be worthwhile to note that this feed system has two housing cylindrical points in series which would not be the case in a real turbopump. The two joints are a test fixture design only. No attempt was made at this time to correct the stuck piston ring, but it will be replaced for the next series of turbopump tests.

The rotating assembly was instrumented for X and Y distance detectors in front of the first impeller and between the turbine bearing and turbine and an axial distance detector at the pump inlet. These distance detectors were made with the most appropriate materials for LOX compatibility considerations. The tip was constructed of alumina ceramic. This material required additional thickness that inhibited the sensitivity of the probe. Calibrating the instrumentation at room temperature for cryogenic operation was less successful than anticipated. The turbine end and axial distance detector was off scale during the high speed test. The pump end X and Y distance probe signals combined to display a shaft orbit. Several orbits for the pump end at approximately 70,000 rpm are shown in Figure 5.1-7. A 0.002 step in the shaft was used for signal generation and calibration. Due to the reduced sensitivity of the detector the magnitude of the trace is not accurate, but the trace was steady and repeatable indicating a stable shaft condition.

5.2 CONCLUSIONS

1. A hydrostatic self-aligning bearing system was demonstrated for high pressure, high speed cryogenic turbomachinery applications.
2. The rotor-bearing mass-elastic system operated sub-critical over the full speed range with ample margin.
3. The tests performed demonstrated stable rotor motion for the design throughout the speed range necessary for throttleable engine turbopump operation.
4. A hydrostatic thrust bearing design incorporating seals is capable of supporting the high axial load imposed by pump and turbine.

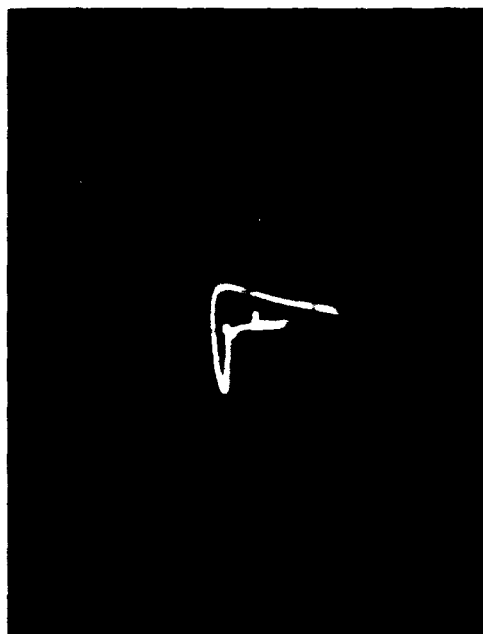
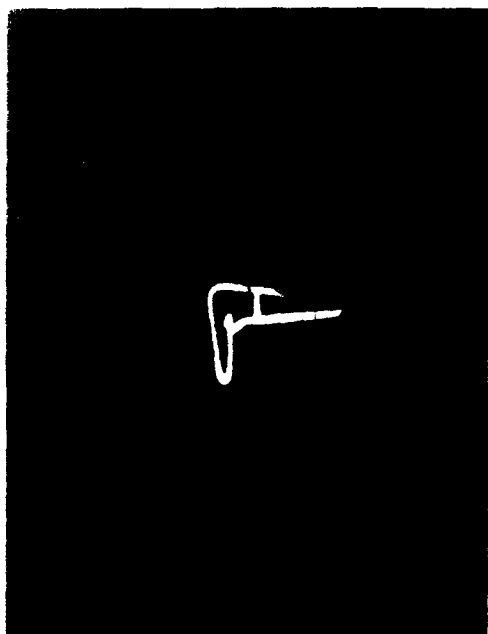
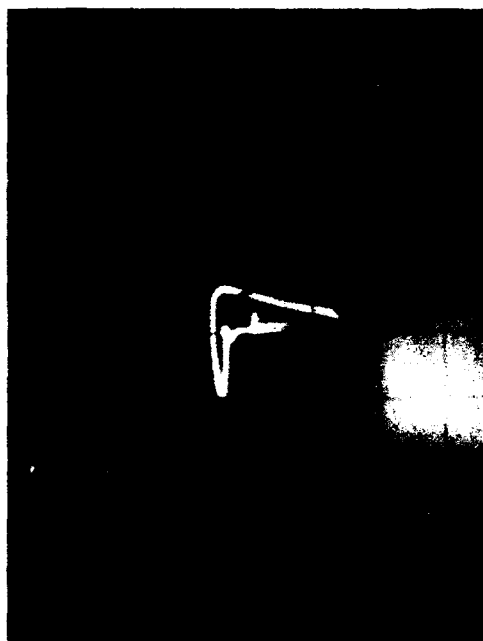
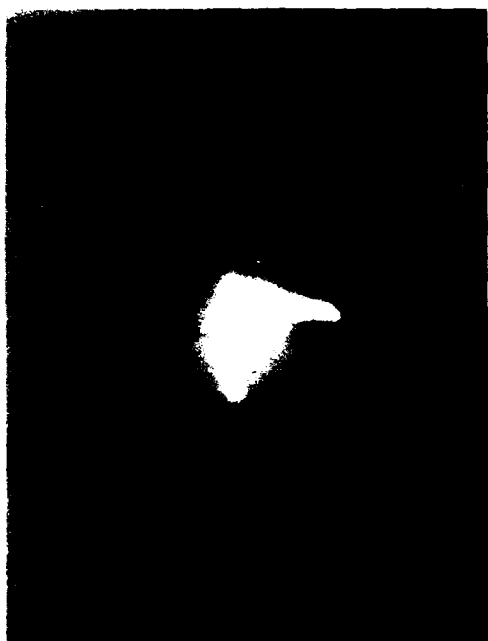


Figure 5.1 - "X" vs. "Y" Orbits at 72,000 ft

5.2, Conclusions, cont.

5. Accurate axial control of impellers by stiff hydrostatic thrust bearings makes close clearance open impellers feasible.
6. Cryogenic (-300°F) and high pressure (3500 psi) deflections were accommodated by this self-aligning rotor-bearing system and housing without rubbing.
7. A bearing tester program is both expensive and time consuming. The full benefit of such a program comes only from comparisons of more than one bearing design.
8. Conducting a bearing tester program is complicated by problems involving the tester rather than the test article. The bearing performed better than the test apparatus in this program.
9. No evidence of metallurgical phase change or thermal gradient produced distortion of parts was found over the room temperature to -300°F temperature range experienced.

6.0 REFERENCES

1. Schoenman, L., "Selection of Burn-resistant Materials for Oxygen-Driven Turbopumps," AIAA/ASME/SAE 20th Joint Propulsion Conference Paper No. AIAA-84-1287, June 11-13, 1984.
2. Schoenman, L., "Advanced Cryogenic OTV Engine Technology," AIAA/ASME/ASME 21st Joint Propulsion Conference Paper No. AIAA-85-1341, July 8-10, 1985.
3. Schoenman, L., "Oxygen TPA Material Ignition Study," Aerojet TechSystems Report 238772-M-42, pp. 23-33, November 1986.
4. Schoenman, L., "Friction Rubbing Test Results of Dissimilar Materials in High-Pressure Oxygen," Aerojet TechSystems Report 23772-M-32, Appendix A, January 1986.
5. Schoenman, L., Stoltzfus, J. and Kazaroff, V., "Friction Induced Ignition of Metals In High Pressure Oxygen," ASTM Publication STP986, Sept. 1988.
6. Cooper, L.P and Scheer, D.D., "Status of Advanced Propulsion for Space Based Orbital Transfer Vehicle," NASA TM 88848, October 1986.
7. Holtzmann, W.A. and Hayden, W.R., "Integrated Control and Health Management, Phase II Final Report", Aerojet TechSystems, prepared for NASA Lewis Research Center, NAS 3-23772, Report CR-182122, October 1988.
8. Buckman, P.S., "Preliminary Bearing Design for LOX Turbopump," Task B.3, Contract NAS 3-23772, NASA Lewis Research Center, April 1984.
9. Buckmann, P.S., "Freon Hydrostatic Bearing Test Report," NASP Contract, Aerojet TechSystems, Sacramento, California, August 1986.
10. Stepanoff, A.J., Centrifugal and Axial Flow Pumps, J. Wiley, New York, 1948.

6.0, References (cont.)

11. McBride, R.W., Optimizing Turbine Stage Efficiency by Selecting and Matching Reaction, Velocity Ratio, and Clearance Ratio, Turbodyne Corp., Steam Turbine Div., Weilsville, N.Y. ASME Paper No. 77-WA/FE-10, August 1, 1978.
12. Kacker, S.C., and Okapuu, C., A Mean Line Prediction Method for Axial Flow Turbine Efficiency, Pratt & Whitney Aircraft of Canada Ltd, ASME Paper No. 81-GT-58, December 9, 1980.
13. Denton, J.D., A Survey and Comparison of Methods for Predicting the Profile Loss of Turbine Blades, Institution of Mechanical Engineering, July 1972.
14. Hass, J.E., and Kofskey, M.G., Effect of Rotor Tip Clearance and Configuration on Overall Performance of a 12.77-Centimeter Tip Diameter Axial-Flow Turbine, Lewis Research Center, ASME Paper No. 79-FT-42, December 13, 1978.

7.0 SYMBOLS AND UNITS

SYMBOLS

<u>Symbol</u>	<u>Definition</u>
C	Clearance
F	Filter, Fuel, Load
Gal	Gallon
GH ₂	Gaseous Hydrogen
GN ₂	Gaseous Nitrogen
"G's"	Number standard earth gravities
LN ₂	Liquid Nitrogen
LOX	Liquid Oxygen
O	Oxygen
N	Angular Speed
NPSH	Net Positive Suction Head
P	Pressure
RPM	Parts per million
Q	Gallons per minute
R	Radius
t	Time
T	Temperature
TBD	To Be Determined
TPA	Turbopump Assembly
X	Lateral motion
Y	Vertical motion
Z	Axial motion

UNITS

<u>Units</u>	<u>Definition</u>
°F	Degree Fahrenheit
Ft	Feet
GPM, gpm	Gallons per minute
in.	inch
lbf, lb, LB	Pound force
lb/sec	pounds/second
psi	Pounds per square inch
psig	Pounds per square inch gage
°R	Degree Rankine
RPM, rpm	Revolutions per minute
sec	Seconds
μ	Microinch

APPENDIX A

PORT INSTRUMENT LOCATION/
IDENTIFICATION SCHEME

SUBJECT APPENDIX

OTV LOX BEARING TESTER
PORT/INSTRUMENT LOCATION
IDENTIFICATION SCHEME

WORK ORDER

2459-54

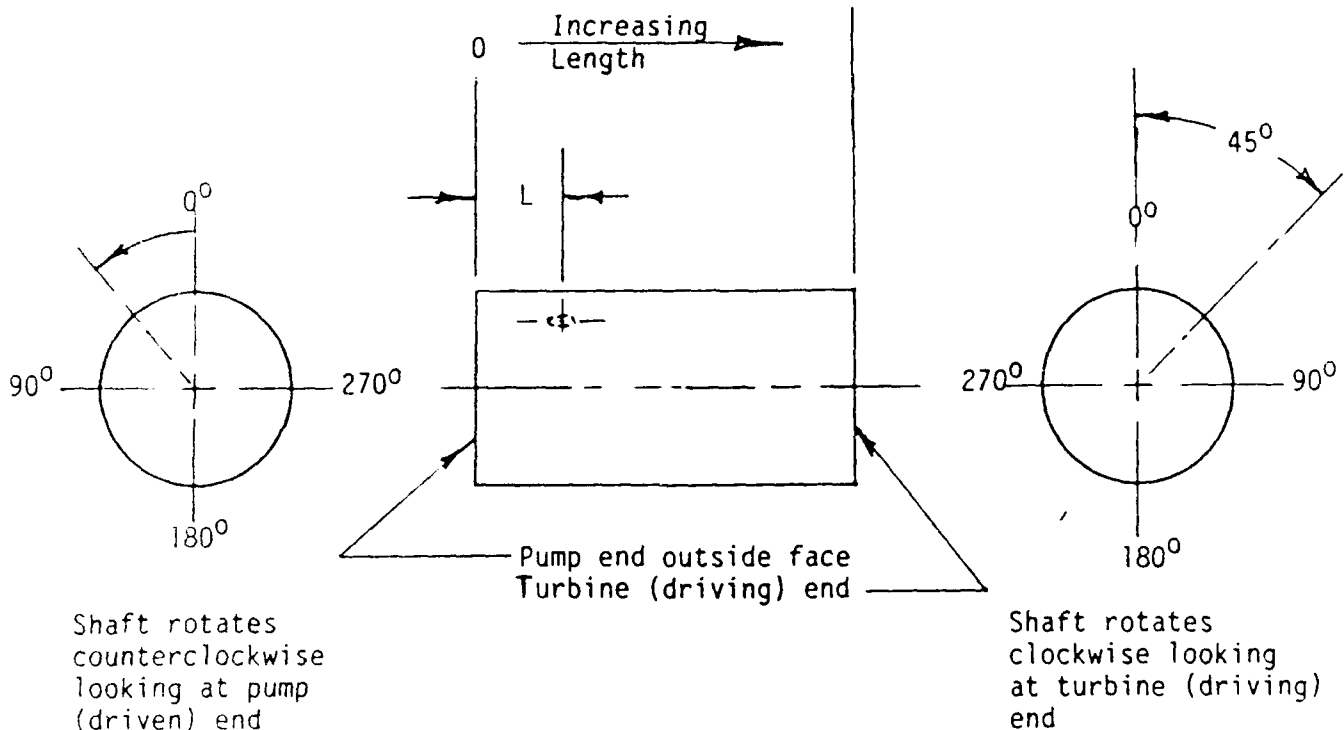
DATE

4/29/86

BY

R. L. Sabiers

CHK BY



EXAMPLE:

Port location illustrated on cylinder outside diameter is noted as (L,45) for "L" distance from outside surface of the pump end in a plane 45 degrees from the vertical center line in a clockwise direction when looking from the turbine end. Location designator ignores radial distance. This location symbolism is used on the following pages to define the tester port locations for bearing tester tests only. Parameters without channel symbol numbers will be used later for the turbopump testing.

TWO WIRE CHANNELS

<u>Symbol and Number</u>	<u>Name</u>	<u>Test Area Nomenclature</u>	<u>Units</u>	<u>Tester Drawing Port Nomenclature, Location (inch,degrees)</u>
①	Housing exterior temp. at turbine	TH7	°F	(4.82,0)
②	Turbine bearing inlet temperature	TBI	°F	
③	Pump bearing flow meter	FMPBI	gpm	PBI
④	Pump discharge flow meter	FMPD	gpm	
⑤	Turbine bearing flow meter	FMTBI	gpm	TBI
⑥	Pump first stage discharge temp.	TPD	°F	TSD1
⑥	Pump first stage discharge temp.	TPD	°F	TSD2
⑦	Flow meter pump suction	FMSI	gpm	
⑧	Housing exterior temp. at turbine bearing	TTH8	°F	(3.79,0)
⑨	Housing exterior temp. at turbine bearing	TIPH10	°F	(0.25,0)
⑩	Pump bearing exit temperature	TPBEC	°F	PBE1
⑩	Pump bearing exit temperature	TPBEC	°F	PBE2
⑪	Pump bearing exit flow meter	FMPBE	gpm	PBE1(2.54,120)
⑪	Pump bearing exit flow meter	FMPBE	gpm	PBE2(2.54,300)
⑫	Turbine bearing exit temperature	TTBEC	°F	TBE1
⑫	Turbine bearing exit temperature	TTBEC	°F	TBE2
⑫	Turbine bearing exit temperature	TTBEC	°F	TBE3
⑬	Turbine bearing exit flow meter	FMTBE	gpm	TBE1(4.71,0)
⑬	Turbine bearing exit flow meter	FMTBE	gpm	TBE2(4.71,180)

TWO WIRE CHANNELS (Continued)

<u>Symbol and Number</u>	<u>Name</u>	<u>Test Area Nomenclature</u>	<u>Units</u>	<u>Tester Drawing Port Nomenclature, Location (inch, degrees)</u>
(13)	Turbine bearing exit flow meter	FMTBE	gpm	TBE3(4.71,300)
(14)	Pump suction exit temperature	TSE	°F	
(15)	Pump suction exit flow meter	FMSE	gpm	
(16)	Speed test drive turbine and torque meter	NDIM	rpm	
(18)	Drive turbine exhaust bearing temperature	TDTEB	°F	1197921
(19)	Drive turbine inlet bearing temperature	TDTIB	°F	1197921
(20)	Distance detector turbine 120°	DDTX	inch	(4.08,120)
(21)	Distance detector turbine 210°	DDTY	inch	(4.08,210)
(22)	Distance detector pump 120°	DDPX	inch	(1.0,120)
(23)	Distance detector pump 210°	DDPY	inch	(1.0,210)
(24)	Distance detector pump axial	DDPZ	inch	(-1.23,¢)
(24)	Speed tester/turbopump	NT	rpm	(-1.23,¢)
	Pump suction temperature	TS	°F	
	Second stage discharge temperature	TPD	°F	
	Second stage discharge temperature	TPD	°F	
	Pump bearing inlet temperature	TBI	°F	

TRANSDUCER CHANNELSPRESSURE CHANNELS

<u>Symbol and Number</u>	<u>Name</u>	<u>Test Area Nomenclature</u>	<u>Units</u>	<u>Tester Drawing Port Nomenclature, Location (inch,degrees)</u>
1	Torque	TQ	in.lb.	
2	Run tank pressure	PBRT	psig	
3	Pump bearing inlet pressure	PPBI	psig	PBI(2.06,330)
4	Turbine bearing inlet pressure	PTBI	psig	TBI(3.63,45)
5	Turbine bearing exit pressure	PTBE	psig	TBE1(4.71,180)
6	Turbine exhaust pressure	PTD-1	psig	(5.81,90)
7	Pump pressure (mid)	PTM1	psig	PP1(0.0,330)
8	Pump bearing exit pressure	PPBE	psig	PBE1(2.54,120)
8	Pump bearing exit pressure	PPBE	psig	PBE2(2.54,300)
9	Pump pressure (tip)	PTT2	psig	PP2(0.0,300)
10	Turbine bearing cavity pressure	PTBC	psig	TBCP(4.64,45)
11	Suction pressure	PS	psig	
12	Second stage discharge pressure	PD2-1	psig	2SD1(3.03,70)
12	Second stage discharge pressure	PD2-2	psig	2SD2(3.03,250)
13	Pump peripheral pressure	PPP1	psig	PPP1(0.0,0)
14	Second stage suction pressure	PS2I-1	psig	2SI1(3.37,0)
14	Second stage suction pressure	PS2I-2	psig	2SI2(3.37,180)
15	Drive turbine inlet	PTI	psig	
16D	Mid diaphragm bearing side temp.	TDDB	°F	TBE3(4.71,0)
16N	Min diaphragm bearing side temp.	TDNB	°F	TBE3(4.71,0)
16X	Max diaphragm bearing side temp.	TDXB	°F	TBE3(4.71,0)

TRANSDUCER CHANNELS
PRESSURE CHANNELS
(Continued)

<u>Symbol and Number</u>	<u>Name</u>	<u>Test Area Nomenclature</u>	<u>Units</u>	<u>Tester Drawing Port Nomenclature, Location (inch, degrees)</u>
①7	Housing exterior temp. at pump bearing	THX9	°F	(1.78, 0)
◇17D	Mid diaphragm turbine side temp.	TDDT	°F	TEP1(-, 90)
◇17N	Min diaphragm turbine side temp.	TDNT	°F	TEP1(-, 90)
◇17X	Max diaphragm turbine side temp.	TDXT	°F	TEP1(-, 90)
◇18	First stage discharge pressure	PD1-1	psig	LSD1(1.55, 70)
◇19	First stage discharge pressure	PD1-2	psig	LSD2(1.55, 250)
◇20	Turbine exhaust pressure	PGN-2	psig	(5.81, 270)
	Turbine exhaust pressure	PTE	psig	TEP(5.03, 225)
	Boost pump discharge pressure	PBPD	psig	BPP(0.86, 15)
	Pump peripheral pressure	PPP2	psig	PPP2(0.0, 270)
	Pump peripheral pressure	PPP3	psig	PPP3(0.0, 180)
	Pump peripheral pressure	PPP4	psig	PPP4(0.0, 90)
	Turbine inlet pressure	PTI	psig	(6.96, ϕ)

HIGH FREQUENCY CHANNELS

<u>Symbol and Number</u>	<u>Name</u>	<u>Test Area Nomenclature</u>	<u>Units</u>	<u>Tester Drawing Port Nomenclature, Location (inch,degrees)</u>
1	Accelerometer turbine end - Vertical	GTK	"G's"	(6.86,0)
2	Accelerometer turbine end - Horizontal	GTY	"G's"	(6.86,270)
3	Accelerometer pump end - axial	GPZ	"G's"	(-0.56,180)
4	Accelerometer pump end - vertical	GPX	"G's"	(0.81,0)
5	Accelerometer pump end - horizontal	GPY	"G's"	(0.81,270)
6	Accelerometer drive turbine - vertical	GDTX	"G's"	1197921
7	Accelerometer drive turbine - horizontal	GDTY	"G's"	1197921
8	Accelerometer drive turbine - axial	GDTZ	"G's"	1197921

APPENDIX B
INSTRUMENTATION LIST

SUBJECT

APPENDIX B
OTV LOX BEARING TESTER
INSTRUMENTATION LIST

DATE

WORK ORDER

BY

R. L. Sabiers

CHK BY

DATE

4/30/86

The instrumentation list is divided into the three functional types of wiring used to transmit the electrical output of the instruments: (1) a two-wire system, (2) a transducer system and a high frequency system.

The two wire system is tabulated on Pages B-2 and B-3. The location of the sensor is number coded, (n), on the flow diagram Figure B-1.

The transducer system is tabulated on Pages B-5 and B-6. The location of the sensor is number coded, n, on the flow diagram Figure B-2.

The high frequency system is tabulated on Page B-8. The location of the sensor is number coded, n, on the flow diagram Figure B-3.

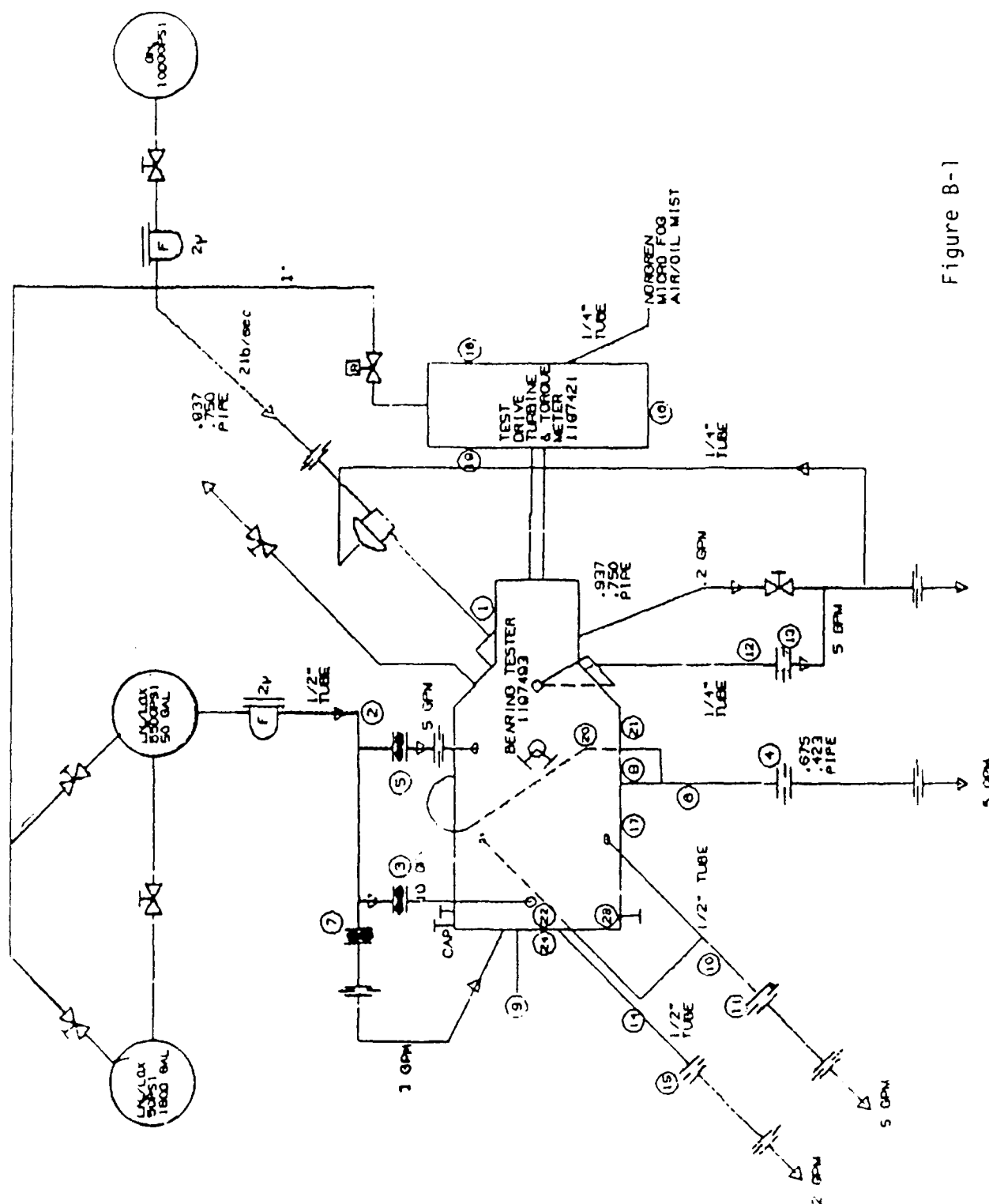
TEST SERIES ACHANNEL CATEGORY - 2-WIRE

<u>Ch</u> <u>No.</u>	<u>Instrument</u> <u>Designation</u>	<u>Port</u> <u>Identification</u>	<u>Function</u>	<u>Type</u>	<u>Range-Units</u>
①	TTH7		Turbine Housing Exterior 7 Temperature	C/A (K)	+100°F to -400°F
②	TBI		Bearing Inlet Temperature	C/A (K)	+100°F to -400°F
③	FMPBI	PBI	Pump Bearing Inlet Flow Meter	Turbine	0.5 GPM to 15
④	FMPD	2SD1 2SD2	Pump Discharge Flow Meter	Orifice	0.5 GPM to 15
⑤	FMTBI	TBI	Turbine Bearing Inlet Flow Meter	Turbine	0.5 GPM to 15
⑥	TPD	TSD1 TSD2	Pump Discharge Temperature	C/A (K)	+100°F to -400°F
⑦	FMSI		Pump Suction Inlet Flow Meter	Turbine	0.5 GPM to 15
⑧	TTBH8		Turbine Bearing Housing Exterior 8	C/A (K)	+100°F to -400°F
⑨	TIPH10		First Stage Pump Housing Exterior 10	C/A (K)	+100°F to -400°F
⑩	TPBEC	PBE1 PBE2	Pump Bearing Exit Combined Temperature	C/A (K)	+100°F to -400°F
⑪	FMPBE	PBE1 PBE2	Pump Bearing Exit Flow Meter	Orifice	0.5 GPM to 15
⑫	TTBEC	TBE1 TBE2 TBE3	Turbine Bearing Exit Combined Temperature	C/A (K)	+100°F to -400°F
⑬	FMTBE	TBE1 TBE2 TBE3	Turbine Bearing Exit Flow Meter	Orifice	0.5 GPM to 15

TEST SERIES ACHANNEL CATEGORY - 2-WIRE (Continued)

Ch No.	Instrument Designation	Port Identification	Function	Type	Range-Units
(14)	TSE		Pump Suction Exit Temperature	C/A (K)	+100°F to -400°F
(15)	FMSE		Pump Suction Exit Flow Meter	Orifice	0.5 GPM to 15
(16)	NDTM		Speed-Drive Turbine		0.0 RPM to 100,000
(17)	THX9		Housing External Temperature-Pump Bearing 9	C/A (K)	+100°F to -400°F
(18)	TDTEB		Drive Turbine Exhaust Bearing Temperature	C/A (K)	+100°F to -400°F
(19)	TDTIB		Drive Turbine Inlet Bearing Temperature	C/A (K)	+100°F to -400°F
(20)	DDTX		Distance Detector Turbine 120° 74792		0.001 In. to 0.010
(21)	DDTY		Distance Detector Turbine 210° 74792		0.001 In. to 0.010
(22)	DDPX		Distance Detector Pump 120° 74792		0.001 In. to 0.010
(23)	DDPY		Distance Detector Pump 210° 74792		0.001 In. to 0.010
(24)	DDPZ NT		Distance Detector & Speed Pump Axial		0.001 In. to 0.010 2000 RPM to 100,000

Figure B-1
 OTV TEST SERIES "A" & "B"
 LN2 BEARING TESTER FLOW DIAGRAM
 TEMPERATURE, DISTANCE,
 SPEED AND FLOW, METERS
 TWO WIRE SYSTEM



TEST SERIES A CHANNEL CATEGORY - TRANSDUCER

Ch No.	Instrument Designation	Port Identification	Function	Type	Range-Units
1	TQ		Torque	BLH Electronics 434376	IN-LB
2	PBRT		Bearing Run Tank Pressure	SG Tabor	0-6K PSIG
3	PPBI	P3I	Pump Bearing Inlet Pressure	SG Tabor	0-6K PSIG
4	PTBI	TPI	Turbine Bearing Inlet Pressure	SG Tabor	0-3K PSIG
5	PTBE	TBE1 TBE2 TBE3	Turbine Bearing Exit Pressures	SG Tabor	0-3K 0-3K 0-3K PSIG
6	PTD	TDI	Turbine Exit Pressure	SG Tabor	0-3K PSIG
7	PIM1	PP1	Impeller Wall Mid Pressure	SG Tabor	0-3K PSIG
8	PPBE	PBE1 PBE2	Pump Bearing Exit Pressures	SG Tabor	0-3K 0-3K PSIG
9	PIT2	PP2	Impeller Wall Tip Pressure	SG Tabor	0-3K PSIG
10	PTPG	TBCP	Turbine Bearing Cavity Pressure	SG Tabor	0-3K PSIG
11	PS		Suction Pressure	SG Tabor	0-3K PSIG
12	PD2-1 PD2-2	2SD1 2SD2	Second Stage Discharge Pressures	SG Tabor	0-3K 0-3K PSIG
13	PCW	PPPI	Cutwater Wall Pressure	SG Tabor	0-3K PSIG
14	P2SI-1 P2SI-2	2SI1 2SI2	Second Stage Inlet Pressures	SG Tabor	0-3K 0-3K PSIG
15	PTT		Drive Turbine Inlet Pressure	SG Tabor	0-50 PSIA

TEST SERIES ACHANNEL CATEGORY - TRANSDUCERS (Continued)

<u>Ch</u> <u>No.</u>	<u>Instrument</u> <u>Designation</u>	<u>Port</u> <u>Identification</u>	<u>Function</u>	<u>Type</u>	<u>Range-Units</u>
16N	TDNB	TBE3	Min. Diaph. Bearing Temperature	C/A (K)	+100°F -400°F
16D	TDDB	TBE3	Mid. Diaph. Bearing Temp.	C/A (K)	+100°F -400°F
16X	TDXB	TBE3	Max. Diaph. Bearing Temp.	C/A (K)	+100°F -400°F
17N	TDNT	TD2	Min. Diaph. Turbine Temp.	C/A (K)	+100°F -400°F
17D	TDDT	TD2	Mid. Diaph. Turbine Temp.	C/A (K)	+100°F -400°F
17X	TDXT	TD2	Max. Diaph. Turbine Temp.	C/A (K)	+100°F -400°F
18	PD1-1	1SD1	First Stage Pump SG Tabor Discharge Pressure		0-3K PSIG
19	PD1-2	1SD2	First Stage SG Tabor Discharge Pressure		0-3K PSIG
20	PGN2	TD2	GN ₂ Turbine SG Tabor Discharge Supply Pressure		0-6K PSIG

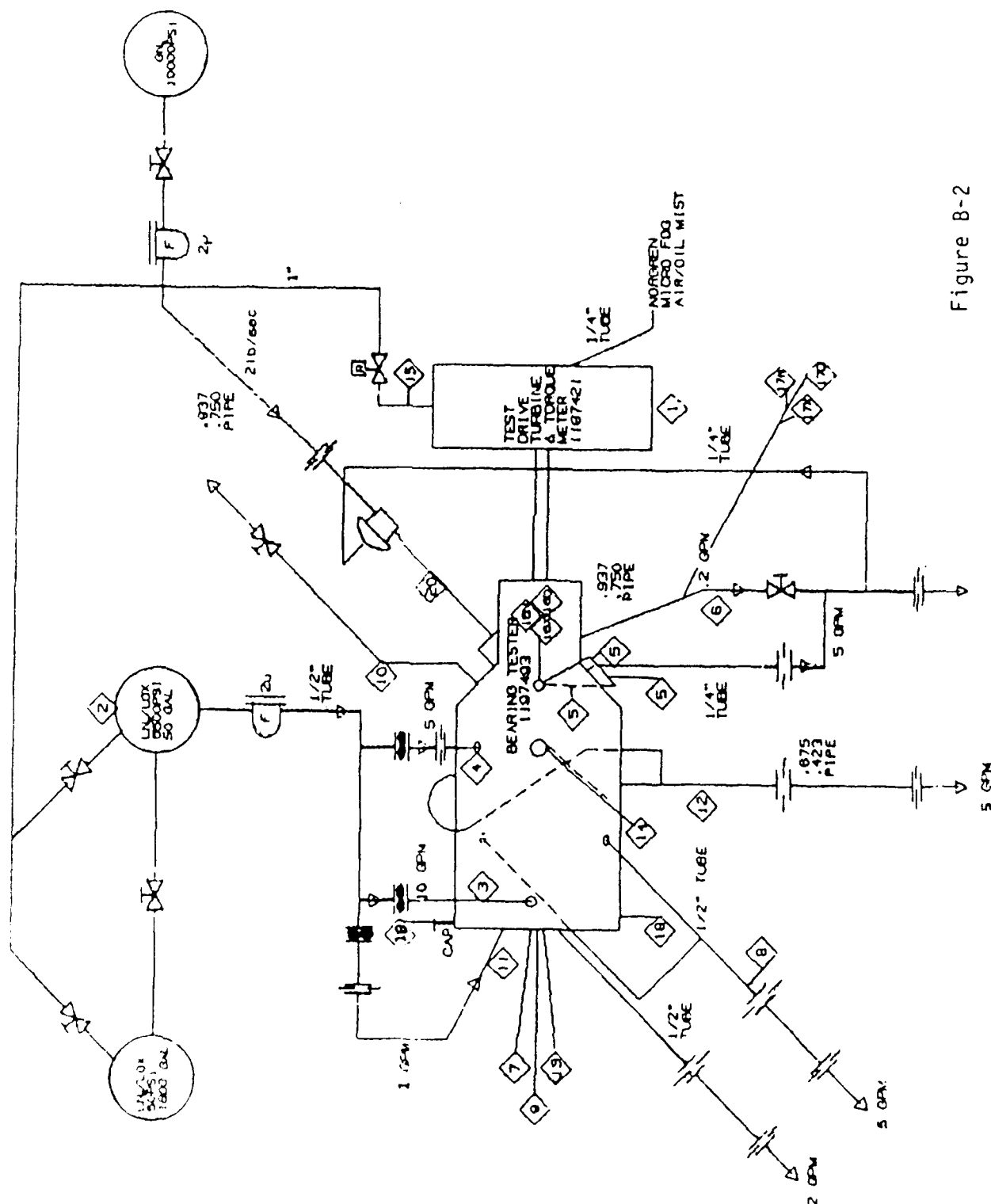


Figure B-2

QTV TEST SERIES "A" & "B"
LN2 BEARING TESTER FLOW DIAGRAM

PRESSURE TRANSDUCERS
AND TEMPERATURES
FOUR WIRE SYSTEM

TEST SERIES A CHANNEL CATEGORY - HIGH FREQUENCY

Ch No.	Instrument Designation	Function	Type	Range-Units
1	GTX	Accelerometer - Turbine End 0°	Endevco 2272	0-10 G's 10-5K CPS
2	GTY	Accelerometer Turbine End 270°	Endevco 2272	0-10 G's 10-5K CPS
3	GPZ	Accelerometer Pump End Axial	Endevco 2272	0-10 G's 10-5K CPS
4	GPX	Accelerometer Pump End 0°	Endevco 2272	0-10 G's 10-5K CPS
5	GPY	Accelerometer Pump End 270°	Endevco 2272	0-10 G's 10-5K CPS
6	GDTX	Accelerometer Drive Turbine 0°	Endevco 2272	0-10 G's 10-5K CPS
7	GDTY	Accelerometer 90° Drive Turbine	Endevco 2272	0-10 G's 10-5K CPS
8	GDTZ	Accelerometer Drive Turbine Axial	Endevco 2272	0-10 G's 10-5K CPS

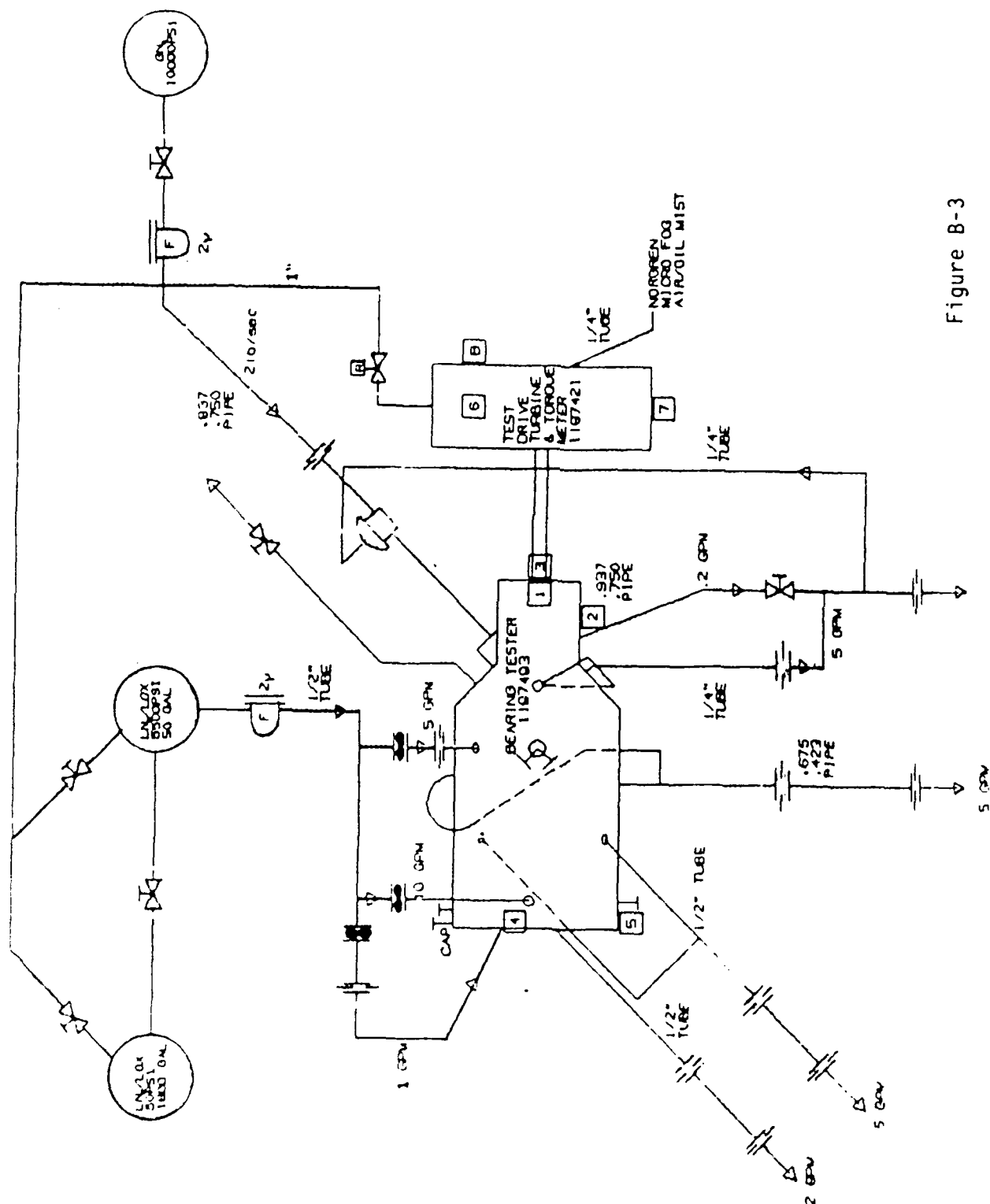


Figure B-3

QTV TEST SERIES "A" & "B"
LN2 BEARING TESTER FLOW DIAGRAM

HIGH-FREQUENCY
ACCELEROMETERSHIGH-FREQUENCY
ACCELEROMETERSHIGH-FREQUENCY
ACCELEROMETERS

Report Documentation Page

1. Report No. NASA CR-185175		2. Government Accession No.		3. Recipient's Catalog No.	
4. Title and Subtitle Orbital Transfer Vehicle Oxygen Turbopump Technology Final Report, Volume I—Design, Fabrication, and Hydrostatic Bearing Testing				5. Report Date December 1990	
				6. Performing Organization Code	
7. Author(s) P.S. Buckmann, W.R. Hayden, S.A. Lorenc, R.L. Sabiers, and N.R. Shimp				8. Performing Organization Report No. Aerojet 2459-54-2	
				10. Work Unit No. 591-41-11	
5. Performing Organization Name and Address GENCORP Aerojet TechSystems Aerojet Propulsion Division P.O. Box 13222 Sacramento, California 95813-6000				11. Contract or Grant No. NAS3-23772	
				13. Type of Report and Period Covered Contractor Report Final	
12. Sponsoring Agency Name and Address National Aeronautics and Space Administration Lewis Research Center Cleveland, Ohio 44135-3191				14. Sponsoring Agency Code	
15. Supplementary Notes Project Manager, Margaret Proctor, Space Propulsion Technology Division, NASA Lewis Research Center.					
16. Abstract This report covers the design, fabrication, and initial testing of a rocket engine turbopump (TPA) for the delivery of high - pressure liquid oxygen using hot oxygen for the turbine drive fluid. This TPA is basic to the dual expander engine which uses both oxygen and hydrogen as working fluids. Separate tasks addressed the key issue of materials for this TPA. All material selections emphasized compatibility with hot oxygen. The OX TPA design uses a two-stage centrifugal pump driven by a single-stage axial turbine on a common shaft. The first pump stage incorporates an inducer section for improved suction performance. Inter-stage pump flow is routed external to the main housing through two ducts connecting first-stage discharge to second stage entry. The shaft is supported by two journal type hydrostatic bearings supplied with high pressure LOX from the second-stage pump discharge. The design includes provision for future addition of a low speed boost pump to the engine for operation with the low pump suction pressure of flight tankage. The design also includes ports for three shaft displacement/speed sensors, various temperature measurements, and accelerometers. The unique spherical hydrostatic bearing design was considered a radical enough departure from current design to warrant a bearing test program. Testing proceeded with great care as nearly all the hardware was unique, required considerable fabrication time, and there were no spares. The Series A testing demonstrated bearing chilldown and integrity at low speed operation. An incompletely resolved problem was the rotor binding caused by pressure changes as the tester was chilled to liquid nitrogen temperatures. Series B testing demonstrated the bearing operation at high speed. The maximum speed attained was 72 000 rpm. The bearing operated satisfactorily with no load or stability problems. Post test examination of the journal and thrust bearing surfaces showed no evidence of operating wear. Additional testing which used ambient oxygen as the turbine drive gas and liquid oxygen in the pump is discussed in Volume II of this report.					
17. Key Words (Suggested by Author(s)) Orbital transfer vehicle engine; OTV; OTVE; Oxygen turbopump; Hot GOX turbine; LOX turbopump; Self-aligning bearings; Spherical seat bearings; Hydrostatic bearings; Monel; Bearing tests; Expander cycle engine			18. Distribution Statement Unclassified - Unlimited Subject Category 20		
19. Security Classif. (of this report) Unclassified		20. Security Classif. (of this page) Unclassified		21. No. of pages 239	
				22. Price All	